Physics of Alfvén waves and energetic particles in burning plasmas

Liu Chen*

Institute for Fusion Theory and Simulation and Department of Physics, Zhejiang University, Hangzhou, 310027 People's Republic of China, China and Department of Physics and Astronomy, University of California, Irvine, California 92697-4575, USA

Fulvio Zonca

C.R. ENEA Frascati–C.P. 65, 00044 Frascati, Italy and Institute for Fusion Theory and Simulation and Department of Physics, Zhejiang University, Hangzhou, 310027 People's Republic of China, China

(published 23 March 2016)

Dynamics of shear Alfvén waves and energetic particles are crucial to the performance of burning fusion plasmas. This article reviews linear as well as nonlinear physics of shear Alfvén waves and their self-consistent interaction with energetic particles in tokamak fusion devices. More specifically, the review on the linear physics deals with wave spectral properties and collective excitations by energetic particles via wave-particle resonances. The nonlinear physics deals with nonlinear wave-wave interactions as well as nonlinear wave-energetic particle interactions. Both linear as well as nonlinear physics demonstrate the qualitatively important roles played by realistic equilibrium nonuniformities, magnetic field geometries, and the specific radial mode structures in determining the instability evolution, saturation, and, ultimately, energetic-particle transport. These topics are presented within a single unified theoretical framework, where experimental observations and numerical simulation results are referred to elucidate concepts and physics processes.

DOI: 10.1103/RevModPhys.88.015008

CONTENTS

*liuchen@uci.edu

I. INTRODUCTION

Since the mid 20th century, mankind has pursued magnetic fusion energy (MFE) research, which has reached a crucial stage with the construction of the International Thermonuclear Experimental Reactor (ITER) (Tamabechi *et al.*, 1991; Aymar *et al.*, 1997). The purpose of ITER is investigating the physics of burning plasmas, where deuterium-tritium (D-T) fusion reactions

$$\mathrm{D} + \mathrm{T} \rightarrow {}^4\mathrm{He}(3.52\ \mathrm{MeV}) + n(14.06\ \mathrm{MeV})$$

produce α particles and neutrons. In ideal conditions for a fusion reactor, α particles thermalize (slow down) due to Coulomb collisions with the thermal plasma and sustain the fusion process by supplying the power input required to keep the plasma in "ignition" condition. Thus, α particles need to have sufficiently good confinement.

In toroidally symmetric magnetic fusion experimental devices (tokamaks), e.g., ITER, the geometry of the confining equilibrium magnetic field $\boldsymbol{B}_0$ is conceived to ensure properly confined charged-particle orbits, including fusion α particles. While transport due to classical collisional processes is sufficiently small, the concern is transport via collective fluctuations driven unstable by α particles via wave-particle resonances. Such collective instabilities may be toroidal symmetry breaking and, thus, lead to enhanced α-particle loss. Such "anomalous" enhanced loss is, of course, detrimental to the success of MFE research.

In order to achieve wave-particle resonances, the α-particle characteristic dynamical frequencies need to match the wave frequencies of collective instabilities. As typically α-particle velocity-space distribution function is isotropic and, after slowing down due to Coulomb collisions, decreases with energy; i.e., a velocity-space gradient is stabilizing, no collective fluctuations around the cyclotron frequency (or "gyrofrequency") will be excited. That is, the relevant instability drive is due to the finite real-space gradients. The dynamical frequencies are, thus, associated with the guiding-center motion, i.e., transit, bounce, and precessional frequencies in, e.g., a tokamak device. The corresponding wave frequencies then fall inside the magnetohydrodynamic (MHD) regime (Alfvén, 1942, 1950), which are $\mathcal{O}(10^{-2})$ smaller than the ion gyrofrequency Ω_i for typical tokamak parameters. As to the three finite-frequency MHD modes, the most relevant one is the nearly incompressible, anisotropic shear Alfvén wave (SAW) with dispersion relation $\omega = k_\parallel v_A$. Here $k_\parallel = \boldsymbol{k}\cdot\boldsymbol{B}_0/B_0$ is the parallel wave number and $v_A = B_0/\sqrt{4\pi\varrho_{m0}}$ is the Alfvén speed, with ϱ_{m0} the plasma mass density. The compressional, fast Alfvén wave with $\omega_f \simeq k v_A$ tends to have frequencies at least $\mathcal{O}(10)$ higher than those of SAW and generally is more difficult to excite. The slow sound wave with $\omega_s \simeq k_\parallel c_s$ (c_s is the ion sound speed) is also typically stable due to significant ion Landau damping with $T_e \sim T_i$, where T_e and T_i are, respectively, thermal electron and ion temperatures. This discussion is also applicable to energetic, fast (relative to the thermal background plasma) charged particles produced by auxiliary heating sources such as radio-frequency waves and/or neutral beam injection. Collective excitations of SAW instabilities by energetic, fast particles (EPs) and the ensuing nonlinear consequences on EP confinement as well as, on longer time scales, the confinement and stability of thermal background plasmas are, thus, crucial issues for both present-day MFE devices and future burning-plasma experiments.

A. Historical review

Energetic particles in burning plasmas consist of electrically charged fusion products as well as suprathermal ions and electrons, generated by external power sources that are used for heating and current drive or, more generally, for tailoring and controlling equilibrium plasma profiles. The possible detrimental roles of SAWs on EP confinement in burning plasmas was brought to researchers' attention since the pioneering works by Kolesnichenko and Oraevskij (1967), Belikov, Kolesnichenko, and Oraevskij (1968), Mikhailovskii (1975), and Rosenbluth and Rutherford (1975). In particular, Kolesnichenko and Oraevskij (1967) suggested that instabilities may be caused by fusion products, and Belikov, Kolesnichenko, and Oraevskij (1968) showed for the first time the existence of SAW instabilities with $\omega \simeq k_\parallel v_A$ driven by monoenergetic EPs. As the characteristic frequencies of EP motions in fusion devices are of the same order of those typical of SAWs, and the SAW group velocity is parallel to $\boldsymbol{B}_0$, resonant wave-particle interactions may directly excite a variety of SAWs as well as yield an efficient transport channel for EPs.

In the 1980s, increasing theoretical attention was devoted to the analysis of the effects of fusion α's in burning plasmas, e.g., in the works by Kolesnichenko (1980) and Tsang, Sigmar, and Whitson (1981). However, the problem of SAWs interactions with EPs and of related transport processes became an issue of immediate practical interest at the time of the first observation of the fishbone mode instability in the Poloidal Divertor eXperiment (PDX) tokamak (McGuire *et al.*, 1983), causing dramatic global losses of EPs due to a secular transport process (White *et al.*, 1983). This instability was explained as resonant excitation of an internal kink mode and its self-consistent nonlinear interplay with the EP nonuniform source (Chen, White, and Rosenbluth, 1984; Coppi and Porcelli, 1986). After fishbone observation and theoretical interpretation, MHD modes were considered on the

same footing as SAWs concerning their possible effect on EPs confinement. Essential physics ingredients in these analyses were nonuniform equilibrium profiles of EP sources, of SAW continuous spectrum (Chen, White, and Rosenbluth, 1984; Cheng, Chen, and Chance, 1985; Chen, 1988, 1994), the corresponding continuum damping by phase mixing (Grad, 1969), the specific equilibrium geometries of magnetized plasmas, and the resultant frequency gaps inside the SAW continuum (Pogutse and Yurchenko, 1978; D'Ippolito and Goedbloed, 1980; Kieras and Tataronis, 1982). In the same years, further demonstration of the articulated role played by EPs in tokamak plasmas came with the evidence of "sawtooth"[1] stabilization in plasma discharges with additional heating (Campbell *et al.*, 1988) observed in the Joint European Torus (JET) (Rebut, Bickerton, and Kenn, 1985). This was explained with the strong stabilizing effect of magnetically trapped EPs on the internal kink mode (Coppi *et al.*, 1988; White *et al.*, 1988) and is an important example of plasma operation control by external power input.

An important theoretical result was that discrete Alfvén eigenmodes (AEs), such as toroidal AEs (TAEs), can exist essentially free of continuum damping in the frequency gaps of the SAW continuous spectrum (Cheng, Chen, and Chance, 1985). Experimental observations of TAEs (Heidbrink *et al.*, 1991; Wong *et al.*, 1991) and of lower frequency AEs dubbed beta-induced AEs (BAEs) (Heidbrink, Strait *et al.*, 1993), and, most importantly, the evidence that these modes may have significant impact on EP transport were the findings that brought significant and continuing attention to the physics of SAWs and EPs in burning plasmas. In fact, only a small fraction of fusion α's or EP losses can be tolerated in ITER without significantly degrading the fusion yield or damaging the plasma facing components (ITER Physics Expert Group on Energetic Particles, Heating and Current Drive, 1999; Fasoli *et al.*, 2007; Pinches *et al.*, 2015).

Another important theoretical prediction was the existence of energetic-particle continuum modes (EPMs) (Chen, 1994), i.e., non-normal modes of the SAW continuous spectrum, which emerge as discrete fluctuations at the frequency that maximizes wave-EP power exchange above the threshold condition associated with continuum damping. In this respect, fishbones could be considered the first example of EPM. In the presence of EPM and/or fishbones, the low critical level of tolerable EP losses in a fusion device can become more severe. In fact, being non-normal modes, both fishbones and EPMs maintain maximum wave-EP power exchange and ensuing EP transport through their nonlinear evolution by phase locking with resonant particles via frequency sweeping (Briguglio, Zonca, and Vlad, 1998; Vlad *et al.*, 2004, 2013; Zonca *et al.*, 2005, 2015b; Briguglio *et al.*, 2007). In turn, phase locking is responsible for the secular transport process first introduced by White *et al.* (1983) to explain fishbone induced EP losses. Intuitively, secular losses of EPs are characterized by a different energy spectrum than EP diffusive losses and tend to be more critical, since resonant EPs are typically lost before significant thermalization (White *et al.*, 1983; Chen, 1988). The self-consistent nonlinear interplay of EP spatial distributions with the EPM radial mode structures plays a crucial role in all of these processes. Experimental observations of EPMs and corresponding EP transport came right after their theoretical prediction (Gorelenkov *et al.*, 2000; Gorelenkov and Heidbrink, 2002). Meanwhile, first spectacular observations of these phenomena, dubbed abrupt large amplitude events (ALEs) (Shinohara *et al.*, 2001), were reported in the JT-60U tokamak (Shinohara *et al.*, 2004) and are among the clearest experimental evidences of strong EP redistributions along with observations of EP losses and redistributions in the Doublet III-D (DIII-D) (Duong *et al.*, 1993; Strait *et al.*, 1993; Heidbrink and Sadler, 1994) and National Spherical Torus eXperiment (NSTX) tokamaks (Fredrickson *et al.*, 2009; Podestà *et al.*, 2009, 2011).

Since the early evidence of AEs and EPMs in tokamak plasmas, a whole "zoology" of modes have been observed (Heidbrink, 2002), with a classification following the qualitative features of experimental measurements. All these fluctuations can be actually understood and explained within the theoretical framework based on one single general fishbonelike dispersion relation (GFLDR) (Zonca and Chen, 2014b, 2014c), first introduced for the description of the fishbone mode (Chen, White, and Rosenbluth, 1984), and later on derived for different branches of SAW fluctuations, demonstrating its general validity (Zonca and Chen, 2006, 2007; Chen and Zonca, 2007a; Zonca *et al.*, 2007a; Chen, 2008). The usefulness of the GFLDR theoretical framework stands in its capability of providing a simple description of the underlying physics and extracting the distinctive features of the different AE and EPM branches that have been observed experimentally or in numerical simulations. Furthermore, the GFLDR also naturally introduces the spatiotemporal scales of the process involved, explaining thereby the connection between MHD fluctuations, SAWs, and drift wave turbulence (DWT). The historical review of various experimental observations of AE and EPM and their theoretical interpretations is further articulated in Secs. III and IV. Successful feedbacks between theory and experiment in this area were made possible by the development of impressive diagnostic techniques as well as numerical simulation capabilities, accompanied by detailed physics understanding. Meanwhile, one element of enrichment was brought by the fruitful exchanges between MFE tokamak and stellarator expert communities (Kolesnichenko *et al.*, 2011; Toi *et al.*, 2011).

Of the two "routes" to nonlinear dynamics of EP-driven SAW instabilities (Chen and Zonca, 2013), i.e., nonlinear wave-wave and wave-EP interactions (cf. Sec. IV), the former one was historically addressed first in the classic work by Hannes Alfvén, demonstrating the existence of the pure "Alfvénic state," where SAW can exist in uniform, incompressible MHD plasmas independently of their amplitude due to the cancellation of Reynolds and Maxwell stresses and the incompressible plasma motion produced by SAW (Alfvén, 1942, 1950; Walén, 1944). However, nonlinear SAW-EP interactions have attracted most of the interest until recently because of the important role of EP transport in burning plasmas.

Within the first route, it is illuminating to explore the various nonlinear wave-wave interactions that could lead to the breaking of the Alfvénic state (Chen and Zonca, 2013).

[1]This name refers to the "shape" of the time trace of plasma electron temperature on the magnetic axis.

The effect of plasma compressibility in the macroscopic MHD limit was investigated by Sagdeev and Galeev (1969), demonstrating the decay instability of a SAW into an ion sound wave (ISW) and a backscattered SAW. Later, plasma compressibility effects were explored by Hasegawa and Chen (1976) for microscale fluctuations with wavelengths of the order of the thermal ion Larmor radius. This analysis not only generalized the MHD results on the decay instability, but demonstrated important consequences on plasma transport due to the different features of scattered SAW fluctuation spectra. These processes are discussed in Sec. IV.B, while Sec. IV.C analyzes examples of processes that could break the Alfvénic state in toroidal geometry as well as lead to cross-scale couplings among MHD fluctuations, SAWs, and DWT.

Within the second route (cf. Sec. IV.D), the first nonlinear analysis of "thermonuclear Alfvén instability" was reported by Belikov, Kolesnichenko, and Oraevskij (1974), using the quasilinear description of a weakly turbulent plasma (Vedenov, Velikhov, and Sagdeev, 1961; Drummond and Pines, 1962). This case shows the important influence of original works on nonlinear wave-particle dynamics in one-dimensional (1D) systems, investigated by pioneers in the early 1960s (O'Neil and Malmberg, 1968), adopting the paradigmatic case of the interaction of a suprathermal electron beam with a plasma in a strong axial magnetic field. This system provides the framework in which various processes were investigated and understood, such as mode dispersion relations, Landau damping in a finite-amplitude wave (Mazitov, 1965; O'Neil, 1965), and nonlinear behavior due to wave-particle interactions (O'Neil, Winfrey, and Malmberg, 1971). The interest for the beam-plasma system was revived in the 1990s, when it was proposed as a paradigm for interpreting experimental observation of AEs excitation by EPs and related nonlinear dynamics processes near marginal stability (Berk, Breizman, and Ye, 1992a; Breizman, Berk, and Ye, 1993; Berk, Breizman, and Pekker, 1996; Berk, Breizman, and Petiashvili, 1997; Breizman *et al.*, 1997), based on their one-to-one correspondence with the evolution of the "bump-on-tail" instability (Langmuir wave) in a 1D uniform plasma (Berk and Breizman, 1990a, 1990b, 1990c). This bump-on-tail paradigm, recently reviewed by Breizman and Sharapov (2011), was extensively applied for comparisons of theoretical model predictions with experimental observations. There are, however, processes crucial to the dynamics of toroidal plasmas such as fishbone induced EP losses (White *et al.*, 1983) as well as nonlinear EPM dynamics and ensuing EP transport (Briguglio, Zonca, and Vlad, 1998; Zonca *et al.*, 2000, 2005; Vlad *et al.*, 2004), which would require theoretical analyses based on an alternative "fishbone" paradigm (Chen and Zonca, 2013; Zonca *et al.*, 2015b). Magnetic field geometry and plasma nonuniformities play major roles in this fishbone paradigm. In particular, nonlinear dynamics due to the self-consistent interplay of fluctuations evolution and EP transport leads typically to secular EP losses due to EPMs, fishbones, and phase locking of fluctuations with resonant particles via frequency sweeping. Ultimately, it is possible to demonstrate the unification of these two paradigms for nonlinear wave-EP interactions (cf. Sec. IV.D), based on the solution of the Dyson equation for the EP distribution function (Al'tshul' and Karpman, 1965).

Because of the intrinsic complexity involved in a self-consistent nonlinear description of SAW fluctuations with EPs, EP transport in burning plasmas has typically been addressed by test-particle methods (Hsu and Sigmar, 1992; Sigmar *et al.*, 1992), i.e., removing the possible feedback of EP redistributions on a given fluctuation spectrum (cf. Sec. V). As AE fluctuations are local in nature and have generally small intensity [see, e.g., Heidbrink (2008)], EP redistributions by AEs are expected to be typically small, unless stochastization threshold of EP motions in phase space is reached in the presence of many modes. Realistic predictions of test-particle transport in ITER are, however, still not available. In fact, not only is the threshold for stochastic EP transport sensitive to details of the underlying physics and adopted model (White *et al.*, 2010a, 2010b), but predicting EP redistributions and losses requires necessarily realistic sources, geometries, and boundary conditions. Such thorough and detailed calculation of AE spectra in ITER with comprehensive global gyrokinetic and/or extended hybrid MHD-gyrokinetic codes (cf. Sec. II) could be likely available in the near future due to the progress in both computational capabilities and understanding of essential physics ingredients.

B. Scope of the present review

The first and thorough experimental review of SAW and EP physics in burning plasmas was given by Heidbrink and Sadler (1994). This work was followed by that of Wong (1999), which was focused on experiments in the Tokamak Fusion Test Reactor (TFTR) (Grove and Meade, 1985) but provided a general overview in this area. A dedicated review of α-particle physics experiments in TFTR was given by Zweben *et al.* (2000), while high performance D-T experiments in JET (Gibson, 1998) were stable to SAW excited by fusion α's (Sharapov *et al.*, 1999). Meanwhile, the ITER Physics Expert Group on Energetic Particles, Heating and Current Drive (1999) gave the first review of the physics of SAW and EPs in ITER plasmas, which was updated later on (Fasoli *et al.*, 2007), while the most recent review of this topic can be found in Pinches *et al.* (2015).

Basic theoretical reviews can be found in Mahajan (1995), analyzing the general linear properties of the SAW fluctuation spectrum, and in Chen and Zonca (1995), with a discussion of the complications and twists of SAW physics in realistic toroidal geometries. A general overview of both linear and nonlinear SAW and EP physics was given by Vlad, Zonca, and Briguglio (1999), along with a discussion of numerical simulation results using the hybrid MHD-gyrokinetic model (Park *et al.*, 1992). The work by Pinches *et al.* (2004) mainly focused on the interplay between advancements in nonlinear theory, also reviewed by Breizman (2006), and comparisons with experimental data. Other brief overviews are available, with emphasis on the self-consistent interaction of nonlinear SAW dynamics with EP transport and complex behavior in burning plasmas (Zonca *et al.*, 2006; Chen and Zonca, 2007a).

Key issues for burning plasmas were summarized by Heidbrink (2002) and a general review of basic physics of SAWs and EPs in toroidal plasmas was given by Heidbrink (2008). An updated view of experimental results since Wong

(1999) and Heidbrink (2002) and of the further progress in nonlinear theory comparison with experimental data was presented by Breizman and Sharapov (2011). Recent overview works meanwhile focused on the progress made in developing innovative diagnostic techniques and on the modeling effort for the interpretation of the corresponding observations (Sharapov *et al.*, 2013; Gorelenkov, Pinches, and Toi, 2014) as well as on the kinetic models and numerical solution strategies adopted in comparisons of numerical simulation results to experiments (Lauber, 2013). For stellarators, a recent experimental review can be found in Toi *et al.* (2011), while theoretical aspects were reviewed by Kolesnichenko *et al.* (2011), with emphasis on both the "affinity and difference between energetic-ion-driven instabilities in 2D and 3D toroidal systems."

The scope of this review is to provide a comprehensive analysis of physics processes involved with SAW and EP behavior in burning plasmas within a unified and self-contained theoretical framework. As prevalent Alfvénic fluctuations are in the MHD frequency range ($|\omega| \ll \Omega_i$), basic equations are derived from the nonlinear gyrokinetic equation (Frieman and Chen, 1982); cf. Sec. II. Most detailed derivations, which interested readers can find in Zonca and Chen 2014b, 2014c), are omitted in Sec. II. The main scope of Sec. II is the discussion of fundamental physics processes described by basic equations, especially their characteristic spatial and temporal scales.

Experimental observations and numerical simulation results are important elements of existing literature in this area and are referred to in this work as a means for elucidating theoretical concepts. Thus, this review offers different levels of reading that are merged and integrated into the same narrative to address the different aspects that may be of interest to theoreticians, modelers, and/or experimentalists. The GFLDR (cf. Sec. III.C) provides the foundation for the unified theoretical framework used throughout this work and is derived and discussed in Zonca and Chen (2014b, 2014c). The present review shows the usefulness of the GFLDR theoretical framework in suggesting the interpretation of experimental observations and numerical simulation results on the basis of the underlying physics. In this respect, various models and computation techniques with different levels of approximation can also be employed to validate and verify theoretical predictions.

The application of the GFLDR theoretical framework to nonlinear SAW and EP dynamics (cf. Sec. IV) allows separating wave-wave and wave-EP nonlinear interactions based on the respective spatiotemporal scales and unifying the bump-on-tail and fishbone paradigms for nonlinear SAW-EP interactions (Zonca *et al.*, 2015b) based on the solution of the Dyson equation for the EP distribution function. It also naturally yields to the formulation of a general nonlinear Schrödinger equation (NLSE) with integrodifferential nonlinear terms (cf. Sec. IV.A), which can be used to draw analogies between this area of MFE and neighboring fields of physics research, such as fluid turbulence, condensed matter, nonlinear dynamics and complexity, fractional kinetics, and accelerator physics (cf. Secs. IV.D and IV.E). This unified approach also elucidates the role of EPs as mediators of cross-scale coupling and long time-scale behavior in burning plasmas (Zonca, 2008; Zonca and Chen, 2008; Zonca *et al.*, 2013), reviewed by Zonca *et al.* (2015a).

In spite of the broad range of topics discussed in this review, it is far from being complete. A summary of relevant issues left out of this work is given in Sec. VI, along with elements for reflections on some of the major research topics in the MFE field for the next decade or so, in the perspective of ITER operations.

II. BASIC EQUATIONS AND CONCEPTS

In this section, we consider a magnetized plasma in general geometry and briefly review equations for low-frequency electromagnetic fluctuations, produced by the self-consistent charged-particle motion. The low-frequency ordering in magnetized plasmas is referred as usual to oscillation frequencies that are much smaller than the ion cyclotron frequency Ω_i, where $\Omega = eB_0/mc$, with the subscript i denoting ions, B_0 denotes the strength of the local equilibrium magnetic field, e stands for the generic particle electric charge, and m for its mass. Similarly, the subscript e refers to electrons and the subscript E denotes EPs, which may be ions and/or electrons.

A self-consistent description of low-frequency fluctuations is based on the derivation of gyrokinetic Maxwell equations (Antonsen and Lane, 1980; Catto, Tang, and Baldwin, 1981; Frieman and Chen, 1982),[2] expressed in terms of moments of the gyrocenter Vlasov (Boltzmann) distribution. Within this approach, one can systematically decouple (Rutherford and Frieman, 1968; Taylor and Hastie, 1968) the nearly periodic particle gyromotion (Kruskal, 1962; Northrop, 1963) from the fluctuation dynamics. This is achieved in two steps (Dubin *et al.*, 1983; Hahm, 1988; Hahm, Lee, and Brizard, 1988; Brizard, 1989), based on asymptotic decoupling of the fast gyromotion time scale from a set of Hamilton equations by Lie-transform methods (Littlejohn, 1982; Brizard, 1990; Qin and Tang, 2004). First, the guiding-center Hamilton equations are derived eliminating the gyroangle dependence due to the gyromotion of charged particles about $\boldsymbol{B}_0$. Second, the new gyrocenter Hamilton equations are obtained eliminating the gyroangle dependence in the perturbed guiding-center equations due to the presence of electromagnetic fluctuations. In this way (Brizard and Hahm, 2007), it is possible to construct the gyrocenter magnetic moment as an adiabatic invariant corresponding to the fast and nearly periodic particle gyromotion in the gyrocenter gyroangle, while the guiding-center magnetic moment adiabatic invariance is modified by the introduction of low-frequency fluctuations (Taylor, 1967).

In the following, we discuss equations governing the low-frequency response of a quasineutral, finite-β, magnetized plasma, with $\beta = 8\pi P/B_0^2$ defined as the ratio between kinetic and magnetic energy densities. We describe the low-frequency plasma oscillations in terms of three fluctuating scalar fields, having chosen to work in the Coulomb gauge: the scalar potential perturbation $\delta\phi$, the parallel (to $\boldsymbol{b} = \boldsymbol{B}_0/B_0$) magnetic field perturbation $\delta B_\parallel$, and the parallel (to $\boldsymbol{b}$) vector potential fluctuation $\delta A_\parallel$. For simplicity and hence clarity, we,

[2]See Brizard and Hahm (2007) for a recent and comprehensive review.

unless otherwise explicitly stated, neglected in this review plasma rotation effects, which may be important in practical applications (see, e.g., Secs. III.C and V.B) and can be, in principle, included via extensions of the present theoretical framework.

A. Gyrokinetic ordering of physical quantities

The ordering of spatiotemporal scales and fluctuation strength is the usual one in gyrokinetic theory. The background plasma is described by means of the small parameter $\epsilon_B \equiv \rho_i/L_B$, with ρ_i denoting the ion Larmor radius and

$$|\rho_i \nabla \ln B_0| \sim \epsilon_B \quad \text{and} \quad \left|\frac{1}{\Omega_i}\frac{\partial}{\partial t}\ln B_0\right| \sim \epsilon_B^3. \tag{2.1}$$

A similar ordering is introduced for the background Vlasov (Boltzmann) distribution function f_0:

$$|\rho_i \nabla \ln f_0| \sim \epsilon_F \quad \text{and} \quad \left|\frac{1}{\Omega_i}\frac{\partial}{\partial t}\ln f_0\right| \sim \epsilon_F^3. \tag{2.2}$$

The usefulness of having separate orderings, based on ϵ_B and ϵ_F, is the possibility of introducing ϵ_B/ϵ_F as an auxiliary ordering parameter for exploiting the inverse aspect-ratio expansion in $a/R_0 \sim \epsilon_B/\epsilon_F$, with a and R_0 the torus minor and major radii, respectively. The time-scale ordering of Eqs. (2.1) and (2.2) is consistent with the transport time-scale ordering (Hinton and Hazeltine, 1976), as noted by Frieman and Chen (1982).

Spatial and temporal scales in the fluctuation fields $(\delta\phi, \delta A_\parallel, \delta B_\parallel)$ and distribution function (δf) are described in terms of the ordering parameters $(\epsilon_\perp, \epsilon_\omega)$

$$|\boldsymbol{k}_\perp \rho_i| \sim \epsilon_\perp \sim 1 \quad \text{and} \quad \left|\frac{\omega}{\Omega_i}\right| \sim \epsilon_\omega \ll 1, \tag{2.3}$$

with $\boldsymbol{k}$ and ω the wave vector and angular frequency, and the subscript $\perp$ indicating the component perpendicular to $\boldsymbol{b}$. The ordering for $k_\parallel$ is obtained from the condition that strong wave-particle interactions may be accounted for, i.e., denoting by v_{ti} the ion characteristic (thermal) speed

$$\omega \sim k_\parallel v_{ti} \quad \text{and} \quad \left|\frac{k_\parallel}{\boldsymbol{k}_\perp}\right| \sim \frac{\epsilon_\omega}{\epsilon_\perp}. \tag{2.4}$$

The ordering of Eqs. (2.3) and (2.4) may be applied either to thermal ions as usual or to EPs, yielding to a broad range of frequency and wavelength spectra of fluctuations that can be described within the present theoretical framework (cf. Secs. II.B, II.D, and II.E as well as Sec. III).

When investigating fluctuations of the Alfvén branch, the $|k_\parallel/\boldsymbol{k}_\perp|$ ratio reflects the frequency ratio of shear to compressional waves. In most of this work (see Secs. II.D and II.E), we assume that these frequency scales are well separated for this is the condition under which SAW and DAW (drift Alfvén wave) are most easily excited by both thermal plasma and EPs in fusion plasmas. Meanwhile, when considering compressional Alfvén waves (CAWs), the frequency ordering reads $\omega/\Omega_i \sim |\boldsymbol{k}_\perp| v_A/\Omega_i \sim |\boldsymbol{k}_\perp \rho_i|/\beta^{1/2}$, so that the oscillation frequency can no longer be considered small compared with Ω_i for typical conditions in fusion plasmas. In this case, a high-frequency gyrokinetic description of linear plasma dynamics may still be derived (Chen and Tsai, 1983; Tsai, Van Dam, and Chen, 1984; Lashmore-Davies and Dendy, 1989; Qin, Tang, Lee, and Rewoldt, 1999; Qin, Tang, and Lee, 2000), but its discussion is outside the scope of this review. Note that while the condition $|k_\parallel/\boldsymbol{k}_\perp| \simeq \epsilon_\omega/\epsilon_\perp \ll 1$ is consistent with gyrokinetic ordering, it is in general not necessary (Qin, Tang, and Rewoldt, 1998, 1999; Brizard and Hahm, 2007).

The relative fluctuation levels are estimated by the ordering parameter ϵ_δ:

$$\epsilon_\perp \left|\frac{\delta f}{f_0}\right| \sim \left|\frac{\delta \boldsymbol{B}_\perp}{B_0}\right| \sim \left|\frac{\delta \dot{\bar{\boldsymbol{X}}}_\perp}{v_{ti}}\right| \sim \epsilon_\delta \ll 1, \tag{2.5}$$

with $\delta\dot{\bar{\boldsymbol{X}}}_\perp$ the perturbed gyrocenter velocity [cf. Eq. (2.25)]

$$|\delta \dot{\bar{\boldsymbol{X}}}_\perp| \sim \left|\frac{c\delta \boldsymbol{E}_\perp}{B_0}\right| \sim \left|v_\parallel \frac{\delta \boldsymbol{B}_\perp}{B_0}\right| \sim \left|\epsilon_\perp \frac{e}{T_i}\delta\phi\right| v_{ti} \sim \left|\epsilon_\perp \frac{e}{T_i}\frac{v_\parallel}{c}\delta A_\parallel\right| v_{ti} \tag{2.6}$$

and T_i stands for the ion characteristic (thermal) energy. Finally, due to the condition $|k_\parallel/\boldsymbol{k}_\perp| \ll 1$, the compressional component of the magnetic field fluctuation[3] $\delta B_\parallel$ satisfies the perpendicular pressure balance (Chen and Hasegawa, 1991)

$$\nabla_\perp (B_0 \delta B_\parallel + 4\pi \delta P_\perp) \simeq 0. \tag{2.7}$$

Thus, $\delta B_\parallel$ is ordered as

$$\left|\frac{\delta B_\parallel}{B_0}\right| \sim \beta\epsilon_\delta \ll 1 \Rightarrow \left|\mu \frac{\nabla_\perp \delta B_\parallel}{\Omega_i}\right| \sim \beta \epsilon_\perp \epsilon_\delta v_{ti} \tag{2.8}$$

which applies in general for both low- and high-β magnetized plasmas. Here $\mu = v_\perp^2/(2B_0)$ is the magnetic moment.

In Sec. II.B, we summarize equations governing the low-frequency response of a quasineutral, finite-β, magnetized plasma, which apply for arbitrary β, i.e., in both space (Chen and Hasegawa, 1991), for $\beta \sim 1$, and laboratory plasmas (Hahm, Lee, and Brizard, 1988), for $\beta \ll 1$. The simplified equations for $\beta \ll 1$, more readily adopted for the description of DAW dynamics in tokamaks which are the main focus of this review, will be discussed in Sec. II.D. Finally, the further limiting case of governing equations that may be generally adopted for investigating DAW excitation by EPs in burning plasmas is given in Sec. II.E.

B. Theoretical model and formal governing equations

Consistent with the gyrokinetic wavelength ordering, discussed in Sec. II.A, we assume $k^2\lambda_D^2 \sim \lambda_D^2/\rho_i^2 = \Omega_i^2/\omega_{pi}^2 \ll 1$, with λ_D the Debye length and ω_{pi} the ion plasma frequency.

[3]This denomination is due to the fact that $\delta B_\parallel$ modifies the magnetic energy density at order ϵ_δ.

Thus, Poisson's equation becomes the quasineutrality condition

$$\sum e\langle \delta f\rangle_v = 0, \tag{2.9}$$

where $\sum$ implicitly indicates summation on all particle species and $\langle\cdots\rangle_v$ denotes integration in velocity space.

The equation for $\delta B_\parallel$ is readily obtained from the perpendicular component of the low-frequency Ampère's law (without displacement current, since $|\boldsymbol{k}|^2c^2 \gg |\omega|^2$)

$$\nabla_\perp \delta B_\parallel = \boldsymbol{\kappa}\delta B_\parallel + \nabla_\parallel \delta \boldsymbol{B}_\perp + (\nabla \boldsymbol{b})\cdot \delta \boldsymbol{B}_\perp + \frac{4\pi}{c}\sum e\langle \boldsymbol{b}\times \boldsymbol{v}_\perp \delta f\rangle_v. \tag{2.10}$$

Here $\nabla_\parallel \equiv \boldsymbol{b}\cdot\nabla$, $\nabla_\perp \equiv \nabla - \boldsymbol{b}\nabla_\parallel$, $\boldsymbol{\kappa}\equiv \boldsymbol{b}\cdot\nabla\boldsymbol{b}$ is the equilibrium magnetic field curvature, and the perpendicular magnetic field fluctuation can be expressed as

$$\delta \boldsymbol{B}_\perp = \nabla_\perp \delta A_\parallel \times \boldsymbol{b} + (\boldsymbol{b}\times\boldsymbol{\kappa})\delta A_\parallel + \boldsymbol{b}\times\nabla_\parallel \delta \boldsymbol{A}_\perp + (\boldsymbol{b}\times\nabla\boldsymbol{b})\cdot\delta\boldsymbol{A}_\perp. \tag{2.11}$$

The equation for $\delta A_\parallel$ can be written in terms of the vorticity equation

$$\nabla\cdot\delta\boldsymbol{j} = \boldsymbol{B}_0\cdot\nabla\left(\frac{\delta j_\parallel}{B_0}\right) + \nabla\cdot\delta\boldsymbol{j}_\perp = 0. \tag{2.12}$$

Here the fluctuating parallel current density is expressed in terms of $\delta A_\parallel$ via the parallel component of the low-frequency Ampère's law

$$\begin{aligned}\delta j_\parallel &= \frac{c}{4\pi}\boldsymbol{b}\cdot\nabla\times(\nabla\times\delta\boldsymbol{A})\\ &= \frac{c}{4\pi}\{[-\nabla^2+\kappa^2+(\nabla\boldsymbol{b}):(\nabla\boldsymbol{b})]\delta A_\parallel + (\nabla\times\boldsymbol{b})_\parallel \delta B_\parallel\\ &\quad + (\nabla\boldsymbol{b}):(\nabla\delta\boldsymbol{A}_\perp) + \nabla\cdot[(\nabla\boldsymbol{b})\cdot\delta\boldsymbol{A}_\perp]\\ &\quad + (\boldsymbol{\kappa}\cdot\nabla\boldsymbol{b})\cdot\delta\boldsymbol{A}_\perp + (\boldsymbol{b}\cdot\nabla\delta\boldsymbol{A}_\perp)\cdot\boldsymbol{\kappa}\},\end{aligned} \tag{2.13}$$

while the fluctuating perpendicular current is obtained from the perpendicular component of the force balance

$$\frac{\partial}{\partial t}\delta(\varrho_m\boldsymbol{u}) = -\nabla\cdot\delta\mathcal{P} + \delta\left(\frac{\boldsymbol{j}\times\boldsymbol{B}}{c}\right). \tag{2.14}$$

Here as usual we introduced the fluctuating plasma mass density and flow

$$\delta\varrho_m = \sum m\langle\delta f\rangle_v \quad\text{and}\quad \delta(\varrho_m\boldsymbol{u}) = \sum m\langle\boldsymbol{v}\delta f\rangle_v, \tag{2.15}$$

as well as the perturbed stress tensor $\delta\mathcal{P}$

$$\delta\mathcal{P} = \sum m\langle\boldsymbol{v}\boldsymbol{v}\delta f\rangle_v. \tag{2.16}$$

Equation (2.14) is readily solved for $\delta\boldsymbol{j}_\perp$ and yields

$$\left(1+\frac{\delta B_\parallel}{B_0}\right)\delta\boldsymbol{j}_\perp = \frac{c}{B_0}\boldsymbol{b}\times\left[\frac{\partial}{\partial t}\delta(\varrho_m\boldsymbol{u}) + \nabla\cdot\delta\mathcal{P}\right] - \boldsymbol{j}_{\perp 0}\frac{\delta B_\parallel}{B_0} + (j_{\parallel 0}+\delta j_\parallel)\frac{\delta\boldsymbol{B}_\perp}{B_0}. \tag{2.17}$$

Substituting back into Eq. (2.12), one obtains the general form of the vorticity equation

$$B_0\left(\boldsymbol{b}+\frac{\delta\boldsymbol{B}_\perp}{B_0}\right)\cdot\nabla\left(\frac{\delta j_\parallel}{B_0}\right) + \delta\boldsymbol{B}_\perp\cdot\nabla\left(\frac{j_{\parallel 0}}{B_0}\right) + \delta B_\parallel\nabla_\parallel\left(\frac{\delta j_\parallel}{B_0}+\frac{j_{\parallel 0}}{B_0}\right) - (\boldsymbol{j}_0+\delta\boldsymbol{j})\cdot\nabla\left(\frac{\delta B_\parallel}{B_0}\right) + \nabla\cdot\left[\frac{c}{B_0}\boldsymbol{b}\times\left(\frac{\partial}{\partial t}\delta(\varrho_m\boldsymbol{u}) + \nabla\cdot\delta\mathcal{P}\right)\right] = 0. \tag{2.18}$$

Equations (2.9), (2.10), and (2.18) form the closed set of dynamic equations formally governing the low-frequency response of a quasineutral, finite-β, magnetized plasma, once the perturbed particle distribution function δf is given and the perpendicular magnetic field fluctuation is obtained by Eq. (2.11). Note that they still hold for finite plasma rotation, about which no assumption has been made so far. Meanwhile, Eqs. (2.13) and (2.17) are considered as definitions for $\delta j_\parallel$ and $\delta\boldsymbol{j}_\perp$, and Eqs. (2.15) and (2.16) are used for $\delta(\varrho_m\boldsymbol{u})$ and $\delta\mathcal{P}$. In fact, given $\delta A_\parallel$ and $\delta B_\parallel = \boldsymbol{b}\cdot\nabla\times\delta\boldsymbol{A}$, and noting the Coulomb gauge $\nabla\cdot\delta\boldsymbol{A}=0$, $\delta\boldsymbol{A}_\perp$ is uniquely determined. By construction, Eqs. (2.9), (2.10), and (2.18), for wavelengths that are much longer than the Debye length, are completely equivalent to the gyrokinetic Maxwell equations (Brizard and Hahm, 2007), once the perturbed particle fluid moments are expressed in terms of the perturbed gyrocenter fluid moments (Brizard, 1992). These equations are also equivalent to the formulation adopted in most literature, once the parallel Ampère's law is employed in the vorticity equation (2.18).

C. Ordering estimates of vorticity equation and physical time scales

Unlike most treatments available in the literature, the present theoretical framework does not assume any particular ordering of the perpendicular wavelength with respect to characteristic equilibrium spatial scales: this is the reason why Eqs. (2.10), (2.11), and (2.13) maintain terms that depend on equilibrium geometry, which may be important when treating long-wavelength modes (Qin, Tang, and Rewoldt, 1998, 1999; Brizard and Hahm, 2007). However, while the nonlinear formal kinetic equations governing collisionless plasmas in the drift-kinetic limit (vanishing Larmor radius) were given by Kulsrud (1983), expressions of the perturbed particle in terms of the perturbed gyrocenter fluid moments (Brizard, 1992), valid for general low-frequency fluctuations and at arbitrary wavelengths are still not available at present. Nonetheless, Eqs. (2.9), (2.10), and (2.18) allow a detailed discussion of the relative importance of various contributions and, ultimately, the derivation of a set of reduced nonlinear equations, which will be used in the present work.

The first term in the vorticity equation (2.18) represents the linear magnetic field line bending, which we denote as $\mathcal{O}(1)$. The second one is its nonlinear extension, related to the

perpendicular Maxwell stress, ordered as $\sim\epsilon_\perp\epsilon_\delta/\epsilon_\omega$ (cf. Sec. II.A). The third term, representing the kink drive, is of the order of $\sim\epsilon_F/\epsilon_\perp$. Meanwhile, the fourth to seventh terms containing $\delta B_\parallel$ are, respectively, of the order of $\beta\epsilon_\delta$, $\beta\epsilon_B/\epsilon_\perp$, $\beta^2\epsilon_F/\epsilon_B$, and $\beta^2\epsilon_\perp\epsilon_\delta/\epsilon_\omega$. The last two terms in Eq. (2.18) represent the plasma inertia response and the stress tensor contribution, which includes the usual Reynolds stress as well as the divergence of the nonlinear diamagnetic current. The linear plasma inertia response is of the order of $\sim\omega^2/k_\parallel^2 v_A^2$, whereas its nonlinear contribution is an order $\sim\epsilon_\delta/\epsilon_\perp$ higher. The stress tensor linear contribution is of the same order as the inertia term, while the nonlinear pressure stress tensor response is $\sim(\epsilon_\delta\epsilon_\perp/\epsilon_\omega)(\omega^2/k_\parallel^2 v_A^2)$, the same as the Maxwell stress.

From these estimates, we note that while the perpendicular Maxwell stress and the pressure stress tensor contribution are of the same order, $\sim\epsilon_\perp\epsilon_\delta/\epsilon_\omega$, the inertia (polarization) nonlinearity is of the order of $\sim\epsilon_\delta/\epsilon_\perp$. Therefore, we can anticipate that for $\epsilon_\perp^2\sim\epsilon_\omega$ there will be a transition from nonlinear dynamics dominated by the polarization response (Sagdeev and Galeev, 1969), where the nonlinear MHD description is reasonably applicable, to a regime where dominant nonlinear interactions are due to the pressure stress tensor and Maxwell stress, which is the typical condition of gyrokinetic plasma behavior. This transition, first pointed out by Hasegawa and Chen (1976) for kinetic Alfvén waves (KAWs), is further discussed in Sec. IV.B and has important consequence on the spectral features of Alfvén waves and related transport processes (Chen and Zonca, 2011).

Applying the same orderings to other terms in Eq. (2.18), it can also be concluded that in tokamaks of current interest, where $\beta\lesssim\mathcal{O}(\epsilon_B/\epsilon_F)\sim\mathcal{O}(10^{-1})$, the linear terms $\propto\delta B_\parallel$ are $\sim\beta\epsilon_B/\epsilon_\perp$ and $\sim\beta^2\epsilon_F/\epsilon_\omega\sim\beta^2\epsilon_F/\epsilon_B\lesssim\beta$ and, hence, generally negligible. However, more careful consideration is needed concerning the nonlinear behavior. For $\epsilon_\omega>\epsilon_\perp^2$, the polarization nonlinearity overwhelms the Maxwell stress and the pressure stress tensor nonlinearity, and the nonlinear $\delta B_\parallel$ contribution is negligible provided that

$$\mathcal{O}(\epsilon_\delta/\epsilon_\perp)\gg\mathcal{O}(\beta\epsilon_\delta;\beta^2\epsilon_\perp\epsilon_\delta/\epsilon_\omega)$$
$$\Rightarrow\mathcal{O}(\epsilon_\perp^{-1})>\mathcal{O}(\epsilon_\omega^{1/2}/\epsilon_\perp)>\mathcal{O}(1)>\beta,$$

which is readily satisfied for laboratory plasmas. In the opposite limit, $\epsilon_\omega<\epsilon_\perp^2$, Maxwell stress and pressure stress tensors are also typically larger than the nonlinear $\delta B_\parallel$ contribution, since

$$\mathcal{O}(\epsilon_\perp\epsilon_\delta/\epsilon_\omega)\gg\mathcal{O}(\beta\epsilon_\delta;\beta^2\epsilon_\perp\epsilon_\delta/\epsilon_\omega).$$

However, for long-wavelength incompressible SAWs in uniform plasmas, satisfying $\omega^2=k_\parallel^2 v_A^2$, Reynolds and Maxwell stresses cancel exactly, yielding the well-known properties of the *Alfvénic state* (Alfvén, 1942, 1950; Walén, 1944; Elsasser, 1956; Hasegawa and Sato, 1989), discussed in Sec. IV.B. Although a realistic system can approach only the Alfvénic state, it is in this case important to make sure that residual effects of nonexact cancellations of Reynolds and Maxwell stresses remain more significant than the $\delta B_\parallel$ nonlinear term.

Since it is possible to formally write $\omega=\omega_0+i\partial_t$, with ω_0 the typical linear mode frequency, the significance of the nonlinear terms also depends on the relative time scales of the phenomena they produce in the dynamic evolution of the system. Ignoring the nonlinear $\delta B_\parallel$ contribution for $\epsilon_\omega<\epsilon_\perp^2$ thus sets a minimum constraint on both the linear (γ_L) and nonlinear (τ_{NL}^{-1}) rates, i.e.,

$$|\gamma_L/\omega_0|\sim|\omega_0\tau_{NL}|^{-1}\gg\mathcal{O}(\beta\epsilon_\delta;\beta^2\epsilon_\perp\epsilon_\delta/\epsilon_\omega).$$

Thus, one needs to keep these self-consistency requirements in mind when making numerical simulations or theoretical analyses close to the marginal stability condition and/or examining a long time-scale behavior. In fact, nonlinear Alfvén wave behavior and self-consistent interactions with EPs in fusion plasmas (see Sec. IV) are characterized by $\tau_{NL}\sim\gamma_L^{-1}\sim\epsilon_B\epsilon_F^{-1}\beta^{-1}\omega^{-1}\ll\epsilon_B^{-1}\epsilon_\omega^{-1}\Omega^{-1}$. For typical low-$\beta$ toroidal plasmas [$\beta\lesssim\mathcal{O}(\epsilon_B/\epsilon_F)\sim\mathcal{O}(10^{-1})$], which are the main focus of this work, $\propto\delta B_\parallel$ terms in Eq. (2.18) typically affect the mode dynamics on time scales that are longer than τ_{NL}. Thus, they can be consistently neglected in the present analysis. However, these terms may become important when considering longer time-scale behavior, e.g., $\tau_{NL}\sim\epsilon_\omega^{-1}\omega^{-1}$, where $\beta^2\ll\epsilon_\omega/\epsilon_\perp$ may not be so well satisfied in tight aspect-ratio tokamaks (Cox and MAST Team, 1999; Ono *et al.*, 2000). These self-consistency requirements on linear and nonlinear rates must also be obeyed when looking at mode nonlinear dynamics to explore the global variations of plasma equilibrium on the transport time scale [see Eqs. (2.1) and (2.2)]. Although this is an important issue as the forefront of magnetic fusion research, it is outside the scope of this review.

In Sec. II.D, the reduced nonlinear gyrokinetic forms of governing equations are derived specifically for low-β plasmas, which may be readily adopted for the description of the DAW dynamics in tokamaks (Mikhailovskii and Rudakov, 1963; Hasegawa and Chen, 1976; Tang and Luhmann, 1976; Chen *et al.*, 1978; Tang, Connor, and Hastie, 1980; Frieman and Chen, 1982; Hahm, Lee, and Brizard, 1988; Scott, 1997).

D. Reduced equations for low-β drift Alfvén waves

Since all the works in this review are limited to time scales

$$|\omega_0\tau_{NL}|^{-1}\sim|\gamma_L/\omega_0|\gg\epsilon_\omega,$$

we may self-consistently neglect $\delta B_\parallel$ terms (cf. Sec. II.C) and following Chen *et al.* (2001) derive the nonlinear gyrokinetic vorticity equation by taking moments of the nonlinear gyrokinetic equation of Frieman and Chen (1982). Note that this is equivalent to describing the gyrocenter Hamiltonian up to $\sim\epsilon_\delta$ linear terms. For longer time scales, we need to include $\sim\epsilon_\delta^2$ terms to ensure the exact conservation of the gyrokinetic energy (Brizard and Hahm, 2007).

It can be readily shown that the particle distribution function f can be written as

$$f=e^{-\rho\cdot\nabla}\left[\bar{F}-\frac{e}{m}\left(\frac{\partial\bar{F}}{\partial\mathcal{E}}+\frac{1}{B_0}\frac{\partial\bar{F}}{\partial\mu}\right)\langle\delta L_g\rangle\right]+\frac{e}{m}\left[\frac{\partial\bar{F}}{\partial\mathcal{E}}\delta\phi+\frac{1}{B_0}\frac{\partial\bar{F}}{\partial\mu}\delta L\right],\tag{2.19}$$

where $\bar{F}$ is the gyrocenter distribution function (Brizard and Hahm, 2007), $e^{-\boldsymbol{\rho}\cdot\boldsymbol{\nabla}}$ is the transformation from guiding center to particle coordinates, $\boldsymbol{\rho} \equiv \Omega^{-1}\boldsymbol{b}\times\boldsymbol{v}$, $\langle\cdots\rangle$ denotes gyrophase averaging, $\mathcal{E} = v^2/2$ is the energy per unit mass, μ is the magnetic moment adiabatic invariant $\mu = v_\perp^2/(2B_0)+\cdots$, and

$$\delta L_g = \delta\phi_g - \frac{v_\parallel}{c}\delta A_{\parallel g} = e^{\boldsymbol{\rho}\cdot\boldsymbol{\nabla}}\delta L = e^{\boldsymbol{\rho}\cdot\boldsymbol{\nabla}}\left(\delta\phi - \frac{v_\parallel}{c}\delta A_\parallel\right). \quad (2.20)$$

In Eq. (2.19), all terms that are not acted upon by $e^{-\boldsymbol{\rho}\cdot\boldsymbol{\nabla}}$ are the adiabatic response of the particle distribution function, the other terms representing the nonadiabatic response of the guiding-center distribution. Up to order $\mathcal{O}(\epsilon_\delta)$, one can further reduce Eq. (2.19) to the following decomposition for the fluctuating particle distribution function (Frieman and Chen, 1982):

$$\delta f = e^{-\boldsymbol{\rho}\cdot\boldsymbol{\nabla}}\left[\delta g - \frac{e}{m}\frac{1}{B_0}\frac{\partial\bar{F}_0}{\partial\mu}\langle\delta L_g\rangle\right] + \frac{e}{m}\left[\frac{\partial\bar{F}_0}{\partial\mathcal{E}}\delta\phi + \frac{1}{B_0}\frac{\partial\bar{F}_0}{\partial\mu}\delta L\right], \quad (2.21)$$

where the fluctuating gyrocenter distribution function $\delta\bar{F}$ is related to the nonadiabatic response δg as

$$\delta\bar{F} = \delta g + \frac{e}{m}\frac{\partial\bar{F}_0}{\partial\mathcal{E}}\langle\delta L_g\rangle, \quad (2.22)$$

and δg obeys the following nonlinear gyrokinetic equation (Frieman and Chen, 1982):

$$\begin{aligned}\left(\frac{\partial}{\partial t} + v_\parallel\nabla_\parallel + \boldsymbol{v}_d\cdot\boldsymbol{\nabla}_\perp\right)\delta g &= -\left(\frac{e}{m}\frac{\partial}{\partial t}\langle\delta L_g\rangle\frac{\partial\bar{F}_0}{\partial\mathcal{E}} + \frac{c}{B_0}\boldsymbol{b}\times\boldsymbol{\nabla}\langle\delta L_g\rangle\cdot\boldsymbol{\nabla}\bar{F}_0\right)\\ &\quad - \frac{c}{B_0}\boldsymbol{b}\times\boldsymbol{\nabla}\langle\delta L_g\rangle\cdot\boldsymbol{\nabla}\delta g. \end{aligned} \quad (2.23)$$

Here the magnetic-drift velocity $\boldsymbol{v}_d$ is

$$\boldsymbol{v}_d = \frac{\boldsymbol{b}}{\Omega}\times(\mu\boldsymbol{\nabla}B_0 + \boldsymbol{\kappa}v_\parallel^2) \simeq \frac{(\mu B_0 + v_\parallel^2)}{\Omega}\boldsymbol{b}\times\boldsymbol{\kappa}, \quad (2.24)$$

where $\boldsymbol{\nabla}B_0 \simeq \boldsymbol{\kappa}B_0$ in the low-β limit and is consistent with well-known cancellations in the linear vorticity equation, arising from the perpendicular pressure balance, Eq. (2.7), and plasma equilibrium condition (Hasegawa and Sato, 1989). In the long-wavelength limit, Eq. (2.23) has to be slightly modified to account for the perturbed gyrocenter motion at $\mathcal{O}(\epsilon_\delta)$ being given by (Brizard and Hahm, 2007)

$$\begin{aligned}\delta\dot{\bar{\boldsymbol{X}}}_\perp &= \frac{c}{B_0}\boldsymbol{b}\times\boldsymbol{\nabla}\langle\delta L_g\rangle + \frac{v_\parallel}{B_0}\boldsymbol{\kappa}\langle\delta A_{\parallel g}\rangle\\ &= \frac{c}{B_0}\boldsymbol{b}\times\boldsymbol{\nabla}\langle\delta\phi_g\rangle + v_\parallel\frac{\langle\delta\boldsymbol{B}_{\perp g}\rangle}{B_0}, \end{aligned} \quad (2.25)$$

with $\langle\delta\boldsymbol{B}_{\perp g}\rangle = \boldsymbol{\nabla}\times\boldsymbol{b}\langle\delta A_{\parallel g}\rangle$. As shown by Qin, Tang, and Rewoldt (1998, 1999), this distinction is important for the linear response only, since the nonlinear $\boldsymbol{E}\times\boldsymbol{B}$ convection and nonlinear line bending are small at $\epsilon_\perp^2 < \epsilon_\omega$ (see Sec. II.B). For simplicity and hence clarity, Eq. (2.23) assumes no equilibrium plasma rotation that, however, can be taken into account by nonlinear gyrokinetic theory [see, e.g., Brizard and Hahm (2007)].

The following nonlinear gyrokinetic vorticity equation (Chen *et al.*, 2001) can then be derived from Eq. (2.23) acted upon by $\sum e e^{-\boldsymbol{\rho}\cdot\boldsymbol{\nabla}}$ and integrated in velocity space (Zonca and Chen, 2014b):

$$\begin{aligned} &B_0\left(\nabla_\parallel + \frac{\delta\boldsymbol{B}_\perp}{B_0}\cdot\boldsymbol{\nabla}\right)\left(\frac{\delta j_\parallel}{B_0}\right) - \boldsymbol{\nabla}\cdot\sum\left\langle\frac{e^2}{m}\frac{2\mu}{\Omega^2}\left(B_0\frac{\partial\bar{F}_0}{\partial\mathcal{E}} + \frac{\partial\bar{F}_0}{\partial\mu}\right)\left(\frac{J_0^2-1}{\lambda^2}\right)\right\rangle_v\boldsymbol{\nabla}_\perp\frac{\partial}{\partial t}\delta\phi\\ &\quad - \sum ec\boldsymbol{b}\times\boldsymbol{\nabla}\left\langle\frac{2\mu}{\Omega^2}\bar{F}_0\left(\frac{J_0^2-1}{\lambda^2}\right)\right\rangle_v\cdot\boldsymbol{\nabla}\nabla_\perp^2\delta\phi + \frac{c}{B_0}\boldsymbol{b}\times\boldsymbol{\kappa}\cdot\boldsymbol{\nabla}\sum\langle m(\mu B_0 + v_\parallel^2)J_0\delta g\rangle_v\\ &\quad + \delta\boldsymbol{B}_\perp\cdot\boldsymbol{\nabla}\left(\frac{j_{\parallel 0}}{B_0}\right) + \sum e\left\langle J_0\left[\frac{c}{B_0}\boldsymbol{b}\times\boldsymbol{\nabla}(J_0\delta\phi)\cdot\boldsymbol{\nabla}\delta g\right] - \frac{c}{B_0}\boldsymbol{b}\times\boldsymbol{\nabla}\delta\phi\cdot\boldsymbol{\nabla}(J_0\delta g)\right\rangle_v\\ &\quad + \frac{c}{B_0}\boldsymbol{b}\times\boldsymbol{\nabla}\delta\phi\cdot\boldsymbol{\nabla}\left[\boldsymbol{\nabla}\cdot\sum\left\langle\frac{e^2}{m}\frac{2\mu}{\Omega^2}\frac{\partial\bar{F}_0}{\partial\mu}\left(\frac{1-J_0^2}{\lambda^2}\right)\right\rangle_v\boldsymbol{\nabla}_\perp\delta\phi\right] = 0. \end{aligned} \quad (2.26)$$

Here J_0 is the Bessel function of argument λ and $\lambda^2 = 2\mu B_0 k_\perp^2/\Omega^2$. Nonlinear plasma behavior enters implicitly, in the pressure curvature coupling with δg, and explicitly, through the perpendicular Maxwell stress (nonlinear line bending) and the next to last term on the left-hand side, which can be shown to be connected with nonlinear diamagnetic response and gyrokinetic generalization of the Reynolds stress. Note that Eq. (2.26) is pertinent to the short-wavelength regime ($\epsilon_\perp^2 > \epsilon_\omega$), consistent with the gyrokinetic ordering discussed in Sec. II.A. In the $\epsilon_\perp^2 \lesssim \epsilon_\omega$ long-wavelength limit, it is necessary to include an additional term on the left-hand side of Eq. (2.26), representing the divergence of the nonlinear polarization current due to mass density fluctuation, i.e.,

$$-\frac{c^2}{4\pi}\boldsymbol{\nabla}\cdot\left(\frac{\delta\varrho_m}{\varrho_{m0}v_A^2}\boldsymbol{\nabla}_\perp\frac{\partial}{\partial t}\delta\phi\right). \tag{2.27}$$

Meanwhile, the quasineutrality condition equation (2.9) can be rewritten as

$$\sum\left\langle\frac{e^2}{m}\frac{\partial\bar{F}_0}{\partial\mathcal{E}}\right\rangle_v\delta\phi+\boldsymbol{\nabla}\cdot\sum\left\langle\frac{e^2}{m}\frac{2\mu}{\Omega^2}\frac{\partial\bar{F}_0}{\partial\mu}\left(\frac{J_0^2-1}{\lambda^2}\right)\right\rangle_v\boldsymbol{\nabla}_\perp\delta\phi+\sum\langle eJ_0(\lambda)\delta g\rangle_v=0. \tag{2.28}$$

The presence of J_0 and of velocity-space integrals involving δg in Eqs. (2.26) and (2.28) shows that they are integrodifferential equations. Given that $\delta\boldsymbol{B}_\perp=[\boldsymbol{\nabla}\times(\boldsymbol{b}\delta A_\parallel)]_\perp$ and $\delta B_\parallel=(\boldsymbol{\nabla}\times\boldsymbol{b})_\parallel\delta A_\parallel$,[4] these equations are closed by the nonlinear gyrokinetic equation (2.23), along with Eq. (2.25), and by the reduced form of the parallel Ampère's law, Eq. (2.13),

$$\delta j_\parallel=\frac{c}{4\pi}\boldsymbol{b}\cdot\boldsymbol{\nabla}\times(\boldsymbol{\nabla}\times\delta\boldsymbol{A})=\frac{c}{4\pi}[-\nabla^2+\kappa^2+(\boldsymbol{\nabla}\boldsymbol{b}):(\boldsymbol{\nabla}\boldsymbol{b})+(\boldsymbol{\nabla}\times\boldsymbol{b})_\parallel^2]\delta A_\parallel. \tag{2.29}$$

Equations (2.26)–(2.29) are the *governing gyrokinetic equations* for low-β DAWs, adopted throughout this work to investigate their nonlinear dynamics on time scales $\gamma_L\tau_{NL}\sim 1$.

Equations (2.26)–(2.29) need to be supplemented by equations governing *zonal structures*, i.e., for fluctuations that have $k_\parallel\equiv 0$ identically in the whole plasma[5] and play crucial roles in regulating DAW dynamics, as shown in Sec. IV. First we note that Eqs. (2.26) and (2.28) are not independent for $\delta\phi_z$ (Chen *et al.*, 2001), with the subscript z standing for *zonal*. While Eq. (2.26) governs the evolution of $\delta\phi_z$, $\delta A_{\parallel z}$ is governed by Eq. (2.29), with the zonal current $\delta j_{\parallel z}$ computed from the solution of Eq. (2.23). Assuming consistently throughout this review that $\delta j_\parallel$ is carried by electrons and that $k_\perp^2\delta_e^2\sim\epsilon_\perp^2\delta_e^2/\rho_i^2\ll 1$, with $\delta_e=c/\omega_{pe}$ the collisionless skin depth and ω_{pe} the electron plasma frequency, Eq. (2.29) for the zonal current becomes essentially $\delta j_{\parallel ze}\simeq 0$, which reads

$$\frac{\partial}{\partial t}\delta A_{\parallel z}=\left(\frac{c}{B_0}\boldsymbol{b}\times\boldsymbol{\nabla}\delta A_\parallel\cdot\boldsymbol{\nabla}\delta\psi\right)_z, \tag{2.30}$$

after a straightforward calculation of δf_{ze} from Eq. (2.23),

$$\frac{\partial}{\partial t}\delta f_{ze}=\frac{e}{T_e}\frac{v_\parallel}{c}\bar{F}_{0e}\left(\frac{\partial}{\partial t}\delta A_\parallel-\frac{c}{B_0}\boldsymbol{b}\times\boldsymbol{\nabla}\delta A_\parallel\cdot\boldsymbol{\nabla}\delta\psi\right)_z,$$

with $\delta\psi$ defined by

$$\boldsymbol{b}\cdot\boldsymbol{\nabla}\delta\psi\equiv-\frac{1}{c}\frac{\partial}{\partial t}\delta A_\parallel, \tag{2.31}$$

for given $\delta A_\parallel$ with $k_\parallel\neq 0$. Note that Eq. (2.30) can also be readily derived from a massless electron force balance along $\boldsymbol{B}_0$. When considering DAWs excited by EPs, Eq. (2.26) can be further reduced, as done in Sec. II.E.

E. Drift Alfvén waves excited by energetic particles in low-β fusion plasmas

In burning plasmas, EPs are characterized by an energy density, which is comparable to that of the thermal plasma, so that $\beta_E\sim\beta$. However, due to the significantly higher energy $T_{0i}/T_{0E}=\mathcal{O}(10^{-2})$, the EP density is typically low, $n_{0E}/n_{0i}\sim T_{0i}/T_{0E}$. Thus, it is generally possible to consider reactor relevant plasmas consisting of two components (Chen, White, and Rosenbluth, 1984): a core or thermal plasma component, essentially providing an isotropic Maxwellian background made of electrons (e) and ions (i), and an energetic component (E), which is often anisotropic and non-Maxwellian.

A detailed discussion of the general wavelength and frequency orderings for the case of DAWs resonantly excited by EPs in space plasmas was given by Chen and Hasegawa (1991) and later by Zonca and Chen (2006) for low-β laboratory plasmas, where

$$n_{0E}/n_{0i}\sim T_{0i}/T_{0E}=\mathcal{O}(10^{-2})\lesssim\beta_i\sim\beta_E\lesssim\mathcal{O}(10^{-1}). \tag{2.32}$$

Meanwhile, most unstable EP-driven modes are characterized by $|k_\theta\rho_E|\lesssim 1$ (Berk, Breizman, and Ye, 1992b; Fu and Cheng, 1992; Tsai and Chen, 1993; Chen, 1994), where ρ_E is the EP Larmor radius. More precisely, ρ_E represents the characteristic EP magnetic-drift orbit width, corresponding to the relevant wave-particle resonance and typically larger than the EP Larmor radius. Finally, thermal electrons typically have $v_{te}\gg v_A$, corresponding to $\beta\gg m_e/m_i$, and hence can be approximated as a massless fluid. These orderings, in addition to those of Sec. II.A and the low-β assumption used in Sec. II.D, allow us to further simplify Eqs. (2.26) and (2.28), while maintaining an accurate description of nonlinear dynamics of SAW excited by EPs.

From Eq. (2.23), the thermal electron response as a massless fluid ($|v_\parallel\nabla_\parallel|\gg|\partial_t|$ and $|v_\parallel\delta\boldsymbol{B}_\perp|\gg|c\delta\boldsymbol{E}_\perp|$) is

$$\left(\boldsymbol{b}+\frac{\delta\boldsymbol{B}_\perp}{B_0}\right)\cdot\boldsymbol{\nabla}\delta g_e=-\left(\frac{e}{m_e c}\frac{\partial\delta A_\parallel}{\partial t}\frac{\partial\bar{F}_{0e}}{\partial\mathcal{E}}+\frac{\delta\boldsymbol{B}_\perp}{B_0}\cdot\boldsymbol{\nabla}\bar{F}_{0e}\right). \tag{2.33}$$

Here e denotes the positive electron charge and core electron response due to particles near the trapped to circulating particle boundary has been neglected. Using Eq. (2.33) for a Maxwellian electron core to explicitly evaluate the corresponding perturbed electric charge and recalling Eq. (2.31), the quasineutrality condition, Eq. (2.28) acted upon by $(\boldsymbol{b}+\delta\boldsymbol{B}_\perp/B_0)\cdot\boldsymbol{\nabla}$ can be cast as (Zonca and Chen, 2014b)

[4]Note that $\delta B_\parallel$ includes a further contribution due to $\delta\boldsymbol{A}_\perp$, which ensures that Eq. (2.7) is fulfilled. This contribution is accounted for implicitly, when using the expression of magnetic drifts given by Eq. (2.24), as discussed by Chen and Hasegawa (1991).

[5]See Diamond *et al.* (2005) for a recent review on the physics of zonal structures.

$$\frac{n_{0e}e^2}{T_{0e}}\left[\boldsymbol{b}\cdot\boldsymbol{\nabla}(\delta\phi-\delta\psi)+\frac{\delta\boldsymbol{B}_\perp}{B_0}\cdot\boldsymbol{\nabla}\delta\phi\right] = \left(\boldsymbol{b}+\frac{\delta\boldsymbol{B}_\perp}{B_0}\right)\cdot\boldsymbol{\nabla}\sum_{\neq e}(e\langle\delta f\rangle_v+e\langle\bar{F}_0\rangle_v), \tag{2.34}$$

where $\sum_{\neq e}$ denotes a summation on particle species except for core electrons and equilibrium charge neutrality has been used explicitly. Note that Eq. (2.34) is just the extended Ohm's law

$$\left(\boldsymbol{b}+\frac{\delta\boldsymbol{B}_\perp}{B_0}\right)\cdot\delta\boldsymbol{E}=-\left(\boldsymbol{b}+\frac{\delta\boldsymbol{B}_\perp}{B_0}\right)\cdot\frac{\boldsymbol{\nabla}P_e}{n_{0e}e}, \tag{2.35}$$

having assumed isothermal electron response. Furthermore, the ordering of Eq. (2.32) allows ignoring the contribution of EPs to the plasma density,[6] while the wavelength ordering $|k_\theta\rho_E|\lesssim 1$ indicates that $\epsilon_\perp\ll 1$ for the core plasma component. Thus, the quasineutrality condition, Eq. (2.28) or (2.34), at the lowest order reduces to the ideal MHD approximation $\delta E_\parallel=0$ or $\delta\phi=\delta\psi$.

The gyrokinetic vorticity equation is also greatly simplified with the additional ordering introduced in this section and can be shown to yield [see Zonca and Chen (2014b) for details]

$$\begin{aligned}
&B_0\left(\nabla_\parallel+\frac{\delta\boldsymbol{B}_\perp}{B_0}\cdot\boldsymbol{\nabla}\right)\left(\frac{\delta j_\parallel}{B_0}\right)\\
&-\frac{c^2}{4\pi}\boldsymbol{\nabla}\cdot\left\{\left[\left(1+\frac{\delta\varrho_m}{\varrho_{m0}}\right)\frac{1}{v_A^2}+\frac{3\pi}{B_0^2}\left(\frac{P_{0\perp i}}{\Omega_i^2}+\frac{P_{0\perp E}}{\Omega_E^2}\right)\nabla_\perp^2\right]\boldsymbol{\nabla}_\perp\frac{\partial}{\partial t}\delta\phi\right\}\\
&+\frac{c^2}{4\pi}\boldsymbol{b}\times\boldsymbol{\nabla}\left[\frac{4\pi}{B_0^2}\left(\frac{P_{0\perp i}}{\Omega_i}+\frac{P_{0\perp E}}{\Omega_E}\right)\right]\cdot\boldsymbol{\nabla}\nabla_\perp^2\delta\phi\\
&+\frac{c}{B_0}\boldsymbol{b}\times\boldsymbol{\kappa}\cdot\boldsymbol{\nabla}\sum\langle m(\mu B_0+v_\parallel^2)J_0\delta g\rangle_v+\delta\boldsymbol{B}_\perp\cdot\boldsymbol{\nabla}\left(\frac{j_{\parallel 0}}{B_0}\right)\\
&+\sum_{\neq e}\frac{ec}{2\Omega^2}\{\boldsymbol{b}\times\boldsymbol{\nabla}(\nabla_\perp^2\delta\phi)\cdot\boldsymbol{\nabla}\langle\mu\delta g\rangle_v-\boldsymbol{b}\times\boldsymbol{\nabla}\delta\phi\cdot\boldsymbol{\nabla}\langle\mu\nabla_\perp^2\delta g\rangle_v\\
&-\nabla_\perp^2[\boldsymbol{b}\times\boldsymbol{\nabla}\delta\phi\cdot\boldsymbol{\nabla}\langle\mu\delta g\rangle_v]\}=0.
\end{aligned}\tag{2.36}$$

Here we used the definition $P_{0\perp}=\langle m\mu B_0\bar{F}_0\rangle_v$ and adopted the long-wavelength limit for both thermal and energetic ions. In this way, note that energetic ions,[7] even though they do not contribute to plasma inertia due to Eq. (2.32), contribute both to a finite Larmor radius correction to the plasma inertia (KAW) (Briguglio *et al.*, 1995) and to the diamagnetic response (Wang *et al.*, 2011; Lauber *et al.*, 2012) (see Sec. III.C), for these terms depend explicitly on perpendicular pressure. Note also that we omitted the long-wavelength formal expansions of pressure gradient curvature coupling for simplicity and clarity of the physics presentation.

In the case of highly energetic ions, the gyrokinetic vorticity equation (2.26), formally viewed as the fluctuating charge continuity equation, i.e., $\boldsymbol{\nabla}\cdot\delta\boldsymbol{j}=0$, can be read as currents in the core component balancing the "charge uncovering" (charge separation) effect due to the large EP orbits (Rosenbluth, 1982; Berk *et al.*, 1985). This interpretation was originally proposed by Rosenbluth (1982) in stability analyses of tandem mirror and elmo bumpy torus configurations. The corresponding reduced form of Eq. (2.26) can then be obtained taking $J_0\to 0$ in EP contributions, while the thermal plasma component is still described by the long-wavelength limit as in Eq. (2.36). This approach to charge uncovering was reproposed by Mikhailovskii *et al.* (2004) and Sharapov, Mikhailovskii, and Huysmans (2004) to investigate the effects of nonresonant EPs on MHD instabilities. A general description, valid for arbitrary wavelengths, can be obtained by noting that magnetic-drift orbits of highly suprathermal EPs are typically much larger than their Larmor radius. Thus, taking the drift-kinetic limit ($J_0=1$) for EPs is consistent with both small and large EP magnetic-drift orbit limits and adequately renders both resonant and nonresonant EP dynamics, including their nearly adiabatic response to short-wavelength modes [see Zonca and Chen (2006) for an in-depth discussion of these issues]. For this reason, EP contribution to KAW and diamagnetic terms can be formally neglected in Eq. (2.36), which further reduces to

$$\begin{aligned}
&B_0\left(\nabla_\parallel+\frac{\delta\boldsymbol{B}_\perp}{B_0}\cdot\boldsymbol{\nabla}\right)\left(\frac{\delta j_\parallel}{B_0}\right)\\
&-\frac{c^2}{4\pi}\boldsymbol{\nabla}\cdot\left\{\left[\left(1+\frac{\delta\varrho_m}{\varrho_{m0}}\right)\frac{1}{v_A^2}+\frac{3\pi}{B_0^2}\left(\frac{P_{0\perp i}}{\Omega_i^2}\right)\nabla_\perp^2\right]\boldsymbol{\nabla}_\perp\frac{\partial}{\partial t}\delta\phi\right\}\\
&+\frac{c^2}{4\pi}\boldsymbol{b}\times\boldsymbol{\nabla}\left[\frac{4\pi}{B_0^2}\left(\frac{P_{0\perp i}}{\Omega_i}\right)\right]\cdot\boldsymbol{\nabla}\nabla_\perp^2\delta\phi\\
&+\frac{c}{B_0}\boldsymbol{b}\times\boldsymbol{\kappa}\cdot\boldsymbol{\nabla}\sum\langle m(\mu B_0+v_\parallel^2)J_0\delta g\rangle_v\\
&+\delta\boldsymbol{B}_\perp\cdot\boldsymbol{\nabla}\left(\frac{j_{\parallel 0}}{B_0}\right)+\sum_{\neq e}\frac{ec}{2\Omega^2}\{\boldsymbol{b}\times\boldsymbol{\nabla}(\nabla_\perp^2\delta\phi)\cdot\boldsymbol{\nabla}\langle\mu\delta g\rangle_v\\
&-\boldsymbol{b}\times\boldsymbol{\nabla}\delta\phi\cdot\boldsymbol{\nabla}\langle\mu\nabla_\perp^2\delta g\rangle_v-\nabla_\perp^2[\boldsymbol{b}\times\boldsymbol{\nabla}\delta\phi\cdot\boldsymbol{\nabla}\langle\mu\delta g\rangle_v]\}=0.
\end{aligned}\tag{2.37}$$

Here the nonlinear stress tensor is due to thermal ions only and $J_0\to 1$ in the EP pressure gradient curvature coupling term. It is also worthwhile noting that Eq. (2.37) correctly describes reactor relevant plasma conditions, since $\beta_E\sim(\tau_{sd}/\tau_E)\beta_i$ and the energetic ion (collisional) slowing down time on thermal electrons τ_{sd} is short compared to the energy confinement time τ_E. Equation (2.37) is crucial for the validity of many of the hybrid MHD-gyrokinetic descriptions of SAW excitations by energetic ions (Park *et al.*, 1992, 1999; Briguglio *et al.*, 1995; Todo *et al.*, 1995; Briguglio, Zonca, and Vlad, 1998; Todo and Sato, 1998), which have provided the first successful numerical simulation approach to this problem.

In the linear limit, Eq. (2.37) coincides with the gyrokinetic vorticity equation discussed by Qin, Tang, and Rewoldt (1998, 1999) and, dropping KAW and diamagnetic terms as well, with the reduced form of the linear kinetic-MHD model by Brizard (1994).

[6] In doing so, some attention must be paid to applications to present day experiments, where suprathermal particles may not be as energetic and low density as estimated in Eq. (2.32).

[7] Suprathermal electrons, if present, give a negligible contribution to KAW and diamagnetic terms.

III. LINEAR ALFVÉN WAVE PHYSICS IN NONUNIFORM PLASMAS

Shear Alfvén waves are anisotropic electromagnetic waves existing in magnetized plasmas, which have parallel wavelengths $\lambda_\parallel \sim L_\parallel$ comparable to the system size along the equilibrium magnetic field $\boldsymbol{B}_0$. They can, however, have a wide range in the perpendicular wavelengths $\lambda_\perp, \rho_i < \lambda_\perp < L_\perp$, with ρ_i the ion Larmor radius and $L_\perp$ the system size perpendicular to $\boldsymbol{B}_0$. The SAW frequency is $\omega \simeq k_\parallel v_A \sim \mathcal{O}(v_A/L_\parallel)$ much less than the ion cyclotron frequency Ω_i. Here notations are those introduced in Sec. II.

SAW dynamics is, hence, of low frequency and macroscopic scales and, therefore, may cause significant perturbations in the bulk of the plasma. Furthermore, SAW dynamics is nearly incompressible, whereas CAW and slow sound waves tend to be stabilized by finite magnetic and/or plasma compression as well as finite ion Landau damping. These are the primary reasons why SAWs play many important roles in laboratory and space plasmas. Some examples are (1) heating of laboratory (Grossman and Tataronis, 1973; Chen and Hasegawa, 1974a; Hasegawa and Chen, 1974; Tataronis, 1975) and solar corona plasmas (Ionson, 1982); (2) resonant interactions with EPs produced during high-power neutral beam and/or radio-frequency laboratory heating experiments or with alpha particles produced in D-T fusion plasmas (Kolesnichenko and Oraevskij, 1967; Belikov, Kolesnichenko, and Oraevskij, 1968; Mikhailovskii, 1975; Rosenbluth and Rutherford, 1975; Kolesnichenko, 1980; Tsang, Sigmar, and Whitson, 1981; Chen, 1988; Fu and Van Dam, 1989a, 1989b), which is the main subject of this review work; (3) cross-field transport in magnetospheric plasmas, e.g., the day-side magnetopause (Hasegawa and Mima, 1978); and (4) acceleration of electrons along the auroral field lines (Hasegawa, 1976).

One of the most important properties of SAW is that its group velocity $\boldsymbol{v}_g$ is directed along $\boldsymbol{B}_0$, i.e., $\boldsymbol{v}_g \simeq \boldsymbol{v}_A$. In nonuniform plasmas with spatially varying v_A this property can then lead to singular oscillations at the local SAW frequency, for the wave energy is "confined" to the local field line. As the local SAW frequency varies continuously, we then have oscillations which constitute the so-called SAW continuous spectrum or continuum (Grad, 1969). The existence of SAW continuum then suggests that at the layer where the frequency of the applied radio-frequency source matches the local SAW frequency, the wave equation has a singular point leading to resonant wave absorption and the Alfvén wave heating scheme (Grossman and Tataronis, 1973; Chen and Hasegawa, 1974a, 1974b; Hasegawa and Chen, 1974). That the wave solution becomes singular is due to the inadequacy of ideal MHD approximation. Including microscopic kinetic effects, such as finite ion Larmor radii (FLR), removes the singular behavior by allowing small but finite $\boldsymbol{v}_g$ across $\boldsymbol{B}_0$. That is, we have the linear mode conversion of resonant SAW to KAW (Hasegawa and Chen, 1975, 1976).

More generally, plasma nonuniformity and equilibrium magnetic field geometry not only modify the SAW frequency spectrum, causing the existence of gaps in the continuum (Pogutse and Yurchenko, 1978; D'Ippolito and Goedbloed, 1980; Kieras and Tataronis, 1982), but may also cause collective oscillations, i.e., discrete AEs within the gaps (Cheng, Chen, and Chance, 1985). These fundamental concepts and processes of SAW in nonuniform plasmas are briefly reviewed in this section, since basic theoretical reviews of linear SAW spectrum properties are available in the literature for both 1D systems (Mahajan, 1995) and axisymmetric toroidal (2D) plasmas (Chen and Zonca, 1995). Numerical simulations of stability properties of SAW excited by EP in tokamak plasmas were extensively discussed by Vlad, Zonca, and Briguglio (1999), and in the recent review by Lauber (2013), focused on kinetic models, numerical solution strategies, and comparison to tokamak experiments. Similarities and differences of these physics with those of SAW in 3D toroidal equilibria were given by Kolesnichenko *et al.* (2011) and Toi *et al.* (2011). This section is also devoted to the formulation of the GFLDR, which provides a unified theoretical framework for describing and understanding the various branches of SAW fluctuations (Zonca and Chen, 2014b, 2014c). The GFLDR can also be extended to nonlinear analyses and will be the starting point for our discussion of nonlinear SAW physics and their interactions with EPs in Sec. IV.

A. Continuous spectrum, kinetic Alfvén waves, and global Alfvén eigenmodes

Considering a 1D plasma slab confined in straight magnetic field (Chen and Hasegawa, 1974a; Goedbloed, 1984), one can demonstrate that the governing equation for the plasma displacement in the direction of nonuniformity (say x) becomes singular at

$$\omega^2 = \omega_A^2(x) \equiv k_\parallel^2(x) v_A^2(x) \tag{3.1}$$

and

$$\omega^2 = \omega_S^2(x) \equiv [1 + v_S^2(x)/v_A^2(x)]^{-1} k_\parallel^2(x) v_S^2(x), \tag{3.2}$$

corresponding to the appearance of two continuous spectra with $v_S^2(x) = \Gamma P_0(x)/\varrho_{m0}(x)$ representing the sound speed and Γ the appropriate adiabatic index. Meanwhile, adopting the slow sound wave approximation ($v_S^2/v_A^2 \to 0$) and assuming, for simplicity, that $\varrho_0 = \varrho_0(x)$ while $\mathbf{B}_0 = B_0 \mathbf{e}_z$, it is possible to show that the plasma displacement $\delta\xi_x$ becomes logarithmically singular as the SAW resonance is approached. In fact, the SAW group velocity is directed along $\boldsymbol{B}_0$. Thus, the latter one "piles up" wave energy at the radial location where the SAW spectrum is resonantly excited, explaining the origin of "local singular oscillations" (Chen and Zonca, 1995).

Resonant excitation is connected with SAW resonant absorption (Chen and Hasegawa, 1974a, 1974b). In fact, a finite amount of wave energy can be absorbed at the SAW resonant layer. Meanwhile, the time-averaged energy absorption rate is given by the Poynting flux into that infinitely narrow layer, and it occurs on time scales $\sim(\omega_A' \Delta x)^{-1}$, with Δx the perturbation "radial" extent.[8] Corresponding to this,

[8]Here "radial" stands for the direction of nonuniformity, which is generally identified as the gradient of the equilibrium magnetic flux.

the radial wave vector $|k_x| \sim |\omega_A'(x)t|$ and, thus, $|k_x| \to \infty$ as $t \to \infty$, i.e., the wave function becomes singular in the asymptotic time limit, in agreement with the eigenmode analysis. While $\delta\xi_x \sim (1/t)\exp[-i\omega_A(x)t]$ as $t \to \infty$ because of phase mixing of the SAW continuous spectrum (Barston, 1964; Grad, 1969; Sedláček, 1971), the binormal ($\boldsymbol{e}_y = \boldsymbol{e}_z \times \boldsymbol{e}_x$) plasma displacement $\delta\xi_y \sim \exp[-i\omega_A(x)t]$ does not decay algebraically in time and represents the undamped oscillations at frequencies of the SAW continuum, which are routinely observed in the Earth's magnetosphere (Engebretson *et al.*, 1987) and have also been demonstrated by ideal MHD initial value numerical simulations [see, e.g., Vlad, Zonca, and Briguglio (1999)].

When the ideal MHD model breaks down at very short scales, the typically most relevant new dynamics are associated with charge separation, i.e., with the finite $\delta E_\parallel$ fluctuations due to FLR (ρ_i), small but finite electron inertia and finite plasma resistivity. In the presence of finite $\delta E_\parallel$, additional effects due to wave-particle interactions also appear, which yield collisionless wave dissipation (Landau damping). Incorporating such "kinetic" effects essentially allows finite energy propagation across the resonant surfaces. Thus, wave energy will no longer pile up at these radial locations and all wave-function singularities are removed on short scales. A dedicated monograph on KAWs was given by Wu (2012). Here we limit our discussion to the case in which $m_e/m_i \ll \beta_e \ll 1$. Furthermore, for simplicity, we also assume $(k_x^2 + k_y^2)\rho_i^2 \equiv k_\perp^2\rho_i^2 \ll 1$. It is then possible to show that the Wentzel-Kramers-Brillouin (WKB) local dispersion relation of KAWs is an extension of Eq. (3.1):

$$\omega^2 = (1 + k_\perp^2\rho_K^2)\omega_A^2, \tag{3.3}$$

where (Hasegawa and Chen, 1975, 1976)

$$\rho_K^2 = [(3/4)(1 - i\delta_i) + (T_e/T_i)(1 - i\delta_e)]\rho_i^2 - i\eta c^2/4\pi\omega. \tag{3.4}$$

Here terms $\propto 3/4$ and T_e/T_i represent, respectively, FLR corrections to plasma inertia and parallel electric field, δ_i and δ_e indicate ion and electron Landau damping contributions, and η is plasma resistivity.

That KAW possesses finite $\delta E_\parallel$ not only modifies the linear wave properties but also, perhaps more significantly, the nonlinear particle and wave dynamics. More specifically, $\delta E_\parallel$ may lead to phase-space transport, i.e., heating, acceleration, and cross-field transport (Hasegawa and Chen, 1976; Chen, 1999). In addition, KAW could break the so-called nonlinear pure Alfvénic state (Alfvén, 1942, 1950; Walén, 1944; Elsasser, 1956; Hasegawa and Sato, 1989) (cf. Sec. IV.B) and lead to enhanced rates of nonlinear mode-coupling effects such as parametric decay instabilities (DuBois and Goldman, 1965, 1967; Nishikawa, 1968; Kaw and Dawson, 1969) (cf. Sec. IV.B) as well as the generation of convective cells or zonal structures (Hasegawa, Maclennan, and Kodama, 1979) (cf. Secs. IV.B and IV.C).

In addition to the local oscillations of the SAW continuum, a global AE (GAE) (Appert *et al.*, 1982; Ross, Chen, and Mahajan, 1982; Mahajan, Ross, and Chen, 1983; Goedbloed, 1984) may also exist in a 1D nonuniform plasma. Such global modes, if destabilized by EPs, could affect confinement over a large region of the plasma. In order to minimize damping due to coupling with the SAW continuum, global mode structures are preferentially excited near regions where the resonant energy absorption rate $\propto \omega_A'$ vanishes, i.e., near an extremum of the SAW continuous spectrum (cf. Sec. III.B for further discussion). Detailed analyses of mode structures, frequencies, and stability properties can be found in Appert *et al.* (1982), Ross, Chen, and Mahajan (1982), Mahajan, Ross, and Chen (1983), Goedbloed (1984), and Mahajan (1995). In the presence of nonideal terms, such as, e.g., resistivity or FLR effects, other discrete, closely spaced (in frequency), localized (in radius) kinetic GAE modes (KGAEs) also exist in addition to GAEs (Mahajan, 1995). These modes "replace" the SAW continuous spectrum, due to the trapping of KAW as a bound state in the radial region where the mode frequency exceeds the local SAW continuum frequency. That nonideal effects discretize the SAW continuum is a general result that will be further discussed in Sec. III.B.

B. Alfvén eigenmodes and energetic-particle modes in two-dimensional toroidal plasmas

In nearly 2D or 3D toroidal devices, the main additional complication that modifies the SAW fluctuation spectrum with respect to the 1D case is due to modulations of v_A along $\mathbf{B}_0$. This causes the loss of translational symmetry for SAWs traveling along $\mathbf{B}_0$ and sampling regions of periodically varying v_A. Similar to electron wave packets traveling in a 1D periodic lattice of period L [see, e.g., Kittel (1971)], SAWs in toroidal systems are characterized by gaps in their continuous spectrum, corresponding to the formation of standing waves at the Bragg reflection condition, i.e.,

$$k_\parallel = \frac{\ell}{2L_0}, \qquad \omega^2 = \frac{\ell^2 v_A^2}{4L_0^2}, \qquad \ell \in \mathbb{N}, \tag{3.5}$$

with $L = 2\pi L_0$ the connection length[9] and v_A being a "typical" value of the Alfvén speed on the reference magnetic surface. In tokamak plasmas, the existence of gaps in the SAW continuous spectrum was discussed by Pogutse and Yurchenko (1978), D'Ippolito and Goedbloed (1980), and Kieras and Tataronis (1982). In this case, given that $L_0 \simeq qR_0$ for circular plasmas with large aspect ratio R_0/a [see Sec. II, the remark following Eq. (2.2)], q being the safety factor (representing the pitch of equilibrium magnetic field lines winding on a given flux surface), the dominant frequency gap occurs at $v_A/(2qR_0)$ and is due to the finite poloidal asymmetry of the system (Kieras and Tataronis, 1982). Other gaps also generally exist at $\omega = \ell v_A/(2qR_0)$, due to either noncircularity of the magnetic flux surfaces ($\ell = 2, 3, \ldots$) (Betti and Freidberg, 1991), to the anisotropic trapped EP population ($\ell = 1, 2, 3, \ldots$) (Van Dam and Rosenbluth, 1998), or to finite-β (mainly $\ell = 2$, with β the ratio between kinetic and magnetic pressures) (Zheng and

[9]It is the length of a magnetic field line connecting two distinct points on a magnetic surface where the SAW frequency is the same.

Chen, 1998a, 1998b). A low-frequency gap, corresponding to $\ell = 0$, also exists because of finite plasma compressibility (Chu *et al.*, 1992, 1993; Turnbull *et al.*, 1993) at $\omega \simeq \beta_i^{1/2} v_A/R_0 \ll v_A/R_0$.

In order to nullify or minimize continuum damping, discrete AEs must be localized in the SAW continuum frequency gaps and/or around radial positions, where $(d/dr)\omega_A(r) = 0$ (cf. Sec. III.A). The degeneracy of AE mode frequency with the continuous spectrum is removed by equilibrium nonuniformities, which make it possible for these fluctuations to exist as discrete modes. Continuing further the analogy with the 1D periodic lattice case, discrete AE can be localized in the continuum frequency gaps because of MHD and/or kinetic effects due to both thermal plasma and/or EPs, which play the role of "defects" (Zonca *et al.*, 2006; Chen and Zonca, 2007a). The particular role of EPs in the resonant excitation of SAWs was noted already in the late 1960s and 1970s along with the possible detrimental effects of collective SAW fluctuations as well as of lower frequency MHD modes on EP confinement (see Sec. I.A).

Discrete AEs existing in the various frequency gaps have accordingly been given different names. The first example is TAE (Cheng, Chen, and Chance, 1985) for $\omega \simeq v_A/(2qR_0)$. This is a particularly important case for it was the first demonstration of the existence of AEs in toroidal plasmas, thereby fixing a paradigm for subsequent AE investigations. Other examples are the ellipticity induced AE (EAE) (Betti and Freidberg, 1991, 1992) for $\omega \simeq v_A/(qR_0)$ and noncircular triangularity (or other shaping effects) induced AE (NAE) (Betti and Freidberg, 1991, 1992) for $\omega \simeq \ell v_A/(2qR_0)$ and $\ell \geq 3$, as shown by Eq. (3.5). The low-frequency SAW continuum frequency gap at $\omega \simeq \beta_i^{1/2}(7/4 + T_e/T_i)^{1/2} v_A/R_0$ (Mikhailowskii, 1973; Kotschenreuther, 1986; Zonca, Chen, and Santoro, 1996) deserves a special note, since the mode frequency can be comparable with thermal ion diamagnetic (ω_{*pi}) and/or transit (ω_{ti}) frequencies, i.e., $|\omega| \sim \omega_{*pi} \sim \omega_{ti}$. This is the frequency range where SAWs may exist as MHD fluctuations and/or their kinetic or resistive counterparts. We generally refer to this frequency gap as the kinetic thermal ion (KTI) gap (Chen and Zonca, 2007a). In fact, the ideal MHD accumulation point, $\omega = 0$ at $k_\parallel = 0$ from Eq. (3.5), is shifted either by the ion diamagnetic drift, as in the kinetic ballooning mode (KBM) case (Biglari and Chen, 1991), or by parallel and perpendicular ion compressibility, as for BAEs (Heidbrink, Strait *et al.*, 1993; Turnbull *et al.*, 1993), or, more generally, by the combined effects of finite ion temperature gradient ($\boldsymbol{\nabla} T_i$) and wave-particle resonances with thermal ions, as for the Alfvén ion temperature gradient (AITG) driven mode (Zonca *et al.*, 1999). For the AITG, the SAW continuum accumulation point could be shifted to the complex ω plane (Mikhailowskii, 1973; Kotschenreuther, 1986; Zonca, Chen, and Santoro, 1996) and, thus, become unstable for modes with sufficiently short wavelength ($\lambda_\perp \gtrsim \rho_i$). The mode localization condition inside the frequency gap then leads to the excitation of unstable discrete AITG even in the absence of EP drive (Zonca, Chen, and Santoro, 1996; Zonca *et al.*, 1998, 1999; Nazikian *et al.*, 2006). In this case, they are sometimes referred to as beta-induced temperature gradient eigenmodes (Mikhailovskii and Sharapov, 1999a, 1999b). The predominance of either an ion diamagnetic drift (KBM) or parallel and perpendicular ion compressibility (BAE) in the KTI frequency gap depends on both wave number and plasma equilibrium nonuniformity: AITGs are typically excited when both effects are of the same order (Zonca, Chen, and Santoro, 1996; Zonca *et al.*, 1999). Thus, two bands of low-frequency Alfvénic activities are generally expected, with varying frequency-dependent geodesic curvature coupling to the ion-acoustic wave (Chavdarovski and Zonca, 2009, 2014; Lauber *et al.*, 2009; Zonca *et al.*, 2010), of which—in the long-wavelength limit—the lower one refers to the ion diamagnetic frequency, consistent with recent numerical simulation results and experimental observations (Curran *et al.*, 2012; Lauber *et al.*, 2012). Another low-frequency fluctuation branch also exists, characterized by strong coupling of the SAW to the ion-acoustic wave and called the beta-induced Alfvén acoustic eigenmode (BAAE) (Gorelenkov *et al.*, 2007, 2009; Gorelenkov, Berk *et al.*, 2007), which, however, is affected by strong Landau damping, unless $T_e/T_i \gg 1$ (Zonca *et al.*, 2010). In this respect, experimental observation of BAAEs in NSTX and JET (Gorelenkov *et al.*, 2007; Gorelenkov, Berk *et al.*, 2007) with $T_e/T_i \sim 1$ is somewhat "puzzling." Experimental evidence of BAAEs is also reported in DIII-D (Gorelenkov *et al.*, 2009), ASDEX Upgrade (Curran *et al.*, 2012), and HL-2A (Yi *et al.*, 2012). This "puzzle" may be actually understood with a proper kinetic treatment of low-frequency Alfvénic and acoustic modes, which demonstrates that strong coupling of KBM and BAAE branches may occur and affect mode frequency, polarization, and damping rate, suggesting such fluctuations may indeed be observed in this "strong coupling" condition due to reduced damping (Chavdarovski and Zonca, 2014).

Consistently with the fact that degeneracy of AE frequency with the SAW continuum is removed by equilibrium nonuniformities, various local plasma profiles can produce variants of the AEs mentioned previously. In the case of TAEs with low magnetic shear values, $|s| = |(r/q)dq/dr| \ll 1$ typical of the plasma near the magnetic axis, they have been called core-localized TAEs (Berk, Van Dam *et al.*, 1995; Fu, 1995) or also tornado modes (Kramer *et al.*, 2004) when they are excited within the $q = 1$ magnetic flux surface. GAEs may also exist (cf. Sec. III.A), although they tend to be more strongly damped due to coupling with the continuous spectrum (Li, Mahajan, and Ross, 1987; Weiland, Lisak, and Wilhelmsson, 1987; Cheng, Fu, and Van Dam, 1988; Fu *et al.*, 1989) and are localized in both frequency and radial position near $(d/dr)\omega_A(r) = 0$. A special case of $(d/dr)\omega_A(r) = 0$ is given by hollow-q profiles, characterized by negative magnetic shear $s < 0$ inside the minimum-q surface. For these equilibria, a frequency gap is formed in the local SAW continuous spectrum, where AE can be excited (Berk *et al.*, 2001) yielding the so-called Alfvén cascades (ACs) (Sharapov *et al.*, 2001) or reversed-shear AE (RSAE) (Kimura *et al.*, 1998; Takechi *et al.*, 2002). These modes have frequencies that are typically less than that of TAEs, although there are experimental observations of RSAE near the EAE and NAE gaps (Kramer and Fu, 2006; Kramer *et al.*, 2008).

In addition, a variety of kinetic counterparts of ideal AEs also exists, in analogy to the existence of KAW as a counterpart of SAWs, discussed in Sec. III.A. Typical examples are kinetic TAE (KTAE) that are obtained when, e.g.,

finite resistivity (Cheng, Chen, and Chance, 1985) or FLR effects are accounted for, as in Mett and Mahajan (1992a, 1992b), Berk, Mett, and Lindberg (1993), and Candy and Rosenbluth (1993, 1994). Similarly, one could show that kinetic BAE (KBAE) also exist (Zonca *et al.*, 1998, 1999; Wang, Zonca, and Chen, 2010; Wang *et al.*, 2011) as the granularity of the SAW continuum becomes evident when the plasma response is probed on sufficiently short spatial scales and sufficiently long temporal scales (Chen and Zonca, 1995; Zonca and Chen, 1996). The most practically important consequence of KAW is their excitation by mode conversion (Hasegawa and Chen, 1975, 1976), mostly via FLR effects, due to the radial singular structures of SAW continuous spectrum (cf. Sec. III.A). Since KAW are not generally absorbed locally nearby the mode conversion layer in high temperature plasmas (Jaun, Fasoli, and Heidbrink, 1998; Jaun *et al.*, 2000; Kolesnichenko *et al.*, 2005), mode structures, and stability properties of SAWs are truly kinetic and global in nature, and it becomes crucial to properly account for all these physics in realistic comparisons with experimental observations and in stability predictions in reactor relevant conditions.

A final important class of Alfvénic fluctuations in 2D nonuniform systems is given by EPMs (Chen, 1994), which originate at marginal stability as non-normal modes of the SAW continuous spectrum and are resonantly excited at the characteristic frequency of EP motions. The excitation condition of EPM is independent of the existence of AE inside the frequency gaps, but it requires that the mode drive is sufficiently strong to overcome continuum damping (cf. Sec. III.C). Being connected with a condition on the beam energy density, EPM can manifest themselves in a variety of different forms, the best known and first observed of which is the fishbone mode (McGuire *et al.*, 1983), i.e., an internal kink oscillation with toroidal mode number $n = 1$, which is resonantly excited typically by the toroidal precession resonance with magnetically trapped EPs (Chen, White, and Rosenbluth, 1984). As for AE, the fishbone "gap mode" also exists, for weaker EP beam power density, in the low-frequency KTI gap, dominated by diamagnetic response and smoothly connecting with the ideal and resistive internal kink mode for vanishing kinetic effects (Coppi and Porcelli, 1986).

As all instabilities that tap the expansion free energy from EP spatial gradients, AE and EPM have both linear growth and transport rates (Chen, 1999) proportional to the mode number; thus, short wavelengths tend to be favored. On the other hand, due to the orbit-averaging effect in wave-particle interactions, the typical lower bound for $\lambda_\perp$ is set by the characteristic EP orbit width ρ_E, which, in toroidal devices, is determined by magnetic drifts and is generally larger than the Larmor radius (Berk, Breizman, and Ye, 1992b; Fu and Cheng, 1992; Tsai and Chen, 1993; Chen, 1994). For this reason, modes with $\lambda_\perp \gtrsim \rho_E$ are expected to play a dominant role both for resonant excitations of collective SAWs and DAWs and for producing fluctuation enhanced EP transport. This condition corresponds to $n_{\max} q \lesssim r/\rho_E$ for the maximum toroidal mode number of linearly excited Alfvénic modes. Generally, AEs in the same gap have nearly degenerate frequency for the various toroidal mode numbers, as in the case of TAE (Cheng, Chen, and Chance, 1985). Moreover, each nth mode has $\sim O(nqr/R_0)$ different possible realizations (radial eigenstates) of AE localized at different radial locations. Thus, within the TAE gap we may expect $\sim O(n^2 qr/R_0)$ AEs forming a "dense population of eigenmodes (lighthouses) with unique (equilibrium-dependent) frequencies and locations" (Chen and Zonca, 2007a). In Secs. V and VI, the significant implications of this fact on the nonlinear AE physics are discussed.

In Sec. III.C, we discuss how all this Alfvén zoology (Heidbrink, 2002) can be described by one single dispersion relation (GFLDR) written in a general "fishbonelike" form, which can be adopted for linear stability studies as well as for systematic extensions to the nonlinear regime (cf. Sec. IV.A) (Zonca and Chen, 2014b, 2014c).

C. The general fishbonelike dispersion relation

We assume that the equilibrium $\boldsymbol{B}_0$ can be expressed in the usual form

$$\boldsymbol{B}_0 = F(\psi)\boldsymbol{\nabla}\varphi + \boldsymbol{\nabla}\varphi \times \boldsymbol{\nabla}\psi, \tag{3.6}$$

where φ is the physical toroidal angle, identifying the symmetry of the system at equilibrium, and ψ is the poloidal magnetic flux function. Moreover, we use a straight magnetic field line toroidal coordinates system (r, θ, ζ), where r is a radial-like coordinate depending only on the magnetic flux function ψ,[10] while θ and ζ are periodic anglelike variables, the latter being the ignorable (symmetry) coordinate of the plasma equilibrium. More precisely, ζ is the general toroidal angle defined by

$$\boldsymbol{B}_0 \cdot \boldsymbol{\nabla}\zeta / \boldsymbol{B}_0 \cdot \boldsymbol{\nabla}\theta = q(r), \tag{3.7}$$

where $q(r)$ is the safety factor profile and θ is chosen such that the Jacobian $\mathcal{J} = (\boldsymbol{\nabla}\psi \times \boldsymbol{\nabla}\theta \cdot \boldsymbol{\nabla}\zeta)^{-1}$ satisfies the condition of $\mathcal{J}B_0^2$ being a flux function, i.e., (r, θ, ζ) are Boozer coordinates (Boozer, 1981, 1982). A scalar function $f(r, \theta, \zeta)$, describing a generic fluctuating field, can be decomposed as a Fourier series

$$f(r, \theta, \zeta) = \sum_{n\in\mathbb{Z}} e^{in\zeta} F_n(r, \theta) = \sum_{m,n\in\mathbb{Z}} e^{in\zeta - im\theta} f_{m,n}(r), \tag{3.8}$$

where $\mathbb{Z}$ denotes the set of integers, and the toroidal Fourier components $F_n(r, \theta)$ are independent in the linear limit, while the poloidal Fourier components $f_{m,n}(r)$ are not, due to the equilibrium geometry. Note that, for simplicity, time dependences are assumed implicit. The GFLDR derivation is based on the construction of a nonlinear functional form $\delta\mathcal{L}(\delta\phi, \delta\psi)$ from Eqs. (2.26) and (2.28) (Chen and Hasegawa, 1991; Edery *et al.*, 1992). The final result can be put in close connection with various forms of the MHD energy principle (Bernstein *et al.*, 1958; Kruskal and Oberman, 1958; Rosenbluth and Rostoker, 1959; Taylor and Hastie, 1965; Antonsen, Lane, and Ramos, 1981; Antonsen and Lee, 1982; Van Dam, Rosenbluth, and

[10] One possible choice is $r/a = (\psi - \psi_0)^{1/2}/(\psi_a - \psi_0)^{1/2}$, with ψ_0 the value of ψ on the magnetic axis and ψ_a its value at the plasma minor radius $r = a$.

Lee, 1982; Porcelli and Rosenbluth, 1998), due to the fact that, in the long-wavelength limit, Eqs. (2.26)–(2.29) can be cast as Eqs. (2.34)–(2.37), i.e., they recover reduced MHD as a limiting case of nonlinear gyrokinetic equations and their linearized form reduces to the kinetic-MHD equations discussed in Sec. II.E. When nonlinear terms are included, $\delta\mathcal{L}(\delta\phi,\delta\psi)$ is generally not variational, although $\delta\mathcal{L}(\delta\phi,\delta\psi)=0$ by definition, when the functional is computed for the actual solution of Eqs. (2.34) and (2.37).

The construction of the GFLDR assumes that fluctuations are characterized by two radial scales, due to the existence of the SAW continuous spectrum. As a result, the contribution from regular regions δW is readily separated from that due to singular layers $-\delta I$, yielding $\delta\mathcal{L}=\delta W-\delta I$. Radial scale separation can be explicitly accounted for by adopting the mode structure decomposition approach discussed by Zonca, Chen, and White (2004) and Lu, Zonca, and Cardinali (2012),[11] which, for short-wavelength modes, reduces to the well-known "ballooning representation" (Coppi, 1977; Glasser, 1977; Lee and Van Dam, 1977; Connor, Hastie, and Taylor, 1978, 1979; Pegoraro and Schep, 1978; Dewar *et al.*, 1981; Hazeltine, Hitchcock, and Mahajan, 1981; Dewar *et al.*, 1982), and consists of writing a generic fluctuating field $f(r,\theta,\zeta)$, decomposed as in Eq. (3.8), in the form

$$f(r,\theta,\zeta)=\sum_{m,n\in\mathbb{Z}}e^{in\zeta-im\theta}\int_{-\infty}^{\infty}e^{i(m-nq)\vartheta}\hat{f}_n(r,\vartheta)d\vartheta$$
$$=\sum_{m,n\in\mathbb{Z}}e^{in\zeta-im\theta}\int_{-\infty}^{\infty}e^{i(m-nq)\vartheta}\mathcal{P}_{Bn}(r,\vartheta)[f]d\vartheta. \quad (3.9)$$

Equation (3.9) introduces and defines the projection operator $\mathcal{P}_{Bn}(r,\vartheta):f(r,\theta,\zeta)\mapsto\hat{f}_n(r,\vartheta)$, with $\hat{f}_n(r,\vartheta)$ satisfying regularity conditions at $|\vartheta|\to\infty$ (Zonca and Chen, 2014b), and ϑ corresponds to an extended poloidal angle. In fact, multiplication by a periodic function $p(\theta)$ in (r,θ) space corresponds to multiplication by a periodic function $p(\vartheta)$ in (r,ϑ) space and $\boldsymbol{b}\cdot\boldsymbol{\nabla}\mapsto(\mathcal{J}B_0)^{-1}\partial_\vartheta$. Finally, when operating on a function in this ballooning representation, we find

$$\boldsymbol{\nabla}_\perp\mapsto\boldsymbol{\nabla}r\left(-inq'\vartheta+\frac{\partial}{\partial r}\right)+in\boldsymbol{\nabla}\zeta+\boldsymbol{\nabla}\theta\left(\frac{\partial}{\partial\vartheta}-inq\right)$$
$$-\frac{\boldsymbol{b}}{\mathcal{J}B_0}\frac{\partial}{\partial\vartheta}, \quad (3.10)$$

with q' denoting the radial derivative of $q(r)$, defined by Eq. (3.7), with respect to r. Introducing the magnetic shear as

$$s=s(r)=rq'(r)/q(r), \quad (3.11)$$

and adopting the notation

$$\delta\hat{\Psi}_n\equiv\hat{\kappa}_\perp\delta\hat{\psi}_n \quad\text{and}\quad k_\vartheta^2\hat{\kappa}_\perp^2\equiv-\nabla_\perp^2, \quad (3.12)$$

it can be shown that δI is given by (Zonca and Chen, 2014b)

$$\delta I=\frac{2\pi^2c^2}{|\omega|^2}\sum_{n\in\mathbb{Z}}\left.\frac{|k_\vartheta|(d\psi/dr)}{|s|^2\mathcal{J}B_0^2}\right|_{r=r_0,\vartheta=0}(\delta\hat{\Psi}^\dagger_{-n0^+}\delta\hat{\Psi}_{n0^+})i|s|\Lambda_n, \quad (3.13)$$

with the summation on all singular layer contributions left implicit. Furthermore, $\delta\psi^\dagger$ is the adjoint of $\delta\psi$ with the definition by Gerjuoy, Rau, and Spruch (1983), $\delta\hat{\Psi}_{n0^+}=\delta\hat{\Psi}_n(r_0,\vartheta\to0^+)$ is used as normalization, and Λ_n is obtained from

$$i\Lambda_n\equiv\tfrac{1}{2}(\delta\hat{\Psi}^\dagger_{-n0^+}\delta\hat{\Psi}_{n0^+})^{-1}[\delta\hat{\Psi}^\dagger_{-n}(\vartheta)\partial_\vartheta\delta\hat{\Psi}_n(\vartheta)]_{\vartheta\to0^-}^{\vartheta\to0^+}, \quad (3.14)$$

i.e., from the solution of Eq. (2.37) for $\hat{\kappa}_\perp^2=k_\perp^2/k_\vartheta^2\simeq s^2\vartheta^2|\boldsymbol{\nabla}r|^2\gg1$ with outgoing wave boundary conditions, corresponding to causality constraints. Thus, Eq. (3.13) contains the information on the sharp varying structures of SAW fluctuation associated with the continuous spectrum. Meanwhile, one can show that (Zonca and Chen, 2014b)

$$\delta W=\lim_{\vartheta_1\to\infty}(2\pi)^3\int_0^a dr\frac{d\psi/dr}{2}\int_{-\vartheta_1}^{\vartheta_1}\mathcal{J}d\vartheta$$
$$\times\sum_{n,\ell\in\mathbb{Z}}e^{-2\pi inq\ell}\left\{\mathcal{P}_{B-n}(r,\vartheta)[\delta\boldsymbol{B}^\dagger]\cdot\mathcal{P}_{Bn}(r,\vartheta+2\pi\ell)\left[\frac{\delta\boldsymbol{B}}{4\pi}\right]\right.$$
$$+\mathcal{P}_{B-n}(r,\vartheta)[\partial_t^{-1}\delta\phi^\dagger]\mathcal{P}_{Bn}(r,\vartheta+2\pi\ell)$$
$$\times\left[-\frac{c^2}{4\pi}\boldsymbol{\nabla}\cdot\left(\frac{1}{v_A^2}\boldsymbol{\nabla}_\perp\frac{\partial}{\partial t}\delta\phi\right)+\frac{c^2}{4\pi}\boldsymbol{b}\times\boldsymbol{\nabla}\left[\frac{4\pi}{B_0^2}\left(\frac{P_{0\perp i}}{\Omega_i}\right)\right]\right.$$
$$\left.\cdot\boldsymbol{\nabla}\nabla_\perp^2\delta\phi+\frac{c}{B_0}\boldsymbol{b}\times\boldsymbol{\kappa}\cdot\boldsymbol{\nabla}\sum\langle m(\mu B_0+v_\parallel^2)J_0\delta g\rangle_v\right.$$
$$\left.\left.+\delta\boldsymbol{B}_\perp\cdot\boldsymbol{\nabla}\left(\frac{j_{\parallel0}}{B_0}\right)\right]\right\}. \quad (3.15)$$

Formally nonlinear terms due to core plasma dynamics (cf. Secs. II.D and II.E) may be dropped in the expression for δW (Zonca and Chen, 2014b). For the same reason, thermal ion FLR terms are dropped and $\delta\phi=\delta\psi$ is explicitly imposed in Eq. (3.15). As in ideal MHD, most important destabilization effects come from the last two terms, the "ballooning interchange" and the "kink" drive, respectively (Furth *et al.*, 1965; Greene and Johnson, 1968; Freidberg, 1987). Note that the expression for δW is still nonlinear due to the implicit nonlinear response included in the ballooning-interchange contribution, which also maintains FLR effects of EPs. Adopting the normalization for δW in Eq. (3.15) as in Eq. (3.13), it is possible to rewrite (Zonca and Chen, 2014b)

$$\delta W=\frac{2\pi^2c^2}{|\omega|^2}\sum_{n\in\mathbb{Z}}\left.\frac{|k_\vartheta|(d\psi/dr)}{|s|^2\mathcal{J}B_0^2}\right|_{r=r_0,\vartheta=0}(\delta\hat{\Psi}^\dagger_{-n0^+}\delta\hat{\Psi}_{n0^+})\delta\hat{W}_n. \quad (3.16)$$

Thus, the GFLDR is derived from $\delta\mathcal{L}=\delta W-\delta I=0$ combining Eqs. (3.13) and (3.16), and for a single-n toroidal mode, is given by

[11]This representation relies solely on the Poisson summation formula and its general properties. A thorough discussion of these issues and of applications of Eq. (3.9) to Alfvén waves was given by Zonca and Chen (2014b).

$$i|s|\Lambda_n = \delta\hat{W}_{nf} + \delta\hat{W}_{nk}. \tag{3.17}$$

The generalized inertia term $\Lambda_n(\omega)$ accounts for the thermal ion response and can be extended to include EP effects for long-wavelength modes (Briguglio *et al.*, 1995), as well as, for shorter wavelength modes, thermal ion FLR effects. Meanwhile, Λ_n can also be modified to include the stress tensor, Maxwell stress, and polarization nonlinearity, by including the corresponding terms from Eq. (2.37) (see Sec. IV.C). Same as the inertia term, the potential energy $\delta\hat{W}_n$ accounts for both linear and nonlinear responses due to the presence of δg in Eq. (3.15). The right-hand side of Eq. (3.17) also distinguishes between "fluid" ($\delta\hat{W}_{nf}$) and kinetic ($\delta\hat{W}_{nk}$) contributions to the potential energy $\delta\hat{W}_n$ (Chen, White, and Rosenbluth, 1984). The expression for $\delta\hat{W}_{nf}$ is obtained from Eq. (3.16) using the fluid limit for the gyrokinetic particle response δg in Eq. (3.15), while $\delta\hat{W}_{nk}$ accounts for the remaining kinetic particle response. In the low-frequency limit ($|\Lambda_n^2| \ll 1$), $\delta\hat{W}_{nf}$ is independent of ω and reduces to the well-known MHD limiting forms. Meanwhile, $\delta\hat{W}_{nk}(\omega)$ is always a function of ω, as it reflects resonant as well as nonresonant wave-particle interactions. Dispersion relations in a form similar to Eq. (3.17) have been derived in many works on the effect of EPs on low-frequency MHD modes by precession resonance (Chen, White, and Rosenbluth, 1984; Rewoldt and Tang, 1984; Spong *et al.*, 1985; Weiland and Chen, 1985; White *et al.*, 1985; Biglari and Chen, 1986; Coppi and Porcelli, 1986; White, Romanelli, and Bussac, 1990). Meanwhile, the generality of Eq. (3.17) and its applicability to low-frequency MHD modes (Chen, White, and Rosenbluth, 1984; Liljeström and Weiland, 1992), as well as to KBM (Biglari and Chen, 1991; Tsai and Chen, 1993) and higher frequency SAWs (Chen, 1988; Chen *et al.*, 1989; Biglari, Zonca, and Chen, 1992), was formulated by Chen (1994) and Zonca, Chen, and Santoro (1996) and formalized by Zonca *et al.* (1999, 2007a), Zonca and Chen (2006, 2007), and Chen and Zonca (2007a). When magnetic shear vanishes at one isolated singular layer ($s = 0$ at $r = r_0$ where $k_{\|n} = k_{\|n0}$), it is possible to construct the (local) extension of Eq. (3.17) that, for $|\Lambda_n^2| \ll 1$, becomes (Zonca *et al.*, 2007a)

$$iS(\Lambda_n^2 - k_{\|n0}^2 L_0^2)^{1/2}[(1/n)k_{\|n0}L_0 - (i/n)(\Lambda_n^2 - k_{\|n0}^2 L_0^2)^{1/2}]^{1/2} = \delta\hat{W}_{nf} + \delta\hat{W}_{nk}, \tag{3.18}$$

originally derived by Hastie *et al.* (1987) for internal kink mode stability analyses, where

$$S^2 = r_0^2 q''(r_0)/q(r_0)^2. \tag{3.19}$$

The GFLDR generally demonstrates the existence of two types of modes (Zonca and Chen, 2006): a discrete gap mode, or AE, for $\mathbb{R}\mathrm{e}\Lambda_n^2 < 0$, and an EPM (Chen, 1994) for $\mathbb{R}\mathrm{e}\Lambda_n^2 > 0$. The combined effect of $\delta\hat{W}_{nf}$ and $\delta\hat{W}_{nk}$ determines the existence conditions of AEs, and various effects in $\delta\hat{W}_{nf}$ and $\delta\hat{W}_{nk}$ can lead to AE localization in various gaps, i.e., to different species of AE (Chen and Zonca, 2007a). The transition between AE and EPM is generally continuous with varying plasma parameters and a net distinction is possible only when the distance of the mode frequency from the SAW accumulation point ($\Lambda_n = 0$) is larger than the mode linear growth rate γ_L or the characteristic inverse nonlinear time τ_{NL}^{-1} (cf. Sec. II.C). In the low-frequency limit ($|\Lambda_n^2| \ll 1$), when the AE frequency is above the SAW continuum accumulation point ω_ℓ, the causality constraint for AE existence inside the SAW frequency gap is (Chen and Zonca, 2007a; Zonca and Chen, 2014b)

$$\delta\hat{W}_{nf} + \mathbb{R}\mathrm{e}\delta\hat{W}_{nk} > 0. \tag{3.20}$$

Similarly, for AE frequency below the SAW continuum accumulation point ω_u, the AE existence condition becomes

$$\delta\hat{W}_{nf} + \mathbb{R}\mathrm{e}\delta\hat{W}_{nk} < 0. \tag{3.21}$$

For EPM meanwhile the $i\Lambda_n$ term in Eq. (3.17) represents continuum damping and the threshold in EP drive for mode excitation. In fact, near marginal stability,

$$\delta\hat{W}_{nf} + \mathbb{R}\mathrm{e}\delta\hat{W}_{nk} = 0, \Rightarrow \text{determines } \omega_0,$$
$$\frac{\gamma_L}{\omega_0} = \frac{|s|^{-1}\mathbb{I}\mathrm{m}\delta\hat{W}_{kn} - \Lambda_n}{(-\omega_0|s|^{-1}\partial\mathbb{R}\mathrm{e}\delta\hat{W}_n/\partial\omega_0)}, \Rightarrow \text{determines } \gamma_L. \tag{3.22}$$

Equations (3.17) and (3.18) are global by construction and can be used for computing the (generally nonlinear) mode dispersion relation. The fact that Eqs. (3.17) and (3.18) follow from a variational principle, at least in the linear limit, allows evaluating $\delta\hat{W}_{nf}$ and $\delta\hat{W}_{nk}$ by trial function method, thus, even with realistic mode structures obtained numerically. Furthermore, Λ_n can generally be computed by solving an ordinary (nonlinear) differential equation with outgoing wave boundary conditions, Eq. (2.37) [or Eq. (2.26) in the same limit, accounting for full FLR effects (Connor, Tang, and Taylor, 1983)] for $\hat{\kappa}_\perp^2 = k_\perp^2/k_\vartheta^2 \simeq s^2\vartheta^2|\boldsymbol{\nabla} r|^2 \gg 1$, which can be done analytically in many cases of practical interest (Zonca and Chen, 2014b, 2014c), or numerically. The generality of Eqs. (3.17) and (3.18) makes them applicable to a variety of MHD modes as well (Zonca and Chen, 2014b, 2014c), e.g., internal and/or external kink modes by suitable extension of $\delta\hat{W}_{nf}$ and $\delta\hat{W}_{nk}$ expressions. Stability of these modes is expected to be strongly influenced by plasma rotation, due to the ideal MHD coupling with sound (Bondeson and Ward, 1994; Betti, 1995) and Alfvén waves (Gregoratto *et al.*, 2001; Zheng, Kotschenreuther, and Chu, 2005), or due to resistive layer (Finn, 1995; Gimblett and Hastie, 2000) and viscous boundary layer damping (Fitzpatrick and Aydemir, 1996). However, even stronger effects are expected when resonant interactions are accounted for with thermal ions at the bounce or transit frequencies (Bondeson and Chu, 1996; Liu *et al.*, 2004), or with either trapped thermal ions or electrons at the precession frequency (Hu and Betti, 2004). Experimental evidence also suggests the existence of EP-driven external kink modes (Heidbrink *et al.*, 2011; Okabayashi *et al.*, 2011), which are the EPM counterpart of the resistive wall mode (RWM) (Pfirsch and Tasso, 1971). Recent reviews of the physics of internal kink (sawtooth) stabilization (Chapman *et al.*, 2007; Graves *et al.*, 2010, 2012) and analyses of high-β regimes for the demonstration power plant (DEMO)

(Chapman, Kemp, and Ward, 2011) confirm the necessity of thorough kinetic models for the description of the plasma operation control in burning plasmas.

For short-wavelength SAW with radially localized mode structures, the mode structure decomposition of Eq. (3.9) reduces to the ballooning representation

$$f(r,\theta,\zeta) = \sum_{m,n\in\mathbb{Z}} A_n(r) e^{in\zeta - im\theta} \int e^{i(m-nq)\vartheta} \hat{f}_{0n}(r,\vartheta) d\vartheta = \sum_{m,n\in\mathbb{Z}} A_n(r) e^{in\zeta - im\theta} \int e^{i(m-nq)\vartheta} \mathcal{P}_{Bn}(r,\vartheta)[f_{0n}] d\vartheta, \tag{3.23}$$

where $\mathcal{P}_{Bn}(r,\vartheta): f_{0n}(r; nq-m) \mapsto \hat{f}_{0n}(r,\vartheta)$ and the functions $f_{0n}(r; nq-m)$ are nearly invariant under radial translations by multiples of $(nq')^{-1}$, while the radial envelope functions $A_n(r)$ have characteristic spatial dependences on mesoscales, intermediate between the perpendicular wavelength and the equilibrium scale length (Zonca and Chen, 1993; Zonca, 1993a). Because of the spatial scale separation among $f_{0n}(r; nq-m)$, $A_n(r)$, and equilibrium nonuniformities, it is possible to use the eikonal ansatz $A_n(r) \sim \exp[i\int nq'\theta_k(r)dr]$ (Dewar *et al.*, 1981, 1982). Thus, Eq. (3.10) becomes

$$\boldsymbol{\nabla}_\perp \mapsto ik_\vartheta \boldsymbol{\nabla} r(s\vartheta - s\theta_k) + in\boldsymbol{\nabla}\zeta + ik_\vartheta r\boldsymbol{\nabla}\theta \tag{3.24}$$

and Eq. (2.37) can be rewritten as

$$\left(\frac{\partial^2}{\partial\vartheta^2} - \frac{\partial_\vartheta^2\hat{\kappa}_\perp}{\hat{\kappa}_\perp}\right)\delta\hat{\Psi}_n - \frac{\mathcal{J}^2B_0^2}{v_A^2}\frac{\partial}{\partial t}\left[\frac{\partial}{\partial t} + i\omega_{*pi} - \frac{3}{4}k_\vartheta^2\rho_i^2\hat{\kappa}_\perp^2\left(\frac{\partial}{\partial t} + i\omega_{*pi} + i\omega_{*Ti}\right)\right]\delta\hat{\Phi}_n - \frac{4\pi\mathcal{J}^2B_0}{ck_\vartheta^2\hat{\kappa}_\perp}\boldsymbol{b}\times\boldsymbol{\kappa}\cdot\boldsymbol{\nabla}\sum\left\langle m(\mu B_0 + v_\parallel^2)J_0\frac{\partial}{\partial t}\delta\hat{g}_n\right\rangle_v + [\text{nonlinear terms}] = 0. \tag{3.25}$$

Here we introduced the notation $\delta\hat{\Phi}_n \equiv \hat{\kappa}_\perp\delta\hat{\phi}_n$, as in Eq. (3.12), and $\omega_{*pi} = \omega_{*ni} + \omega_{*Ti}$, with

$$\omega_{*ni} = \left(\frac{T_0c}{en_0B_0}\right)_i (\boldsymbol{b}\times\boldsymbol{\nabla}n_{0i})\cdot\boldsymbol{k}_\perp, \qquad \omega_{*Ti} = \left(\frac{c}{eB_0}\right)_i (\boldsymbol{b}\times\boldsymbol{\nabla}T_{0i})\cdot\boldsymbol{k}_\perp, \tag{3.26}$$

for Maxwellian thermal plasma ions, and $\boldsymbol{k}_\perp = -i\boldsymbol{\nabla}_\perp$. Furthermore, we have omitted the kink drive, for it scales as n^{-1} (cf. Sec. II.C), and the nonlinear terms, since they are analyzed specifically in Sec. IV.C. Equations (3.13) and (3.16) meanwhile become

$$\delta I = \frac{2\pi^2c^2}{|\omega|^2}\sum_{n\in\mathbb{Z}}\int_0^a dr \frac{|k_\vartheta|^2(d\psi/dr)}{\mathcal{J}B_0^2}\bigg|_{\vartheta=0} \times (\delta\hat{\Psi}^\dagger_{-n0^+}\delta\hat{\Psi}_{n0^+})i\Lambda_n, \tag{3.27}$$

$$\delta W = \frac{2\pi^2c^2}{|\omega|^2}\sum_{n\in\mathbb{Z}}\int_0^a dr \frac{|k_\vartheta|^2(d\psi/dr)}{\mathcal{J}B_0^2}\bigg|_{\vartheta=0} \times (\delta\hat{\Psi}^\dagger_{-n0^+}\delta\hat{\Psi}_{n0^+})\delta\bar{W}_n, \tag{3.28}$$

with the ballooning $\delta\bar{W}_n$ expressed as, noting that $\delta\hat{\Psi}^\dagger_{-n0^+}\delta\hat{\Psi}_{n0^+} = \delta\hat{\Phi}^\dagger_{-n0^+}\delta\hat{\Phi}_{n0^+}$,

$$\delta\bar{W}_n = \delta\bar{W}_{nf} + \delta\bar{W}_{nk} = (\delta\hat{\Phi}^\dagger_{-n0^+}\delta\hat{\Phi}_{n0^+})^{-1}\frac{1}{2}\int_{-\infty}^{\infty}\left[\left(\frac{\partial}{\partial\vartheta}\delta\hat{\Phi}_{-n}\right)^\dagger\left(\frac{\partial}{\partial\vartheta}\delta\hat{\Phi}_n\right) + \frac{\partial_\vartheta^2\hat{\kappa}_\perp}{\hat{\kappa}_\perp}\delta\hat{\Phi}^\dagger_{-n}\delta\hat{\Phi}_n + \delta\hat{\Phi}^\dagger_{-n}\frac{\mathcal{J}^2B_0^2}{v_A^2}\frac{\partial}{\partial t}\left(\frac{\partial}{\partial t} + i\omega_{*pi}\right)\delta\hat{\Phi}_n + \delta\hat{\Phi}^\dagger_{-n}\frac{4\pi\mathcal{J}^2B_0}{ck_\vartheta^2\hat{\kappa}_\perp}\boldsymbol{b}\times\boldsymbol{\kappa}\cdot\boldsymbol{\nabla}\sum\left\langle m(\mu B_0 + v_\parallel^2)J_0\frac{\partial}{\partial t}\delta\hat{g}_n\right\rangle_v\right]d\vartheta. \tag{3.29}$$

Here Λ_n, $\delta\bar{W}_n$, and other physical quantities are dependent on r, due to the global equilibrium profile variations. For very localized modes, whose radial envelope variation $A_n(r)$ on mesoscales can be ignored, a direct comparison of Eqs. (3.16) and (3.28) yields $\delta\hat{W}_n = |s|\delta\bar{W}_n$ and the GFLDR becomes a local dispersion relation.

In the more general case, where global plasma nonuniformities play important roles, the GFLDR can be cast as

$$[i\Lambda_n - (\delta\bar{W}_f + \delta\bar{W}_k)_n]A_n(r) = D_n(r,\theta_k,\omega)A_n(r) = 0, \tag{3.30}$$

with $D_n(r,\theta_k,\omega)$ playing the role of a local dispersion function. This equation can be generally solved using the fact that $\omega = \omega_0 + i\partial_t$, with ω_0 the typical (linear) mode frequency (cf. Sec. II.C). In fact, we can describe the spatiotemporal evolution of SAW wave packets in toroidal plasmas expanding the solutions of Eq. (3.30) about the characteristics

$$D_n(r,\theta_{k0}(r),\omega_0) = 0. \tag{3.31}$$

Then, letting $A_n(r) = \exp(-i\omega_0 t)A_{n0}(r,t)$, with $\partial_t A_{n0}(r,t) \sim \gamma_L A_{n0}(r,t) \sim \tau_{NL}^{-1}A_{n0}(r,t)$ (cf. Secs. II.C and IV.A), the spatiotemporal evolution equation for $A_{n0}(r,t)$ is

$$\frac{\partial D_n}{\partial \omega_0}\left(i\frac{\partial}{\partial t}\right)A_{n0}+\frac{\partial D_n}{\partial \theta_{k0}}\left(-\frac{i}{nq'}\frac{\partial}{\partial r}-\theta_{k0}\right)A_{n0}+\frac{1}{2}\frac{\partial^2 D_n}{\partial \theta_{k0}^2}\left[\left(-\frac{i}{nq'}\frac{\partial}{\partial r}-\theta_{k0}\right)^2 A_{n0}-\frac{i}{nq'}\frac{\partial \theta_{k0}}{\partial r}A_{n0}\right]=S_n(r,t). \tag{3.32}$$

The $S_n(r,t)$ on the right-hand side can represent either a source term or nonlinear interactions (cf. Sec. IV.A). The solution of Eq. (3.32) identifies important time scales, such as the inverse linear growth time γ_L^{-1} and the formation time of the global eigenmode structure τ_A, which is of the order of the wave-packet bounce time between WKB turning points (Zonca, Chen, and White, 2004). It can be shown that the global mode dispersion relation is (Zonca and Chen, 1993; Zonca, 1993a, 1993b)

$$\Phi_0(\omega_0)=\oint nq'\theta_{k0}dr-k\pi=2\ell\pi, \qquad \ell\in\mathbb{N}. \tag{3.33}$$

Here $k=0$ or $k=1$, respectively, for librations or rotations of θ_{k0} characteristics of Eq. (3.31).

Detailed applications of the GFLDR theoretical framework to various branches of the SAW spectrum in toroidal plasmas (cf. Sec. III.B) and their experimental observations are given by Zonca and Chen (2014c). In this work, we are mainly interested in the extensions of those analyses to nonlinear phenomena (cf. Sec. IV).

IV. NONLINEAR ALFVÉN WAVE BEHAVIOR AND SELF-CONSISTENT INTERACTIONS WITH ENERGETIC PARTICLES

The ordering estimates of the vorticity equation in Sec. II.C introduce two different nonlinear dynamic regimes in the long-wavelength limit. For $\epsilon_\omega > \epsilon_\perp^2$, nonlinear wave-wave interactions are determined by the polarization (inertia) nonlinearity and the MHD plasma description is reasonably accurate. Meanwhile, for $\epsilon_\omega < \epsilon_\perp^2$, Maxwell stress and pressure stress tensor nonlinearity become dominant and kinetic theory becomes necessary at increasingly shorter wavelengths. Thus, the nonlinear dynamics of Alfvén waves crucially depends on the existence of the so-called Alfvénic state (cf. Sec. II.C), where Reynolds and Maxwell stresses cancel exactly and large amplitude SAW can be supported. Consequently, physics processes that are responsible for breaking the Alfvénic state are of great importance for the nonlinear evolution of the SAW spectrum.

As anticipated in Sec. III, the GFLDR theoretical framework provides a useful starting point for our analyses of nonlinear physics of SAW, DAW, and EPs in burning plasmas. Section IV.A discusses the general theoretical approach adopted here, which is formulated as a NLSE with integro-differential nonlinear terms. That equation is then used in later sections to investigate nonlinear processes affecting DAW behavior.

Many of these issues can be analyzed and illuminated in uniform plasmas and are presented in Sec. IV.B, where the finite ion compressibility effect (polarization nonlinearity) is analyzed in the long-wavelength limit, showing that it yields the decay of a SAW into another SAW and an ISW (Sagdeev and Galeev, 1969) (cf. Sec. IV.B.1). However, for sufficiently short wavelength there is a transition to nonlinear behavior dominated by Reynolds and Maxwell stresses, which requires accounting for wavelengths comparable with the ion Larmor radius (Hasegawa and Chen, 1975, 1976). In this case, KAWs break the ideal Alfvénic state and the three-wave SAW decay is taken over by the three-wave KAW decay (Hasegawa and Chen, 1976). Such a transition has important consequences on plasma transport, since SAW decay preserves the anisotropy of the initial $\boldsymbol{k}_\perp$ spectrum, while KAW decay tends to make it isotropic (cf. Sec. IV.B.2). These findings, thus, demonstrate that, in general, it may be necessary to adopt the kinetic description in the study of DAW turbulence. The breaking of the Alfvénic state by KAWs also affects the nonlinear excitation of convective cells, as shown in Sec. IV.B.3. Convective cells are the uniform plasma counterpart of zonal flows and fields in toroidal systems. Studying convective cells thus provides useful insights to understanding the more complex nonlinear interplay between Alfvén waves and zonal structures (ZS) (cf. Sec. II.D), which will be further discussed later in this section and in Sec. VI within a broader physics framework.

In Sec. IV.C, we show how geometry of the plasma equilibrium and spatial nonuniformities affect, both qualitatively and quantitatively, the nonlinear processes discussed previously. The tokamak counterpart of the SAW decay process in a uniform plasma is TAE frequency cascading via nonlinear Landau damping (Hahm and Chen, 1995), discussed in Sec. IV.C.1. At shorter wavelengths, as in the KAW decay, polarization nonlinearity becomes subdominant, and Maxwell stress and pressure stress tensor (including Reynolds stress; cf. Secs. II.B and II.D) nonlinear terms determine the cross section of TAE frequency cascading. This analysis, however, remains to be carried out. In Sec. IV.C.2, we also discuss the generation of ZS by finite-amplitude TAE (Spong, Carreras, and Hedrick, 1994; Todo, Berk, and Breizman, 2010; Chen and Zonca, 2012) as the toroidal geometry analog of the generation of convective cells by KAW. These various processes may by themselves yield to TAE or AE saturation levels that possibly explain some experimental observations. More generally, however, saturation levels ($|\delta B_r/B_0| \sim 10^{-3}$) expected for the individual nonlinear interactions are larger than observed values ($|\delta B_r/B_0| \lesssim 5\times 10^{-4}$) [see, e.g., Heidbrink *et al.* (2008)]. It is nonetheless important to identify and keep these processes in account, especially in conditions where a number of nonlinear interactions may be simultaneously active and ultimately determine the AE fluctuation amplitude. In addition to regulating turbulence intensity and plasma transport, coherent nonlinear interaction of AE and ZS may influence fine structures of the AE frequency spectrum (cf. Sec. IV.C.2), as is the case of modulation interactions due to wave-particle nonlinear dynamics (Fasoli *et al.*, 1998) (cf. Sec. IV.D.3 and related discussion in Sec. IV.D.6). Finally, we analyze the AE nonlinear interplay with the SAW continuous spectrum in nonuniform systems, which may yield either enhanced continuum damping (Vlad *et al.*, 1992; Zonca *et al.*, 1995; Chen *et al.*, 1998) (cf. Sec. IV.C.3) or nonlinear instability, as in the

case with finite-amplitude MHD activity (Biancalani *et al.*, 2010a, 2010b, 2011) (cf. Sec. IV.C.4).

The nonlinear wave-particle interaction of AEs and EPMs with EPs is discussed in Sec. IV.D. We start from the analysis of the nonlinear dynamics of a nearly monochromatic energetic electron beam in a 1D plasma (O'Neil, Winfrey, and Malmberg, 1971; O'Neil and Winfrey, 1972), given in Sec. IV.D.1, for this is the classical problem on which the mode dispersion relation and nonlinear behavior in a beam-plasma system were formulated and understood for the first time. The 1D beam-plasma problem is also important for understanding aspects of the nonlinear interaction of AE with EPs. In fact, there are currently two paradigms for discussing these physics. One is the bump-on-tail paradigm, which is based on wave trapping in uniform plasma, including effects of source and dissipation,[12] that occurs due to wave-particle "resonance detuning." This paradigm was extensively developed by Berk and Breizman (1990a, 1990b, 1990c) and applied to explain experimental observations [see Breizman and Sharapov (2011) for a recent review]. The other paradigm may be called the fishbone paradigm (Chen and Zonca, 2013; Zonca *et al.*, 2015b) in which the role of magnetic field geometry and plasma nonuniformity is crucial, and wave-particle interaction may be limited due to the finite radial localization of the mode structures, i.e., "radial decoupling" (Chen, White, and Rosenbluth, 1984; Briguglio, Zonca, and Vlad, 1998; Zonca *et al.*, 2005). Furthermore, the self-consistent interplay of instabilities and EP transport may lead to secular EP losses due to phase locking of fluctuations and resonant particles via frequency sweeping (White *et al.*, 1983).

The nonlinear physics of the bump-on-tail paradigm are analyzed in Sec. IV.D.2, stemming from the original works by Berk and Breizman (1990a, 1990b, 1990c). Its applications to AE experimental observations are discussed in Sec. IV.D.3, which also addresses its underlying assumptions and its consequent validity limits. Some of these limitations can be overcome by approximate numerical simulation models, based on perturbative treatment of EPs, which are presented in Sec. IV.D.4. The bump-on-tail paradigm applies sufficiently close to marginal stability, when fluctuation-induced radial particle excursions are smaller than the mode radial wavelength. For sufficiently strong external power inputs and, therefore, EP power density sources, nonlinear EP excursions explore regions of radially varying mode structures and thus a transition typical of nonuniform plasmas is expected in the AE nonlinear dynamics (Zonca *et al.*, 2005), while EP redistributions occur on mesoscales. The general theoretical framework, formulated in Sec. IV.D.5, allows one to describe the transition from uniform to nonuniform plasma behavior, illuminated by recent numerical simulation results (Wang *et al.*, 2012; Zhang, Lin, and Holod, 2012; Briguglio *et al.*, 2014) and to unify bump-on-tail and fishbone paradigms (Zonca *et al.*, 2015b). Effects of such a transition become more important as drive strength increases and are most apparent for EPMs (cf. Sec. IV.D.6) and fishbones (cf. Sec. IV.D.7), which are characterized by the nonperturbative interplay of nonlinear mode dynamics and EP transport processes.

Further remarks and discussion related to the general theoretical formulation of Sec. IV.A are presented in Sec. IV.E, where possible interesting connections to other fields of physics research are also discussed.

A. General theoretical approach

Here we further elaborate on the GFLDR theoretical framework and derive a general form of governing equations for addressing nonlinear physics of SAW, DAW, and EPs in burning plasmas. Equation (3.32) describes the spatiotemporal evolution of DAW wave packets in toroidal plasmas due to the influence of external sources and/or nonlinear dynamics. From Eq. (3.30), a useful formal interpretation of the left-hand side is obtained isolating linear terms in the local dispersion function $D_n(r,\theta_{k0}(r),\omega_0)$, while nonlinear and external source terms are collected on the right-hand side. Thus,

$$\begin{aligned} S_n(r,t) &= -D_n^{NL} + S_n^{\mathrm{ext}}(r,t) \\ &= \left(\delta\bar{W}_f^{NL} + \delta\bar{W}_k^{NL}\right)_n - i\Lambda_n^{NL} + S_n^{\mathrm{ext}}(r,t), \end{aligned} \tag{4.1}$$

where $S_n^{\mathrm{ext}}(r,t)$ explicitly denotes external sources, the superscript NL stands for nonlinear, and the definition of the various terms follows from Eqs. (3.13), (3.16), (3.27), and (3.28). In general, $S_n(r,t)$ can be written symbolically, in terms of amplitude expansion, as (Chen, Zonca, and Lin, 2005; Zonca *et al.*, 2006)

$$\begin{aligned} S_n(r,t) - S_n^{\mathrm{ext}}(r,t) = (C_{n,0} + C_{0,n}) \circ A_{n0}(r,t) A_{z0}(r,t) \\ + \sum_{n'+n''=n}^{n',n''\neq n} C_{n',n''} \circ A_{n'0}(r,t) A_{n''0}(r,t), \end{aligned} \tag{4.2}$$

where $C_{n',n''}$ are generally integrodifferential operators, which imply nonlocal interactions in the n toroidal mode number space and whose composition with (action on) A_{z0}, A_{n0} is denoted by "$\circ$," and A_{z0} and A_{n0} are, respectively, the radial envelope functions of the zonal and $n \neq 0$ components. Here we included nonlinear dynamics that modify the $n = 0$ "zonal" particle distribution function $\delta\bar{F}_z$, given by Eq. (2.22) (Zonca *et al.*, 2000). Therefore, A_{z0} not only represents the amplitude of ZS, but it also symbolically indicates the nonlinear distortion of the equilibrium particle distribution function. This distortion effect enters Eq. (4.1) through velocity-space integrals, implying that A_{z0}, when accounting for interactions with $\delta\bar{F}_z$, is by itself a nonlinear function of A_{n0} and that the dependence is quadratic, $A_{z0} \propto |A_{n0}|^2$. As explained in Sec. IV.D.5.b, we refer to these contributions as phase-space ZS (Zonca *et al.*, 2013, 2015b). Thus, the source term in Eq. (4.1) is intended to contain a cubic nonlinearity with respect to the envelope function

[12] Source and dissipation account for the generation of the EP population by external heating and/or current drive systems in toroidal plasmas of fusion interest as well as for the relaxation of their distribution function via Coulomb collisions (Berk and Breizman, 1990a).

$A_{n0}(r,t)$. The last term in Eq. (4.2) accounts for three-wave interactions and, in general, nonlocal spectral transfers. Combining all the various terms, Eq. (3.32) can be cast in the form of a NLSE with integrodifferential terms

$$\frac{\partial D_n^L}{\partial \omega_0}\left(i\frac{\partial}{\partial t}\right)A_{n0}(r,t)+\frac{\partial D_n^L}{\partial \theta_{k0}}\left(-\frac{i}{nq'}\frac{\partial}{\partial r}-\theta_{k0}\right)A_{n0}(r,t)+\frac{1}{2}\frac{\partial^2 D_n^L}{\partial \theta_{k0}^2}\left[\left(-\frac{i}{nq'}\frac{\partial}{\partial r}-\theta_{k0}\right)^2-\frac{i}{nq'}\frac{\partial \theta_{k0}}{\partial r}\right]A_{n0}(r,t)=S_n^{\mathrm{ext}}(r,t)+(C_{n,0}+C_{0,n})\circ A_{n0}(r,t)A_{z0}(r,t)+\sum_{n'+n''=n}^{n',n''\neq n}C_{n',n''}\circ A_{n'0}(r,t)A_{n''0}(r,t). \tag{4.3}$$

Note that Eq. (4.3) describes both short-wavelength modes, for which Eq. (3.32) was derived, and global long-wavelength modes with one isolated singular layer. The argument yielding Eq. (4.3) from Eqs. (3.30) and (3.32) can be repeated for the GFLDR in the form of Eq. (3.17). As a result, one obtains Eq. (4.3) again, provided that $\theta_{k0}=\partial/\partial r=0$ is assumed, i.e., considering A_{n0} as the amplitude of the n mode at the singular layer (cf. Sec. IV.D.7). The same also applies for the vanishing magnetic shear case, Eq. (3.18). Thus, we may consider Eq. (4.3) as the general form of governing equations for addressing nonlinear physics of Alfvén waves and EPs in burning plasmas. Expressions of the nonlinear-coupling operators $C_{n',n''}$ depend on the specific nonlinear interactions, and some examples are discussed in the remainder of this section.

Equation (4.3) demonstrates that observations of the EP-driven DAW spectrum are expected to be largely described by linear physics, as noted experimentally by Van Zeeland *et al.* (2006), while nonlinear dynamics can be understood as coupling of relevant degrees of freedom on a time scale $\tau_{NL}\sim\gamma_L^{-1}$ [cf. Sec. II.C and Zonca and Chen (2014b), and Zonca *et al.* (2015a, 2015b) for an in-depth discussion of this point]. Furthermore, Eq. (4.3) allows us to readily recognize the various spatiotemporal scales for the nonlinear dynamic evolution of DAWs. In addition to the inverse linear growth rate γ_L^{-1} and the formation time of the global eigenmode structure τ_A (Zonca, Chen, and White, 2004) (cf. Sec. III.C), in fact, one can identify nonlinear processes and corresponding time scales separating ideal region response from singular layer dynamics, as suggested by Eq. (4.1). Recalling that $\tau_{NL}\sim\gamma_L^{-1}$, different behavior is expected for $\tau_A<\tau_{NL}\sim\gamma_L^{-1}$, typical of AE, and for $\tau_A\sim\tau_{NL}\sim\gamma_L^{-1}$, which generally applies for EPM.

Equation (4.3) is also a useful starting point for constructing reduced nonlinear dynamic models with various levels of approximation for understanding selected aspects of the processes under investigation. Different terms entering Eq. (4.3) can be evaluated either analytically or with simplified numerical descriptions, helping, thus, building models with reliable predictive capabilities. Three-wave couplings modify the nonlinear dynamics via the processes discussed in Secs. IV.B and IV.C, which are the dominant nonlinear dynamics of the DAW spectrum caused by the core plasma component (cf. Sec. II.E) and directly affecting fluctuation-induced transport of the thermal plasma. Meanwhile, for a spectrum of low-amplitude fluctuations, $|\delta \boldsymbol{B}_\perp/B_0|\sim 10^{-4}$ with $|\gamma_L/\omega_0|\sim|\omega_0\tau_{NL}|^{-1}\ll 1$ as in the case of DAWs excited by EPs (cf. Sec. II.E), transport processes are dominated by wave-particle resonant interactions (White *et al.*, 1983, 2010a, 2010b) and by the evolution of phase-space ZS (cf. Sec. IV.D). Nonlinear wave-wave couplings and wave-particle interactions for DAW excited by EPs are historically considered separately, for simplicity and clarity of the analysis. However, noting that the existence of the SAW continuous spectrum could lead to the excitation of short-wavelength modes via resonant mode conversion of longer scale lengths excited by EPs, EPs could then act as mediators of cross-scale couplings (Zonca, 2008; Zonca and Chen, 2008)[13] and play a unique role in determining complex behavior in burning plasmas (see also Secs. IV.E and VI.B). Thus, a comprehensive understanding of the nonlinear physics of DAW instabilities excited by EPs would require a self-consistent treatment of both nonlinear wave-wave and wave-particle interactions and is beyond the scope of this review. Here, we mainly focus on nonlinear dynamics of single-n modes[14] and separate the analysis of wave-wave and wave-particle nonlinear interactions in order to delineate more clearly the underlying physics mechanisms.

B. Nonlinear shear Alfvén waves in uniform plasmas

Let us first explore the simple limit of an infinite, uniform plasma with $\boldsymbol{B}_0=B_0\hat{\boldsymbol{z}}$. Within the generally valid approximation of the quasineutrality condition and $m_i\gg m_e$, we have the following one-fluid equation of motion:

$$\varrho_m(\partial_t+\boldsymbol{u}\cdot\nabla)\boldsymbol{u}=-\nabla\cdot\boldsymbol{P}+\boldsymbol{j}\times\boldsymbol{B}/c, \tag{4.4}$$

where $\varrho_m=\sum_j n_j m_j\simeq n_i m_i$ and $\boldsymbol{u}\simeq\boldsymbol{u}_i$. Equation (4.4) is readily obtained from Eq. (2.14) decomposing the stress tensor as pressure and Reynolds stress, as usual, i.e., defining $\mathcal{P}\equiv\boldsymbol{P}+\varrho_m\boldsymbol{u}\boldsymbol{u}$. Letting $\boldsymbol{u}=\boldsymbol{u}_0+\delta\boldsymbol{u}$, etc., and noting $\boldsymbol{u}_0=\boldsymbol{j}_0=0$, Eq. (4.4) becomes

$$(\varrho_{m0}+\delta\varrho_{m0})(\partial_t+\delta\boldsymbol{u}\cdot\nabla)\delta\boldsymbol{u}=-\nabla\cdot\delta\boldsymbol{P}+\delta\boldsymbol{j}\times\boldsymbol{B}/c. \tag{4.5}$$

We further assume that SAW and CAW frequencies are well separated ($|\nabla_\perp|\gg|\nabla_\parallel|$) and $\beta\ll 1$. Thus, Eqs. (2.7) and (2.8) apply and only dynamics of SAW and ISW are kept. If we now further make the crucial assumption that all the interacting waves are SAWs, which are nearly incompressible, we then have $\nabla\cdot\delta\boldsymbol{u}\simeq 0$ and $\delta\varrho_m\simeq 0$, $\delta\boldsymbol{P}\simeq 0$. Then, Eq. (4.5) becomes

$$\varrho_{m0}\partial_t\delta\boldsymbol{u}=\boldsymbol{F}_p^{(2)}+\delta\boldsymbol{j}\times\boldsymbol{B}_0/c, \tag{4.6}$$

where the nonlinear ponderomotive force $\boldsymbol{F}_p^{(2)}$ is defined as

[13]This aspect was recently explored by Qiu, Zonca, and Chen (2012) in connection with the analysis of radial structures of EP-driven geodesic acoustic modes (Berk *et al.*, 2006; Fu, 2008).

[14]Note that, in toroidal geometry, this corresponds anyhow to many coupled poloidal Fourier harmonics in Eq. (3.23) and, due to nonlinear interactions, to the coupling of different radial states (not necessarily eigenstates) of the same toroidal mode n.

$$\boldsymbol{F}_p^{(2)} = \delta\boldsymbol{j}\times\delta\boldsymbol{B}/c - \varrho_{m0}\delta\boldsymbol{u}\cdot\nabla\delta\boldsymbol{u} = -\nabla(\delta B)^2/(8\pi) - \boldsymbol{Mx} - \boldsymbol{Re},$$

and

$$\boldsymbol{Mx} = -(\delta\boldsymbol{B}\cdot\nabla)\delta\boldsymbol{B}/(4\pi) \simeq -(\delta\boldsymbol{B}_\perp\cdot\nabla)\delta\boldsymbol{B}_\perp/(4\pi),$$
$$\boldsymbol{Re} = \varrho_{m0}(\delta\boldsymbol{u}\cdot\nabla)\delta\boldsymbol{u} \simeq \varrho_{m0}(\delta\boldsymbol{u}_\perp\cdot\nabla)\delta\boldsymbol{u}_\perp, \tag{4.7}$$

are, respectively, the divergence of Maxwell and Reynolds stresses. The approximations are justified since $\beta \ll 1$ and $|\nabla_\perp| \gg |\nabla_\parallel|$; both $\delta B_\parallel$ and $\delta u_\parallel$ are, hence, suppressed here. Equation (4.6) may be regarded as the basic equation for SAW interactions subject to the above constraints.

Equation (4.6) gives $\delta\boldsymbol{j}_\perp$ as

$$\delta\boldsymbol{j}_\perp = \delta\boldsymbol{j}_\perp^{(1)} + \delta\boldsymbol{j}_\perp^{(2)}, \tag{4.8}$$

where $\delta\boldsymbol{j}_\perp^{(1)} = (c/B_0)\boldsymbol{b}\times\varrho_{m0}\partial_t\delta\boldsymbol{u}_\perp$ is the polarization current, and $\delta\boldsymbol{j}_\perp^{(2)}$ is the nonlinear current

$$\delta\boldsymbol{j}_\perp^{(2)} = -(c/B_0)\boldsymbol{b}\times\boldsymbol{F}_p^{(2)}. \tag{4.9}$$

For SAW dynamics, Eqs. (2.12) and (2.13), $\nabla^2\delta A_\parallel \simeq \nabla_\perp^2\delta A_\parallel = -(4\pi/c)\delta j_\parallel$, yield the following vorticity equation:

$$(\boldsymbol{b}\cdot\nabla)(-c/4\pi)\nabla_\perp^2\delta A_\parallel + \nabla_\perp\cdot\delta\boldsymbol{j}_\perp = 0, \tag{4.10}$$

where $\delta\boldsymbol{B} = \nabla\times\delta\boldsymbol{A}$, $\delta\boldsymbol{E} = -(\nabla\delta\phi + \partial_t\delta\boldsymbol{A}/c)$, and $\delta\boldsymbol{A} \simeq \delta A_\parallel\boldsymbol{b}$. Thus, we have $\delta\boldsymbol{E}_\perp \simeq -\nabla_\perp\delta\phi$ and $\delta E_\parallel = -\boldsymbol{b}\cdot\nabla\delta\phi - \partial_t\delta A_\parallel/c$. Adopting the flux function $\delta\psi$ defined in Eq. (2.31), Eq. (4.10) can be written as

$$(c^2/4\pi)(\boldsymbol{b}\cdot\nabla)^2\nabla_\perp^2\delta\psi + \partial_t(\nabla_\perp\cdot\delta\boldsymbol{j}_\perp) = 0. \tag{4.11}$$

We now make the final MHD approximations,

$$\delta\boldsymbol{u}_\perp \simeq (c/B_0)\delta\boldsymbol{E}_\perp\times\boldsymbol{b} = (c/B_0)\boldsymbol{b}\times\nabla_\perp\delta\phi, \tag{4.12}$$

and

$$\delta E_\parallel = -\boldsymbol{b}\cdot\nabla(\delta\phi - \delta\psi) \simeq 0. \tag{4.13}$$

Equation (4.11) then becomes

$$c^2[(\boldsymbol{b}\cdot\nabla)^2 - v_A^{-2}\partial_t^2]\nabla_\perp^2\delta\phi + 4\pi\partial_t[\nabla\cdot\delta\boldsymbol{j}_\perp^{(2)}] = 0, \tag{4.14}$$

and

$$\nabla\cdot\delta\boldsymbol{j}_\perp^{(2)} = -(c/B_0)\boldsymbol{b}\cdot\nabla\times(\boldsymbol{Re} + \boldsymbol{Mx}). \tag{4.15}$$

Equation (4.15) has the interesting properties that $\nabla_\perp\cdot\delta\boldsymbol{j}_\perp^{(2)} = 0$ if $\boldsymbol{Re} + \boldsymbol{Mx} = 0$ or

$$\delta\boldsymbol{u}_{\perp w}/v_A = \pm\delta\boldsymbol{B}_{\perp w}/B_0. \tag{4.16}$$

Equation (4.16) is the Walén relation (Walén, 1944). In terms of $\delta\phi$ and $\delta A_\parallel$, we have

$$\delta\phi_w/v_A = \pm\delta A_{\parallel w}/c$$

or

$$\partial_t(\delta\phi_w/v_A) = \mp(\boldsymbol{b}\cdot\nabla)\delta\psi_w = \mp(\boldsymbol{b}\cdot\nabla)\delta\phi_w. \tag{4.17}$$

Equation (4.17) thus demonstrates that given the Walén relation, Eq. (4.16),

$$[(\boldsymbol{b}\cdot\nabla)^2 - v_A^{-2}\partial_t^2]\delta\phi_w = 0, \tag{4.18}$$

and Eq. (4.14) is self-consistently satisfied regardless of the magnitude of $\delta\phi_w$ and δA_w or $\delta\boldsymbol{u}_{\perp w}$ and $\delta\boldsymbol{B}_{\perp w}$. This is the celebrated Alfvénic state (Alfvén, 1942, 1950; Walén, 1944; Elsasser, 1956; Hasegawa and Sato, 1989). That is, a purely copropagating $[\partial_t + (\boldsymbol{b}\cdot\nabla)]\delta\phi_{w+} = 0$ or counterpropagating $[\partial_t - (\boldsymbol{b}\cdot\nabla)]\delta\phi_{w-} = 0$ finite-amplitude SAW is a self-consistent solution to the nonlinear SAW equation (4.14). Nonlinear interactions thus can occur only among oppositely propagating SAWs. There exists a vast amount of literature [see, e.g., Biskamp (1993)] investigating the consequences of such interactions within the incompressibility and ideal MHD assumptions, and we will not go into details here. Instead, this paper focuses on effects relevant to fusion plasmas, which break the constraints leading to the existence of Alfvénic states. More specifically, in the following sections, we investigate nonlinear SAW dynamics including effects of finite compressibility, ion Larmor radii, and geometries.

1. Effects of finite ion compressibility

By relaxing the incompressibility constraints, it was first shown by Sagdeev and Galeev (1969) that a SAW can parametrically decay into an ISW and a backscattered SAW. Specifically, let us consider the three-wave interactions among the pump SAW $\Omega_0 = (\omega_0, \boldsymbol{k}_0)$, the daughter ISW $\Omega_s = (\omega_s, \boldsymbol{k}_s)$, and the lower-sideband SAW $\Omega_- = (\omega_-, \boldsymbol{k}_-)$, where $\omega_- = \omega_s - \omega_0$ and $\boldsymbol{k}_- = \boldsymbol{k}_s - \boldsymbol{k}_0$. Note that, in the Ω_s mode, the dynamics is predominantly along $\boldsymbol{B}_0$. One can then show that the dominant nonlinear effect of SAW on the Ω_s mode enters via the parallel ponderomotive force, i.e.,

$$\boldsymbol{b}\cdot(\delta\boldsymbol{j}_\perp\times\delta\boldsymbol{B}_\perp)_s/c = -\nabla_\parallel(\delta B_\perp^2)_s/(8\pi) = -n_0e\nabla_\parallel\delta\phi_{ps}, \tag{4.19}$$

$\delta\boldsymbol{B}_\perp = \sum_{\boldsymbol{k}}\delta\boldsymbol{B}_{\boldsymbol{k}\perp}\exp(-i\omega_{\boldsymbol{k}}t + i\boldsymbol{k}\cdot\boldsymbol{x})$, $(\delta B_\perp^2)_s = \delta\boldsymbol{B}_{0\perp}\cdot\delta\boldsymbol{B}_{-\perp}$, and $\delta\phi_{ps}$ is the corresponding ponderomotive potential. That is,

$$\varrho_{m0}(-i\omega_s)\delta u_{\parallel s} = -ik_{s\parallel}(\delta P_s + \delta\boldsymbol{B}_{0\perp}\cdot\delta\boldsymbol{B}_{-\perp}/8\pi). \tag{4.20}$$

Applying the equation of state, we have $\delta P_s = (\gamma_e T_e + \gamma_i T_i)\delta n_s \equiv T\delta n_s$. The continuity equation $n_0 k_{s\parallel}\delta u_{\parallel s} = \omega_s\delta n_s$ then yields

$$\omega_s^2\epsilon_s\delta\varrho_{ms} = k_{s\parallel}^2\delta\boldsymbol{B}_{0\perp}\cdot\delta\boldsymbol{B}_{-\perp}/(8\pi) \tag{4.21}$$

and, with $c_s^2 \equiv T/m_i$,

$$\epsilon_s = 1 - k_{s\parallel}^2 c_s^2/\omega_s^2. \tag{4.22}$$

As to the Ω_- SAW sideband, the dominant coupling effect to Ω_s is via $\delta\varrho_{ms}$ in the polarization current, i.e.,

$$\begin{aligned}\delta \boldsymbol{j}_{\perp -}^{(2)} &= (c/B_0)\boldsymbol{b}\times[\delta\varrho_{ms}\partial_t\delta\boldsymbol{u}_\perp]_- \\ &= (c/B_0)\delta\varrho_{ms}(i\omega_0)\boldsymbol{b}\times\delta\boldsymbol{u}_{\perp 0}^*.\end{aligned} \tag{4.23}$$

The vorticity equation (4.14), for the Ω_- mode, then becomes

$$\epsilon_{A-}k_{-\perp}^2\delta\phi_- = (\delta\varrho_{ms}/\varrho_{m0})(\boldsymbol{k}_{0\perp}\cdot\boldsymbol{k}_{-\perp})\delta\phi_0^*, \tag{4.24}$$

where

$$\epsilon_{A-} = 1 - k_{-\parallel}^2 v_A^2/\omega_-^2, \tag{4.25}$$

and we noted $\delta\phi_{0,-} \simeq \delta\psi_{0,-}$. Equation (4.21) along with Eq. (4.24) then yields the following parametric dispersion relation:

$$\epsilon_s\epsilon_{A-} = \frac{1}{2}k_{0\perp}^2\rho_s^2\cos^2\theta_c\left(\frac{k_{-\parallel}}{k_{0\parallel}}\right)|\Phi_0|^2, \tag{4.26}$$

where $\Phi_0 = e\delta\phi_0/T$, $\rho_s = c_s/\Omega_i$, and θ_c is the angle between $\boldsymbol{k}_{0\perp}$ and $\boldsymbol{k}_{-\perp}$. For resonant decays, we have $\omega_s = i\gamma + \omega_{sr}$, $\omega_{sr} = k_{s\parallel}c_s$, $\omega_- = i\gamma + (\omega_{sr} - \omega_0)$, $\omega_0 - \omega_{sr} = |k_{-\parallel}|v_A$, and Eq. (4.26) then reduces to

$$\frac{\gamma^2}{\omega_0\omega_{sr}} = \frac{1}{8}k_{0\perp}^2\rho_s^2\cos^2\theta_c\left(\frac{k_{-\parallel}}{k_{0\parallel}}\right)|\Phi_0|^2. \tag{4.27}$$

Equation (4.27) shows that instability sets in when $k_{0\parallel}/k_{-\parallel} > 0$. Since $|\omega_0| \gg |\omega_s|$, we have $|\omega_-| \simeq \omega_0$, $k_{-\parallel} = k_{s\parallel} - k_{0\parallel} \simeq k_{0\parallel}$, or $k_{s\parallel} \simeq 2k_{0\parallel}$, and meanwhile, $\omega_-/k_{-\parallel} \simeq -v_A$, i.e., the parallel phase velocity of the lower-sideband SAW is opposite to that of the pump wave. Equation (4.27) also shows that the parametric instability maximizes around $\theta_c = 0$, i.e., $\boldsymbol{k}_{-\perp}$ aligns with $\boldsymbol{k}_{0\perp}$. This carries a significant implication to the transport process induced by the SAW turbulence (cf. Sec. IV.B.2). Note also that including damping of the SAW sideband and ISW in Eq. (4.27) would lead to a threshold in $|\Phi_0|$.

For fusion plasmas, we have typically $T_e \sim T_i$ and the ISW becomes a quasimode due to significant ion Landau damping. In this case, we need to treat ions kinetically and the corresponding parametric decay process becomes a nonresonant decay via nonlinear ion Landau damping (Sagdeev and Galeev, 1969; Cohen and Dewar, 1974; Kulsrud, 1978). Since nonlinearities enter via ion dynamics only, for the Ω_s ion sound wave, we have $\delta n_{se}/n_0 = e\delta\phi_s/T_e$ with $\delta\phi_s$ being the self-consistent electrostatic potential, and

$$\delta n_{si}/n_0 = -e\chi_{is}(\delta\phi_s + \delta\phi_{ps}). \tag{4.28}$$

Here $\delta\phi_{ps}$ is given by Eq. (4.19) and

$$\begin{aligned}\chi_{is} &= (1/T_i)\langle F_{0i}k_{s\parallel}v_\parallel/(k_{s\parallel}v_\parallel - \omega_s)\rangle_v \\ &= (1/T_i)[1 + \xi_s Z(\xi_s)],\end{aligned} \tag{4.29}$$

$\langle\cdots\rangle_v$ denotes $\int d\boldsymbol{v}(\cdots)$, F_{0i} is taken to be Maxwellian, $Z(\xi_s)$ is the plasma dispersion function [see, e.g., Stix (1992)], $\xi_s = \omega_s/|k_{s\parallel}|v_{ti}$ and $v_{ti} = (2T_i/m_i)^{1/2}$. The quasineutrality condition then gives

$$\epsilon_{sk}\delta\phi_s = -T_e\chi_{is}\delta\phi_{ps}, \tag{4.30}$$

where

$$\epsilon_{sk} = 1 + T_e\chi_{is}. \tag{4.31}$$

Equations (4.19) and (4.30) then yield

$$\epsilon_{sk}\frac{\delta\varrho_{ms}}{\varrho_{m0}} = -\frac{\chi_{is}}{8\pi n_0}\delta\boldsymbol{B}_{0\perp}\cdot\delta\boldsymbol{B}_{-\perp}. \tag{4.32}$$

Note that for $|\omega_s| \gg |k_{s\parallel}v_{ti}|$ Eq. (4.32) recovers the fluid result of Eq. (4.21) with $c_s^2 = T_e/m_i$.

Substituting Eq. (4.32) into Eq. (4.24), with $\Phi_0 \equiv e\delta\phi_0/T_e$, and proceeding as in the previous one-fluid analysis, one readily derives the following parametric decay dispersion relation:

$$\epsilon_{sk}\epsilon_{A-} = -\frac{1}{2}T_e\chi_{is}k_{0\perp}^2\rho_s^2\cos^2\theta_c\left(\frac{k_{-\parallel}}{k_{0\parallel}}\right)|\Phi_0|^2. \tag{4.33}$$

While Ω_s is a quasimode since $|\mathrm{Im}\epsilon_{sk}| \sim O(1)$, Ω_- remains a normal mode. Thus, let $\omega_- = \omega_{-r} + i\gamma$ and $\omega_{-r} = \omega_{sr} - \omega_0 = |k_{-\parallel}|v_A$; the imaginary part of Eq. (4.33) then yields, noting $T_e\chi_{is} = \epsilon_{sk} - 1$,

$$\frac{2\gamma}{\omega_0} = \frac{1}{2}k_{0\perp}^2\rho_s^2\cos^2\theta_c\left(\frac{k_{-\parallel}}{k_{0\parallel}}\right)\frac{T_e\mathbb{I}\mathrm{m}\chi_{is}}{|\epsilon_{sk}|^2}|\Phi_0|^2, \tag{4.34}$$

where, from Eq. (4.29),

$$\begin{aligned}\mathbb{I}\mathrm{m}\chi_{is} &= (1/T_i)\mathbb{I}\mathrm{m}[\xi_s Z(\xi_s)] \\ &\simeq (\pi/T_i)\omega_{sr}\langle F_{0i}\delta(k_{s\parallel}v_\parallel - \omega_{sr})\rangle_v.\end{aligned} \tag{4.35}$$

Thus, the nonresonant decay maximizes around $|\omega_{sr}| = |\omega_0 + \omega_{-r}| \approx |k_{s\parallel}v_{ti}| = |k_{0\parallel} + k_{-\parallel}|v_{ti}$. Since $|\omega_0| \simeq |\omega_{-r}| \gg |k_\parallel v_{ti}|_{0,-}$, maximal interaction requires $k_{0\parallel}k_{-\parallel} > 0$, i.e., $k_{-\parallel} \simeq k_{0\parallel}$, $k_{s\parallel} \simeq 2k_{0\parallel}$, and $\omega_-/k_{-\parallel} \simeq -v_A$, similar to resonant decay. Furthermore, from Eqs. (4.34) and (4.35), the decay instability ($\gamma > 0$) occurs when $\omega_{sr} > 0$, i.e., $|\omega_{-r}| = |\omega_{sr} - \omega_0| < \omega_0$; that is, the parametrically excited lower-sideband SAW has a real frequency lower than ω_0, $|\omega_{-r}| \simeq \omega_0 - 2k_{0\parallel}v_{ti}$, and a parallel phase velocity opposite to that of the pump wave. Again, including finite damping of the SAW sideband and ISW would lead to a threshold in $|\Phi_0|$.

We note that the current analysis has assumed (Chen and Zonca, 2011, 2013)

$$|k_\perp\rho_s|_{0,-}^2 < |\omega_0/\Omega_i| \ll 1. \tag{4.36}$$

Equation (4.36) is the same condition derived in Sec. II.C, discussing the transition between nonlinear (MHD) dynamics dominated by the polarization response to a regime where dominant nonlinear (gyrokinetic) interactions are due to the

pressure stress tensor (cf. the introduction to Sec. IV) and Maxwell stress. Thus, for SAWs with $|k_\perp\rho_s| > |\omega_0/\Omega_i|^{1/2} \sim \mathcal{O}(10^{-1})$ typically we need to employ the nonlinear gyrokinetic equation (2.23), and the parametric decay processes are significantly altered both quantitatively and qualitatively (cf. Sec. IV.B.2).

2. Parametric decays of kinetic Alfvén waves

We now consider three-wave interactions among Ω_0, Ω_s, and Ω_- with $\beta \ll 1$ as in Sec. IV.B.1, but $|k_\perp\rho_i|$ formally of $\mathcal{O}(1)$. Here we sketch only the derivations and refer to Chen and Zonca (2011) for details. Following Frieman and Chen (1982), we can adopt the nonlinear gyrokinetic theoretical framework of Sec. II.D. Thus, assuming that both electrons and ions have $\bar{F}_0 = F_M \equiv n_0 F_0$, with F_0 taken to be Maxwellian, Eq. (2.21) yields

$$\delta f = -(e/T)F_M\delta\phi + \exp(-\boldsymbol{\rho}\cdot\boldsymbol{\nabla})\delta g, \tag{4.37}$$

while Eq. (2.23) for δg becomes

$$(\partial_t + v_\parallel \boldsymbol{b}\cdot\boldsymbol{\nabla} + \langle\delta\boldsymbol{u}_{Eg}\rangle\cdot\boldsymbol{\nabla})\delta g = (e/T)F_M\partial_t\langle\delta L_g\rangle. \tag{4.38}$$

Here we introduced the notation $\langle\delta\boldsymbol{u}_{Eg}\rangle = (c/B_0)\boldsymbol{b}\times\boldsymbol{\nabla}\langle\delta L_g\rangle$. In terms of Fourier modes, Eq. (4.38) can be expressed as

$$\begin{aligned} &i(k_\parallel v_\parallel - \omega_k)\delta g_k - (c/B_0)\Lambda_{k'}^{k''}[\langle\delta L_g\rangle_{k'}\delta g_{k''} - \langle\delta L_g\rangle_{k''}\delta g_{k'}] \\ &\quad = -i\omega_k(e/T)F_M\langle\delta L_g\rangle_k, \end{aligned} \tag{4.39}$$

where $\Lambda_{k'}^{k''} \equiv \boldsymbol{b}\cdot(\boldsymbol{k}'_\perp\times\boldsymbol{k}''_\perp)$. Meanwhile, the quasineutrality condition, Eq. (2.28), becomes

$$(1+T_i/T_e)\delta\phi_k = (T_i/n_0e)\langle J_k\delta g_{ki} - \delta g_{ke}\rangle_{\boldsymbol{v}}, \tag{4.40}$$

where e stands for the (positive) electron charge, and the vorticity equation (2.26) can be written as

$$\begin{aligned} &ik_\parallel\delta j_{\parallel k} - i\frac{c^2}{4\pi}\frac{\omega_k k_\perp^2}{v_A^2 b_k}(1-\Gamma_k)\delta\phi_k \\ &\quad = -\Lambda_{k'}^{k''}\left(\delta A_{\parallel k'}\frac{\delta j_{\parallel k''}}{B_0} - \delta A_{\parallel k''}\frac{\delta j_{\parallel k'}}{B_0}\right) \\ &\qquad + \frac{ec}{B_0}\Lambda_{k'}^{k''}\langle[(J_kJ_{k'} - J_{k''})\delta L_{k'}\delta g_{k''i} \\ &\qquad - (J_kJ_{k''} - J_{k'})\delta L_{k''}\delta g_{k'i}]\rangle_{\boldsymbol{v}}, \end{aligned} \tag{4.41}$$

with $\delta j_{\parallel k} = (c/4\pi)k_\perp^2\delta A_{\parallel k}$. Here $\langle\delta L_g\rangle_k = J_k(\delta\phi - v_\parallel\delta A_\parallel/c)_k \equiv J_k\delta L_k$, $J_k = J_0(k_\perp\rho)$, and $\boldsymbol{k} = \boldsymbol{k}' + \boldsymbol{k}''$. Furthermore, $b_k = k_\perp^2\rho_i^2 = k_\perp^2(T_i/m_i)/\Omega_i^2$, $\Gamma_k = \langle J_k^2F_{0i}\rangle_{\boldsymbol{v}} = I_0(b_k)\exp(-b_k)$, I_0 is the modified Bessel function, and $|k_\perp\rho_e| \ll 1$ was assumed. On the right-hand side of Eq. (4.41) the first term represents the usual Maxwell stress, whereas the second term reduces to the well-known Reynolds stress for $k_\perp\rho_i \ll 1$. Noting the ordering $|k_\parallel v_{te}| \gg |\omega_k| \gg |k_\parallel v_{ti}|$, with v_{te} and v_{ti} denoting electron and ion thermal velocities, and defining $\delta\psi_k = (\omega\delta A_\parallel/ck_\parallel)_k$ from Eq. (2.31), we can readily recover the following linear KAW results (Hasegawa and Chen, 1975, 1976):

$$\delta\psi_k \simeq [1+\tau(1-\Gamma_k)]\delta\phi_k \equiv \sigma_k\delta\phi_k, \tag{4.42}$$

where $\tau = T_e/T_i$, and the KAW linear dispersion relation (cf. Sec. III.A)

$$\omega^2/(k_\parallel^2v_A^2) \simeq \sigma_k b_k/(1-\Gamma_k). \tag{4.43}$$

As to the excitation of ISW, Ω_s, by the two KAWs, Ω_0 and Ω_-, we note that due to the frequency ordering discussed in Sec. IV.B.1 Ω_s is predominantly an electrostatic mode. Equation (4.39) can then be used to calculate linear and nonlinear responses of δg_s for both electrons and ions. Substituting these results into the quasineutrality condition (4.40), we then obtain

$$\epsilon_{sK}\delta\phi_s = -i(c/B_0\omega_-)\Lambda_0^s\beta_1\delta\phi_-\delta\phi_0, \tag{4.44}$$

where

$$\epsilon_{sK} = 1+\tau+\tau\Gamma_s\xi_sZ(\xi_s), \tag{4.45}$$

$$\beta_1 = \tau F_1[1+\xi_sZ(\xi_s)] + \sigma_-\sigma_0, \tag{4.46}$$

ϵ_{sK} is the short-wavelength extension of ϵ_{sk} introduced in Eq. (4.31), $F_1 = \langle J_sJ_0J_-F_{0i}\rangle_{\boldsymbol{v}}$, J_s, J_0, J_- stand for $J_0(k_\perp\rho)$ computed at $k_{\perp s}, k_{\perp 0}, k_{\perp -}$, respectively, and we applied the corresponding linear KAW wave properties, noting that Ω_0 and Ω_- are normal modes.

Since Ω_s could be a heavily damped quasimode (cf. Sec. IV.B.1), we need to include both linear and nonlinear responses of δg_s in its coupling to Ω_- via Ω_0. The corresponding quasineutrality condition (4.40) then becomes

$$\delta\psi_- = [\sigma_- + \sigma_-^{(2)}]\delta\phi_- + D_1\delta\phi_s\delta\phi_0^*, \tag{4.47}$$

where σ_- is defined in Eq. (4.42),

$$\sigma_-^{(2)} = \left(\frac{c}{B_0\omega_-}\Lambda_0^s\right)^2\left[\tau[1+\xi_sZ(\xi_s)]\langle J_0^2J_-^2\rangle_i - \frac{k_{\parallel 0}}{k_{\parallel -}}\sigma_0^2\sigma_-\right]|\delta\phi_0|^2 \tag{4.48}$$

and

$$D_1 = -i(c/B_0\omega_-)\Lambda_0^s\tau[1+\xi_sZ(\xi_s)]F_1. \tag{4.49}$$

Proceeding in the same way, we may compute Eq. (4.41) for the KAW sideband. In this case, the Maxwell stress does not contribute to the nonlinear dynamics for Ω_s is a predominantly electrostatic mode. Thus, the parametric decay is mediated by the generalized Reynolds' stress in Eq. (4.41). Applying the results of δg_s derived earlier, we can obtain

$$\begin{aligned} &k_{\perp -}^2[(1-\Gamma_- + \alpha_-^{(2)})b_-^{-1}\delta\phi_- - (k_\parallel^2v_A^2/\omega^2)_-\delta\psi_-] \\ &\quad = (D_2/\rho_s^2)\delta\phi_s\delta\phi_0^*, \end{aligned} \tag{4.50}$$

where $\rho_s^2 = \tau\rho_i^2$ and $\alpha_-^{(2)}$ and D_2 are due to the nonlinear ion response

$$\alpha_-^{(2)} = (c/B_0\omega_-)^2\Lambda_0^{s2}[1+\xi_s Z(\xi_s)][\langle J_0^2 J_-^2 F_{0i}\rangle_{\boldsymbol{v}} - F_1]|\delta\phi_0|^2, \tag{4.51}$$

$$D_2 = i(c/B_0\omega_-)\Lambda_0^s\tau\{[1+\xi_s Z(\xi_s)]F_1 - \xi_s Z(\xi_s)\Gamma_s - \Gamma_0\}. \tag{4.52}$$

Combining Eqs. (4.47) and (4.50), we then obtain the following equation for the Ω_- KAW modified by the nonlinear coupling between Ω_s and Ω_0 modes:

$$b_{s-}(\epsilon_{AK-} + \epsilon_{AK-}^{(2)})\delta\phi_- = i(c/B_0\omega_-)\Lambda_0^s\beta_2\delta\phi_s\delta\phi_0^*, \tag{4.53}$$

where $b_{s-} = \tau b_-$,

$$\epsilon_{AK-} = [(1-\Gamma_-)/b_- - (k_\parallel^2 v_A^2/\omega^2)_-\sigma_-] \tag{4.54}$$

is the short-wavelength extension of Eq. (4.25),

$$\epsilon_{AK-}^{(2)} = [\alpha_-^{(2)}/b_- - (k_\parallel^2 v_A^2/\omega^2)_-\sigma_-^{(2)}], \tag{4.55}$$

and

$$\begin{aligned}\beta_2 &= \left(\frac{F_1}{\Gamma_s}\right)(\epsilon_{sK}-\sigma_s)\left[1-\left(\frac{k_\parallel^2 v_A^2}{\omega^2}\right)_- b_{s-}\right] - \epsilon_{sK} + \sigma_0 \\ &= [(\epsilon_{sK}-\sigma_s)F_1/\Gamma_s + \sigma_-(\sigma_0-\sigma_s)]/\sigma_- \\ &= \beta_1/\sigma_- - \epsilon_{sK}.\end{aligned} \tag{4.56}$$

Combining Eqs. (4.44) and (4.53), the resultant parametric instability dispersion relation becomes

$$\epsilon_{sK}(\epsilon_{AK-} + \Delta_{A-}^{(2)} + \chi_{A-}^{(2)}) = C_k|\Phi_0|^2, \tag{4.57}$$

where $\Phi_0 = e\delta\phi_0/T_e$, $C_k = (\lambda H)^2$,

$$\begin{aligned}\Delta_{A-}^{(2)} = &[(\sigma_s/\Gamma_s)(F_1^2/\Gamma_s - G) + (\sigma_- - 2F_1/\Gamma_s - \sigma_0 k_{\parallel 0}/k_{\parallel -})\sigma_0\sigma_- \\ &+ \sigma_0^2\sigma_-^2 k_{\parallel 0}/k_{\parallel -}]\lambda^2|\Phi_0|^2,\end{aligned} \tag{4.58}$$

$$\chi_{A-}^{(2)} = \epsilon_{sK}(\lambda^2/\Gamma_s)G|\Phi_0|^2, \tag{4.59}$$

$$\lambda^2 = (\Omega_i/\omega_0)^2\rho_s^4\Lambda_0^{s2}/(\sigma_- b_{s-}), \tag{4.60}$$

$$G = \langle J_0^2 J_-^2 F_{0i}\rangle_{\boldsymbol{v}} - F_1^2/\Gamma_s, \tag{4.61}$$

and

$$H = (\sigma_0\sigma_- - F_1\sigma_s/\Gamma_s). \tag{4.62}$$

Note also that, in Eq. (4.61), $G \geq 0$ from Schwartz inequality. On the left-hand side of Eq. (4.57), the $\Delta_{A-}^{(2)}$ term describes the nonlinear frequency shift only, while the contribution $\chi_{A-}^{(2)}$ accounts for processes involving resonant wave-particle interactions due to low-frequency nonlinear thermal ion response to Ω_0 and Ω_- KAW modes. Therefore, this process involves spectral transfer of fluctuation energy toward the low-frequency region and is generally referred to as nonlinear ion Compton scattering (Sagdeev and Galeev, 1969). Meanwhile, the nonresonant scatterings of Ω_0 off the fluctuations due to the Ω_s mode are described by the right-hand side, which thus accounts for shielded-ion scatterings. Ignoring nonlinear frequency shift and keeping terms relevant to the stability analysis, the resultant parametric dispersion relation becomes

$$\epsilon_{sK}(\epsilon_{AK-} + \chi_{A-}^{(2)}) = C_k|\Phi_0|^2. \tag{4.63}$$

The term $\chi_{A-}^{(2)}$ in Eq. (4.63) is absent in the previous drift-kinetic analysis (Hasegawa and Chen, 1975, 1976). This can be understood, since $|G| \sim \mathcal{O}(k_\perp^4\rho_i^4)$ for $|k_\perp\rho_i| \ll 1$ and the drift-kinetic analysis formally keeps only $\mathcal{O}(k_\perp^2\rho_i^2)$ terms. Meanwhile, for $|k_\perp\rho_i| \ll 1$, $H \simeq \tau(b_0 + b_- + \tau b_0 b_- - b_s)$, and the drift-kinetic results are recovered.

For $T_e \gtrsim 5T_i$, both Ω_s and Ω_- are weakly damped normal modes, and Eq. (4.63) yields the following resonant-decay dispersion relation:

$$(\gamma+\gamma_{dA-})(\gamma+\gamma_{ds}) = (\lambda H|\Phi_0|)^2\left[-\frac{\partial\epsilon_{sKr}}{\partial\omega_{sr}}\frac{\partial\epsilon_{AK-r}}{\partial\omega_{A-r}}\right]^{-1}, \tag{4.64}$$

where γ is the parametric growth rate, γ_{dA-} and γ_{ds} are, respectively, the linear damping rates of the KAW sideband and ISW, and ω_{A-r} and ω_{sr} are the corresponding normal mode frequencies, i.e., $\epsilon_{AK-r}(\omega_{A-r}) = 0$ and $\epsilon_{sKr}(\omega_{sr}) = 0$, $-\partial\epsilon_{AK-r}/\partial\omega_{A-r} \simeq 2(1-\Gamma_-)/(\omega_{0r}b_-)$ and $\partial\epsilon_{sKr}/\partial\omega_{sr} \simeq 2\sigma_s/\omega_{sr}$. Note that, similar to the Sec. IV.B.1 analysis for SAW, KAW parametric decay instability requires $\omega_{0r}\omega_s > 0$, i.e., $-\omega_{0r} < \omega_{A-r} < 0$, having chosen $\omega_{0r} > 0$ without loss of generality.

For $T_e \sim T_i$, Ω_s becomes a quasimode, while $\Omega_- \simeq -\Omega_A \equiv -(\omega_A, \boldsymbol{k}_A)$ remains a KAW normal mode. The growth rate of the parametric decay instability is then given by

$$\begin{aligned}(\gamma+\gamma_{dA-})\left(-\frac{\partial\epsilon_{AK-r}}{\partial\omega_{A-r}}\right) &= \mathbb{I}\mathrm{m}\left[\chi_{A-}^{(2)} - \frac{C_k}{\epsilon_{sK}}|\Phi_0|^2\right] \\ &= |\lambda\Phi_0|^2[G/\Gamma_s + H^2/|\epsilon_{sK}|^2]\mathbb{I}\mathrm{m}\epsilon_{sK},\end{aligned} \tag{4.65}$$

where again $G \geq 0$,

$$\mathbb{I}\mathrm{m}\epsilon_{sK} = \tau\Gamma_s\mathbb{I}\mathrm{m}[\xi_s Z_s(\xi_s)], \tag{4.66}$$

and $\xi_s = (\omega_0 - \omega_{Ar})/|k_{\parallel 0} - k_{\parallel A}|v_{ti}$. In Eq. (4.65), the G and H^2 terms correspond, respectively, to the nonlinear ion Compton and shielded-ion scatterings. Note that for $|k_\perp\rho_i| \sim \mathcal{O}(1)$, $G \sim H^2 \sim |\epsilon_{sK}|$, the two scattering processes are additive and have comparable magnitudes. Similar to previous studies (Sagdeev and Galeev, 1969; Hasegawa and Chen, 1976), Eq. (4.66) indicates that the scattering is maximized when $k_{\parallel 0}k_{\parallel A} < 0$, i.e., the backscattered KAW daughter wave (since $\omega_{0r}\omega_{Ar} > 0$), and $\gamma > 0$ requires $\xi_s > 0$, i.e., $\omega_0 > \omega_{Ar}$, or the parametric decay process leads to cascading in KAW frequencies. Note also that, while for $|k_\perp\rho_i| \ll 1$, γ increases with $|k_\perp|$, it decreases as $|k_\perp\rho_i|^{-1}$ for

$|k_\perp \rho_i| \gg 1$, and, thus, the decay processes tend to maximize around $|k_\perp \rho_i| \sim \mathcal{O}(1)$.

It is illuminating to compare the present results with those derived in Sec. IV.B.1. In fact, if in Eq. (4.63)

$$C_k = (\Omega_i/\omega_0)^2(\tau b_0/\sigma_-)H^2 \sin^2\theta_c \tag{4.67}$$

is replaced by

$$C_I = [\tau b_0/(\gamma_e + \gamma_i T_i/T_e)]\cos^2\theta_c, \tag{4.68}$$

one readily recovers Eq. (4.26) in the MHD limit. For $k_\perp \rho_i \sim \mathcal{O}(1)$, $H \sim \mathcal{O}(1)$, and $|C_k|/|C_I| \sim \mathcal{O}(\Omega_i^2/\omega_0^2) \gg 1$. In fact, for $|k_\perp \rho_i| < 1$, $\sigma_- \simeq 1$, $H \sim k_\perp^2 \rho_i^2 \tau$, and $|C_k|/|C_I| \sim (\Omega_i/\omega_0)^2 (k_\perp \rho_i)^4$, that is, consistent with the general discussion of Sec. II.C, the kinetic process dominates for $k_\perp^2 \rho_i^2 > |\omega_0/\Omega_i| \sim 10^{-2}$ typically. Thus, while the ideal MHD theory holds for $k_\perp^2 \rho_i^2 \ll 1$ in the linear physics description, it breaks down much earlier in nonlinear physics applications. Furthermore, C_k and C_I peak, respectively, at $\theta_c = \pi/2$ and $\theta_c = 0$. Thus, while the ideal MHD results predict KAWs are excited with $\boldsymbol{k}_{-\perp}$ parallel to the pump $\boldsymbol{k}_{0\perp}$, the kinetic excitation process shows that $\boldsymbol{k}_{-\perp}$ is predominantly perpendicular to $\boldsymbol{k}_{0\perp}$. This difference has significant qualitative implications to plasma transport induced by KAWs. More specifically, let the pump KAW be excited via resonant mode conversion and thus $\boldsymbol{k}_{0\perp} \simeq k_{0r}\boldsymbol{\nabla} r$. Ideal MHD theory would predict the KAW spectrum peaks along k_r with little k_θ components in the $\boldsymbol{b} \times \boldsymbol{\nabla} r$ direction and, hence, little radial transport. On the other hand, the kinetic theory predicts the KAW spectrum with significant k_θ components and, hence, significant radial plasma transport. These findings thus question the applicability of MHD based theories for realistic comparisons with experimental measurements and observations of Alfvénic fluctuation spectra and related transport even more severely than those stemming from accurate linear physics descriptions.

3. Nonlinear excitation of convective cells by kinetic Alfvén waves

Zonal structures, such as zonal flows, are known to play crucial roles in dynamically regulating plasma transport in tokamak plasmas. The analogs in uniform plasma are the convective cells, which have been extensively studied in the 1970s (Taylor and McNamara, 1971; Okuda and Dawson, 1973; Chu, Chu, and Ohkawa, 1978; Lin, Dawson, and Okuda, 1978) in the context of cross-field transport (Shukla *et al.*, 1984), especially with regard to potential applications to space plasmas. In particular, it is worthwhile mentioning the extensive studies of convective cells excitation by KAW in the context of the generation of turbulence flows in the upper ionosphere (Sagdeev, Shapiro, and Shevchenko, 1978).

As can be anticipated from previous discussions on the Alfvénic state, since SAWs participating in the ZS nonlinear generation are copropagating along $\boldsymbol{B}_0$, nontrivial finite nonlinear couplings have long been known to rely on deviations from the ideal MHD approximations. Nonetheless, previous theoretical analyses often rely on two limiting assumptions: (i) neglecting FLR corrections to the Reynolds stress, and (ii) decoupling between the electrostatic (ESCC, described by $\delta\phi_z$ only) and the magnetostatic (MSCC, described by $\delta A_{\parallel z}$ only) convective cells. Both assumptions, as will be shown, could lead to erroneous conclusions on the spontaneous excitation of convective cells by KAW.[15] The details of the analysis are complicated and, in the following, we simply demonstrate that one needs to employ the nonlinear gyrokinetic equation in order to properly account for the finite nonideal effects.

Let $\Omega_0 = (\omega_0, \boldsymbol{k}_0)$ be the pump KAW, $\Omega_z = (\omega_z, \boldsymbol{k}_z)$ be the zonal mode, and $\Omega_+ = (\omega_+, \boldsymbol{k}_+)$ and $\Omega_- = (\omega_-, \boldsymbol{k}_-)$ be the upper- and lower-sideband KAWs, respectively. Here we note that $|\omega_z| \simeq 0$, $\boldsymbol{k}_z \cdot \boldsymbol{b} = 0$, and $\omega_\pm = \omega_z \pm \omega_0$, $\boldsymbol{k}_\pm = \boldsymbol{k}_z \pm \boldsymbol{k}_0$. We also assume $\boldsymbol{k}_z \perp \boldsymbol{k}_{0\perp}$, which maximizes the nonlinear coupling. Let us first consider how the zonal mode is generated by KAWs. The vorticity equation (4.10) for the Ω_z mode is given by $\nabla_\perp \cdot \delta \boldsymbol{j}_{z\perp} = 0$, or

$$-i\omega_z \frac{c^2}{B_0^2}\varrho_{m0} k_z^2 \delta\phi_z = -\langle \nabla_\perp \cdot \delta \boldsymbol{j}_\perp^{(2)} \rangle_z, \tag{4.69}$$

where in terms of Fourier modes $\delta\phi_k$ and $\delta\psi_k \equiv (k_\parallel c/\omega_k)\delta A_{\parallel k}$ Eq. (4.15) becomes (Chen and Zonca, 2013)

$$\langle \nabla \cdot \delta \boldsymbol{j}_\perp^{(2)} \rangle_z = -\frac{1}{2}\left(\frac{c}{B_0}\right)^3 \varrho_{m0} \sum_{\boldsymbol{k}'+\boldsymbol{k}''=\boldsymbol{k}_z} \Lambda_{k'}^{k''}(k''^2_\perp - k'^2_\perp) \times \left[G_{k'}G_{k''}\delta\phi_{k'}\delta\phi_{k''} - \left(\frac{k'_\parallel v_A}{\omega_{k'}}\right)\left(\frac{k''_\parallel v_A}{\omega_{k''}}\right)\delta\psi_{k'}\delta\psi_{k''}\right], \tag{4.70}$$

$\Lambda_{k'}^{k''} = (\boldsymbol{k}'_\perp \times \boldsymbol{k}''_\perp)\cdot \boldsymbol{b}$ was defined in Sec. IV.B.2 and in the Reynolds stress, Eq. (4.7), we have

$$\delta \boldsymbol{u}_{\perp k} = i\frac{c}{B_0}(\boldsymbol{b} \times \boldsymbol{k}_\perp) G_k \delta\phi_k, \tag{4.71}$$

with G_k accounting for the ion FLR effects. In the small b_k limit, $G_{k'}G_{k''} \simeq 1 - (3/4)(b_{k'} + b_{k''})$, having used the notations of Sec. IV.B.2. Equation (4.70) provides the following illuminating perspectives in the long-wavelength ($|k_\perp \rho_i|, |k_\perp \rho_s| \to 0^+$) limit. First, we have $G_k \to 1$, and $\delta E_{\parallel k} \to 0$ for KAW, such that $\delta\phi_k = \delta\psi_k$. Meanwhile, $|\omega_k| \to |k_\parallel v_A|$. The same limiting behaviors apply for KAW pump and sideband modes. Now with $k''_\parallel = k_{z\parallel} - k'_\parallel$, $k_{z\parallel} = 0$, $\omega_{k''} = \omega_z - \omega_{k'}$, and $|\omega_z| \ll |\omega_k|$, we have $\boldsymbol{k}''_\parallel = -\boldsymbol{k}'_\parallel$ and $\omega_{k''} \simeq -\omega_{k'}$, and thus, $\langle \nabla \cdot \delta \boldsymbol{j}_\perp^{(2)} \rangle_z \to 0$ in this limit. This, in fact, can be expected since, in the $|k_\perp \rho_i| \to 0$ limit, $\boldsymbol{k}'$ and $\boldsymbol{k}''$ modes reduce to copropagating ideal MHD SAWs, which do not interact nonlinearly.

It is, therefore, clear that in order to nonlinearly generate $\delta\phi_z$ in uniform plasmas, one needs to introduce finite $|k_\perp \rho_i|$ effects, which, in turn, induce finite $\langle \nabla \cdot \delta \boldsymbol{j}_\perp \rangle_z$ by modifying the various terms mentioned previously. To properly take into account FLR corrections to the Reynolds stress, one needs to

[15] See, e.g., the recent analysis and summary of previous literatures on this topic given by Zhao *et al.* (2011).

employ the nonlinear gyrokinetic equation. Noting that, for the KAWs, we have $v_e \gg |\omega_k/k_\parallel| \gg v_i$ and $|\delta\psi_k| \sim |\delta\phi_k|$, Eq. (4.41) for the scalar potential $\delta\phi_z$ then becomes, in the $b_k \ll 1$ limit,

$$-i\omega_z b_z \delta\phi_z = \frac{c}{2B_0}\rho_i^2 \sum_{\boldsymbol{k}'+\boldsymbol{k}''=\boldsymbol{k}_z} \Lambda_{k'}^{k''}(k''^2_\perp - k'^2_\perp) \times \left\{ \delta\phi_{k'}\delta\phi_{k''}\left[1 - \frac{3}{4}(b_{k'} + b_{k''})\right] - \left(\frac{k'_\parallel v_A}{\omega_{k'}}\right)\left(\frac{k''_\parallel v_A}{\omega_{k''}}\right)\delta\psi_{k'}\delta\psi_{k''}\right\}, \tag{4.72}$$

where the b_k terms inside the angle bracket may be regarded as the ion FLR corrections to the Reynolds stress. Meanwhile, the equation governing the vector potential $\delta A_{z\parallel}$ can be derived from Eq. (2.30) and is given by

$$\delta A_{z\parallel} = (i/2) \sum_{\boldsymbol{k}'+\boldsymbol{k}''=\boldsymbol{k}_z} \Lambda_{k'}^{k''}(\delta A_{k'\parallel}\delta A_{k''\parallel}/k'_\parallel B_0). \tag{4.73}$$

For the KAW sidebands Ω_+ and Ω_- we have, from Eq. (4.40), noting $|\omega_k/k_\parallel| \ll v_e$ and again $b_k \ll 1$,

$$(1+\tau b_k)\delta\phi_k - \delta\psi_k = -i(c/B_0)\Lambda_{k_z}^{k''}(\delta\phi_{k''}/\omega_{k''}) \times (1+\tau b_0)(\delta\phi_z - \delta\psi_z), \tag{4.74}$$

where $\boldsymbol{k}=\boldsymbol{k}_\pm$, $\boldsymbol{k}''=\pm\boldsymbol{k}_0$, $\boldsymbol{k}=\boldsymbol{k}''+\boldsymbol{k}_z$, and $\delta\psi_z \equiv \omega_0\delta A_{z\parallel}/ck_{0\parallel}$. Furthermore, Eq. (4.41) can be shown to become

$$k_\perp^2[(1-3b_k/4)\delta\phi_k - (k_\parallel^2 v_A^2/\omega_k^2)\delta\psi_k] = i(c/B_0)\Lambda_{k_z}^{k''}(k''^2_\perp - k_z^2)(\delta\phi_{k''}/\omega_k) \times [(1-3b_0/4)(\delta\phi_z - \delta\psi_z) - (3/4)b_z\delta\phi_z]. \tag{4.75}$$

Equations (4.72)–(4.75) are the desired set of equations for Ω_+, Ω_-, and Ω_z coupled via Ω_0.

To analyze the modulational stability properties of Ω_z, we first note that Ω_0 is a normal KAW mode and thus $\epsilon_{AK0}=0$, where, consistent with Eq. (4.54),

$$\epsilon_{AKk} = 1 - (3/4)b_k - (k_\parallel^2 v_A^2/\omega_k^2)(1+\tau b_k) \tag{4.76}$$

is the KAW linear dielectric constant in the $b_k \ll 1$ limit. Letting $\omega_z = i\gamma_z$, we then have

$$\epsilon_{AK\pm} \simeq \pm[2\omega_0/(\omega_0 \pm i\gamma_z)^2][1-(3/4)(b_0+b_z)] \times (i\gamma_z \mp \Delta \mp \gamma_z^2/2\omega_0), \tag{4.77}$$

where $\Delta \simeq (\omega_0/2)(\tau+3/4)b_z$ is the frequency mismatch between ω_0 and the normal mode frequency of Ω_+ and Ω_-. Substituting Eqs. (4.74) and (4.75) into Eq. (4.72), taking Eq. (4.77) into account and noting that on the right-hand side of Eq. (4.72) $\boldsymbol{k}'=\boldsymbol{k}_-$ and $\boldsymbol{k}''=\boldsymbol{k}_0$ as well as $\boldsymbol{k}'=\boldsymbol{k}_+$ and $\boldsymbol{k}''=-\boldsymbol{k}_0$, we have

$$\delta\phi_z = -\alpha_\phi(\delta\phi_z - \delta\psi_z)/(\gamma_z^2+\Delta^2), \tag{4.78}$$

where

$$\alpha_\phi = \left|\frac{ck_zk_{0\perp}\delta\phi_0}{B_0}\right|^2 \frac{b_0[(\tau+3/4)(2b_0+b_z)]}{b_0+b_z}. \tag{4.79}$$

Similarly, Eq. (4.73) reduces to

$$\delta\psi_z = -\alpha_\psi(\delta\phi_z - \delta\psi_z)/(\gamma_z^2+\Delta^2), \tag{4.80}$$

where

$$\alpha_\psi = \left|\frac{ck_zk_{0\perp}\delta\phi_0}{B_0}\right|^2 \frac{b_0b_z(\tau+3/4)}{b_0+b_z}. \tag{4.81}$$

Equations (4.78) and (4.81) then yield the following dispersion relation for the modulational excitation of the Ω_z zonal mode:

$$1 = -(\alpha_\phi - \alpha_\psi)/(\gamma_z^2+\Delta^2). \tag{4.82}$$

Note that $\alpha_\phi - \alpha_\psi > 0$. Hence, $\gamma_z^2 = -\omega_z^2 < 0$ and KAW cannot spontaneously excite convective cells or zonal structures in the $b_k \ll 1$ limit regardless of the $\tau = T_e/T_i$ value (Chen and Zonca, 2013), consistent with some of the recent results by Zhao *et al.* (2011) and in contrast with the analyses of Onishchenko *et al.* (2004), Pokhotelov *et al.* (2004), and Mikhailovskii *et al.* (2007).

Equations (4.78) and (4.80) are, respectively, the generating equations for ESCC and MSCC. Thus, it is readily noted that they are excited by KAW simultaneously as $|\delta\psi_z/\delta\phi_z| = \mathcal{O}(1)$. Artificially assuming that $\delta\psi_z$ is suppressed yields the incorrect ESCC dispersion relation, Eq. (4.82) with $\alpha_\psi = 0$, but still the correct qualitative conclusion that ESCCs are not spontaneously excited by KAW in the long-wavelength limit. However, the analogous assumption that $\delta\phi_z$ is suppressed delivers the erroneous MSCC dispersion relation, Eq. (4.82) with $\alpha_\phi = 0$, as well as the erroneous claim that MSCC can be spontaneously excited by KAW for $b_k \ll 1$ [see, e.g., the discussion given by Zhao *et al.* (2011)].

C. Nonlinear mode coupling of shear Alfvén waves in toroidal plasmas

In this section, we illustrate how equilibrium geometry and plasma nonuniformity can contribute to breaking the Alfvénic state. As a counterpart of a "pump" SAW exciting a lower frequency "daughter" SAW via nonlinear Landau damping in a uniform plasma (cf. Sec. IV.B.1), Sec. IV.C.1 discusses TAE frequency cascading (Hahm and Chen, 1995). Similarly, Sec. IV.C.2 addresses the generation of ZS by finite-amplitude TAE (Spong, Carreras, and Hedrick, 1994; Todo, Berk, and Breizman, 2010; Chen and Zonca, 2012) as a toroidal geometry analog of convective cells generated by KAW (cf. Sec. IV.B.3). Particular emphasis is given on the importance of spontaneous versus forced generation of ZS (Chen and Zonca, 2012), given their potentially important self-regulatory roles on Alfvénic oscillations and, more broadly, on DAW turbulence.

As geometry effects importantly affect the SAW continuous spectrum (cf. Sec. III.B), Sec. IV.C.3 discusses how AE nonlinear effects modify the SAW continuum and, thereby, lead to enhanced continuum damping (Vlad *et al.*, 1992; Zonca *et al.*, 1995; Chen *et al.*, 1998). Finite-amplitude MHD activity can also yield to deformation of the SAW continuum, as illustrated in Sec. IV.C.4. However, due to a quasistatic helical deformation of the axisymmetric tokamak equilibrium, this effect may be destabilizing for BAEs (Marchenko and Reznik, 2009; Biancalani *et al.*, 2010a, 2010b, 2011).

1. Toroidal Alfvén eigenmode frequency cascading via nonlinear ion Landau damping

In uniform plasmas (Sec. IV.B), a pump SAW can parametrically excite a daughter SAW with a lower frequency and opposite parallel phase velocity via nonlinear ion Landau damping. Hahm and Chen (1995) applied this frequency cascading mechanism to the nonlinear saturation of TAE with high-n toroidal mode numbers. Because of realistic equilibrium profile variations, there in general exists $O(nq_a)$ TAEs with the same toroidal mode number n. Here q_a is the safety factor at the outmost flux surface. Thus, for $|nq_a| \gg 1/\epsilon = R_0/r$, many TAEs with different mode frequencies may exist within the frequency gaps.

Following Hahm and Chen (1995), let $\boldsymbol{k}'$ be the pump wave, $\boldsymbol{k}$ be the decay wave, and $\boldsymbol{k}'' = \boldsymbol{k} - \boldsymbol{k}'$ be the ISW and applying the parametric decay dispersion relation (4.34) to the wave intensity $I_k = \overline{|\nabla_\perp \phi_k|^2}$, where $\overline{(\cdots)}$ denotes appropriate averaging of $(\cdots)$ over the radial TAE mode structure, we can obtain the following wave-kinetic equation:

$$\frac{\partial}{\partial t} I_k = \gamma_L(\boldsymbol{k}) I_k - \sum_{k'} M_{k,k'} I_{k'} I_k, \tag{4.83}$$

where

$$M_{k,k'} = \frac{\omega'}{2} \frac{\mathbb{I}\mathrm{m}\chi_{is}}{|\epsilon_{sk}|^2} \frac{m_i}{B_0^2} \equiv \omega' V_s, \tag{4.84}$$

χ_{is} and ϵ_{sk} are defined by, respectively, Eqs. (4.29) and (4.31), with $\omega_{sr} = \omega - \omega'$ and $k_{s\|} = k_\| - k'_\|$, and we summed over all the $\boldsymbol{k}'$ pump modes. Now $M_{k,k'}$ has a maximum frequency interaction width $|\omega - \omega'| \simeq |2k'_\| v_{ti}| \sim v_{ti}/qR_0$ and thus if the adjacent TAE's frequency difference $|\Delta\omega| \sim |v_A/(nq^2R_0)|$ is smaller than v_{ti}/qR_0 or $\beta^{1/2} \gg |1/nq|$, we can replace the sum over $\boldsymbol{k}'$ by an integral over ω'; that is, Eq. (4.83) becomes

$$\frac{\partial}{\partial t} I(\omega) = \gamma_L(\omega) I(\omega) - I(\omega) \int_\omega^{\omega_M} d\omega' I(\omega') \omega' V_s(\omega - \omega'). \tag{4.85}$$

Here $I(\omega')$ is the continuum version of $\sum_{k'} I_{k'} \delta(\omega' - \omega_{k'})$, $\omega_M \simeq \omega_u$, the upper TAE gap accumulation point frequency, corresponds to the highest frequency of linearly unstable TAEs. Noting that $I(\omega)$ has a frequency width typically of the order of the frequency gap, $\sim \epsilon v_A/qR_0$, and $V_s(\omega'' = \omega - \omega')$ being an odd function in ω'' with an interacting width $\sim v_{ti}/qR_0$, we can expand the integrand about ω, assuming $\epsilon v_A/qR_0 > v_{ti}/qR_0$ or $\epsilon > \beta_i^{1/2}$, and render Eq. (4.85) into the following differential equation:

$$\frac{\partial}{\partial t} I(\omega) = \gamma_L(\omega) I(\omega) + I(\omega) U_1(\omega) \frac{\partial}{\partial \omega}(\omega I), \tag{4.86}$$

where (Hahm and Chen, 1995)

$$U_1(\omega) = \int_{\omega_M - \omega}^{\omega - \omega_1} (\omega - \omega') V_s(\omega - \omega') d\omega' \simeq \int_{-\infty}^{\infty} \omega'' V_s(\omega'') d\omega'' = \frac{\pi}{2} [(1+\tau) B_0 q R_0]^{-2} \equiv \bar{U}_1. \tag{4.87}$$

Here $\tau \equiv T_e/T_i$ and $\omega_1 \approx \omega_\ell$, the lower TAE gap accumulation point frequency, corresponds to the low-frequency end of $I(\omega)$. Note that $\gamma_L(\omega_1) < 0$ and $I(\omega_1) \simeq 0$. At saturation, $\partial I/\partial t = 0$; Eq. (4.86) then yields

$$I(\omega) \simeq (1/\omega) \int_\omega^{\omega_M} [\gamma_L(\omega')/\bar{U}_1] d\omega'. \tag{4.88}$$

Here the spectral transfer of the wave energy is toward the lower frequency, and we let $I(\omega) \simeq 0$ at the highest frequency end ω_M, i.e., $I(\omega)$ tends to peak away from ω_M. The corresponding overall magnetic fluctuation level $|\delta B_r/B_0| \simeq |ck_\theta \delta\phi/B_0 v_A|$ is then given by

$$\left|\frac{\delta B_r}{B_0}\right|^2 \simeq \left(\frac{k_\theta}{k_r}\right)^2 (1+\tau)^2 \frac{2/\pi}{\omega_A^2} \int_{\omega_1}^{\omega_M} \gamma_L(\omega) \ln\left(\frac{\omega}{\omega_1}\right), \tag{4.89}$$

where $\omega_A = v_A/qR_0$. Expanding $\omega = \omega_1 + (\omega - \omega_1)$, Eq. (4.89) gives the following estimate:

$$\left|\frac{\delta B_r}{B_0}\right|^2 \sim \frac{1}{2\pi} (1+\tau)^2 \left(\frac{\bar{\gamma}_L}{\omega_A}\right) \epsilon^2 \epsilon_{\mathrm{eff}}^2, \tag{4.90}$$

with $\epsilon_{\mathrm{eff}} = 1 - \omega_1/\omega_M$, $\bar{\gamma}_L$ is a typical value of $\gamma_L(\omega)$ and having noted $|k_\theta/k_r| \sim \epsilon$. Quantitatively, with the estimate $|\bar{\gamma}_L/\omega_A| \lesssim O(10^{-2})$, $\epsilon_{\mathrm{eff}} \sim \epsilon \sim 10^{-1}$, and $\tau \lesssim 1$, Eq. (4.90) yields a saturation amplitude at $|\delta B_r/B_0| \lesssim 10^{-3}$.

2. Nonlinear excitation of zonal structures by toroidal Alfvén eigenmodes

Since ZS varies predominantly only radially, the self-regulation of DWT and DAW is achieved via spontaneous excitations of modulational instabilities, and consequently the damping of the driving instabilities via scatterings to the short-radial wavelength stable domain (Chen, Lin, and White, 2000). However, while zonal electric fields and corresponding zonal flows are widely measured in experiments with properties that are consistent with the general theoretical framework (Diamond *et al.*, 2005), zonal magnetic fields and currents predicted theoretically (Chen *et al.*, 2001; Guzdar, Kleva, Das, and Kaw, 2001; Gruzinov *et al.*, 2002; Diamond *et al.*, 2005) have only recently been observed in experiments in the compact helical system (CHS) (Fujisawa *et al.*, 2007).

As TAE plays crucial roles in the SAW instabilities in burning fusion plasmas, it is thus important to understand and assess the possible roles of ZS on the nonlinear dynamics of

TAE. First numerical analyses of this problem were reported by Spong, Carreras, and Hedrick (1994). More recently, numerical simulation results by Todo, Berk, and Breizman (2010) showed that ZS may be force driven by finite-amplitude TAE, while the importance of spontaneous versus forced generation of ZS was emphasized by Chen and Zonca (2012) (cf. Sec. IV).

We follow the theoretical approach of Chen, Lin, and White (2000) and Chen *et al.* (2001), which is also adopted in Sec. IV.B for our treatment of convective cells generated by KAWs in uniform plasmas. Thus, we consider the nonlinear couplings among the pump TAE Ω_0, the upper- and lower-sideband TAEs Ω_+ and Ω_-, and the zonal mode Ω_z. We then have, for example, $\delta\phi = \delta\phi_A + \delta\phi_z$ and $\delta\phi_A = \delta\phi_0 + \delta\phi_+ + \delta\phi_-$.

Assuming $|k_\perp\rho_i|^2 \sim |k_z\rho_s|^2 < \epsilon = r_0/R_0 < 1$, we adopt the ideal MHD approximation and obtain from the vorticity equation of the Ω_z mode Eq. (4.72),

$$-i\omega_z\chi_{iz}\delta\phi_z = -\frac{c}{B_0}k_z k_\theta k_z^2\rho_i^2\left\langle\left(1-\frac{k_{0\parallel}^2 v_A^2}{\omega_0^2}\right)\right\rangle_x (A_0^* A_+ - A_0 A_-), \tag{4.91}$$

where $\chi_{iz} \simeq 1.6q^2\epsilon^{-1/2}k_z^2\rho_i^2$ corresponds to the trapped-ion enhanced polarizability (Rosenbluth and Hinton, 1998), $k_\parallel = (x-j)/qR_0$, $\langle\cdots\rangle_x \equiv \int dx|\Phi_0|^2(\cdots)$, $\langle 1\rangle_x = 1$, $\Phi_0(x-j) = \delta\phi_{n0}(r; nq-m)$ describes the radial dependence of the mth poloidal harmonics [cf. Eq. (3.23)], and A_0 and $A_\pm$ are, respectively, amplitudes of the pump and sidebands. Noting that $|\Phi_0|^2(x)$ is localized at and even[16] with respect to $|x| = 1/2$ with a width $\Delta_x \sim O(\epsilon)$, Eq. (4.91) becomes

$$-i\omega_z\chi_{iz}\delta\phi_z = -(c/B_0)k_z k_\theta k_z^2\rho_i^2(1-\omega_A^2/4\omega_0^2)(A_0^* A_+ - A_0 A_-), \tag{4.92}$$

where $\omega_A = v_A/qR_0$. $\delta A_{z\parallel}$ or $\delta\psi_z \equiv \omega_0\delta A_{z\parallel}/ck_{0\parallel}$ is given by the weighted averaging $\langle\cdots\rangle_x$ of Eq. (4.73),

$$\delta\psi_z = i(ck_z k_\theta/\omega_0 B_0)(A_0^* A_+ + A_0 A_-). \tag{4.93}$$

Including the nonlinear correction to ideal MHD Ohm's law, the nonlinear vorticity equations for the $\Omega_\pm$ sidebands can be rendered into a set of differential-difference equations (Chen and Zonca, 2012), which after weighted averaging yields

$$A_\pm\epsilon_{A\pm}b_\pm = -2i\frac{c}{B_0}k_\theta k_z\omega_0 b_0\begin{pmatrix}A_0\\ A_0^*\end{pmatrix}(\delta\phi-\delta\psi)_z, \tag{4.94}$$

where $b_0 = \rho_i^2\langle|\nabla_0\Phi_0|^2\rangle_x$, $b_+ = \rho_i^2\langle|\nabla_+\Phi_0|^2\rangle = b_0 + b_z$, $b_z = k_z^2\rho_i^2$, and $b_- = b_+$. Meanwhile,

$$\epsilon_{A\pm} = \left(\frac{\omega_A^4}{\epsilon_0\omega^2}\Lambda_{T0}(\omega)D_0(\omega,k_z)\right)_{\omega=\omega_\pm}, \tag{4.95}$$

with $\epsilon_0 = 2(r/R_0 + \Delta')$, Δ' is the radial derivative of the Shafranov shift, $D_0(\omega,k_z) = -2\Gamma_- D(\omega,k_z)$, $\Gamma_\pm = (\omega^2/\omega_A^2)(1\pm\epsilon_0) - 1/4$, and $D(\omega,k_z)$ is the TAE dispersion function consistent with Eq. (3.30) in the notations introduced in Sec. III.C. Meanwhile, $\Lambda_{T0} = -2\Gamma_-\Lambda_T = (-\Gamma_+\Gamma_-)^{1/2}$, consistent with Eq. (3.14).[17] Solutions of $D_0(\omega,k_z) = 0$ are $\omega = \pm\omega_T(k_z)$, with the pump TAE frequency given by $\omega_0 = \omega_T(k_z = 0)$. In light of the general discussion of Sec. IV.A and Eq. (4.95), Eq. (4.94) can be considered as the implicit definition of $\propto \Lambda_n^{NL}$ term in Eq. (4.1), showing that the effect of ZS on TAE nonlinear dynamics results in a renormalization of the (sideband) inertia. This, in general, is also the case for other types of AEs (cf. Sec. IV.D.7).

Combining Eq. (4.94) with Eqs. (4.92) and (4.93) and letting $-i\omega_z = \gamma_z$ yield

$$\delta\phi_z = 2i\left(\frac{c}{B_0}k_\theta k_z\right)^2\frac{b_z}{\chi_{iz}}\left(1-\frac{\omega_A^2}{4\omega_0^2}\right)\times\frac{\omega_0 b_0}{\gamma_z b_+}|A_0|^2\left(\frac{1}{\epsilon_{A+}}-\frac{1}{\epsilon_{A-}}\right)(\delta\phi-\delta\psi)_z, \tag{4.96}$$

$$\delta\psi_z = 2\left(\frac{c}{B_0}k_\theta k_z\right)^2\frac{b_0}{b_+}|A_0|^2\left(\frac{1}{\epsilon_{A+}}+\frac{1}{\epsilon_{A-}}\right)\times(\delta\phi-\delta\psi)_z. \tag{4.97}$$

Noting that $D_0(\omega_\pm,k_z) = \pm(\partial D_0/\partial\omega_0)(i\gamma_z \mp \Delta_T)$, with $\Delta_T \equiv \omega_T(k_z) - \omega_0$, Eqs. (4.96) and (4.97) further reduce to, in analogy with Eqs. (4.78) and (4.80),

$$\begin{aligned}\delta\phi_z &= 2\left(\frac{c}{B_0}k_\theta k_z|A_0|\right)^2\left(\frac{\omega_0^2}{\omega_A^2}-\frac{1}{4}\right)\left(\frac{b_z}{\chi_{iz}}\right)\frac{b_0}{b_+}\frac{\epsilon_0}{\Lambda_{T0}(\omega_0)}\\ &\quad\times\frac{2\omega_0/\omega_A^2}{\partial D_0/\partial\omega_0}\frac{(\delta\phi-\delta\psi)_z}{\gamma_z^2+\Delta_T^2}\\ &\equiv -\alpha_{\phi T}\frac{(\delta\phi-\delta\psi)_z}{\gamma_z^2+\Delta_T^2},\end{aligned} \tag{4.98}$$

$$\begin{aligned}\delta\psi_z &= -2\left(\frac{c}{B_0}k_\theta k_z|A_0|\right)^2\left(\frac{b_0}{b_+}\right)\left(\frac{\Delta_T}{\omega_0}\right)\frac{\epsilon_0\omega_0^2/\omega_A^2}{\Lambda_{T0}(\omega_0)}\\ &\quad\times\frac{2\omega_0/\omega_A^2}{\partial D_0/\partial\omega_0}\frac{(\delta\phi-\delta\psi)_z}{\gamma_z^2+\Delta_T^2}\\ &\equiv -\alpha_{\psi T}\frac{(\delta\phi-\delta\psi)_z}{\gamma_z^2+\Delta_T^2}.\end{aligned} \tag{4.99}$$

Equations (4.98) and (4.99) then yield the following desired dispersion relation:

[16]This is valid strictly for TAEs near SAW continuum accumulation points. However, TAE mode structures have generally mixed parity (Zonca and Chen, 1993, 1996; Zonca, 1993a; Chen and Zonca, 1995). Here we strictly follow Chen and Zonca (2012) and assume $|\Phi_0|^2(x)$ is even, noting that the present analysis is readily generalized to mixed parity modes.

[17]Here we adopt the notations of Chen and Zonca (2012) and use D_0 and Λ_{T0}, symmetric with respect to lower and upper continuum accumulation points, rather than D and Λ_T that, for TAE, is the notation for Λ_n obtained from Eq. (3.14), having dropped the subscript n for simplicity.

$$\gamma_z^2 = \alpha_{\psi T} - \alpha_{\phi T} - \Delta_T^2, \tag{4.100}$$

i.e., instability will set in when

$$\left(\frac{c}{B_0\omega_0}k_\theta k_z|A_0|\right)^2 \frac{b_0}{b_+}\frac{\epsilon_0\omega_0^2/\omega_A^2}{\Lambda_{T0}(\omega_0)}\frac{4\omega_0/\omega_A^2}{\partial D_0/\partial\omega_0} \times\left[\frac{\Delta_T}{\omega_0}+\frac{b_z}{\chi_{iz}}\left(1-\frac{\omega_A^2}{4\omega_0^2}\right)\right] > \left(\frac{\Delta_T}{\omega_0}\right)^2. \tag{4.101}$$

Note that $|\Delta_T/\omega_0| \sim O(\epsilon_0)$ and $|b_z(1-\omega_A^2/4\omega_0^2)/\chi_{iz}| \sim O(\epsilon_0^{3/2}/q^2)$. Meanwhile, we typically have $\omega_0(\partial D_0/\partial\omega_0) > 0$ (Chen and Zonca, 2012). Thus, Eq. (4.101) becomes

$$\Delta_T/\omega_0 > 0 \tag{4.102}$$

and

$$\left(\frac{c}{B_0\omega_0}k_\theta k_z|A_0|\right)^2 \frac{b_0}{b_+}\frac{\epsilon_0\omega_0^2/\omega_A^2}{\Lambda_{T0}(\omega_0)}\frac{4\omega_0/\omega_A^2}{\partial D_0/\partial\omega_0} > \frac{\Delta_T}{\omega_0}. \tag{4.103}$$

This inequality essentially determines the condition for the spontaneous excitation of the zonal field $\delta\psi_z$, given by Eq. (4.99), which dominates over the usual zonal flow $\delta\phi_z$ because of the enhanced trapped-ion polarizability. The sign of Δ_T/ω_0 depends on the specific equilibria and plasma parameters and must be computed for individual cases. For the case of nearly circular plasmas with monotonic q profiles, $\Delta_T/\omega_0 < 0$ (Zonca and Chen, 1993; Zonca, 1993a), so that Eq. (4.102) is violated. However, Eq. (4.101) can still be satisfied for mode frequencies in the upper TAE gap, $\omega_0^2 > \omega_A^2/4$, and small $|\Delta_T/\omega_0|$, with $\delta\phi_z$ dominating over $\delta\psi_z$. Note that, especially when strongly driven by EPs, TAE modes tend to be characterized by $\omega_0^2 < \omega_A^2/4$. This may provide a plausible explanation for the numerical simulation results by Todo, Berk, and Breizman (2010), where the ZS response to TAE is found to be force driven rather than spontaneously excited (cf. Secs. IV.C.3 and IV.D.4).

In order to give a quantitative estimate for the onset condition of the modulational instability, Eq. (4.101), we recall that TAE linear stability analysis yields (Chen and Zonca, 2012)

$$\frac{\epsilon_0\omega_0^2/\omega_A^2}{\Lambda_{T0}(\omega_0)}\frac{4\omega_0/\omega_A^2}{\partial D_0/\partial\omega_0} \sim 1.$$

Thus, considering $b_z \lesssim k_\theta^2\rho_i^2 \sim \epsilon_0 b_0$ and $2qR_0k_{\|0} \simeq 1$, the threshold condition for spontaneous excitation of the most unstable zonal mode with $b_0 \sim \epsilon_0$ becomes

$$\left(\frac{c}{B_0\omega_0}k_\theta k_z|A_0|\right)^2 \sim \left|\frac{\Delta_T}{\omega_0}\right| \sim \epsilon_0\frac{b_z}{k_\theta^2\rho_i^2} \sim \frac{b_z}{\epsilon_0}, \quad \Leftrightarrow \left|\frac{\delta B_r}{B_0}\right|_{\rm th}^2 \sim \frac{\rho_i^2}{4\epsilon_0 q^2 R_0^2}. \tag{4.104}$$

For some typical tokamak parameters, this estimate yields $|\delta B_r/B_0|_{\rm th}^2 \sim \mathcal{O}(10^{-8})$, suggesting that spontaneous excitation of ZS may be a process effectively competing with other nonlinear dynamics in determining the saturation level of TAE and other AE modes if constraints specified below Eq. (4.103) can be satisfied.

Coherent nonlinear interactions of AE and ZS if spontaneously excited, in addition to playing important self-regulatory roles in AE nonlinear dynamics, could also influence fine structures of the AE frequency spectrum. These features in experimental observations [see, e.g., Fasoli *et al.* (1998) and the review by Breizman and Sharapov (2011)] are generally interpreted as evidence of modulation interactions due to wave-particle nonlinear dynamics (cf. Sec. IV.D.3). In principle, it should be possible to discriminate these different underlying nonlinear physics processes on the basis, e.g., of the different scaling of the frequency splitting with the "pump AE" amplitude, given by Eq. (4.100) in the case of modulation interactions of TAE and ZS.

3. Toroidal Alfvén eigenmode saturation via nonlinear modification of local continuum

Since the difference between TAE frequency and the lower or upper SAW continuum accumulation frequencies is relatively small, $|\Delta\omega| \lesssim \epsilon v_A/qR_0$ with $\epsilon \equiv r/R_0$, an efficient nonlinear saturation mechanism is via nonlinear modification of the local SAW continuum structures, such that the frequency difference $\Delta\omega$ vanishes due to the corresponding nonlinear frequency shift. Within the general theoretical framework of Sec. IV.A, this process is accounted for by the $\propto \Lambda_n^{NL}$ term in Eq. (4.1). As the TAE frequency gap is due to the coupling of $(m \pm 1, n)$ and (m, n) modes, the contribution to Λ_n^{NL} may be produced by $(m = \pm 1, n = 0)$ components of $\delta\boldsymbol{E} \times \boldsymbol{b}$ flow and $\delta\boldsymbol{B}_\perp$ field line bending, rather than by the generation of ZS discussed in Sec. IV.C.2. So far two such mechanisms have been proposed. One depends on the nonlinear modification in the magnetic surface structure (Zonca *et al.*, 1995) and the other depends on the nonlinear modification in the density structures (Chen *et al.*, 1998). Although of different underlying nature, these two processes are described by essentially the same nonlinear equations. Therefore, we discuss in some detail only the former.

In general, mechanisms for nonlinear modification of the local SAW continuum structures at short-radial scales mentioned previously yield mode saturation above a critical amplitude threshold because of the appearance of fine scales in the mode structure, i.e., of enhanced mode damping in the presence of finite dissipation. This phenomenon may be physically interpreted as mode conversion to short scale damped oscillations, produced by the TAE modes due to the nonlinear SAW continuum distortion. Note that this mechanism is different from that discussed by Todo, Berk, and Breizman (2010, 2012a, 2012b), which is connected with power transfer to nonlinear driven oscillations, which are damped possibly through the fine structures connected with resonant excitation of higher toroidal mode-number continuous spectra (cf. Sec. IV.D.4).

Let us consider a local TAE structure that consists of toroidal mode number n and poloidal mode numbers m and $m+1$, with given frequency ω_0. The dominant nonlinear interactions yield a low-frequency fluctuation with $(m = 1, n = 0)$ and a $(2m+1, 2n)$ component at $2\omega_0$, which can be

expressed as (Vlad *et al.*, 1992, 1995; Zonca *et al.*, 1995; Vlad, Zonca, and Briguglio, 1999)

$$\delta\phi_{1,0} = -\frac{ck_{\theta 0}}{\omega_0 B_0}\frac{\partial}{\partial r}(\delta\phi^*_{m,n}\delta\phi_{m+1,n}),$$
$$\delta A_{\parallel 1,0} = \frac{c^2 k_{\theta 0}}{\omega_0 B_0 v_A}\left(\delta\phi^*_{m,n}\frac{\partial}{\partial r}\delta\phi_{m+1,n} - \delta\phi_{m+1,n}\frac{\partial}{\partial r}\delta\phi^*_{m,n}\right), \tag{4.105}$$

$$\frac{\partial}{\partial r}\delta\phi_{2m+1,2n} = \frac{ck_{\theta 0}}{\omega_0 B_0}\left(2\frac{\partial}{\partial r}\delta\phi_{m,n}\frac{\partial}{\partial r}\delta\phi_{m+1,n} - \delta\phi_{m,n}\frac{\partial^2}{\partial r^2}\delta\phi_{m+1,n} - \delta\phi_{m+1,n}\frac{\partial^2}{\partial r^2}\delta\phi_{m,n}\right),$$
$$\delta A_{\parallel 2m+1,2n} = -\frac{c^2 k_{\theta 0}}{\omega_0 B_0 v_A}\left(\delta\phi_{m+1,n}\frac{\partial}{\partial r}\delta\phi_{m,n} - \delta\phi_{m,n}\frac{\partial}{\partial r}\delta\phi_{m+1,n}\right). \tag{4.106}$$

These equations can be derived from Eqs. (2.35) and (2.37), neglecting thermal ion compressions and EP contribution in the singular layer (cf. Sec. III). Furthermore, we have assumed $|n| \gg 1$ for simplicity and defined $k_{\theta 0} = -m/r_0$, with r_0 the radial position of the considered local TAE frequency gap. In particular, in Eq. (4.105), we have also neglected the effect of thermal ion Landau damping, considering a very narrow TAE spectrum centered at ω_0. The effect of ion Landau damping may become important for a broader TAE frequency spectrum and can be included in the present analysis following the derivations of Secs. IV.B and IV.C.1. It is also worthwhile noting that due to toroidal geometry $(2m, 2n)$ and $(2m+2, 2n)$ Fourier modes are nonlinearly driven at $2\omega_0$ in addition to the $(2m+1, 2n)$ harmonic given by Eq. (4.106). These modes may locally interact with the SAW continuum since the frequency gap at $\simeq v_A/qR_0$ is very narrow for toroidal equilibria with circular flux surfaces (Zheng and Chen, 1998a, 1998b). In this case, the effect of the $2n$ nonlinear mode can be significant and contribute to the saturation of the pump TAE mode (Todo, Berk, and Breizman, 2012b). More generally, however, the $(2m, 2n)$ and $(2m+2, 2n)$ modes at $2\omega_0$ do not locally interact with the SAW continuum, due to the frequency gap at $\simeq v_A/qR_0$ produced by finite magnetic flux surface ellipticity (Betti and Freidberg, 1991). Therefore, in the typical case of elongated plasmas, the effect of $(2m, 2n)$ and $(2m+2, 2n)$ results in a nonlinear frequency shift $\mathcal{O}(\epsilon)$ smaller than that due to the $(2m+1, 2n)$ harmonic given in Eq. (4.106), and thus can be neglected (Vlad *et al.*, 1992, 1995; Zonca *et al.*, 1995).

Adopting the general notation of Eq. (3.23) for the fluctuating fields structure, let us define

$$U = 8\sqrt{2}mqs\left(\frac{R_0}{r_0}\right)\left(\frac{\beta b_s}{\epsilon_0^3}\right)^{1/2}\frac{e}{T_e+T_i}\delta\phi_{0n}(r; nq-m),$$
$$V = 8\sqrt{2}mqs\left(\frac{R_0}{r_0}\right)\left(\frac{\beta b_s}{\epsilon_0^3}\right)^{1/2}\frac{e}{T_e+T_i}\delta\phi_{0n}(r; nq-m-1), \tag{4.107}$$

where $b_s = k_{\theta 0}^2(T_e+T_i)/m_i\Omega_i^2$. Meanwhile, the dimensionless time can be defined as $\tau \equiv \epsilon_0 v_A t/4qR_0$, and the corresponding dimensionless radial coordinate is $x \equiv (4/\epsilon_0)(nq-m-1/2)$. The effect of the nonlinearly driven $(m=1, n=0)$ and $(2m+1, 2n)$ components on the pump TAE mode is obtained by direct substitution of Eqs. (4.105) and (4.106) into the coupled vorticity equations for (m, n) and $(m+1, n)$ modes near r_0 (cf. Sec. II). The final governing equations are

$$(i\partial_\tau - x)\partial_x U + \partial_x V - \partial_x^2|V|^2\partial_x U = \bar{A},$$
$$(i\partial_\tau + x)\partial_x V + \partial_x U - \partial_x^2|U|^2\partial_x V = -\bar{A}. \tag{4.108}$$

Here $\bar{A}$ and $\bar{B}$ are defined as

$$\begin{pmatrix}\bar{A}\\ \bar{B}\end{pmatrix} = \frac{8}{\sqrt{\pi}}mq\left(\frac{R_0}{r_0}\right)\left(\frac{\beta b_s}{\epsilon_0^3}\right)^{1/2}\frac{e}{T_e+T_i}\begin{pmatrix}A(0)\\ B(0)\end{pmatrix}, \tag{4.109}$$

where $A(0) \equiv A(\theta=0)$ and $B(0) \equiv B(\theta=0)$, given the representation of the TAE fluctuation field as $\delta\hat{\Phi}_n = A(\theta)\cos(\theta/2) + B(\theta)\sin(\theta/2)$ (cf. Sec. III) (Cheng, Chen, and Chance, 1985). The local TAE dispersion relation in the form of the GFLDR (cf. Secs. III.C and IV.C.2) is obtained from the solutions of Eq. (4.108) with the matching condition

$$\int_{-\infty}^{\infty}\partial_x U dx = -\int_{-\infty}^{\infty}\partial_x V dx = -\pi\bar{B}. \tag{4.110}$$

Since the ratio $\bar{B}/\bar{A}$ depends only on $\delta\hat{W}_f$ in the absence of EPs, Eq. (4.110) describes the nonlinear frequency shift with respect to ω_0, produced by the finite TAE amplitude. It can be shown that, above a certain critical $\bar{A} = \bar{A}_c(\delta\hat{W}_f)$, the solutions of Eq. (4.108) start producing fine radial structures due to enhanced interaction with the local continuous spectrum. The critical fluctuation level for this to occur can be estimated as

$$\left(\frac{\delta B_r}{B_0}\right)_c \sim \frac{1}{8|s|mq}\frac{r_0}{R_0}\epsilon_0^{3/2}|U| \sim \frac{1}{4|s|mq}\left(\frac{r_0}{R_0}\right)^{5/2}\bar{A}_c(\delta\hat{W}_f) \lesssim 10^{-3}\bar{A}_c(\delta\hat{W}_f). \tag{4.111}$$

As $\bar{A}_c(\delta\hat{W}_f) \ll 1$ for some choice of plasma equilibrium profiles (nonlinear) enhanced continuum damping may effectively yield mode saturation.

Again we note that the local SAW continuum may also be modified via nonlinear density changes (Chen *et al.*, 1998). The corresponding critical fluctuation level for enhanced continuum damping is given by

$$\left(\frac{\delta B_r}{B_0}\right)_c \sim (\beta\epsilon_0^3)^{1/2}\bar{\mathcal{A}}_c(\delta\hat{W}_f) \lesssim 10^{-2}\bar{\mathcal{A}}_c(\delta\hat{W}_f). \tag{4.112}$$

The critical amplitude in Eq. (4.112) is typically larger than that in Eq. (4.111). That is, the dominant mechanism for nonlinearly enhanced continuum damping is expected to be

due to the nonlinear modification in the magnetic surface structure and plasma flow.

4. Alfvén eigenmodes in the presence of a finite-size magnetic island

Theoretical analyses of Alfvénic fluctuations in the presence of a finite-size magnetic island were originally motivated by the experimental observation of BAEs in Frascati Tokamak Upgrade (FTU) (Annibaldi, Zonca, and Buratti, 2007), where they are excited without EP drive but in the presence of a sufficiently large magnetic island (Buratti *et al.*, 2005), as also reported in the Tokamak EXperiment for Technology Oriented Research (TEXTOR) (Zimmermann *et al.*, 2005) and the Chinese Toroidal Device–2A (HL-2A) (Chen *et al.*, 2011).

Theoretically, the low-frequency magnetic island can be considered as a nonaxisymmetric distortion of the tokamak equilibrium, and a detailed analysis was given by Biancalani *et al.* (2010a, 2010b, 2011). This situation has evident analogies with the formation of frequency gaps in the SAW continuous spectrum in helical devices [see, e.g., Kolesnichenko *et al.* (2011) and Toi *et al.* (2011)]. A case of particular interest is when the toroidal periodicity of the singular perturbations representing the SAW continuum coincides with that of the magnetic island, assumed to have (m_0, n_0) poloidal and toroidal mode numbers. In this case, the SAW continuous spectrum is qualitatively modified (Biancalani *et al.*, 2011). In particular, the BAE frequency is upshifted by the finite-size magnetic island to

$$\omega_{BAE} = \omega_{BAE0}\left[1 + \frac{n_0^2 s^2 q_0^2}{4}\frac{W_{isl}^2}{r_0^2}\frac{\omega_A^2}{\omega_{BAE-CAP}^2}\right]^{1/2}. \quad (4.113)$$

Here ω_{BAE0} is the BAE frequency in the reference axisymmetric tokamak equilibrium without magnetic island, W_{isl} stands for the magnetic island (half) width, $\omega_{BAE-CAP}$ denotes the BAE continuum accumulation point frequency defined as $\Lambda_n^2(\omega_{BAE-CAP}) = 0$, $\omega_A = v_A/q_0R_0$, $q_0 = m_0/n_0$, r_0 is the island O-point position, and s is the magnetic shear. Equation (4.113) has been successfully tested against FTU experimental observations for sufficiently small magnetic island width (Tuccillo *et al.*, 2011).

The actual physics determining the threshold in magnetic island size for BAE excitation has not been fully clarified. Two possible mechanisms have been proposed so far: (i) the core plasma profiles, modified inside the finite-size magnetic island, along with the modified SAW continuum structures, may alter the stability properties of BAE modes and eventually excite them even in the absence of EPs (Biancalani *et al.*, 2011); and (ii) the island-induced modification of the thermal ion equilibrium distribution function (Smolyakov, Garbet, and Ottaviani, 2007) may be sufficient to yield a change in sign of ion Landau damping and cause mode excitation (Marchenko and Reznik, 2009).

D. Nonlinear wave-particle dynamics

As remarked in the introduction to Sec. IV, there are currently two paradigms for discussing nonlinear interactions of Alfvénic fluctuations with EPs in fusion plasmas (Chen and Zonca, 2013; Zonca *et al.*, 2015b): the bump-on-tail and the fishbone paradigms. It is possible to adopt the former one provided that the system is sufficiently close to marginal stability. In particular, the nonlinear modification of resonant EP orbits must be small compared with the characteristic fluctuation wavelength (Berk and Breizman, 1990b, 1990c). Thus, this model can account only for local EP transport in the presence of an isolated resonance, i.e., unless the threshold is exceeded for the onset of stochasticity in the particle phase space due to resonance overlap (cf. Secs. V.A and VI.A). The essential physics of the bump-on-tail paradigm are the same as those originally introduced in the analysis of the temporal evolution of a small cold electron beam interacting with a plasma in a 1D system (Al'tshul' and Karpman, 1965; Mazitov, 1965; O'Neil, 1965; O'Neil, Winfrey, and Malmberg, 1971) and are discussed in Sec. IV.D.1. There we also give the self-consistent nonlinear solution for the low-frequency beam distribution function in the presence of a periodic fluctuation, as derived by Al'tshul' and Karpman (1965). In fact, this is the solution of the Dyson equation for a 1D uniform plasma, which is the starting point for its extension to nonuniform systems (Zonca *et al.*, 2005) and provides the theoretical basis for the construction of the fishbone paradigm later on. The dynamics of the nonlinear beam-plasma system with sources and collisions are analyzed in Sec. IV.D.2, based on the original works by Berk and Breizman (1990a, 1990b, 1990c). These include steady-state and bursting behaviors (periodic and chaotic) (Berk, Breizman, and Ye, 1992a; Breizman, Berk, and Ye, 1993; Berk, Breizman, and Pekker, 1996; Breizman *et al.*, 1997), the formation of hole and clump pairs in the resonant particle phase space (Berk, Breizman, and Petiashvili, 1997; Breizman *et al.*, 1997; Berk *et al.*, 1999), and the existence of subcritical states (Berk *et al.*, 1999). Applications of the 1D bump-on-tail paradigm to AE experimental observations are discussed in Sec. IV.D.3, with notable examples being fine structures (frequency splitting) of AE spectral lines (Fasoli *et al.*, 1998) as well as AE adiabatic frequency chirping (Pinches *et al.*, 2004; Vann, Dendy, and Gryaznevich, 2005; Gryaznevich and Sharapov, 2006), where the mode frequency sweeping rate is much less than the wave-particle trapping frequency $|\dot{\omega}| \ll \omega_B^2$. Section IV.D.3 also addresses the assumptions underlying the 1D bump-on-tail paradigm and analyzes its validity limits.

One approximate method for analyzing finite AE mode width effects is based on perturbative treatment of EPs and prescribed AE structures, which ultimately yields AE nonlinear dynamics in terms of time evolution of wave amplitudes and phases (Chen and White, 1997). Numerical simulation results using this approach are presented in Sec. IV.D.4. In fusion plasmas, however, EP effects are generally nonperturbative and modify the plasma dielectric response as well as the fluctuation structure and frequency. This behavior is related to equilibrium geometry and plasma nonuniformity effects via EP resonance conditions, which depend on EP constants of motion and via finite mode structures, which affect wave-EP interactions. These issues are analyzed in Sec. IV.D.5. First theoretically yielding an estimate of $|\gamma_L/\omega|$ for the transition from local redistributions to mesoscales EP transport and the corresponding shift from the bump-on-tail to the fishbone paradigm. Then

these physics are illustrated by numerical simulation results (Briguglio, Zonca, and Vlad, 1998; Briguglio, 2012; Wang *et al.*, 2012; Zhang, Lin, and Holod, 2012; Briguglio and Wang, 2013). Finally, Sec. IV.D.5 derives the general equations for the nonlinear dynamics of phase-space ZS (PSZS) within the theoretical framework of Sec. IV.A, yielding the generalization of the Dyson equation introduced in Sec. IV.D.1 (Al'tshul' and Karpman, 1965) to nonuniform plasmas with the addition of sources and collisions. This result is then used to discuss the unification of bump-on-tail and fishbone paradigms (Zonca *et al.*, 2015b).

In general, the Dyson equation approach of Sec. IV.D.5 provides an exact description of nonlinear wave-particle interactions for which a numerical solution is necessary. In nonuniform plasmas, with the mode frequency set by the nonlinear dispersion relation, the nonlinear mode evolution is dominated by resonant EPs whose phase is locked with the wave, since these maximize wave-EP power exchange while at the same time are most efficiently displaced by the mode. Depending on the wave dispersive properties, the mode can nonlinearly modify its structure to further enhance the wave-EP power exchange by tapping the steeper spatial gradient regions due to phase-locked resonant EPs. When the mode can readily respond by readapting its frequency and/or mode structure to the modified EP distribution, resonant EP radial motion is secular as long as wave-particle phase locking is maintained, as theoretically predicted (White *et al.*, 1983) and observed experimentally (Duong *et al.*, 1993; Heidbrink, 2008). This process, called "mode-particle pumping" in the original work by White *et al.* (1983), was introduced to explain EP losses due to fishbones in PDX (McGuire *et al.*, 1983). It applies to nonlinear dynamics of radially extended EPM (cf. Sec. IV.D.6) and fishbones (cf. Sec. IV.D.7) and is accompanied by fast nonadiabatic frequency chirping $|\dot{\omega}| \sim \omega_B^2$ with ω_B the wave-particle trapping frequency for fixed ω that suppresses wave-particle trapping as shown in Sec. IV.D.5. The ability to adapt and "follow" phase-locked EPs is characteristic of EPMs, of which fishbones are the first and one well-known example (Chen and Zonca, 2007a), and it is borne in the mode dispersion relation. In fact, nonadiabatic chirping and phase locking can be preserved through the nonlinear phase because nonlinear wave-EP power transfer balances the linear diffusive or dispersive response. Meanwhile, assuming phase locking and additional approximations (to be verified *a posteriori*) allows us to further simplify and solve the Dyson equation for the cases of EPM (Sec. IV.D.6) as well as fishbones (Sec. IV.D.7). For EPM, in particular, Sec. IV.D.6 demonstrates that the general NLSE with integrodifferential nonlinear terms of Sec. IV.A reduces to a special case of the complex Ginzburg-Landau equation (van Saarloos and Hohenberg, 1992; Conte and Musette, 1993), for which the convectively amplified EPM wave packet constitutes an attractor. Section IV.D.6 furthermore discusses the radial modulation effects of the self-consistent interplay of AE and EPM mode structures and EP transport, which are the analogs of the modulation interaction of AE with ZS (Sec. IV.C.2) extended to generally include wave-particle resonance effects in the case of PSZS and, in general, can influence fine features of the AE abd EPM frequency spectra (Sec. IV.D.3).

More generally, the study of convectively amplified EPM wave packets as solitonlike solutions of a complex NLSE introduces analogies with research fields other than plasma physics (cf. Sec. IV.D.6). These include possible formulations of fractional-derivative extensions of the NLSE as well as the Fokker-Planck equation, based on a first-principle physics model derived from general equations governing the nonlinear evolution of a nonuniform plasma system with wave-particle resonant interactions that are responsible for nonlocal spatio-temporal behavior. Further discussion of general implications of the theoretical framework introduced in Sec. IV.A is given in Sec. IV.E.

1. The physics of the collisionless nonlinear beam-plasma system

The temporal evolution of a small cold electron beam interacting with a plasma in a 1D system was described by O'Neil, Winfrey, and Malmberg (1971). Following the linear analysis of O'Neil and Malmberg (1968), let us consider a uniform 1D beam-plasma system, where electrons have density n and are Maxwellian, with a thermal speed v_T significantly lower than the electron beam drifting speed v_D such that thermal electron Landau damping is negligible. Beam electrons of density $n_B \ll n$ have a Lorentzian distribution with velocity spread v_B, while thermal ions are considered as a fixed neutralizing background.

The most unstable wave is a beam mode, which is nearly degenerate with the Langmuir wave, i.e., $\omega = \omega_0 + \delta\omega$ and $k = k_0 + \delta k$, with $\omega_0 = \omega_p$ and $k_0 = \omega_p/v_D$. More precisely, introducing $x = (\delta k/k_0)(2n/n_B)^{1/3}$, $y = (\delta\omega/\omega_0)(2n/n_B)^{1/3}$, and $s = (v_B/v_D)(2n/n_B)^{1/3}$, the most unstable mode for $s = 0$ has $x = 0$, $y = -1/2 + i\sqrt{3}/2$ and group velocity $\partial\omega/\partial k = (2/3)v_D$. The half-width Δk of the linear growth rate spectrum is $\Delta k = (3/2)k_0(n_B/2n)^{1/3}$. For $(n_B/2n)^{1/3} \ll 1$, beam electrons are moving locally over a single wave with relative velocity $\Delta v \sim (n_B/n)^{1/3}v_D$. When the wave grows to an amplitude such that $\phi \sim m\Delta v^2/e \sim (n_B/n)^{2/3}mv_D^2/e$, the wave saturates and starts oscillating (O'Neil, Winfrey, and Malmberg, 1971). Meanwhile, the nonlinear evolution takes place in two stages (Shapiro, 1963): first, the beam-plasma interaction heats the beam, as the nonlinear $\Delta v \gtrsim v_B$; second, the beam distribution is modified (flattened by phase mixing) in velocity space by nonlinear interactions.

Following O'Neil, Winfrey, and Malmberg (1971), we consider $\delta\phi = \delta\phi_0(t)\exp(ik_0x) + \text{c.c.}$, $x = z - v_Dt$, and $\omega_0 = \omega_p$. A general direct solution of the Poisson's equation can be obtained assuming that in one wavelength $2\pi/k_0$ the beam spatial charge is made of $i = 1, 2, 3, \ldots, M$ charge sheets located at x_j with charge $-2\pi en_B/Mk_0$. Thus, recalling that the plasma can be treated as a linear dielectric medium and that the wave is nearly monochromatic and introducing the normalized quantities $\xi_j(\tau) = k_0x_j(t)$, $\tau = \omega_0t(n_B/2n)^{1/3}$, and $\Phi(\tau) = -(2n/n_B)^{2/3}e\delta\phi_0(t)/mv_D^2$,

$$\dot{\Phi}(\tau) = \frac{-i}{M}\sum_{j=1}^{M}\exp\left[-i\xi_j(\tau)\right], \tag{4.114}$$

$$\ddot{\xi}_j(\tau) = -i\Phi(\tau)\exp\left[i\xi_j(\tau)\right] + \text{c.c.}, \tag{4.115}$$

are, respectively, the evolution equation for $\Phi(\tau) = \Phi(0)\exp\left[-i\int_0^\tau y(\tau')d\tau'\right]$, with y the normalized frequency variable introduced earlier, and the equation of motion for the electron beam charge sheets. Equations (4.114) and (4.115) recover the linear dispersion relation $y^3 = 1$ for the most unstable beam mode in the cold beam case. They describe the early nonlinear evolution of the most unstable beam-plasma wave under the single-mode assumption. The numerical solution shows that the fastest growing mode dominates the dynamics and grows until electrons are trapped and begin sloshing back and forth in the wave. Then the wave stops growing and begins oscillating about a mean value due to energy exchange between electrons and the wave itself. This process is similar to the oscillatory behavior observed with an externally launched large amplitude wave (Mazitov, 1965; O'Neil, 1965). Equations (4.114) and (4.115) can be seen as a dynamical system and are formally obtained in the framework of Hamiltonian system theory (Mynick and Kaufman, 1978; Tennyson, Meiss, and Morrison, 1994; Antoni, Elskens, and Escande, 1998). An interesting aspect of this description is that it results in a self-consistent Hamiltonian formulation, which is formally equivalent to that of the free-electron laser dynamics (Antoniazzi *et al.*, 2008). Using the same formulation, it was recently shown (Carlevaro *et al.*, 2014) that the suprathermal electron distribution function in the quasistationary states (intermediate out-of-equilibrium states) produced by the nonlinear evolution of the beam-plasma system are accurately predicted by the maximum entropy principle proposed by Lynden-Bell (Lynden-Bell, 1967; Antoni, Elskens, and Escande, 1998).

Momentum and energy conservation can be derived from Eqs. (4.114) and (4.115), respectively, as

$$|\Phi(\tau)|^2 + \frac{1}{M}\sum_{j=1}^{M}\dot{\xi}_j(\tau) = 0, \tag{4.116}$$

$$\mathbb{R}\text{e}y|\Phi(\tau)|^2 + \frac{1}{4M}\sum_{j=1}^{M}\dot{\xi}_j^2(\tau) = 0, \tag{4.117}$$

yielding $\mathbb{R}\text{e}y(\tau) = (1/4)\sum_j\dot{\xi}_j^2(\tau)/\sum_j\dot{\xi}_j(\tau)$. Noting that $\mathbb{I}\text{m}y(\tau) = (1/2)(d/d\tau)|\Phi(\tau)|^2/|\Phi(\tau)|^2$ by definition, the nonlinear frequency oscillation is always downward as shown by Eq. (4.117), and it occurs with a frequency which is twice that of $|\Phi(\tau)|$ oscillations and maximum negative excursions corresponding to the minima of fluctuation intensity. The excursions of both $\mathbb{R}\text{e}y(\tau)$ and $\mathbb{I}\text{m}y(\tau)$ are $\mathcal{O}(1)$ as can be estimated from the optimal ordering $\dot{\omega} \sim k_0\dot{v} \sim \omega_B^2$.

On long time scales, the wave cannot be considered monochromatic any longer and the total energy dependence of the particle trapping period causes the particle distribution function inside the separatrix to smooth out the increasingly finer structures by phase mixing. This is the coarse-grained distribution function (Sagdeev and Galeev, 1969) and when it is asymptotically formed on long time scales the mode amplitude reaches a steady state (Mazitov, 1965; O'Neil, 1965).[18] Considering $E_z = E_{z0}\sin\xi$ in the wave moving frame, the particle motion is described by

$$\dot{\xi}^2 = (4\omega_B^2/\kappa^2)[1 - \kappa^2\sin^2(\xi/2)], \tag{4.118}$$

where $\omega_B^2 = |ekE_{z0}/m|$ is the trapping frequency of deeply trapped particles, $\kappa^2 = 2eE_{z0}/(kW + eE_{z0})$, and W is the total energy. This is the equation of a nonlinear pendulum with $\kappa^2 < 1$ describing rotations, $\kappa^2 > 1$ denoting oscillations or librations, and $\kappa^2 = 1$ defining the separatrix. Defining $\Delta W = (\partial W/\partial v)\Delta v = \text{const}$, the coarse-grained distribution function is given by (O'Neil, 1965; Sagdeev and Galeev, 1969)

$$[f] = \frac{\oint F_0(v)\Delta v d\xi}{\oint \Delta v d\xi} \simeq F_0(\omega_0/k_0) + \frac{\partial F_0(\omega_0/k_0)}{\partial v}\frac{\oint d\xi/k_0}{\oint d\xi/\dot{\xi}}, \tag{4.119}$$

where $[f] = (2\pi)^{-1}\oint f d\xi$. For $\kappa^2 > 1$, i.e., for trapped particles, it can be noted that $[f] = F_0(\omega_0/k_0)$. Thus, the time asymptotic coarse-grained distribution function takes up the constant value corresponding to the equilibrium particle distribution at resonance. Meanwhile, for circulating particles, $\kappa^2 < 1$,

$$[f] = F_0(\omega_0/k_0) + \frac{\partial F_0(\omega_0/k_0)}{\partial v}\frac{\pi\omega_B/k_0}{\kappa\mathbb{K}(\kappa)}, \tag{4.120}$$

with $\mathbb{K}(\kappa)$ the complete elliptic integral of the first kind. Note that the coarse-grained distribution is continuous at the separatrix $\kappa^2 = 1$ but has discontinuous derivatives. The flattened coarse-grained particle distribution function in the resonance region explains why the nonlinear oscillations eventually fade away due to phase mixing. This is exactly the same time asymptotic state reached when a large amplitude plasma wave is externally driven at a fluctuation level corresponding to $\omega_B \gg \gamma_L$, i.e., the Landau damping due to resonant wave-particle interactions (Mazitov, 1965; O'Neil, 1965). The main difference is in the relative value of fluctuation amplitude oscillations. In the case of a large amplitude wave, the amplitude undergoes small oscillations about an essentially constant value. Meanwhile, for the beam-plasma system, the amplitude is fluctuating by an $\mathcal{O}(1)$ quantity about the mean value as the system evolves from the initial exponential growth, with $\omega_B \ll \gamma_L$, to the saturation phase, with $\omega_B \sim \gamma_L$ (Onishchenko *et al.*, 1970a, 1970b; O'Neil, Winfrey, and Malmberg, 1971; Shapiro and Shevchenko, 1971; O'Neil and Winfrey, 1972). After resonant electrons get trapped and begin sloshing back and forth in the wave, $\mathcal{O}(1)$ amplitude oscillations at ω_B and harmonics

[18] It is worthwhile noting the difference between this time asymptotic equilibrium state, characterized by the coarse-grained distribution function (Sagdeev and Galeev, 1969), and the quasistationary states, which were discussed (Carlevaro *et al.*, 2014) in the context of the Lynden-Bell approach (Lynden-Bell, 1967).

eventually fade away with the wave amplitude reaching a constant level at $\omega_B \simeq 3\gamma_L$ (Levin *et al.*, 1972).

A different approach to the beam-plasma problem was given by Al'tshul' and Karpman (1965) based on the general solution of the nonlinear Poisson equation

$$E_{kz} = -\frac{4\pi}{k} i\delta\hat{Q}_k = \frac{4\pi}{k} ie \int dv \delta f_k, \tag{4.121}$$

with δf_k obtained from the Vlasov equation

$$(\partial_t + ikv)\delta f_k = -\frac{e}{m}\sum_q i(k-q)\delta\phi_{k-q}\frac{\partial}{\partial v} f_q, \tag{4.122}$$

solved for assuming a monochromatic wave. This approach is relevant for the issues dealt with in Secs. IV.D.2–IV.D.7 and is valid in the early nonlinear saturation phase. Furthermore, it touches important aspects of the theory of nonlinear oscillations in collisionless plasmas. Here we sketch its derivations and summarize the main results. Recalling that the thermal plasma is a linear dielectric medium and $\omega = \omega_{k_0} + i\partial_t$ for a nearly monochromatic wave, $(\omega_{k_0}, k_0) = (\omega_p, k_0)$, Eq. (4.121) can be cast as

$$\frac{2}{\omega_p}\frac{\partial}{\partial t}\delta\phi_{k_0} = \frac{4\pi}{k_0^2} ie \int dv \delta f_{Ek_0}, \tag{4.123}$$

where $\sim e^{-i\omega_p t}$ time dependences are extracted, and the subscript E stands for energetic beam electrons (cf. Sec. II.E) and is dropped in the following for simplicity of notation. Introducing the standard definition

$$\begin{aligned} \delta f_k(t) &= \int_{-\infty}^{+\infty} e^{-i\omega t}\delta\hat{f}_k(\omega)d\omega, \\ \delta\hat{f}_k(\omega) &= \frac{1}{2\pi}\int_0^{+\infty} e^{i\omega t}\delta f_k(t)dt \end{aligned} \tag{4.124}$$

for the Laplace transform, the solution of Eq. (4.122) for $k = 0$ is readily obtained as

$$\begin{aligned} \hat{f}_0(\omega) = \frac{i}{2\pi\omega}F_0 + \frac{e}{m}\frac{k_0}{\omega}\int_{-\infty}^{+\infty}\Big[&\delta\hat{\phi}_{k_0}(\omega')\frac{\partial}{\partial v}\delta\hat{f}_{-k_0}(\omega-\omega') \\ &- \delta\hat{\phi}_{-k_0}(\omega')\frac{\partial}{\partial v}\delta\hat{f}_{k_0}(\omega-\omega')\Big]d\omega'. \end{aligned} \tag{4.125}$$

Meanwhile, assuming vanishing initial conditions for δf_{k_0} and $u \equiv v - \omega_p/k_0$,

$$\delta\hat{f}_{k_0}(\omega) = \frac{e}{m}\frac{k_0}{\omega - k_0 u}\int_{-\infty}^{+\infty}\delta\hat{\phi}_{k0}(\omega')\frac{\partial}{\partial u}\hat{f}_0(\omega-\omega')d\omega'. \tag{4.126}$$

By direct substitution of Eq. (4.126) into Eqs. (4.123) and (4.125), one readily obtains, respectively,

$$\begin{aligned} \frac{2}{\omega_p}\frac{\partial}{\partial t}\delta\phi_{k_0} = \frac{\omega_p^2}{nk_0} i\int dv \iint_{-\infty}^{+\infty} e^{-i\omega t}\frac{\delta\hat{\phi}_{k0}(\omega')}{\omega - k_0 u} \\ \times\frac{\partial}{\partial u}\hat{f}_0(\omega-\omega')d\omega d\omega', \end{aligned} \tag{4.127}$$

$$\begin{aligned} \hat{f}_0(\omega) = &\frac{i}{2\pi\omega}F_0 \\ &- \frac{e^2}{m^2}\frac{k_0^2}{\omega}\iint_{-\infty}^{+\infty}\Bigg[\delta\hat{\phi}_{k_0}(\omega')\delta\hat{\phi}_{-k_0}(\omega'') \\ &\times\frac{\partial}{\partial u}\left(\frac{1}{\omega-\omega'+k_0 u}\frac{\partial}{\partial u}\hat{f}_0(\omega-\omega'-\omega'')\right) \\ &+ \delta\hat{\phi}_{-k_0}(\omega')\delta\hat{\phi}_{k_0}(\omega'') \\ &\times\frac{\partial}{\partial u}\left(\frac{1}{\omega-\omega'-k_0 u}\frac{\partial}{\partial u}\hat{f}_0(\omega-\omega'-\omega'')\right)\Bigg]d\omega' d\omega''. \end{aligned} \tag{4.128}$$

This last equation is the analog of the Dyson's equation [see, e.g., Kaku (1993)] in quantum field theory as noted by Al'tshul' and Karpman (1965). The physics processes described by Eqs. (4.127) and (4.128) are schematically depicted in Fig. 1. When Eq. (4.128) is solved by formal expansion in the field amplitudes, the lowest order solution is $\hat{f}_0(\omega) = iF_0/(2\pi\omega)$. Assuming that

$$\delta\hat{\phi}_{k_0}(\omega) = \frac{i}{2\pi}\frac{\delta\phi_{k_0}}{\omega - \omega_{k_0}}, \tag{4.129}$$

with $\delta\phi_{k_0}$ being the k_0 field in the linear approximation, the subsequent steps in the iterative solution of the "Dyson" equation (4.128) will have a second order pole at $\omega = 0$, corresponding to a secular term $\propto t$ in the t representation and to the second order diagram in Fig. 1(b), etc. Similarly, in the solution of Eq. (4.127), a second order pole at $\omega = \omega_{k_0}$ in the nonlinear expression on the right-hand side corresponds to a secular term $\propto t\exp(-i\omega_{k_0}t)$, etc. Even accounting for a complex frequency ω_{k_0} would replace the secular terms $\propto t^\ell$ with terms $\propto (\mathbb{R}e\omega_{k_0}/\mathbb{I}m\omega_{k_0})^\ell \gg 1$ (Montgomery, 1963; Al'tshul' and Karpman, 1965). For this reason, it is crucial to take into account all terms in the Dyson series as shown in Fig. 1 (c) bottom frame. In general, Eqs. (4.127) and (4.128) can be written for a generic fluctuation spectrum of waves with $|\mathbb{I}m\omega_{k_0}/\mathbb{R}e\omega_{k_0}| \ll 1$ assuming that the evolution of the fluctuating fields is dominated by the nonlinear modification of $\hat{f}_0(\omega)$, Eq. (4.128), rather than by the generation of nonlinear harmonics in the fields and the distribution function. For the case of many waves with overlapping resonances, Al'tshul' and Karpman (1965) have demonstrated that Eqs. (4.127) and (4.128) reduce to the well-known quasilinear limit (Vedenov, Velikhov, and Sagdeev, 1961; Drummond and Pines, 1962). In this sense, they can be referred to as generalized quasilinear equations (Galeev, Karpman, and Sagdeev, 1965). Meanwhile, in the case of a nearly monochromatic wave with constant amplitude in time, Eq. (4.129), Al'tshul' and Karpman (1965) showed that Eq. (4.128) admits a solution which oscillates around the coarse-grained distribution in the resonant region, with a frequency spectrum given by the wave-particle trapping frequency ω_B and harmonics. More specifically,

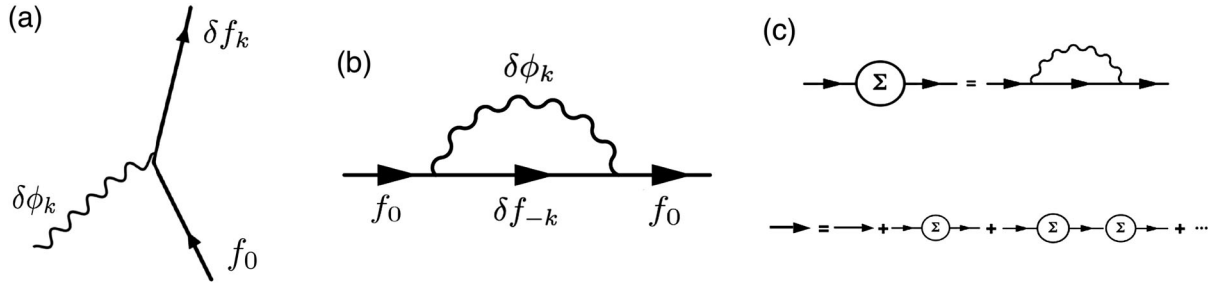

FIG. 1. (a) The generation of the distribution δf_k due to the interaction of f_0 with the field $\delta\phi_k$, corresponding to the solution of Eq. (4.126). (b) Nonlinear distortion of f_0 due to emission and absorption of the field $\delta\phi_k$. (c) The process is defined in the top frame, while the solution of the Dyson equation (4.128) corresponds to the summation of all terms in the Dyson series (bottom) (Al'tshul' and Karpman, 1965).

$$F_0(u,t) = F_0(0) + \frac{\alpha}{k_0}\sum_{\ell=0}^{\infty}\frac{\beta_\ell}{(2\ell+1)}\frac{d}{du}\psi_\ell\left(\frac{k_0 u}{\alpha}\right) \times [1-\cos(\sqrt{2\ell+1}\alpha t)], \tag{4.130}$$

with the notation $\alpha^2 \equiv \sqrt{2}|ek_0E_{k_0}/m| = \sqrt{2}\omega_B^2$, $x = k_0u/\alpha$, and $\psi_\ell(x) \equiv (2^\ell \ell!\pi^{1/2})^{-1/2}e^{-x^2/2}H_\ell(x)$ with $H_\ell(x)$ the Hermite polynomials, and $\beta_\ell \equiv \int_{-\infty}^{\infty}[dF_0(0)/dx]\psi_\ell(x)dx$. Note that Eq. (4.130) describes the oscillations of particles trapped in the wave, which, however, do not decay in time as expected from phase mixing. It was pointed out by O'Neil (1965) that this is due to the assumption of the negligible harmonic generation at $k = \ell k_0$ ($\ell \geq 2$) in both $\delta\phi_k$ and δf_k, which breaks down on long time scales.

2. The nonlinear beam-plasma system with sources and collisions

In a series of papers in the 1990s, Berk and Breizman (1990a, 1990b, 1990c) reconsidered the nonlinear beam-plasma problem (cf. Sec. IV.D.1) including sources and collisions and applied it to the description of nonlinear dynamics of AEs near marginal stability. In this case (Berk and Breizman, 1990a), the coarse-grained distribution function, Eq. (4.119), maintains a residual slope (Zakharov and Karpman, 1962) inside the separatrix including the phase space of wave-trapped resonant particles, so that a steady state can be reached when the residual nonlinear drive balances the background dissipation. The extension of this analysis to electrostatic waves in a plasma slab with a sheared equilibrium magnetic field $\boldsymbol{B}_0$, destabilized by an EP beam with a spatial gradient transverse to $\boldsymbol{B}_0$, was discussed by Berk and Breizman (1990b). Meanwhile, Berk and Breizman (1990c) further extended the same approach to AEs destabilized by nonuniform EP sources. Assumptions of these analyses generally involve (i) one single low-amplitude wave, such that mode structures can be neglected,[19] (ii) finite background dissipation independent of the finite-amplitude wave, and (iii) wave dispersiveness set by the background plasma and independent of the EP dynamics.

a. Steady-state saturation of the collisional beam-plasma system

A steady-state saturation level is reached when background dissipation balances wave drive reduced by nonlinear interactions (cf. Sec. IV.D.1), i.e.,

$$\frac{d}{dt}T = \frac{nm}{2}\int dv v^2\frac{\partial}{\partial t}[f] \simeq \frac{nm}{2}\frac{\omega_0^2}{k_0^2}\int dv\frac{\partial}{\partial t}[f] = -2\gamma_d\mathcal{W}. \tag{4.131}$$

With a source term $Q(v)$ and particle annihilation at a rate $\nu(v)$, the Vlasov equation is

$$\partial_t f + v\partial_x f + \dot{v}\partial_v f = -\nu(v)f + Q(v). \tag{4.132}$$

For $\nu \ll \omega_B$, the lowest order time asymptotic $[f]$ is still given by the coarse-grained distribution function, Eqs. (4.119) and (4.120), which is readily obtained with $F_0(v) = Q(v)/\nu(v)$. At next order in ν/ω_B, the small but finite residual slope within the wave-particle trapping region maintains a residual drive with respect to the linear expression $(dT/dt)_L$, which is given by (Berk and Breizman, 1990a)

$$dT/dt = 1.9(\nu/\omega_B)(dT/dt)_L. \tag{4.133}$$

Thus, noting $(dT/dt)_L = -2\gamma_L\mathcal{W}$, Eqs. (4.131) and (4.133) readily yield the saturation level $\omega_B \simeq 1.9(\nu/\gamma_d)\gamma_L$.

In order to emulate a beam slowing down, Berk and Breizman (1990a) also considered the case of a source at fixed velocity v_0 and particle drag

$$\partial_t f + v\partial_x f + \dot{v}\partial_v f = -\nu(v)f + Q_0\delta(v-v_0) + a\partial_v f. \tag{4.134}$$

Denoting the Heaviside step function as H, the corresponding equilibrium steady-state solution is $F_0 = (Q_0/a)\times \exp[(\nu/a)(v-v_0)]H(v_0-v)$, which again yields the lowest order time asymptotic $[f]$ in terms of the coarse-grained distribution function given by Eqs. (4.119) and (4.120). For $\omega_B^2 > ka$, i.e., for a sufficiently large perturbation, the rate at which particles cross a separatrix width in velocity space

[19]When the Hamiltonian is accidentally degenerate, i.e., the resonance condition is verified for particular values of the action coordinates, the maximum excursion of the action about the resonance scales as the square root of the perturbation strength [see, e.g., Lichtenberg and Lieberman (1983, 2010)].

because of drag is $\nu_{\rm eff} = ka\omega_B^{-1} \sim \nu(\omega/\omega_B)$. Thus, $\omega_B > \nu_{\rm eff} \gg \nu$ and for adiabatically growing wave amplitude trapping regions cannot be filled by drag, so that the distribution function eventually vanishes because of particle annihilation. In this scenario, a discontinuity is expected in the particle distribution function near the separatrix and the residual nonlinear drive is enhanced

$$dT/dt = (16/\pi^2)(\nu_{\rm eff}^2/\nu^2)(\nu/\omega_B)(dT/dt)_L. \tag{4.135}$$

Using this expression, the steady-state saturation level can be computed as for Eqs. (4.131) and (4.133).

In a more realistic description with sources and sinks, the Vlasov equation is (Berk and Breizman, 1990b)

$$d_t f = \nu_d \partial_\lambda (1-\lambda^2)\partial_\lambda f + (\nu/v^2)\partial_v[(v^3+v_c^3)f] + (4\pi v_0^2)^{-2} Q\delta(v-v_0), \tag{4.136}$$

where the term $\propto \nu_d$ on the right-hand side accounts for pitch angle scattering, with $\lambda = \boldsymbol{v}\cdot\boldsymbol{B}_0/vB_0$. Depending on the relative ordering of ν and ν_d, three different regimes can be identified: (i) $\nu_d(\omega^2/\omega_B^2) \ll \nu$, where particles slow down completely, without appreciable pitch angle scattering; (ii) $\nu_d(\omega/\omega_B) \ll \nu < \nu_d(\omega^2/\omega_B^2)$, where particles slow down one separatrix width without appreciable diffusion; and (iii) $\nu \ll \nu_d(\omega/\omega_B)$, where particles are pitch angle scattered before they slow down one separatrix width. The regime to be expected in fusion plasmas is (iii), for which the residual nonlinear drive, with $\nu_{\rm eff} = \nu_d(\omega^2/\omega_B^2) \ll \omega_B$, is given by (Berk and Breizman, 1990b)

$$dT/dt \sim (\nu_{\rm eff}/\omega_B)(dT/dt)_L, \tag{4.137}$$

which with the help of Eq. (4.131) yields the respective saturation level.

b. Collisional beam-plasma system with periodic and chaotic pulsations

Steady-state solutions with constant amplitude are not the only possibility for nonlinear dynamics of the beam-plasma system. Different scenarios are possible depending on the relative ordering of γ_L, $\nu_{\rm eff} \sim \nu_d(\omega^2/\omega_B^2)$, and γ_d (Berk, Breizman, and Ye, 1992a; Breizman, Berk, and Ye, 1993). In Sec. IV.D.1, it was shown that in a region of width $\Delta v \sim \omega_B/k_0$ near an isolated resonance a finite-amplitude wave eventually yields to flattening of the coarse-grained distribution function by phase mixing. Meanwhile, the distribution function is reconstructed at a rate $\nu_{\rm eff}$, while energy is dissipated at a rate γ_d. Thus, for $\gamma_d < \nu_{\rm eff}$, the predicted steady-state level trapping frequency is larger than the linear drive $\omega_B \sim \gamma_L\nu_{\rm eff}/\gamma_d$ and steady-state solutions can be sustained (cf. Sec. IV.D.2.a). Conversely, for $\gamma_d > \nu_{\rm eff}$, the background distribution is not effectively reconstructed and after saturation at $\omega_B \sim \gamma_L$ (cf. Sec. IV.D.1) the mode amplitude decays at rate γ_d, so that fluctuation bursting can be expected. The typical interval between bursts scales as $\sim 1/\nu_{\rm eff}$. Meanwhile, the transition between steady-state and bursting behaviors takes place when $\omega_B \sim \gamma_L$ and $\nu_{\rm eff} = \nu_{\rm eff\,0} = \nu_d\omega^2/\gamma_L^2 \simeq \gamma_d$ (Berk, Breizman, and Ye, 1992a; Breizman, Berk, and Ye, 1993). Numerical particle-in-cell (PIC) simulations of a single Langmuir wave excited by an inverted gradient $F_0(v) = Q(v)/\nu(v)$ confirm analytical predictions about bursting versus steady-state saturation for the bump-on-tail problem (Berk, Breizman, and Pekker, 1995).

Changing the externally imposed dissipation for fixed γ_L changes the qualitative features of numerical solutions of the Vlasov-Poisson system obtained for a monochromatic wave (Berk, Breizman, and Pekker, 1996). In particular, $\omega_B = \alpha(\gamma_L - \gamma_d)$ at the maximum oscillation amplitude, with α varying from $\alpha = 3.2$ to 2.9 when γ_d/γ_L is varied from $\gamma_d/\gamma_L = 0$ to 0.6. More importantly, however, when $\gamma \equiv \gamma_L - \gamma_d$ is reduced to a sufficiently low level, the amplitude of the system oscillates rather than decays at a rate $\sim\gamma_d$ after reaching the peak amplitude at $\omega_B \sim \gamma$. To investigate this phenomenology near marginal stability, the Poisson's equation (4.121) can be replaced by (Berk, Breizman, and Pekker, 1996)

$$\partial_t E_{kz} = 4\pi e \int dv v \delta f_k - \gamma_d E_{kz}, \tag{4.138}$$

in order to introduce an imposed extrinsic damping. Equation (4.138) can be reduced to

$$\frac{2}{\omega_p}\frac{\partial}{\partial t}\delta\phi_{k_0} = \frac{4\pi}{k_0^2} ie \int dv \delta f_{Ek_0} - \frac{2\gamma_d}{\omega_p}\delta\phi_{k_0}, \tag{4.139}$$

i.e., Eq. (4.123) adding an *ad hoc* background dissipation. Meanwhile, the Vlasov equation (4.122) is modified to account for source, sink, and collision terms on the right-hand side in the form of one of the models discussed previously, e.g., Eq. (4.132). Introducing $E = E_0(t)\cos\xi$ with $\xi = k_0 z - \omega_p t = k_0 x$ (cf. Sec. IV.D.1), and dropping subscripts k_0 and E in Eq. (4.139), the solution of Eq. (4.132) can be cast as

$$f = f_0 + \sum_{n=1}^{\infty} \delta f_n e^{in\xi} + \text{c.c.}, \tag{4.140}$$

$$\partial_t f_0 + \nu f_0 = Q(v) - \omega_B^2(t)\partial_u \mathbb{R}\text{e}\delta f_1, \tag{4.141}$$

$$\partial_t \delta f_1 + iu\delta f_1 + \nu\delta f_1 = -(1/2)\omega_B^2(t)\partial_u(f_0 + \delta f_2), \tag{4.142}$$

etc. Here $\omega_B^2(t) = ek_0E_0(t)/m$ and $u = k_0 v - \omega_p$, while Eq. (4.139) becomes

$$\frac{d}{dt}\omega_B^2 = -\frac{\omega_p^2}{n_0}\frac{\omega_0}{k_0}\int_{-\infty}^{\infty} \mathbb{R}\text{e}\delta f_1 du - \gamma_d\omega_B^2. \tag{4.143}$$

For monochromatic fluctuations (dropping δf_2), Eqs. (4.141)–(4.143) are the t representation of Eqs. (4.126)–(4.129) with the addition of finite ν, Q, and γ_d. Near marginal stability $f_0 = F_0 + \delta f_0$, with $F_0 = Q(v)/\nu(v)$, and the problem can be solved iteratively with a perturbative asymptotic expansion based on the ordering $\gamma \equiv \gamma_L - \gamma_d \sim \nu \sim |u| \ll \gamma_L$ and expansion parameter $\omega_B^2/\nu^2 \sim \omega_B^2/u^2 \sim \omega_B^2/\gamma^2 \sim (\gamma/\gamma_L)^{1/2}$, which applies for $\omega_B t \ll 1$ (Berk, Breizman, and Pekker, 1996). The iterative solution corresponds to

$$\delta f_0 = -\int_0^t e^{-\nu(t-t_1)}\omega_B^2(t_1)\partial_u \mathbb{R}\mathrm{e}(\delta f_{1L}+\cdots)dt_1,$$
$$\delta f_1 = -(1/2)\int_0^t e^{-(\nu+iu)(t-t_1)}\omega_B^2(t_1)\partial_u f_0 dt_1, \tag{4.144}$$

where δf_{1L} is the linearized form of δf_1 obtained for $f_0 \to F_0 = Q(v)/\nu(v)$. Introducing $\tau = (\gamma_L - \gamma_d)t$, $\hat{\nu} = \nu/(\gamma_L - \gamma_d)$, and $A(\tau) = (\omega_B^2/\gamma^2)\gamma_L^{1/2}/\gamma^{1/2}$, the validity limits of the asymptotic analysis impose $\tau \ll (\gamma/\gamma_L)^{-1/4}$ (from $\omega_B t \ll 1$) and $A \sim \hat{\nu} \sim 1$. Meanwhile, the iterative solution of Eqs. (4.143) and (4.144) yields

$$\frac{d}{d\tau}A = A - \frac{1}{2}\int_0^{\tau/2} z^2 A(\tau - z)dz \times \int_0^{\tau-2z} A(\tau - z - x)A(\tau - 2z - x)e^{-\hat{\nu}(2z+x)}dx. \tag{4.145}$$

Here the occurrence of the secular term $\propto z^2$ in the normalized time variable is due to the truncation of the Dyson series (cf. Fig. 1), as discussed below Eq. (4.129). Equation (4.145) admits a fixed point solution $A_0 = 2\sqrt{2}\hat{\nu}^2$ which is stable for $\hat{\nu} > \hat{\nu}_{cr} \simeq 4.38$. For $\hat{\nu} < \hat{\nu}_{cr}$, $A(\tau)$ first oscillates and for further decreasing $\hat{\nu}$ it loses the periodic behavior, entering a chaotic regime (Breizman *et al.*, 1997). Meanwhile, for sufficiently low values of $\hat{\nu}$ the system exhibits a finite time singularity which is unphysical and again due to the truncation of the Dyson series.

The work of Berk, Breizman, and Pekker (1996) was generalized by Breizman *et al.* (1997) [see also Berk, Breizman, and Pekker (1997)] to the generic case of weakly unstable modes excited by resonant wave-particle interactions, for which

$$\frac{d}{d\tau}A = A - e^{i\phi}\int_0^{\tau/2} z^2 A(\tau - z)dz \times \int_0^{\tau-2z} A(\tau - z - x)A^*(\tau - 2z - x)e^{-\hat{\nu}(2z+x)}dx. \tag{4.146}$$

Here the factor $e^{i\phi}$ depends on the linear physics of the underlying mode. Breizman *et al.* (1997) also investigated the effect of replacing the source or collisional terms $-\nu(f - F_0)$ and $F_0 = Q(v)/\nu(v)$ with a diffusivelike collision operator $\nu_{\mathrm{eff}}^3(\partial^2/\partial\Omega^2)(f - F_0)$, with $\Omega = \dot{\xi} = \partial H/\partial I$ and (I, ξ) the action-angle coordinates of the relevant wave-particle resonance. Thus, $\exp[-\hat{\nu}(2z + x)]$ in Eq. (4.146) is replaced by $\exp[-\hat{\nu}^3 z^2(2z/3 + x)]$ with $\hat{\nu} = \nu_{\mathrm{eff}}/\gamma$, yielding

$$\frac{d}{d\tau}A = A - e^{i\phi}\int_0^{\tau/2} z^2 A(\tau - z)dz \times \int_0^{\tau-2z} A(\tau - z - x)A^*(\tau - 2z - x)e^{-\hat{\nu}^3 z^2(2z/3+x)}dx. \tag{4.147}$$

Similar to Eq. (4.145), Eqs. (4.146) and (4.147) also admit a fixed point for $\hat{\nu} > \hat{\nu}_{cr}$. At $\hat{\nu} = \hat{\nu}_{cr}$ a first bifurcation occurs and $A(\tau)$ has a solution in the form of a limit cycle, which then goes through subsequent period doubling bifurcations for further decreasing $\hat{\nu}$ and eventually becomes chaotic (Breizman *et al.*, 1997; Fasoli *et al.*, 1998; Heeter, Fasoli, and Sharapov, 2000). In the case of Eq. (4.147), $\hat{\nu}_{cr} \simeq 2.05$ for $|\phi| \ll 1$ (Breizman *et al.*, 1997).

Systematic numerical investigations of the Vlasov-Poisson system were carried out (Vann *et al.*, 2003; Vann, Dendy, and Gryaznevich, 2005; Lesur, Idomura, and Garbet, 2009) in order to characterize the fully nonlinear solutions of Eq. (4.138) and of the Vlasov equation for monochromatic waves with different source, sink, and collisionality models. In particular, Lesur, Idomura, and Garbet (2009) and more recently Lesur and Idomura (2012) adopted a model collision term in the form of Eq. (4.132) and carefully discussed the validity limits of the aforementioned analytical works comparing where appropriate fully nonlinear solutions with analytic ones. It was shown that there are conditions where the thermal plasma does not respond as a linear dielectric medium, e.g., when the resonance involves a finite amount of thermal electrons. The bifurcation diagram in the (γ_d, ν) parameter space, similar to that discussed by Vann *et al.* (2003), confirms that at fixed γ_d and for decreasing values of ν numerical solutions are damped, converge to a steady state (cf. Sec. IV.D.2.a), are periodic, or chaotic, or characterized by frequency sweeping phase-space structures. This latter behavior is discussed in Sec. IV.D.2.c and corresponds to the parameter regime, where the analytic solutions of Eqs. (4.145)–(4.147) exhibit finite time singularity. Furthermore, Lesur, Idomura, and Garbet (2009) demonstrated the existence of subcritical states, consistent with former numerical results that nonlinear excitation of phase-space structures is possible if fluctuation is initialized at sufficiently large amplitude, $\omega_B^2 \sim (\nu + \gamma)^{5/2}(\gamma_L)^{-1/2}$ (Berk *et al.*, 1999). Metastable kinetic modes were also investigated by Nguyen, Lütjens *et al.* (2010), where it was shown that purely nonlinear steady-state regimes are found by numerical simulations, when the nonlinear reduction of the resonant damping rate due to thermal plasma is larger than the corresponding reduction of the EP drive. Such processes may be relevant for BAE nonlinear dynamics, for which purely nonlinear steady-state regimes could exist for typical tokamak equilibrium conditions (Nguyen, Garbet *et al.*, 2010). Nonlinear instabilities of phase-space structures in both marginally unstable and linearly stable (subcritical) regimes were recently discussed by Lesur and Diamond (2013).

c. Nonlinear dynamics of phase-space holes and clumps

For sufficiently small $\hat{\nu}$, Eqs. (4.146) and (4.147) exhibit the same finite time singularity of Eq. (4.145) due to the unphysical truncation of the Dyson series (cf. Fig. 1). This behavior suggests the existence of a fourth dynamic regime of Eqs. (4.145)–(4.147), in addition to steady-state (cf. Sec. IV.D.2.a), periodic, and chaotic regimes (cf. Sec. IV.D.2.b). It was investigated by numerically solving Eq. (4.139) and the Vlasov equation with a variety of source, sink, and collision models (Berk, Breizman, and Pekker, 1997; Berk, Breizman, and Petiashvili, 1997; Breizman *et al.*, 1997; Berk *et al.*, 1999). In particular, it was found that numerical solutions are characterized by the formation of pairs of phase-space holes (Berk, Nielson, and Roberts, 1970;

Dupree, 1982; Berman, Tetreault, and Dupree, 1983; Tetreault, 1983) and clumps (Dupree, 1970, 1972, 1982; Berman, Tetreault, and Dupree, 1983; Tetreault, 1983). After formation, holes and clumps move away from the original resonance in velocity space, corresponding to energy extraction from the particle distribution function and to, respectively, upward (hole) and downward (clump) frequency sweeping phase-space structures, which can be viewed as Bernstein-Greene-Kruskal (BGK) modes (Bernstein, Greene, and Kruskal, 1957). Since the work by Breizman *et al.* (1997), the steady-state, periodic, and chaotic regimes of the solution of the Vlasov-Poisson system are referred to as "soft" nonlinear behavior, to discriminate them from the "hard" nonlinear regime where hole and clump structures are formed. The definition of a hard nonlinear regime is justified by noting that for fixed $\nu_{\rm eff}$ sufficiently low $\hat{\nu}$ can be achieved for sufficiently strong net drive $\gamma = \gamma_L - \gamma_d$. In the work by Berk *et al.* (1999), it was noted that this hard regime is not observed for $\gamma_d/\gamma_L \lesssim 0.4$. On the other hand, Lesur, Idomura, and Garbet (2009) showed that frequency chirping is observed in numerical simulations for γ_d/γ_L as low as $\gamma_d/\gamma_L = 0.2$. In fact, Lilley and Nyqvist (2014) recently demonstrated that holes and clumps may be generated with any small amount of background dissipation, provided that a phase-space plateau is formed by phase mixing and dissipative damping of an unstable kinetic resonance. More precisely, in this case holes and clumps are negative energy waves that grow because of background dissipation.

Equations (4.141)–(4.143) were reconsidered by Lilley, Breizman, and Sharapov (2009) with a model collision term in the form

$$d_t f = (\nu^3 k_0^{-2}\partial_v^2 + \alpha^2 k_0^{-1}\partial_v - \beta)(f - F_0), \tag{4.148}$$

where F_0 is the equilibrium distribution function and ν, α, and β control, respectively, velocity-space diffusion, dynamical friction, and particle annihilation rate. Equations. (4.145)–(4.147) are then generalized to

$$\frac{d}{d\tau}A = A - \frac{1}{2}\int_0^{\tau/2} z^2 A(\tau - z)dz \int_0^{\tau-2z} A(\tau - z - x) \times A^*(\tau - 2z - x)e^{-\hat{\nu}^3 z^2(2z/3+x) - \hat{\beta}(2z+x) + i\hat{\alpha}^2 z(z+x)}dx, \tag{4.149}$$

with $\hat{\nu} = \nu/\gamma$, $\hat{\alpha} = \alpha/\gamma$, $\hat{\beta} = \beta/\gamma$, and $\gamma = \gamma_L - \gamma_d$. For $\hat{\nu} = \hat{\beta} = 0$, i.e., with dominant dynamical friction, Eq. (4.149) always exhibits finite time singularity, in contrast to Eqs. (4.145)–(4.147), whose evolutions exhibit both soft and hard nonlinear dynamic behaviors (cf. Sec. IV.D.2.b). This result is confirmed by numerical solutions of Eqs. (4.139) and (4.148), which show frequency sweeping holes and clumps when dynamical friction is the dominant collisional process (Lilley, Breizman, and Sharapov, 2010).

The first analytical theory of hole-clump frequency sweeping was proposed by Berk, Breizman, and Petiashvili (1997) and Berk *et al.* (1999). There one assumes that the frequency separation of holes and clumps is larger than γ_L and ω_B, so that they are treated independently as isolated structures. Furthermore, both mode amplitude and frequency are postulated to evolve adiabatically, i.e., $|\dot{\omega}| \ll \omega_B^2$, $|\dot{\omega}_B| \ll \omega_B^2$, etc. Defining $\omega = \omega_0 + \delta\omega(t)$, $q = \xi - \int_0^t \delta\omega(t')dt'$, and using the generating function $F_2 = [p + \delta\omega(t)][\xi - \int_0^t \delta\omega(t')dt']$, with $p = \Omega - \omega_0 - \delta\omega(t)$ and $\Omega = \dot{\xi}$, the Hamiltonian is (Berk *et al.*, 1999)

$$\mathcal{H} = p^2/2 - \delta\omega^2/2 - \omega_B^2\cos q + q\delta\dot{\omega}. \tag{4.150}$$

Meanwhile, Eq. (4.139) becomes

$$\left(\frac{d}{dt} + \gamma_d\right)A(t) = -\frac{i}{\pi^2}\frac{\gamma_L}{\partial F_0/\partial\Omega}\int dqdp e^{-iq - i\int_0^t \delta\omega(t')dt'} f(q,p,t). \tag{4.151}$$

Since wave amplitude and frequency change slowly, there exists an adiabatic action invariant and at lowest order particle response is independent of the corresponding angle. Thus, f slightly deviates from the coarse-grained distribution (cf. Sec. IV.D.1) and inside the separatrix $f = F_0 + g$ and at the lowest order

$$g \simeq g_0 = F_0(\omega_0) - F_0(\omega_0 + \delta\omega). \tag{4.152}$$

Furthermore, the dynamics is adiabatic and maintains near marginal stability at every instant. Therefore, frequency sweeping is obtained from the condition of balancing background dissipation with power released by hole and clump motion in phase space (Berk *et al.*, 1999). By means of Eqs. (4.151) and (4.152), it is possible to show that

$$\frac{\omega_B}{\gamma_L} = \frac{16}{3\pi^2}, \quad \text{and} \quad \frac{\delta\omega}{\gamma_L} = \frac{16}{3\pi^2}\sqrt{\frac{2}{3}}(\gamma_d t)^{1/2}, \tag{4.153}$$

having assumed $\hat{g}(x) = [F_0(\omega_0 + x) - F_0(\omega_0)]/F_0'(\omega_0)x \simeq 1$. This result consistently describes the adiabatic evolution of hole and clump structures for times $|\omega_B t| \gg 1$. Note this limit is opposite to the $|\omega_B t| \ll 1$ assumption underlying Eqs. (4.145)–(4.147).

The theory of adiabatic frequency chirping of hole and clump structures in phase space for the bump-on-tail problem near marginal stability was investigated by Breizman (2010). This work further extends the water bag model of driven continuously phase-locked coherent structures in uniform unmagnetized plasmas and of the associated BGK modes (Khain and Friedland, 2007; Barth, Friedland, and Shagalov, 2008). The theoretical analysis assumes the background plasma as a linear dielectric medium (cf. Sec. IV.D.1) and solves Poisson's equation for the BGK mode in terms of the self-similar scalar potential

$$\delta\phi_{k_0} \equiv -(1/e)U[z - s(t); t], \tag{4.154}$$

where $U[z - s(t); t]$ is a periodic function of $z - s(t)$ and a slowly varying function of t. The wave phase velocity $\propto \dot{s} = ds(t)/dt$, with $\dot{s}_0 = \omega_0/k_0$ at the initial time, is determined by the condition that the power released by the phase-space structure motion balances collisional dissipation

due to the friction force exerted by bulk plasma electrons. The exact nonlinear solution of this problem shows that $U[z-s(t);t]$ depends on the narrow depletion (hole) or protrusion (clump) inside the separatrix, i.e., on $F_0(\dot{s})-F_0(\dot{s}_0)$. Meanwhile, assuming that the motion is adiabatic and maintained near marginal stability, the predicted time evolution of the BGK mode recovers Eq. (4.153) in the early stage, where $\dot{s}\simeq\dot{s}_0$. It, however, can significantly depart from that at later times due to significant deviations of $\dot{s}$ from $\dot{s}_0$. In this respect, this model can describe long-range frequency sweeping events (cf. also Sec. IV.D.3), provided that the thermal plasma response remains a linear dielectric medium. For a more detailed description, see the original work (Breizman, 2010) [see also Breizman (2011) and Breizman and Sharapov (2011)].

The first evidence of long-range frequency sweeping was reported in numerical simulations of Eqs. (4.138) and (4.148) with $\alpha=\nu=0$ (Vann, Berk, and Soto-Chavez, 2007). The simulations investigated the nonlinear behavior of strongly driven 1D bump-on-tail systems with comparable values of the thermal plasma and beam densities as well as velocity spread. In these simulations, upward frequency sweeping holes are preferentially formed, connected with strong nonlinear distortions of both thermal and energetic-particle distribution functions (cf. Sec. IV.D.1). Meanwhile, only the time-averaged particle distribution function is maintained near marginal stability. As expected for strongly nonlinear bursting behavior, a structure more stable than the marginal distribution function exists, following which the distribution function is slowly rebuilt by external sources.

For significantly less strong drive and near mode marginal stability, numerical simulation results of Eqs. (4.139) and (4.148) confirm the existence of the long-range frequency sweeping events described by Breizman (2010, 2011) and Breizman and Sharapov (2011), which correspond to convective particle transport in buckets via the adiabatic evolution of the underlying BGK modes. The frequency sweeping phase-space structures described by Lilley, Breizman, and Sharapov (2010) move upward (holes) and downward (clumps) until the nonlinear frequency shift exceeds the frequency width of the linear unstable spectrum, which is much smaller than the frequency of the initial linear instability as assumed in the adopted model.[20] Thus, holes and clumps eventually "stuck up" and, by resonance overlap, cause a relaxation of the particle distribution function to a plateau extending throughout the linearly unstable region (Lilley, Breizman, and Sharapov, 2010), leading to maximized energy extraction from fast particle phase space. This extended flattening was recently shown to be more important near marginal stability than quasilinear diffusion in the presence of many modes (Lilley and Breizman, 2012). Long-range chirping also occurs in the collisionless limit, near marginal stability. In this case, the continuous generation of hole and clump pairs is due to the steepening of the ambient distribution function in the wake of such structures (Lilley, Breizman, and Sharapov, 2010). In fact, phase-space holes and clumps can be generated close as well as far from instability threshold (Lilley and Nyqvist, 2014). However, for increasing instability drive the bump-on-tail paradigm will ultimately break down and one needs to adopt the fishbone paradigm when mesoscale EP physics becomes important (cf. Sec. IV.D.5).

3. The bump-on-tail problem as paradigm for Alfvén eigenmodes near marginal stability

A detailed discussion of applications of the bump-on-tail paradigm to AE nonlinear dynamics was given in Breizman and Sharapov (2011). Here we present only the main findings and discuss the underlying physics basis for such applications.

The first application of the bump-on-tail paradigm to experimental observations is the interpretation of the pitchfork splitting of TAE spectral lines in JET during ion cyclotron resonance heating (ICRH) (Fasoli *et al.*, 1998; Heeter, Fasoli, and Sharapov, 2000) as manifestation of the soft nonlinear regime discussed in Sec. IV.D.2. More precisely, Fasoli *et al.* (1998) used the frequency spectrum of the limit cycle solution of Eq. (4.147) at the bifurcation point, i.e., with $\hat{\nu}=\hat{\nu}_{cr}\simeq 2.05$ for $|\phi|\ll 1$, and compared it with high resolution measurements of TAE frequency. This work motivated further analyses aimed at providing information on the values of γ_L, γ_d, and ν_{eff} from MHD spectroscopy (Fasoli *et al.*, 2002; Pinches *et al.*, 2004; Pinches, Berk *et al.*, 2004) with the advantage of interpreting some features of AE experimental observations and inferring local kinetic plasma parameters, which are otherwise difficult to obtain. Pinches *et al.* (2004) also noted that the frequency chirping expression from Eq. (4.153) agrees with the experimentally observed chirping in experimental devices near marginal stability. Meanwhile, Vann, Dendy, and Gryaznevich (2005) interpreted the observation of frequency chirping AEs in the Mega Ampere Spherical Tokamak (MAST) (Gryaznevich and Sharapov, 2004; Pinches *et al.*, 2004) as evidence of the hard nonlinear regime of the bump-on-tail nonlinear dynamics (Breizman *et al.*, 1997).

The different types of chirping modes observed in MAST (Gryaznevich and Sharapov, 2006; Gryaznevich *et al.*, 2008) have recently attracted significant interest due to the different dynamic behaviors that are predicted by the 1D bump-on-tail paradigm with different collision models and EP sources (Lilley, Breizman, and Sharapov, 2009, 2010). In particular, special emphasis was given to numerical solutions of Eqs. (4.143) and (4.148) showing that frequency sweeping holes and clumps are the only type of nonlinear behavior when dynamical friction dominates (cf. Sec. IV.D.2.c). These findings were proposed by Lilley, Breizman, and Sharapov (2009, 2010) as a possible explanation of why soft nonlinear behavior is expected for ICRH heated plasmas, with prevailing velocity-space diffusion, whereas neutral beam injection (NBI), mostly affected by dynamical friction, generally yields hard nonlinear regimes.[21]

[20] Note that using Eq. (4.138) and including the kinetic response of the thermal plasma component allows the investigation of the nonlinear frequency shift of the order of the linear mode frequency (Vann, Berk, and Soto-Chavez, 2007).

[21] Note that experimental observations of hard nonlinear behavior in ICRH heated plasmas also exist, as in the case of high-frequency fishbones (Nabais *et al.*, 2005; Zonca *et al.*, 2009).

As application of the numerical method by Lesur, Idomura, and Garbet (2009) with a model collision term in the form of Eq. (4.148), Lesur *et al.* (2010) analyzed experimental measurements of quasiperiodic chirping TAE in JT-60U (Oyama, 2009) and developed a fitting procedure for calculating γ_L, γ_d, and collision frequencies from the frequency spectrum provided by Mirnov coil measurements. Reconstructed drive and damping rates are in qualitative and quantitative agreement with experimental findings as are the reconstructed collision frequencies compared with values from experimental equilibrium data. Furthermore, dynamical friction and velocity-space diffusion are found to be essential to reproduce nonlinear features observed in experiments, with dynamical friction playing a crucial role in the asymmetry between hole and clump chirping (Lesur *et al.*, 2010; Lesur and Idomura, 2012), as also noted by Lilley, Breizman, and Sharapov (2009, 2010). These analyses (Lesur *et al.*, 2010) clarify that TAE in JT-60U typically exist in regimes away from marginal stability and that frequency sweeping events are generally nonadiabatic.

As noted earlier, the applicability of the bump-on-tail paradigm to AE nonlinear dynamics requires, in particular, the fluctuation-induced EP excursions be small compared with the radial wavelength (Berk and Breizman, 1990b, 1990c). This allows assuming constant mode amplitude in the radial direction as implicitly required by the formal equivalence $r \leftrightarrow v$. Quantitative discussions on its applicability regime are presented in Sec. IV.D.5. In general, it depends on the type of resonant EPs as well as on the wave dispersive properties and mode structures. For circulating resonant EPs, the validity limits are least stringent and the upper bound on the drive strength is in the range $\gamma_L/\omega_0 \lesssim 10^{-2}$. Meanwhile, for EPMs (Chen, 1994) the bump-on-tail paradigm is not applicable, since mode structure and frequency depend on EPs and the frequency-dependent background damping is due to the SAW continuous spectrum (cf. Secs. III and IV.D.6). The applicability conditions also imply that small EP redistributions are expected in the case of an isolated resonance. Meanwhile, by exchanging $r \leftrightarrow v$, the long-range frequency sweeping events (Breizman, 2010, 2011; Lilley, Breizman, and Sharapov, 2010; Breizman and Sharapov, 2011; Lilley and Breizman, 2012) correspond to local radial perturbations in the EP distribution function propagating across $\boldsymbol{B}_0$ for a distance comparable to the EP equilibrium profile scale length. Thus, the absence of mode structures and plasma nonuniformities in this model renders its generalization to either AE or EPM nonlinear dynamics in toroidal plasmas dubious (cf. Sec. IV.D.5). The original 1D bump-on-tail paradigm was significantly extended by Wang and Berk (2012) and Wang (2013), taking into account the local TAE radial mode structure near one radially isolated gap in the SAW continuous frequency spectrum, but preserving the ansatz of proximity to marginal stability and perturbative EP dynamics (Wang, 2013). Time evolution of the local TAE mode structure is demonstrated to be crucial for describing chirping events with nonlinear frequency shifts comparable with the distance of linear mode frequency from the SAW continuum accumulation point (Wang, 2013), consistent with the results of prior theoretical analyses (Zonca *et al.*, 2000, 2005) and of hybrid MHD-gyrokinetic simulations (Briguglio, Zonca, and Vlad, 1998; Briguglio *et al.*, 2002; Zonca *et al.*, 2002; Vlad *et al.*, 2004; Wang *et al.*, 2012). In this way, it was shown that the predicted chirping may be nonadiabatic, $|\dot{\omega}| \lesssim \omega_B^2$, thereby, challenging the self-consistency of assumptions made for the derivation of model equations (Wang and Berk, 2012; Wang, 2013). These works, nonetheless, suggest that nonadiabatic chirping is naturally developed in nonlinear dynamics of phase-space holes and clumps, as anticipated by Gorelenkov *et al.* (2000), Zonca and Chen (2000), and Zonca *et al.* (2005). Furthermore (Wang, 2013), extended model equations predict the possible penetration of downward frequency sweeping TAE clumps into the lower SAW continuum similar to the long-range chirping mode behavior observed in MAST (Gryaznevich and Sharapov, 2006). As the mode structure evolves into that of an EPM, we note that a nonperturbative treatment of EP nonlinear dynamics becomes, however, in general necessary (cf. Sec. IV.D.6).

Frequency sweeping is an important phenomenon, as recognized since early experimental observations of chirping AEs and EPMs (Heidbrink, 1995; Bernabei *et al.*, 1999; Kramer *et al.*, 1999; McClements *et al.*, 1999; Takechi *et al.*, 1999; Wong, 1999; Gorelenkov *et al.*, 2000) and the first theoretical analyses of these phenomena (Berk and Breizman, 1996) emphasizing that wave-particle energy exchange can be enhanced by resonance sweeping. In particular, Berk and Breizman (1996) showed that this enhancement is higher for adiabatic than for nonadiabatic frequency chirping. This result is consistent with the phenomenology of autoresonance (Meerson and Friedland, 1990), discussed in Sec. IV.E, where adiabatic chirping of a phase-locked resonance structure is imposed externally for optimized energy extraction from the particle phase space. When the system dynamically evolves sufficiently near marginal stability (Sec. IV.D.2.c), the coarse-grained particle distribution function (cf. Sec. IV.D.1) in the hole and clump resonance region preserves its value at the initial linear resonance and its adiabatic dynamics is set by the balance between the power extraction from the particle phase space and the energy dissipation rate (Breizman, 2010). However, for sufficiently strong drive that radial mode structures as well as plasma nonuniformity and equilibrium geometry become important, nonadiabatic frequency sweeping via phase locking becomes the condition for maximized wave-particle power exchange (cf. Sec. IV.D.5) and is associated with rapid EP profile redistributions (Gorelenkov *et al.*, 2000; Zonca and Chen, 2000). For EPM, furthermore, new distinctive features and nonadiabatic bursting behavior (cf. Sec. IV.D.6) are expected due to the interplay among nonlinear dynamics, mode structures, and EP transport.

Deviation from adiabatic frequency sweeping for sufficiently strong drive is also expected in the solutions of the 1D bump-on-tail problem. This is observed by numerical simulations of Eqs. (4.138) and (4.148) with $\alpha = \nu = 0$, showing nonperturbative and fast chirping events with frequency sweeping $\propto t$ rather than $\propto t^{1/2}$ (Vann, Berk, and Soto-Chavez, 2007). These are qualitatively similar to EPM in their general phenomenological features as they involve bursting behavior of a strongly driven nonlinear system.

Nonadiabatic processes also underlie the formation of phase-space structures, such as clumps and holes. In fact, phase-space structures can be formed only for $\omega_B t \sim 1$

(Briguglio *et al.*, 2014; Zonca *et al.*, 2015b). This is the mechanism underlying the continuous generation of hole and clump pairs in the collisionless 1D bump-on-tail problem near marginal stability (Lilley, Breizman, and Sharapov, 2010) (cf. Sec. IV.D.2.c) with similarities to what occurs in the case of EPM nonlinear dynamics (Zonca *et al.*, 2005; Briguglio, 2012; Briguglio *et al.*, 2014) (cf. Sec. IV.D.5). However, the absence of an intrinsic interplay between mode structures and particle transport in the 1D bump-on-tail problem remains a crucial and fundamental difference.

We now briefly remark on the case of many modes, which is less explored than the single-mode case discussed previously. The role of radial mode structures is more subtle in the case of the dense spectrum of AEs characterizing burning plasmas (Chen and Zonca, 2007a) (cf. Sec. III.B), where resonance overlap (Chirikov, 1979) of finite-size phase-space islands can yield enhanced stochastic transport (Hsu and Sigmar, 1992; Sigmar *et al.*, 1992; Breizman, Berk, and Ye, 1993). The qualitative scenario of the onset of stochastic transport within the 1D bump-on-tail paradigm was recently reviewed by Breizman (2011) and Breizman and Sharapov (2011), and the implications of quasilinear diffusion in the presence of many modes were discussed by Lilley and Breizman (2012). Sufficiently above the stochasticity threshold and for a sufficiently dense and broad AE spectrum, finite radial mode structures and thus plasma nonuniformities are not expected to significantly affect diffusive transport. Nonetheless, equilibrium geometry will still play important roles in setting the wave-particle decorrelation time via wave-particle resonance conditions as noted by Zhang *et al.* (2010) on EP turbulent transport (cf. Sec. V.C) and as it more generally applies to turbulent transport [see, e.g., Lin *et al.* (2007) and Feng, Qiu, and Sheng (2013)]. The detailed mechanisms by which a 1D uniform plasma in the presence of many modes reaches the onset condition for diffusive transport by stochastization of particle orbits in the phase space due to resonance overlap (Chirikov, 1979) have been addressed by Breizman, Berk, and Ye (1993). The onset of stochasticity is rarely global in phase space (Lichtenberg and Lieberman, 1983, 2010) and actually the energy release from the particle distribution function in the considered phase-space region affected by diffusive transport may induce the growth of additional fluctuations, otherwise disallowed, in adjacent phase-space domains, where local gradients are enhanced as predicted by Eqs. (4.119) and (4.120). This "domino effect" (Berk, Breizman, Fitzpatrick, and Wong, 1995; Berk *et al.*, 1996) qualitatively resembles that of avalanches in sandpile systems involving self-organized criticality (SOC) (Bak, Tang, and Wiesenfeld, 1987), i.e., of "chain reactions" of transport events. For investigating this process applied to multiple toroidal mode-number AEs, Berk, Breizman, Fitzpatrick, and Wong (1995) introduced a "line-broadened quasilinear burst model" for treating resonance overlap of modes with bursting behavior and applied it to characterize the nonlinear response of driven systems in weak turbulence theory (Berk *et al.*, 1996). It may be expected that near the onset of stochasticity equilibrium geometry and nonuniformity of plasma profiles significantly affect nonlinear dynamics through radial mode structures and their influence on nonlinear particle orbits, whose typical size is of the order of the radial width of the single poloidal Fourier harmonics [see Eq. (3.9)] for typical values of the linear mode growth rate (cf. Sec. IV.D.5). This is supported by recent findings of test-particle simulations of EP transport in DIII-D (White *et al.*, 2010a, 2010b) showing that the stochastic threshold depends on modeling details (cf. Sec. V.A). These issues are further discussed in Sec. VI.A.

4. Numerical simulations of perturbative excitation of Alfvén eigenmodes

For numerical investigation of AE nonlinear dynamics driven by EPs, simplification is possible by considering perturbative EP dynamics.[22] The mode structures meanwhile are computed from a linear stability analysis and taken to be fixed. More specifically, the EP distribution function computed in the given AE fields taking into account sources and collisions yields the corresponding EP currents, which are used to obtain the time evolution of wave amplitudes and phases (Chen and White, 1997). This approach is very efficient and can provide an accurate description of AE nonlinear evolution even in the presence of many modes, provided that the predicted nonlinear frequency shifts are consistent with the fixed radial structure of the single poloidal Fourier harmonics [see Eq. (3.9)].[23] For practical applications and comparisons with experimental observations, however, further simplifications are often employed. In fact, test-particle analyses are often adopted (cf. Sec. V.A), where not only AE mode structures are assumed, but also mode amplitude and phases are given from experimental data.

Perturbative EP numerical analyses were adopted by Wu, Cheng, and White (1994) for investigating the effect of a single TAE mode in typical TFTR and ITER plasmas and by Wu *et al.* (1995), where the saturation level of the bump-on-tail problem in the absence of collisions and background dissipation was found to be $\omega_B \simeq 3.3\gamma_L$, consistent with Levin *et al.* (1972), while the saturation of a $n = 3$ TAE mode in ITER was estimated to scale as $\omega_B \simeq 4\gamma_L$. With a similar approach, Candy *et al.* (1997) developed a Lagrangian representation for AEs time evolution weakly driven by a perturbative EP population. Meanwhile, introducing collisions by Eq. (4.132), Wong and Berk (1998) verified the scaling of the steady-state TAE saturation amplitude predicted by Eq. (4.133) and for decreasing collisionality the existence of amplitude fluctuations, whose downshifted and upshifted frequency components are compatible with the $\propto t^{1/2}$ scaling of Eq. (4.153). A more systematic theoretical framework for handling collisions as in Eq. (4.136) was presented by Chen and White (1997), by means of which Chen *et al.* (1999) verified the theoretically predicted scaling of the saturation amplitude with linear growth rate and collision rate as derived from Eq. (4.137). This approach was used to predict the

[22]This method does not apply to EPMs, for which even the linear description requires a nonperturbative analysis of the EP response (Chen, 1994).

[23]We recall here that the radial structure of poloidal Fourier harmonics changes with the mode frequency and tends to become singular as the accumulation point of the SAW continuous spectrum is approached.

saturation levels of TAE excited by fusion alpha particles in TFTR and to successfully compare theoretical predictions with experimental observations (Gorelenkov *et al.*, 1999). The same approach was used by Bergkvist and Hellsten (2004) to show that ICRH can also have an effect similar to the pitch angle scattering term in Eq. (4.136), pointing out that both processes have a diffusive nature in velocity space, but Coulomb collisions are more effective at low energies while ICRH interactions are more effective at high energies. In plasma scenarios typical for JET and accounting for collisions and ICRH on the same footing, Bergkvist *et al.* (2005) showed that time evolution of TAE amplitude computed with the perturbative analysis of Chen and White (1997) and Chen *et al.* (1999) is consistent with experimental observations and typically dominated by the effect of ICRH. For example, accounting for ICRH effects improves the comparison of the computed numerical TAE spectrum with the observed splitting of TAE spectral lines (Fasoli *et al.*, 1998; Heeter, Fasoli, and Sharapov, 2000). Furthermore, due to the fact that ICRH acts as an effective resonance broadening (Bergkvist, Hellsten,and Holmström, 2007), ICRH is expected to be important in the onset of stochasticity in phase space and enhanced fluctuation-induced transport in the case of resonance overlap due to many modes (cf. Secs. V.A and VI.A). Recently, Fu *et al.* (2010) and Lang and Fu (2011) discussed plasma microturbulence as a possible mechanism to enhance EP phase-space diffusion (cf. Sec. V.C). In particular, letting D_r be the EP radial diffusion coefficient, it was argued that the pitch angle scattering part of the collision operator in Eq. (4.136) near a resonance $\Omega = \omega - k_\parallel v_\parallel = 0$ can be rewritten as

$$\nu_d(1-\lambda^2)(\partial_\lambda \Omega)^2 \partial_\Omega^2 f, \tag{4.155}$$

while the effect of turbulence driven radial diffusion becomes

$$D_r(\partial_r \Omega)^2 \partial_\Omega^2 f, \tag{4.156}$$

to be added on the right-hand side. By comparisons of Eqs. (4.155) and (4.156), Fu *et al.* (2010) and Lang and Fu (2011) concluded that turbulence-induced radial diffusion might be more important than collisional effects in determining the saturation level of EP-driven AEs near marginal stability in burning-plasma experiments.

Hybrid MHD-gyrokinetic codes (Park *et al.*, 1992) (cf. Sec. II.E) were also adopted for the investigation of EP-driven TAE nonlinear dynamics near marginal stability. Simulation results showed the expected scaling $|\delta \boldsymbol{B}_\perp/B_0| \sim (\gamma_L/\omega_0)^2$ at saturation (Fu and Park, 1995; Todo *et al.*, 1995; Park *et al.*, 1999). Deviations from this scaling were shown to occur in hybrid MHD-gyrokinetic numerical simulations of TAEs with increasing EP drive, when the nonlinear EP radial displacement was comparable with the characteristic radial wavelength of the mode (Briguglio, Zonca, and Vlad, 1998) (cf. Sec. IV.D.5). EP losses were also observed in early hybrid MHD-gyrokinetic simulations in the presence of multiple TAEs (Todo and Sato, 1998). Fokker-Planck collision models with source terms were implemented in hybrid MHD-gyrokinetic simulations (Todo *et al.*, 2001; Lang, Fu, and Chen, 2010) and applied to verification of theoretical predictions (Berk *et al.*, 1999) (cf. Sec. IV.D.2) based on the bump-on-tail paradigm (Lang, Fu, and Chen, 2010), as well as to the investigation of recurrent TAE bursts observed in TFTR NBI heated plasmas (Todo, Berk, and Breizman, 2003), for which the numerical repetition time of subsequent TAE bursts is close to experimental values. Neglecting mode-mode nonlinear couplings, the stored beam energy is found to be ~40% of that expected in the absence of fluctuations, although the predicted saturation level of $|\delta \boldsymbol{B}_\perp/B_0| \simeq 2 \times 10^{-2}$ is significantly larger than that observed experimentally, $|\delta \boldsymbol{B}_\perp/B_0| \sim 10^{-3}$. Meanwhile, particle phase-space mapping showed that EP redistributions are due to both resonance overlap of different eigenmodes and stochastization of particle orbits due to secondary and higher order resonances of a single eigenmode. The same numerical simulation was repeated recently (Todo, Berk, and Breizman, 2012a), with the inclusion of MHD mode-mode couplings, finding lower TAE saturations levels and two possible scenarios, i.e., TAE steady-state saturation at $|\delta \boldsymbol{B}_\perp/B_0| \simeq 2 \times 10^{-3}$ for low MHD dissipation coefficients and TAE bursting with peak fluctuation levels at $|\delta \boldsymbol{B}_\perp/B_0| \simeq 5 \times 10^{-3}$ for the higher dissipation case. The lower saturation level in the former case is attributed to the enhanced effective dissipation due to the nonlinearly driven modes, with both $n = 0$ and $n \neq 0$, possibly through the fine structures connected with resonant excitation of higher toroidal mode-number continuous spectra (Todo, Berk, and Breizman, 2010, 2012b). Thus, it is different from the enhanced nonlinear coupling with the SAW continuum or the spontaneous generation of ZS, analyzed in Secs. IV.C.2 and IV.C.3, which are collisionless processes and are expected to play important roles in high temperature burning plasmas.

Model Fokker-Planck collision terms in the form of Eq. (4.136) were also implemented in gyrokinetic codes for investigating nonlinear TAE dynamics as, e.g., by Chen and Parker (2011). There it was shown that an $n = 15$ TAE in ITER, found to be the most unstable mode from previous linear stability analyses of the considered reference scenario (Chen *et al.*, 2010) [see also Gorelenkov *et al.* (2003) and Vlad *et al.* (2006)], nonlinearly evolves up to a peak fluctuation amplitude, consistent with $\omega_B \sim \gamma_L$, and then decays to a steady-state saturation level, which scales as $\nu_d^{2/3}$, consistent with Eq. (4.137) and is typically dominated by pitch angle scattering (Chen and Parker, 2011).

Gyrokinetic and extended hybrid MHD-gyrokinetic codes are becoming of routine use for linear AE and EPM stability studies and comparisons with experimental observations [see Lauber (2013) for an extended and recent review]. Linear spectra and mode structures are then used for perturbative EP transport analyses, as described previously, in present experiments (Schneller *et al.*, 2013) as well as in ITER (Lauber, 2015; Schneller, Lauber, and Briguglio, 2016) (cf. Sec. VI).

5. Nonlinear dynamics of Alfvénic fluctuations in nonuniform toroidal plasmas

Nonlinear wave-particle interactions are significantly modified by geometry of the plasma equilibrium and spatial nonuniformities. In this section, we first present a qualitative discussion of these modifications and the necessary

corresponding deviations from marginal stability. We then give a quantitative and formal description of the same phenomena, based on numerical simulation results and the general theoretical framework introduced in Sec. IV.A. This allows us to ultimately derive general equations for the nonlinear dynamics of PSZS and to demonstrate the unification of bump-on-tail and fishbone paradigms.

A detailed analysis of resonant wave-particle interactions in 2D toroidal plasmas was given by Zonca *et al.* (2013, 2015b), using the general time-scale ordering $|\omega_0\tau_{NL}|^{-1}\sim|\gamma_L/\omega_0|\gg\epsilon_\omega\sim\mathcal{O}(\omega/\Omega_i)$ (Sec. II.D). Thus, the effect of nonlinear dynamics is sufficiently small that wave-particle resonances yield cumulative effects of bounce and transit-averaged processes on unperturbed particle motion. The resonant particle response to a fluctuating field $f(r,\theta,\zeta)$, represented as in Eq. (3.8), can then be written as

$$f(r,\theta,\zeta)=\sum_{m,n,\ell}e^{i(n\bar{\omega}_d+\ell\omega_b)\tau+i\Theta_{n,m,\ell}}\mathcal{P}_{m,n,\ell}\circ f_{m,n}(\bar{r}+\Delta r), \tag{4.157}$$

where $\Theta_{m,n,\ell}$ and Δr are, respectively, the nonlinear wave-particle phase shift and radial displacement, and $\mathcal{P}_{m,n,\ell}\circ f_{m,n}$ stand for "push-forward" operators to magnetic-drift orbit centers (Brizard and Hahm, 2007). This represents a lifting of $f(r,\theta,\zeta)$ to the particle phase space in action-angle coordinates given by $(cm^2\mu/e,\alpha)$, with $\mu=v_\perp^2/(2B_0)+\cdots$ the magnetic moment (see Sec. II) and α the gyrophase, (P_φ,φ), with the canonical toroidal angular momentum P_φ at the leading order

$$P_\phi=\frac{e}{c}\left(F(\psi)\frac{v_\parallel}{\Omega}-\psi\right), \tag{4.158}$$

and by (J,θ_c), with J the "second invariant" and θ_c the respective conjugate canonical angle[24]

$$J=m\oint v_\parallel dl,\qquad \theta_c=\omega_b\int_0^\theta d\theta'/\dot{\theta}'. \tag{4.159}$$

Here dl is the arc length along the particle orbit and we introduced the unified notation of $\omega_b(\mu,J,P_\phi)$,

$$\omega_b(\mu,J,P_\phi)=2\pi\left(\oint d\theta/\dot{\theta}\right)^{-1}, \tag{4.160}$$

for bounce and transit frequency of trapped and circulating particles, respectively. Note that guiding-center equations of motion include first order corrections due to $\boldsymbol{B}_0$ nonuniformity, which are conceptually important for the construction of proper adiabatic invariants and for the accuracy of numerical codes (Brizard and Tronko, 2012). As a consequence, leading order expressions of phase-space actions given earlier may be found to "oscillate" along the particle orbits, especially for EPs in spherical tori (Belova, Gorelenkov, and Cheng, 2003).

[24]A recent review of coordinate systems and their connection with the description of the guiding-center particle motion (see Sec. II) was given by Cary and Brizard (2009).

For given (μ,J,P_ϕ), the particle coordinates (r,θ,ζ) are parametrized as (Zonca *et al.*, 2015b)

$$r=\bar{r}+\tilde{\rho}(\theta_c), \tag{4.161}$$

$$\theta=\tilde{\Theta}_c(\theta_c), \tag{4.162}$$

$$\zeta=\bar{\omega}_d\tau+\bar{q}\theta+\tilde{\Xi}(\theta_c), \tag{4.163}$$

for magnetically trapped particles, while for circulating particles Eq. (4.162) is substituted by

$$\theta=\theta_c+\tilde{\Theta}_c(\theta_c). \tag{4.164}$$

Here $\bar{r}$, $\tilde{\rho}(\theta_c)$, $\tilde{\Theta}_c(\theta_c)$, $\tilde{\Xi}(\theta_c)$, and

$$\bar{q}\equiv\oint qd\theta/\oint d\theta \tag{4.165}$$

are also functions of (μ,J,P_ϕ), which can be computed from equations of motion in the equilibrium $\boldsymbol{B}_0$. Furthermore, the tilde $\tilde{(\,)}$ denotes a generic harmonic function in θ_c with zero average, while the toroidal precessional frequency

$$\bar{\omega}_d(\mu,J,P_\phi)=(2\pi)^{-1}\omega_b\oint(\dot{\zeta}-q\dot{\theta})d\theta/\dot{\theta}. \tag{4.166}$$

In Eq. (4.157), $\ell\in\mathbb{Z}$ stands for the "bounce harmonic," while the $\mathcal{P}_{m,n,\ell}\circ f_{m,n}$ functions are defined as

$$\mathcal{P}_{m,n,\ell}\circ f_{m,n}=(2\pi)^{-1}\lambda_{m,n}\oint\exp\{in\tilde{\Xi}(\theta_c)+i[n\bar{q}(\bar{r})-m]\tilde{\Theta}_c(\theta_c)\}f_{m,n}(\bar{r}+\tilde{\rho}(\theta_c))e^{-i\ell\theta_c}d\theta_c, \tag{4.167}$$

with $\lambda_{m,n}=1$ for trapped particles while for circulating particles, parametrizing $\theta_c=\omega_b\tau$,

$$\lambda_{m,n}=\exp\{i[n\bar{q}(\bar{r})-m]\omega_b\tau\}. \tag{4.168}$$

Furthermore, in Eq. (4.157), $\Delta r=\int_0^\tau\delta\dot{r}d\tau'$ and (Zonca *et al.*, 2013, 2015b)

$$\begin{aligned}\Theta_{n,m,\ell}=&\,n\Delta\zeta-m\Delta\theta+n\left(\frac{\partial\bar{\omega}_d}{\partial P_\phi}\int_0^\tau\delta P_\phi d\tau'+\frac{\partial\bar{\omega}_d}{\partial J}\int_0^\tau\delta Jd\tau'\right)\\&+\ell\left(\frac{\partial\omega_b}{\partial P_\phi}\int_0^\tau\delta P_\phi d\tau'+\frac{\partial\omega_b}{\partial J}\int_0^\tau\delta Jd\tau'\right)-\int_0^\tau\delta\omega d\tau'\\&+[n\bar{q}(\bar{r})-m]\left(\frac{\partial\omega_b}{\partial P_\phi}\int_0^\tau\delta P_\phi d\tau'+\frac{\partial\omega_b}{\partial J}\int_0^\tau\delta Jd\tau'\right)\\&+n\omega_b\frac{d\bar{q}}{d\bar{r}}\int_0^\tau\delta rd\tau'.\end{aligned} \tag{4.169}$$

Here $\Delta\zeta$ and $\Delta\theta$ are the cumulative nonlinear shifts in ζ and θ, while δP_ϕ, δJ, and $\delta r=r-\bar{r}$ are, respectively, the nonlinear deviations from particle constants of motions and the radial nonlinear deviation, and integrations are along unperturbed orbits. Meanwhile, the nonlinear frequency shift

$\delta\omega = \omega(\tau) - \omega_0$ is explicitly taken into account, leaving implicit only the $\sim e^{-i\omega_0 t}$ dependence of the reference linear instability. Note that the last two lines of Eq. (4.169) apply to circulating particles only and are the nonlinear extension of $(-i \ln \lambda_{m,n})$.

Assuming $\Theta_{n,m,\ell}=0$, $\Delta r=0$, and $f(r,\theta,\zeta) \sim \exp(-i\omega_0 t)$, the linear resonance condition may be derived from Eq. (4.157) and yields

$$\omega_0 = \omega(\mu, J, P_\phi) = n\bar{\omega}_d + \ell\omega_b \tag{4.170}$$

for magnetically trapped particles, while for circulating particles,

$$\omega_0 = \omega(\mu, J, P_\phi) = n\bar{\omega}_d + \ell\omega_b + [n\bar{q}(\bar{r}) - m]\omega_b. \tag{4.171}$$

In the presence of fluctuations, Eq. (4.157) accounts for their cumulative effects on multiple bounce and transit periods, discriminating between resonance detuning $\sim \exp(i\Theta_{n,m,\ell})$ and radial decoupling $\sim \mathcal{P}_{m,n,\ell} \circ f_{m,n}(\bar{r} + \Delta r)$ (Zonca *et al.*, 2013; 2015b; Zonca and Chen, 2014a). Wave-particle interactions are thus characterized by finite interaction length Δr_L and finite interaction time τ_{NL}, i.e., the typical spatial and time scales required for particles to effectively lose the resonance condition. Noting that $\Delta r/r \sim \Delta P_\phi/P_\phi \sim (\omega_{*EP}/\omega_0)\Delta\mathcal{E}/\mathcal{E}$ (cf. Sec. II) (Chen, Vaclavik, and Hammett, 1988), with ω_{*EP} the EP diamagnetic frequency and that typically $|\omega_{*EP}/\omega_0| \gg 1$ for SAW and DAW in fusion plasmas, it is possible to simplify Eq. (4.169) and show, for shifted circular magnetic flux surfaces,

$$\begin{aligned} \dot{\Theta}_{n,m,\ell} &\simeq (n\partial_{\bar{r}}\bar{\omega}_d + \ell\partial_{\bar{r}}\bar{\omega}_b)\Delta r - \delta\omega, \\ \dot{\Theta}_{n,m,\ell} &\simeq n(d_{\bar{r}}\bar{q})\omega_t \Delta r - \delta\omega, \end{aligned} \tag{4.172}$$

for magnetically trapped and circulating EPs, respectively. Here we denoted EP transit frequency with ω_t for clarity. In general, we may estimate $\omega_B \sim \dot{\Theta}_{m,n,\ell}$ and, since SAW and DAW are resonantly excited by EPs, $\tau_{NL} \sim (3\gamma_L)^{-1}$ (Zonca *et al.*, 2015b) (cf. Secs. IV.D.2 and IV.D.4).

Near marginal stability and for adiabatic frequency sweeping, $\tau_{NL} \sim \omega_B^{-1} \sim (3\gamma_L)^{-1}$ at saturation. However, Eq. (4.172) suggests that there always exists a special class of "phase-locked" resonant EPs, for which $\omega_B \tau_{NL} \ll 1$ if $\dot{\Theta}_{m,n,\ell}$ is minimized for a proper combination of Δr and $\delta\omega$, yielding nonadiabatic frequency sweeping ($\dot{\omega} \sim \omega_B^2$, cf. Sec. IV.D.5.a). Below we show that important qualitative and quantitative changes take place in the wave-particle nonlinear dynamics when the effect of phase-locked particles is nonperturbative. When fluctuations maintain the wave-particle resonance condition via phase locking through the nonlinear evolution, the chirping rate is proportional to the mode amplitude as observed experimentally by Heidbrink (2008) and Podestà *et al.* (2011), and in numerical simulations of nonlinear EPM evolutions (Briguglio, Zonca, and Vlad, 1998; Vlad, Zonca, and Briguglio, 1999; Briguglio *et al.*, 2002, 2014; Zonca *et al.*, 2002; Vlad *et al.*, 2004) as well as nonlinear fishbone dynamics (Fu *et al.*, 2006; Vlad *et al.*, 2012, 2013). This behavior is also demonstrated analytically for nonlinear EPM dynamics (Zonca *et al.*, 2005). Meanwhile, resonant particle motion is secular and corresponding transport is ballistic and/or convective: this particular nonlinear dynamic regime has been called mode-particle pumping in the original work (White *et al.*, 1983), where it was proposed for interpreting EP transport caused by fishbones (cf. Sec. IV.D.7).

Phase locking can be accounted for by means of $\epsilon_{\dot{\omega}} \leq 1$, defined such that $\dot{\Theta}_{m,n,\ell} \equiv \epsilon_{\dot{\omega}} \dot{\Theta}_{m,n,\ell}(\delta\omega = 0)$ (Zonca *et al.*, 2015b). Thus, $\epsilon_{\dot{\omega}} = 1$ for fixed frequency or adiabatic chirping modes, while $\epsilon_{\dot{\omega}} \ll 1$ for phase-locked fluctuations. The expression of Δr_L is then concisely given as

$$\Delta r_L/r \sim 3\epsilon_{\dot{\omega}}^{-1}\lambda_n^{-1}(\gamma_L/\omega), \tag{4.173}$$

where $\lambda_n = |nrq'|$ for circulating EPs and $\lambda_n = 1$ for trapped EPs, respectively. This expression for $\Delta r_L/r$ implies that circulating EP transport is expected to be mostly diffusive in the presence of many high-n modes, typical of ITER conditions (cf. Secs. V.A and VI.A). On the contrary, magnetically trapped EP transport may be affected by convective (ballistic) processes (cf. Sec. IV.D.6) with intrinsically nonlocal features (Briguglio, Zonca, and Vlad, 1998; Vlad, Zonca, and Briguglio, 1999; Briguglio *et al.*, 2002; Vlad *et al.*, 2004), i.e., characterized by mesoscales larger than $|nq'|^{-1}$, with analogies to electron behavior in gyrokinetic numerical simulations of collisionless trapped electron mode turbulence (Xiao and Lin, 2011). For moderate or low-n fluctuations, more typical of present day tokamaks, the situation is less well defined and requires more articulation as shown hereafter.[25]

a. From local to mesoscale energetic-particle redistributions

In nonuniform plasmas, Eq. (4.173) should be compared with the characteristic scale of $\mathcal{P}_{m,n,\ell} \circ f_{m,n}(\bar{r} + \Delta r)$, Δr_d, i.e., with radial decoupling due to nonlinear wave-particle dynamics. From Eq. (3.23), one can readily write

$$\Delta r_d/r \sim \epsilon_\Delta |nrq'|^{-1}, \tag{4.174}$$

where $\epsilon_\Delta < 1$ controls the perpendicular fluctuation scale (Zonca and Chen, 2014c; Zonca *et al.*, 2015b). From Eqs. (4.173) and (4.174) it is clear that "radial decoupling" becomes just as or more significant than "radial detuning" when

$$\gamma_L/\omega \gtrsim \lambda_n |nrq'|^{-1} \epsilon_{\dot{\omega}} \epsilon_\Delta/3. \tag{4.175}$$

[25]This point, together with similar remarks made earlier about wave-wave couplings (cf. Sec. IV.C) and the different nonlinear dynamic regimes expected in burning plasmas with respect to those in present day devices, suggests that understanding nonlinear SAW and EP physics in existing experiments may be more difficult. This indeed partly applies to sufficiently short time-scale behavior (cf. Secs. II.C and II.D). However, this point also shows the need of theory and numerical simulations for reliable extrapolations of the present understanding of nonlinear SAW dynamics to burning plasma conditions, especially when tackling new physics issues such as those of complex behavior and spatiotemporal cross-scale couplings discussed in Sec. VI.B.

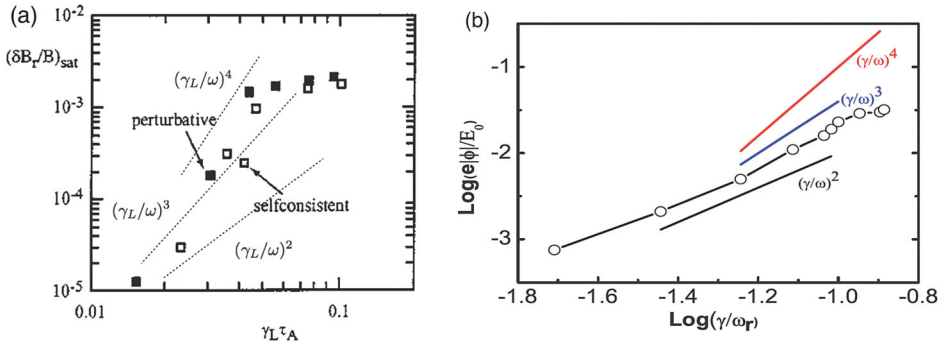

FIG. 2. (a) TAE saturation amplitude vs the normalized linear growth rate, expressed in Alfvén time units $\tau_A = R_0/v_A$ computed at the magnetic axis and with R_0 denoting the geometric center of the circular toroidal plasma (Briguglio *et al.*, 1995). From Briguglio, Zonca, and Vlad, 1998. (b) BAE saturation amplitude, expressed by the peak scalar potential energy normalized with respect to the EP birth energy, whose distribution function is an isotropic slowing down, is shown vs the normalized mode linear growth rate. From Wang *et al.*, 2012.

This condition, which depends on mode dispersive properties via $\epsilon_{\dot{\omega}}\epsilon_\Delta$ and on the type of resonance via λ_n, can also be considered as criterion for estimating the validity limits of the bump-on-tail paradigm. In addition, since significant EP radial redistributions take place on the characteristic fluctuation length scale, both the mode dispersiveness and structures may be affected for nonperturbative EPs, when this condition is satisfied. Equation (4.175) is most restrictive for circulating EPs, for which $\lambda_n = |nrq'|$ and the condition for radial decoupling to become important is

$$\gamma_L/\omega \gtrsim \epsilon_{\dot{\omega}}\epsilon_\Delta/3 \sim 3 \times 10^{-2} \tag{4.176}$$

as an upper bound, having assumed $\epsilon_{\dot{\omega}}\epsilon_\Delta \lesssim 10^{-1}$. Meanwhile, for magnetically trapped EPs, the corresponding condition is $\gamma_L/\omega \gtrsim 10^{-2}$ for moderate mode numbers and $\gamma_L/\omega \gtrsim 10^{-3}$ for the high-n modes expected in ITER.

Once the condition of Eq. (4.175) is exceeded, effects of mode structures become increasingly more important and eventually give rise to novel behavior due to the interplay between mode structures and EP transport (Zonca *et al.*, 2005). This transition can also be understood in terms of EP redistributions, which for isolated resonances change in nature from the local character connected with the short-radial scale of AEs as upper bound to mesoscale features $\gtrsim |nrq'|^{-1}$ (Zonca and Chen, 2014c; Zonca *et al.*, 2015b).

In general, the threshold condition given by Eq. (4.175) can be exceeded in situations of practical interest for trapped as well as circulating particles. In fact, the short time scale ($\tau_{NL}^{-1} \sim \gamma_L$, cf. Secs. II.C, II.D, and IV.A) EP power density is linearly proportional to time and injected power (cf. Sec. IV.D.7). Thus, the effective strength of EP drive is directly controlled by additional power input, which may be tuned equally well to achieve plasma conditions either with AEs excited near marginal stability (cf. Secs. IV.D.3 and IV.D.4) or with strongly driven AE and EPM, as routinely observed in experiments with strong ICRH (Bernabei *et al.*, 1999, 2001; Nabais *et al.*, 2005; Zonca *et al.*, 2009) and neutral NBI (Gryaznevich and Sharapov, 2004, 2006; Lesur *et al.*, 2010; Podestà *et al.*, 2011). It is also interesting to note that the threshold condition can be exceeded nonlinearly, due to the combined effect of different fluctuations. Experimental evidence for this case was given by "TAE avalanches" in NSTX (Fredrickson *et al.*, 2009; Podestà *et al.*, 2009), where significant rapid EP losses occur in bursts of nonadiabatic frequency sweeping modes (Podestà *et al.*, 2011, 2012), which are consistent with the general features of EPMs and cause up to ∼30% EP losses, following the activity of quasiperiodic TAE fluctuations with limited frequency chirping (Fredrickson *et al.*, 2009; Podestà *et al.*, 2009) (cf. Sec. V.B).

The transition from local to mesoscale nonlinear EP redistributions was investigated numerically for the first time by Briguglio, Zonca, and Vlad (1998) for the case of TAE and EPM. In this work, linear TAE and EPM regimes were identified from the behavior of the mode growth rate versus the EP energy density. In the same work it was also shown that TAE to EPM transition is properly described only with a fully nonperturbative treatment of the EPs.

The work by Briguglio, Zonca, and Vlad (1998) confirmed that nonlinear saturation of TAE modes occurs because of wave-particle trapping, as noted earlier (Fu and Park, 1995; Todo *et al.*, 1995). However, for increasing growth rate, EP redistributions by finite-amplitude TAE affect an increasingly broader radial region, which eventually becomes of the same order of the characteristic fluctuations length scale (cf. Sec. IV.D.5.a). This is also visible in the scaling of TAE saturation amplitude versus γ_L shown in Fig. 2(a). When the radial width of the wave-particle resonant region becomes comparable with the finite mode width, the saturation amplitude deviates from the simple scaling $|\delta \boldsymbol{B}_\perp/B_0| \sim (\gamma_L/\omega)^2$ (cf. Secs. IV.D.1 and IV.D.4) and eventually becomes independent of the linear drive. For this case of TAE excited by EPs via transit resonance, the $|\delta \boldsymbol{B}_\perp/B_0| \sim (\gamma_L/\omega)^2$ behavior holds for $\gamma_L/\omega \lesssim 10^{-2}$ consistent with the criterion of Eq. (4.176). The same type of behavior was recently observed in BAE hybrid MHD-gyrokinetic simulations and is reported in Fig. 2(b). The mechanism by which radial decoupling changes the scaling of the saturation amplitude with γ_L/ω_0 was also explained by Wang *et al.* (2012) in terms of a simplified analytical model, which incorporates the wave-particle resonance as well as the finite interaction length due to mode localization. The observed deviation of the mode saturation amplitude from the $\sim(\gamma_L/\omega)^2$ scaling in

simulations (Briguglio, 2012; Briguglio *et al.*, 2012, 2014; Wang *et al.*, 2012; Zhang, Lin, and Holod, 2012) is thus indicative of the increasing importance of radial decoupling with respect to resonance detuning.

Another important aspect of the transition from local to mesoscale EP redistributions is that the system is not near marginal stability, as discussed in Secs. IV.D.2 and IV.D.3, and its dynamics is nonadiabatic. This is due to the nonperturbative power exchange between waves and EPs undergoing an $\mathcal{O}(1)$ variation on the characteristic time τ_{NL} (cf. Sec. IV.D.5.a). These physics are demonstrated in recent numerical simulations of BAE nonlinear dynamics with both gyrokinetic (Zhang, Lin, and Holod, 2012) and hybrid MHD-gyrokinetic (Wang *et al.*, 2012) approaches. In the work by Zhang, Lin, and Holod (2012), BAE was excited predominantly by trapped EPs via precession resonance and the nonlinear mode evolution is characterized by continuous bursting without EP sources or sinks and with EPs assumed to initially have an isotropic Maxwellian distribution function. In the growth phase of the BAE mode, the frequency sweeps downward consistently with the mode dispersion relation, while outward-moving EPs continue driving the mode via maintaining the following phase locking condition from Eqs. (4.172):

$$\delta\dot{\omega} \simeq (n\partial_{\bar{r}}\bar{\omega}_d + \ell\partial_{\bar{r}}\bar{\omega}_b)\Delta\dot{r}. \tag{4.177}$$

EPs that are moving inward and damp the mode are also more easily detuned from resonance. Thus, power transfer from EPs to the wave is maximized as well as are EP nonlinear radial displacement and mode growth. Similar behavior was observed by Wang *et al.* (2012), where BAE is destabilized by EPs via transit resonance and nonlinear mode dynamics is produced uniquely by wave-EP interaction as the thermal ion kinetic response is linearized. In this case, the frequency sweeps upward in the growth phase of the BAE mode, consistent with the mode dispersion relation (Wang *et al.*, 2012). Thus, from Eqs. (4.172) the phase locking condition,

$$\delta\dot{\omega} \simeq n(d_{\bar{r}}\bar{q})\omega_t\Delta\dot{r}, \tag{4.178}$$

is more easily maintained for outward-moving instability-driving EPs with positive parallel velocities. This thus leads to symmetry breaking in $v_\parallel$ for the wave-particle power exchange as well as EP transport.

In both these recent works on nonlinear BAE dynamics, the role of EPs is nonperturbative and results in nonadiabatic frequency chirping $\dot{\omega} \sim \omega_B^2$, while dominant wave-EP resonant interactions satisfy phase locking as expressed by Eqs. (4.177) and (4.178). This can be understood from the estimate $\Delta\dot{r} \sim \delta\dot{\boldsymbol{X}}_\perp$ (cf. Sec. II.D), with

$$\omega_B^2 \simeq \lambda_n|(\omega/r)\delta\dot{\boldsymbol{X}}_\perp| \simeq \lambda_n|(\omega/r)(nq/r)(c/B_0)\delta\phi|. \tag{4.179}$$

These results furthermore confirm that PSZS formation and evolution occur on a time scale $\omega_B t \sim 1$, as anticipated in Sec. IV.D.3. Recent and detailed theoretical as well as numerical analyses of these issues were given by Briguglio *et al.* (2014) and Zonca *et al.* (2015a, 2015b).

b. Nonlinear equations for energetic-particle phase-space zonal structures

The self-consistent and generally nonadiabatic nonlinear evolution of Alfvénic fluctuations and resonant EP PSZS is analyzed here allowing the investigation of the transition from local to mesoscale EP redistributions (cf. Sec. IV.D.5.a). The denomination of PSZS follows by analogy that of ZS in configuration space (cf. Secs. IV.A, IV.B.3, and IV.C.2), and, as $n = m = 0$ low-frequency structures in the phase space, they set the dominant nonlinear time scale in resonant wave-particle interactions (Zonca *et al.*, 2015b). As a particular case of theoretical and practical interest, we discuss the fishbone paradigm illustrating the behavior of a magnetized toroidal plasma as a nonautonomous 1D nonuniform system. Then we show that this paradigm reduces to the bump-on-tail paradigm in the proper limit. Thus, phase-space holes and clumps are particular cases of PSZS, where time-scale separation applies between their long characteristic dynamic nonlinear evolution and the much shorter wave-particle trapping time (cf. Secs. IV.D.2 and IV.D.3), and nonlinear particle displacement is small compared with the fluctuation length scale.

For low-frequency fluctuations, the nonlinear description of EP PSZS is obtained from the nonlinear gyrokinetic equations (Frieman and Chen, 1982), i.e., from Eq. (2.21):

$$\delta f_z = \sum_m \{\mathcal{P}_{m,0,0}\circ[J_0(\lambda)\delta g]_{m,0}\} - \left[J_0(\lambda)\left(\frac{e}{m}\frac{1}{B_0}\frac{\partial\bar{F}_0}{\partial\mu}\langle\delta L_g\rangle\right)\right]_{0,0} + \frac{e}{m}\left[\frac{\partial\bar{F}_0}{\partial\mathcal{E}}\delta\phi + \frac{1}{B_0}\frac{\partial\bar{F}_0}{\partial\mu}\delta L\right]_{0,0}, \tag{4.180}$$

where the projection operator $\mathcal{P}_{m,0,0}$ is a particular case, which stands here as the "pullback" operator from magnetic-drift orbit centers (Brizard and Hahm, 2007) of $\mathcal{P}_{m,n,\ell}$ defined in Eq. (4.167) and used in the nonlinear representation of Eq. (4.157). Meanwhile, the evolution equation for the zonal component of δg is obtained from Eq. (2.23) (Zonca *et al.*, 2015b). Assuming that $|k_\parallel| \ll |\boldsymbol{k}_\perp|$ (cf. Sec. II.A), it can be cast as (Zonca *et al.*, 2005)

$$\frac{\partial\delta g_z}{\partial t} = -\mathcal{P}_{0,0,0}\circ\left(\frac{e}{m}\frac{\partial}{\partial t}\langle\delta L_g\rangle_z\frac{\partial\bar{F}_0}{\partial\mathcal{E}}\right)_{0,0} + i\sum_m\mathcal{P}_{m,0,0}\circ\frac{c}{d\psi/dr}\frac{\partial}{\partial r}\sum_n n(\delta g_n\langle\delta L_g\rangle_{-n})_{m,0}, \tag{4.181}$$

where $\sum_n$ stands for a summation on toroidal mode numbers, specified as a subscript of fluctuating fields where needed. In turn, the evolution equation for δg_n is

$$\left(\frac{\partial}{\partial t} - \frac{inc}{d\psi/dr}\langle\delta L_g\rangle_z\frac{\partial}{\partial r} + v_\parallel\nabla_\parallel + \boldsymbol{v}_d\cdot\boldsymbol{\nabla}_\perp\right)\delta g_n = i\frac{e}{m}\left(Q\bar{F}_0 - \frac{nB_0}{\Omega d\psi/dr}\mathcal{P}_{0,0,0}\circ\frac{\partial\delta g_z}{\partial r}\right)\langle\delta L_g\rangle_n. \tag{4.182}$$

Here $Q\bar{F}_0$ is defined as

$$iQ\bar{F}_0 = -\frac{\partial \bar{F}_0}{\partial \mathcal{E}}\frac{\partial}{\partial t} + \frac{\boldsymbol{b}\times\boldsymbol{\nabla}\bar{F}_0}{\Omega}\cdot\boldsymbol{\nabla}, \tag{4.183}$$

the contribution $\propto \langle \delta L_g \rangle_z$ on the left-hand side represents the Doppler-shifted mode frequency due to ZS, while the term $\propto \partial_r \delta g_z$ on the right-hand side accounts for the "radial corrugation" effect of PSZS (cf. Secs. IV.A, IV.D.6, and IV.D.7).

Equations (4.181) and (4.182) along with the field equations for Alfvénic fluctuations, i.e., Eq. (4.3) without the multiple-n coupling term, and Eqs. (2.26) and (2.30) for $\delta\phi_z$ and $\delta A_{\parallel z}$, respectively, fully characterize the short time-scale nonlinear evolution of DAWs and EPs. They are hence the relevant equations for the self-consistent evolution of PSZS excited by EPs and related transport. These equations have so far been investigated only in simplified limits, i.e., either dropping the contribution of wave-particle resonances (Chen, Lin, and White, 2000; Chen *et al.*, 2001; Chen and Zonca, 2007b, 2012, 2013; Guo, Chen, and Zonca, 2009) (cf. Sec. IV.C) or neglecting the effect of ZS, $\langle \delta L_g \rangle_z$ (Zonca *et al.*, 2000, 2005, 2006, 2007b). Thus, the simplified evolution equations for PSZS excited by EPs and related transport, used hereafter, are the NLSE, Eq. (4.3), without the multiple-n coupling term, i.e., the Gross-Pitaevsky (Gross, 1961; Pitaevskii, 1961) or Zakharov (Zakharov, 1968) equation. The NLSE in turn is closed by Eqs. (4.181) and (4.182), rewritten as

$$\frac{\partial F_0}{\partial t} = i\mathcal{P}_{0,0,0}\circ\sum_m \mathcal{P}_{m,0,0}\circ\frac{c}{d\psi/dr}\frac{\partial}{\partial r}\sum_n n(\delta g_n \langle \delta L_g\rangle_{-n})_{m,0}, \tag{4.184}$$

and

$$\left(\frac{\partial}{\partial t} + v_\parallel\nabla_\parallel + \boldsymbol{v}_d\cdot\boldsymbol{\nabla}_\perp\right)\delta g_n = i\frac{e}{m}QF_0\langle \delta L_g\rangle_n. \tag{4.185}$$

Here $F_0 \equiv \bar{F}_0 + \mathcal{P}_{0,0,0}\circ\delta g_z$. Furthermore, we note that for EPs with $|\omega_{*E}| \gg |\omega_0|$ Eq. (4.182) reduces to Eq. (4.185) except for an higher order term. These equations may be used to investigate a number of nonlinear dynamics problems involving a generic DAW spectrum with $|\gamma_L/\omega_0| \sim |\omega_0\tau_{NL}|^{-1} \ll 1$, accounting the reaction of waves on the particle distribution function.

In order to simplify the present analysis further, we restrict Eqs. (4.184) and (4.185) to precessional resonance with magnetically trapped EPs while neglecting finite orbit width effects. Assuming $|\partial_t| \sim n\bar{\omega}_d \ll \omega_b$, the second invariant J, defined in Eq. (4.159), becomes a constant of motion as μ. Then the "bounce averaged" dynamics of magnetized toroidal plasma reduces to that of a nonautonomous 1D nonuniform system, i.e., to the model description adopted in the fishbone paradigm (Zonca *et al.*, 2015b) and used hereafter to demonstrate that in the uniform plasma limit it reduces to the bump-on-tail paradigm. Using Eq. (4.157), we can write $\delta\bar{g}_n$, the bounce averaged expression of δg_n, as

$$\delta\bar{g}_n = e^{in(\zeta-q\theta)}\sum_m \mathcal{P}_{m,n,0}\circ\delta g_{m,n}. \tag{4.186}$$

Meanwhile,

$$\delta\bar{\phi}_n = e^{in(\zeta-q\theta)}\sum_m \mathcal{P}_{m,n,0}\circ\delta\phi_{m,n} = e^{-inq\theta}\overline{e^{inq\theta}\delta\phi_n}, \tag{4.187}$$

with $\overline{(\cdots)} = \tau_b^{-1}\oint(\cdots)d\theta/\dot{\theta}$ denoting bounce averaging. Furthermore, introducing the definition

$$\delta g \equiv \delta K + i(e/m)Q\bar{F}_0\partial_t^{-1}\langle \delta\psi_g\rangle \tag{4.188}$$

and adopting the notation of Eq. (4.124) for the Fourier-Laplace transform, Eq. (4.184) can be solved as

$$\begin{aligned}\hat{F}_0(\omega) = {}& \frac{i}{\omega}\mathrm{St}\hat{F}_0(\omega) + \frac{i}{\omega}\hat{S}_0(\omega) + \frac{i}{2\pi\omega}\bar{F}_0(0)\\ & + \frac{nc}{\omega(d\psi/dr)}\frac{\partial}{\partial r}\int_{-\infty}^{\infty}[\delta\hat{\bar{\phi}}_k(y)\delta\hat{\bar{K}}_{-k}(\omega-y)\\ & - \delta\hat{\bar{\phi}}_{-k}(y)\delta\hat{\bar{K}}_k(\omega-y)]dy.\end{aligned} \tag{4.189}$$

Here we neglected the higher order contribution of reversible processes [see Zonca *et al.* (2015b) for details]. We also included the effect of collisions, formally denoted by $\mathrm{St}\hat{F}_0(\omega)$, and of an external source term $\hat{S}_0(\omega)$, while $\bar{F}_0(0)$ denotes the initial value of F_0 at $t = 0$. Moreover, for clarity, we explicitly indicated dependences on ω only (and y as a dummy integration frequency variable), and the summation on mode numbers has been replaced by an implicit summation on the subscript k, which from now on will be short notation for (m, n). Meanwhile, for EP precessional resonance we readily obtain

$$\delta\hat{\bar{K}}_k(\omega) = \frac{e}{m}\int_{-\infty}^{+\infty}\frac{\hat{\omega}_{dk}}{y}\frac{Q_{k,y}\hat{F}_0(\omega-y)}{n\bar{\omega}_{dk}-\omega}\delta\hat{\bar{\phi}}_k(y)dy, \tag{4.190}$$

where the subscripts in $Q_{k,y}\hat{F}_0$ denote wave number and frequency at which the operator defined by Eq. (4.183) must be evaluated; we introduced the definition

$$e^{-inq\theta}\overline{e^{inq\theta}\omega_d\delta\phi_n} \equiv \hat{\omega}_{dk}\delta\hat{\bar{\phi}}_k. \tag{4.191}$$

It can be verified that Eq. (4.190) gives the linear limit for $\hat{F}_0(\omega) = (2\pi\omega)^{-1}i\bar{F}_0(0)$. Substituting Eq. (4.190) into Eq. (4.189), one obtains

$$\begin{aligned}\hat{F}_0(\omega) = {}& \frac{i}{\omega}\,\mathrm{St}\hat{F}_0(\omega) + \frac{i}{\omega}\hat{S}(\omega) + \frac{i}{2\pi\omega}\bar{F}_0(0)\\ & + \frac{e}{m}\frac{nc}{\omega(d\psi/dr)}\frac{\partial}{\partial r}\iint_{-\infty}^{\infty}\left[\delta\hat{\bar{\phi}}_k(y)\frac{\hat{\omega}_{d-k}}{y'}\right.\\ & \times\frac{Q_{-k,y'}\hat{F}_0(\omega-y-y')}{-n\bar{\omega}_{d-k}+y-\omega}\delta\hat{\bar{\phi}}_{-k}(y')\\ & \left. - \delta\hat{\bar{\phi}}_{-k}(y)\frac{\hat{\omega}_{dk}}{y'}\frac{Q_{k,y'}\hat{F}_0(\omega-y-y')}{n\bar{\omega}_{dk}+y-\omega}\delta\hat{\bar{\phi}}_k(y')\right]dydy'.\end{aligned} \tag{4.192}$$

This equation is the analog of Eq. (4.128), i.e., Dyson's equation in quantum field theory, extended to the case of

nonuniform toroidal plasmas under investigation with the addition of sources and collisions. Following Al'tshul' and Karpman (1965) it is possible to show that in the case of many waves with overlapping resonances Eq. (4.192) reduces to the quasilinear theory of a weakly turbulent plasma (Vedenov, Velikhov, and Sagdeev, 1961; Drummond and Pines, 1962), as noted already for Eqs. (4.127) and (4.128). Similar to Eq. (4.128), Eq. (4.192) can also be considered as a generalized quasilinear equation (Galeev, Karpman, and Sagdeev, 1965) (cf. Sec. IV.D.1), including effects of equilibrium geometries and plasma nonuniformity. It thus addresses resonance detuning and radial decoupling in wave-particle interactions on the same footing, and the present approach may be used to explore the transition of EP transport through stochasticity threshold with all the necessary physics ingredients for a realistic comparison with experimental observations.

In Secs. IV.D.6 and IV.D.7, we focus on the case where the DAW spectrum is very narrow, e.g., the case of a periodic fluctuation (cf. Sec. IV.D.1), whose frequency may be slowly evolving in time, $|\dot{\omega}_k| \ll |\gamma_{Lk}\omega_k|$. Therefore, this case includes both adiabatic ($|\dot{\omega}_k| \ll \omega_B^2$) and nonadiabatic ($|\dot{\omega}_k| \lesssim \omega_B^2$) frequency sweeping and may well represent the nonlinear dynamic evolution of a single toroidal mode-number AE or EPM.[26] Using the representation

$$\delta\hat{\bar{\phi}}_k(\omega) = \frac{i}{2\pi}\frac{\delta\bar{\phi}_{k0}(r,\tau)}{\omega-\omega_k(\tau)},$$
$$\delta\hat{\bar{\phi}}_{-k}(\omega) = \frac{i}{2\pi}\frac{\delta\bar{\phi}_{-k0}(r,\tau)}{\omega+\omega_k^*(\tau)}, \tag{4.193}$$

Equation (4.192) may be reduced to the following form:

$$\hat{F}_0(\omega) = \frac{i}{\omega}\mathrm{St}\hat{F}_0(\omega) + \frac{i}{\omega}\hat{S}(\omega) + \frac{i}{2\pi\omega}\bar{F}_0(0) + \frac{e}{m}\frac{nc}{\omega(d\psi/dr)}\frac{\partial}{\partial r}\left\{\left[\frac{Q^*_{k,\omega_k(\tau)}}{\omega_k^*(\tau)}\frac{\hat{F}_0(\omega-2i\gamma(\tau))}{\omega-\omega_k(\tau)+n\bar{\omega}_{dk}} + \frac{Q_{k,\omega_k(\tau)}}{\omega_k(\tau)}\frac{\hat{F}_0(\omega-2i\gamma(\tau))}{\omega+\omega_k^*(\tau)-n\bar{\omega}_{dk}}\right]\hat{\omega}_{dk}|\delta\bar{\phi}_{k0}(r,\tau)|^2\right\}. \tag{4.194}$$

Here we explicitly denoted the slow time dependence of $\omega_k(\tau)$, i.e., $|\dot{\omega}_k| \ll |\gamma_{Lk}\omega_k|$. Furthermore, we kept the (r,τ) dependences explicit only in $\delta\bar{\phi}_{0k}$, as they emphasize the important role of radial mode structures, which may change in time along with the particle distribution function. Meanwhile, $\gamma_k(\tau) \equiv \mathbb{I}\mathrm{m}[\omega_k(\tau)]$, $(-n)\bar{\omega}_{d-k} = -n\bar{\omega}_{dk}$, $\hat{\omega}_{d-k} = -\hat{\omega}_{dk}$, $Q_{-k,-\omega_k^*(\tau)} = -Q^*_{k,\omega_k(\tau)}$, and Eq. (4.193) is the analog of Eq. (4.129) for frequency sweeping modes.

Equations (4.192) and (4.194) are the general formulation for nonlinear DAW interactions with EPs adopting the fishbone paradigm and thus may be used to demonstrate its unification with the bump-on-tail paradigm (Zonca *et al.*, 2015b). More specifically, the correspondence to the nonlinear beam-plasma system (cf. Sec. IV.D.1) can be readily established ignoring the effect of plasma nonuniformities and geometry. That is, postulating constant $\delta\hat{\bar{\phi}}_k(\omega)$ fluctuations, and letting

$$k_0\frac{\partial}{\partial u} \leftrightarrow -\frac{m}{e}\frac{nc}{d\psi/dr}\frac{\partial}{\partial r}, \tag{4.195}$$

and $n\bar{\omega}_{dk} - \omega_k \simeq n\bar{\omega}_{dk0}(r-r_0)/L_{dk0} \leftrightarrow k_0 u$, with L_{dk0} the characteristic length of variation of $\bar{\omega}_{dk}$,[27] one can draw a one-to-one correspondence between Eqs. (4.126) and (4.190) as well as between Eqs. (4.128) and (4.192), which become identically the same. This also holds for the reduced forms, e.g., Eq. (4.194), once Eqs. (4.129) and (4.193) are introduced, respectively. As pointed out earlier and by Zonca *et al.* (2015b), this reduction of the general formulation illuminates both the validity limits of the bump-on-tail paradigm and its applicability conditions, as well as the qualitative and quantitative differences introduced by equilibrium geometry and plasma nonuniformity.

To be more precise, consider the uniform plasma limit as in Eq. (4.195). Introducing a simple Krook collision operator, Eq. (4.192) then becomes

$$(-i\omega+\nu)\delta\hat{f}_0(\omega) = i\frac{e^2k_0^2}{m^2}\frac{\partial}{\partial u}\iint_{-\infty}^{\infty}\left[\delta\hat{\phi}_{k_0}(y)\frac{-\partial_u\hat{F}_0(\omega-y-y')}{y-k_0u-\omega-i\nu}\delta\hat{\phi}_{-k_0}(y') - \delta\hat{\phi}_{-k_0}(y)\frac{\partial_u\hat{F}_0(\omega-y-y')}{y+k_0u-\omega-i\nu}\delta\hat{\phi}_{k_0}(y')\right]dyd y', \tag{4.196}$$

when expressed for the nonlinear deviation $\delta\hat{f}_0(\omega)$ of the particle distribution function from the equilibrium (initial) value $F_0(0) = Q(v)/\nu(v)$ (cf. Sec. IV.D.2.b). The iterative solution of Eq. (4.144) corresponds to taking $\hat{F}_0(\omega-y-y') = i(2\pi)^{-1}F_0(0)(\omega-y-y')^{-1}$ in Eq. (4.196), i.e., to considering only the first loop in the Dyson series schematically shown in Fig. 1. Moving to the t representation, the recursive solution of Eq. (4.196) is then obtained as

$$\left(\frac{\partial}{\partial t}+\nu\right)\delta f_0 = i\frac{e^2k_0^2}{m^2}\frac{\partial}{\partial u}\iint_{-\infty}^{\infty}e^{-i(y+y')t}\left[\delta\hat{\phi}_{k_0}(y)\frac{\partial_u F_0(0)}{y'+k_0u+i\nu}\delta\hat{\phi}_{-k_0}(y') + \delta\hat{\phi}_{-k_0}(y)\frac{\partial_u F_0(0)}{y'-k_0u+i\nu}\delta\hat{\phi}_{k_0}(y')\right]dyd y', \tag{4.197}$$

which is readily cast as

[26] Here we remind the reader again that one single toroidal mode number involves the coupling of many poloidal harmonics, due to the toroidal geometry of the plasma equilibrium.

[27] Note that Eq. (4.195) implies that directions of incrementing u correspond to decreasing r and vice versa; however, $\bar{\omega}_{dk}$ is generally also a decreasing function of r.

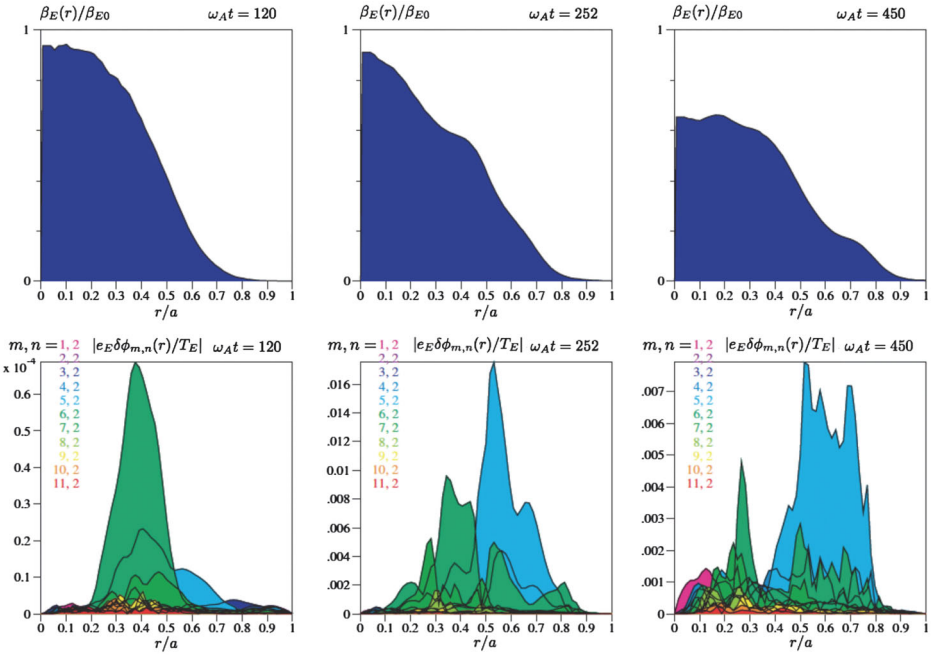

FIG. 3. Radial profiles of β_E and $(m, n = 2)$ Fourier components of the EPM scalar potential fluctuations during the linear growth (left), the end of the EPM avalanche (middle), and saturation phase (right). Time normalization is $\omega_A t$, with $\omega_A = v_A/R_0$ computed at the magnetic axis. From Vlad *et al.*, 2004.

$$\left(\frac{\partial}{\partial t} + \nu\right)\delta f_0 = \frac{\omega_B^2(t)}{4}\frac{\partial}{\partial k_0 u}\int_0^t [e^{-(\nu + ik_0 u)(t-t')} + \text{c.c.}]\omega_B^2(t') \times \frac{\partial F_0(0)}{\partial k_0 u} dt'. \quad (4.198)$$

This equation coincides with Eq. (4.144) noting that here $\omega_B^4 \equiv 4(e/m)^2 k_0^4 |\delta\phi_{k_0}|^2$, in order to preserve the same normalizations of Fourier amplitudes used in Sec. IV.D.2.b. Thus, this is proof that the fishbone paradigm reduces to the bump-on-tail paradigm in the uniform plasma limit.

Finally, as elucidation of Eq. (4.194) in the uniform plasma case, we follow Al'tshul' and Karpman (1965) and assume that the periodic fluctuation of Eq. (4.193) is weakly growing ($\gamma_L \ll \omega_B$) such that Eq. (4.194), with no sources and collisions and accounting for Eq. (4.195), yields the solution of Eq. (4.130). Here we remind one that Eq. (4.130) describes the oscillations of particles that are trapped in the wave, which, however, do not decay in time as expected as a consequence of phase mixing. This limitation is not significant for the analyses of Secs. IV.D.6 and IV.D.7, since phase locking makes wave-particle trapping essentially ineffective; *de facto* suppressing harmonic generation.

6. Nonlinear dynamics of energetic-particle modes and avalanches

The novel feature of EPM nonlinear dynamics in contrast to that of AEs is the interplay between EP transport and mode structure evolution, which is crucially influenced by the structure of the SAW continuous spectrum (Briguglio, Zonca, and Vlad, 1998) [see also Vlad, Zonca, and Briguglio (1999), Briguglio *et al.* (2002, 2007), Vlad *et al.* (2004, 2006, 2009), and Bierwage *et al.* (2011, 2012)].

The first analysis of EPM nonlinear behavior was given by Briguglio, Zonca, and Vlad (1998), reporting numerical results from hybrid MHD-gyrokinetic simulations. In that work, it was shown that unlike in the TAE case EPM saturation occurs because of "macroscopic outward displacement of the energetic-ion population," which is characterized by a convective secular process. There it was also shown that MHD nonlinearities weakly affect the EPM evolution by direct comparison of two different simulations, carried out without and with MHD mode-mode couplings. These results are consistent with theoretical analyses showing the fundamental role played by EPs in determining EPM dispersive properties and threshold conditions (Chen, 1994; Chen and Zonca, 1995; Zonca and Chen, 1996) as well as radial mode structure and spatial localization (Zonca and Chen, 1996, 2000).

Most of the distinctive features of low mode-number EPMs are the same as those typical of fishbone modes (cf. Sec. IV.D.7). However, the nonperturbative interplay of EP transport with mode structures is peculiar to EPM and is most evident as well as relevant for high mode numbers typical of ITER (Briguglio *et al.*, 2002; Vlad *et al.*, 2004; Zonca *et al.*, 2005), since the characteristic scales of EP profiles are longer than the typical mode width (Zonca and Chen, 2000). In these conditions and for sufficiently strong wave-particle power exchange, EP transport occurs in avalanches (Zonca *et al.*, 2015a, 2015b), i.e., as a secular loss process accompanied by a convectively amplified EPM wave packet (Briguglio *et al.*, 2002; Vlad *et al.*, 2004; Zonca *et al.*, 2005) and a local gradient steepening of the EP pressure profile, followed by a relaxation phase (Zonca *et al.*, 2006). This mechanism was demonstrated with hybrid MHD-gyrokinetic numerical simulation results by Vlad *et al.*

(2004), investigating the EPM nonlinear dynamics in the ITER-FEAT (the refined design of the Fusion Energy Advanced Reactor) reversed-shear scenario (see Sec. V.B for more details). The simulation results are summarized in Fig. 3, where β_E radial profiles are shown along with (m,n) Fourier components of the EPM scalar potential fluctuations during the linear growth (left), the end of the EPM avalanche (middle), and saturation phase (right). Meanwhile, Fig. 4 gives evidence of the peak EP pressure gradient value steepening at the location where the EPM wave packet is localized (Zonca and Chen, 2000; Zonca *et al.*, 2005). Thus, an EPM avalanche consists of an unstable wave packet that is convectively amplified as it radially propagates outward, in phase with the strengthening EP free-energy source (pressure gradient). This process continues as long as the EPM wave packet can be amplified by resonant wave-particle interactions. Eventually, the mode saturates due to radial decoupling and relative strengthening of background damping due to plasma nonuniformity. EP transport meanwhile becomes diffusive and the pressure gradient relaxes (Zonca *et al.*, 2006) as shown in Fig. 4. Similar results were obtained by Briguglio *et al.* (2002) studying EP transport in hollow current profile plasmas and showing that the minimum-q magnetic surface is the natural location, where the radial propagations of EPM induced EP avalanches are expected to stop.

These characteristic EPM nonlinear dynamics were studied analytically by Zonca *et al.* (2005) in connection with the transition from local to mesoscale EP redistributions (cf. Sec. IV.D.5). For simplicity, we analyze EPM excitation by precessional resonance with EPs adopting the fishbone paradigm (cf. Sec. IV.D.5.b). We also in order to compare analytic theory with hybrid MHD-gyrokinetic simulations of EPM avalanches assume the following initial (equilibrium) EP isotropic slowing down distribution function:

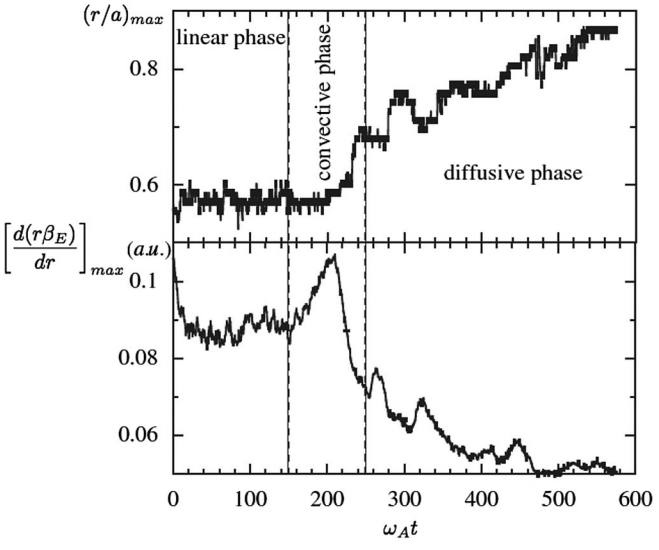

FIG. 4. Radial position $(r/a)_{\max}$ (top) and value of the maximum gradient $[d(r\beta_E)/dr]_{\max}$ vs $\omega_A t$ for the EPM simulation in Fig. 3. The strong convection, characteristic of the avalanche phase, is accompanied by gradient steepening, followed by a relaxation phase, characterized by diffusive EP transport. From Vlad *et al.*, 2004.

$$\bar{F}_0 = \frac{3P_{0E}}{4\pi E_F}\frac{H(E_F/m_E-\mathcal{E})}{(2\mathcal{E})^{3/2}+(2E_c/m_E)^{3/2}}. \tag{4.199}$$

Here H denotes the Heaviside step function and the normalization condition is chosen such that the EP energy density is $(3/2)P_{0E}$ for $E_F \gg E_c$. This condition also implies that EP energy is predominantly transferred to thermal electrons by collisional friction (Stix, 1972) as it occurs for α particles in fusion plasmas. Furthermore, we ignore source and collision terms in Eq. (4.194). The analysis consequently is then reduced to computing the nonlinear contribution to $\delta\bar{W}_{nk}$, which considering Eq. (3.29) together with Eq. (4.190) can be written as

$$\delta\bar{W}_{nk} = \int \mathcal{E}d\mathcal{E}d\lambda \sum_{v_\parallel/|v_\parallel|=\pm}\frac{\pi^2 qR_0}{c^2k_\vartheta^2|s|}\frac{e^2}{m}\left(\frac{\tau_b n^2\bar{\omega}_{dn}^2}{\omega(\tau)}\right) \times\int_{-\infty}^{+\infty}\frac{\omega+\omega(\tau)}{n\bar{\omega}_{dn}-\omega(\tau)-\omega}e^{-i\omega t}Q_{k,\omega(\tau)}\hat{F}_0(\omega)d\omega, \tag{4.200}$$

where $\tau_b = 2\pi/\omega_b$. Note that here $\omega(\tau)=\omega_0(\tau)+i\gamma(\tau)$ is the slowly changing frequency of the periodic EPM allowing nonadiabatic frequency chirping. With the notations of Sec. IV.A and the use of Eq. (4.194), the nonlinear contribution to $\delta\bar{W}_{nk}$ can be written as

$$\delta\bar{W}_{nk}^{NL} \simeq i\int \mathcal{E}d\mathcal{E}d\lambda \sum_{v_\parallel/|v_\parallel|=\pm}\frac{\pi^2 qR_0}{c^2k_\vartheta^2|s|}\frac{e^2}{m}\left(\frac{\tau_b n^2\bar{\omega}_{dn}^2}{\omega(\tau)}\right)k_\vartheta^2 v_E^2\rho_{LE}^2 \times\partial_t^{-2}\frac{\partial^2}{\partial r^2}\left[\left(\int_{-\infty}^{+\infty}\frac{n\bar{\omega}_{dn}(\gamma-i\omega)e^{-i\omega t}Q_{k,\omega(\tau)}\hat{F}_0(\omega)}{(n\bar{\omega}_{dn}-\omega_0)^2+(\gamma-i\omega)^2}d\omega\right) \times\left|\frac{e_E}{T_E}\delta\bar{\phi}_n(r,t)\right|^2\right], \tag{4.201}$$

where $v_E^2 = T_E/m_E$, $T_E = E_F/m_E$, $\rho_{LE}^2 = v_E^2/\Omega_E^2$, and ∂_t^{-2} denotes the action of $-(\omega+2i\gamma)^{-2}$ under the integration in $d\omega$. Meanwhile, the fluctuation intensity in Eq. (4.201) can be rewritten as

$$\left|\frac{e_E}{T_E}\delta\bar{\phi}_n(r,t)\right|^2 = (2\pi)^2\left|\frac{e_E}{T_E}A_n(r,t)\right|^2 \times\sum_{\ell,\ell'}e^{-2\pi i n q'\ell'}\overline{\frac{\delta\hat{\Phi}_{-n}^\dagger}{\hat{\kappa}_\perp}\Big|_{\vartheta=2\pi(\ell-\ell')}}\overline{\frac{\delta\hat{\Phi}_n}{\hat{\kappa}_\perp}\Big|_{\vartheta=2\pi\ell}}. \tag{4.202}$$

Here we used the mode structure decomposition and notations of Eqs. (3.23) and (4.187). Equation (4.202) demonstrates the existence of fine radial structures of the order of or less than $|nq'|^{-1}$, due to nonlinear modulations via wave-particle interactions of the EP radial profiles. While such fine structures are visible in mode structures shown in Fig. 3, they are smoothed out in the pressure profiles due to velocity-space integration. These features are very general and were recently observed in gyrokinetic numerical simulations addressing the effect of ion temperature gradient turbulence driven zonal flows on nonlinear SAW dynamics excited by

EPs (Bass and Waltz, 2010) (cf. Sec. VI.B). These fine structures were demonstrated to be modulationally stable below a critical threshold amplitude of the driving modes (Zonca *et al.*, 2000). For this reason, we consider for now only the $\mathscr{E}' = 0$ component in Eq. (4.202). We will later discuss the conditions under which radial corrugations in the EP profiles are produced spontaneously. Thus, Eq. (4.202) can be rewritten as (cf. Sec. III.C)

$$\left|\frac{e_E}{T_E}\delta\bar{\phi}_n(r,t)\right|^2 \simeq \frac{2\pi^2}{|s|}(\delta\hat{\Phi}^\dagger_{-n0}\delta\hat{\Phi}_{n0})\left|\frac{e_E}{T_E}A_n(r,t)\right|^2 \equiv |\bar{A}_n(r,t)|^2, \tag{4.203}$$

where normalizations are consistent with those of Zonca *et al.* (2005).

Equation (4.201) can be used to formally write the EPM nonlinear equation (Zonca *et al.*, 2005, 2006)

$$D_n(x,-i\partial_x,\omega_0(t)+i\partial_t)\bar{A}_{n0}(x,t) = \delta\bar{W}^{NL}_{nk}\bar{A}_{n0}(x,t), \tag{4.204}$$

where the fast time dependence has been isolated and $\bar{A}_n(r,t) \equiv \bar{A}_{n0}(x,t)\exp[-i\int^t \omega_0(t')dt']$. Equations (4.201) and (4.204) are closed by the leading order evolution equation for $F_0(t)$, i.e.,

$$\frac{\partial}{\partial t}F_0(t) \simeq 2k_\vartheta^2 v_E^2\rho_{LE}^2\left(\frac{n\bar{\omega}_{dn}}{\omega_0}\right)\times\frac{\partial}{\partial r}\left[\left(\int_{-\infty}^{+\infty}\frac{(\gamma-i\omega)}{(n\bar{\omega}_{dn}-\omega_0)^2+(\gamma-i\omega)^2}\times e^{-i\omega t}\frac{\partial\hat{F}_0(\omega)}{\partial r}d\omega\right)|\bar{A}_{n0}(r,t)|^2\right]. \tag{4.205}$$

Note that here we ignored terms $\propto \mathrm{St}\hat{F}_0(\omega)$ and $\propto \hat{S}(\omega)$ in Eq. (4.194), which, however, can be readily included (cf. Sec. IV.D.7). Furthermore, as in the case of Eq. (4.201), ∂_t^{-1} formally applied on the right-hand side when explicitly integrating Eq. (4.205) denotes the action of $(-i\omega+2\gamma)^{-1}$ under the integration in $d\omega$.

The complex features of EPM nonlinear dynamics and more generally of DAW resonantly excited by EPs are visible from the structure of Eq. (4.205). For sufficiently strong (nonperturbative) EP drive, as in the case of EPM, radial structures of $\hat{F}_0(\omega)$ and $|\bar{A}_{n0}|$ vary self-consistently and favor the most unstable growing mode, i.e., the maximization of wave-particle power exchange. Therefore, the mode frequency continuously readjusts to the resonance condition due to mode dispersive properties and radial envelope structures. In turn, particles are most effectively transported outward as they amplify the mode. In Eq. (4.205), phase locking and frequency chirping ensure that $\propto(n\bar{\omega}_{dn}-\omega_0)^2$ in the denominator is essentially vanishing for resonant particles. Thus, the nature of Eq. (4.205) could change from parabolic to hyperbolic for phase-locked particles that play a crucial role in the EPM avalanche of Fig. 3. The hyperbolic nature is intrinsically connected with ballistic resonant particle transport.

The solution of Eqs. (4.201), (4.204), and (4.205) in the early phase of the EPM wave-packet convective amplification (Zonca *et al.*, 2005) is summarized hereafter in order to illustrate the underlying physics (Zonca *et al.*, 2015b). We assume that the nonlinear distortion of the EP distribution function is sufficiently small that $\hat{F}_0(\omega)$ in Eq. (4.201) takes on its equilibrium value, i.e., $\hat{F}_0(\omega) = (2\pi\omega)^{-1}i\bar{F}_0(0)$, with $\bar{F}_0(0)$ chosen as in Eq. (4.199) and

$$\alpha_E = \alpha_{E0}\exp\left(-\frac{(r-r_0)^2}{L_{pE}^2}\right) \simeq \alpha_{E0}\left(1-\frac{x^2/s^2}{k_\vartheta^2 L_{pE}^2}\right), \tag{4.206}$$

with $\alpha_E = -8\pi R_0 q^2 P'_{0E}/B_0^2$, $\alpha_{E0} = \alpha_E(r=r_0)$, and $x = |sk_\vartheta|(r-r_0)$. Assuming that the resonant EPs are deeply magnetically trapped, $\delta\bar{W}^{NL}_{nk}$ can be reduced to

$$\delta\bar{W}^{NL}_{nk0} \simeq \frac{3\pi(r/R_0)^{1/2}\alpha_E}{8\sqrt{2}|s|}i\pi\frac{\omega_0}{\bar{\omega}_{dF}}k_\vartheta^2 v_E^2\rho_{LE}^2\partial_t^{-2}\frac{\partial^2}{\partial r^2}|\bar{A}_{n0}|^2, \tag{4.207}$$

where $\bar{\omega}_{dF} \equiv n\bar{\omega}_{dn}(E=E_F)$, and we assumed that the radial scale of α_E is longer than that of $|\bar{A}_{n0}|$. In Eq. (4.207), it is crucial to note that the entire right-hand side is computed at the instantaneous frequency ω_0 and at the radial location of the EPM wave packet. With $\delta\bar{W}^{NL}_{nk0}$ replacing $\delta\bar{W}^{NL}_{nk}$, Eq. (4.204) recovers the nonlinear EPM envelope equation of Zonca *et al.* (2005), whose solution can be expressed as the convectively amplified propagating (self-similar) wave packet

$$\bar{A}_{n0}(\xi,t) = \bar{U}(\xi)e^{\int_0^t\gamma(t')dt'}, \tag{4.208}$$

with ξ given by

$$\xi-\xi_0 \equiv \frac{k_{n0}}{|sk_\vartheta|}(x-x_0) \equiv \frac{k_{n0}}{|sk_\vartheta|}\left(x-|sk_\vartheta|\int_0^t v_g(t')dt'\right), \tag{4.209}$$

k_{n0} denoting the nonlinear wave vector, and v_g denoting the nonlinear group velocity. Adopting the usual procedure, one first balances the nonlinear term in Eq. (4.204), for $\delta\bar{W}^{NL}_{nk} \to \delta\bar{W}^{NL}_{nk0}$, with the linear dispersiveness in D_n, which for moderate values of $(s, \alpha = -R_0q^2\beta')$ is given by

$$D_n \simeq i\Lambda_T - \frac{|s|\pi}{8}\left(1+2\kappa(s)-\frac{\alpha}{\alpha_{cr}}\right) - \frac{|s|\pi}{8}\kappa(s)\frac{\partial^2}{\partial x^2} - \frac{3\pi(r/R_0)^{1/2}}{8\sqrt{2}|s|}\alpha_{E0}\left(1-\frac{x^2/s^2}{k_\vartheta^2 L_{pE}^2}\right)\times\left\{1+\frac{\omega}{\bar{\omega}_{dF}}\left[\ln\left(\frac{\bar{\omega}_{dF}}{\omega}-1\right)+i\pi\right]\right\}. \tag{4.210}$$

Here $D_n = i\Lambda_T - (\delta\bar{W}^L_{nf}+\delta\bar{W}^L_{nk})$ as in Eq. (3.30), $\Lambda_T = (1/2)(\Gamma_+/\Gamma_-)^{1/2}$ (cf. Sec. IV.C.2), $\alpha_{cr} = s^2/(1+|s|)$, and $\kappa(s) \simeq (1/2)(1+1/|s|)e^{-1/|s|}$ (Zonca and Chen, 1992, 1993; Chen and Zonca, 1995). This optimal balance gives (Zonca *et al.*, 2015b)

$$v_g = \lambda_g \hat{v}_{E\times B}, \qquad k_{n0}^2 = \frac{k_\vartheta^2 s^2 \mathbb{I}\mathrm{m}\delta\bar{W}_{nk}^L(\omega_0)}{\lambda_g^2 \partial^2 D_n/\partial\theta_{k0}^2}, \tag{4.211}$$

where $\hat{v}_{E\times B} = (-k_\vartheta c/B_0)\max[\delta\bar{\phi}_n(r,t)]$ is the EP peak radial $\boldsymbol{E}\times\boldsymbol{B}$ velocity, $\theta_{k0} \equiv -i\partial_x$, and λ_g is a control parameter to be determined as specified by Eq. (4.215). Meanwhile,

letting $\bar{U}(\xi) \equiv e^{i\epsilon_g\xi}U(\xi)$, with $U(\xi) \equiv e^{i\varphi(\xi)}W(\xi)$ and $\epsilon_g \equiv \lambda_g^2 k_{n0} v_g (\mathbb{I}\mathrm{m}\delta\bar{W}_{nk}^L)^{-1}\partial\mathbb{R}\mathrm{e}\delta\bar{W}_{nk}^L/\partial\omega_0$, $U(\xi)$ satisfies the following nonlinear Zonca-Chen equation:

$$\partial_\xi^2 U = (\lambda_0 - \epsilon_g^2)U - 2iU|U|^2, \tag{4.212}$$

which is a particular case of the complex Ginzburg-Landau equation (van Saarloos and Hohenberg, 1992; Conte and Musette, 1993). The solution of Eq. (4.212), discussed by Zonca *et al.* (2015b) in the limit $\epsilon_g \to 0$, is shown in Fig. 5 and is given by $W(\xi) = \mathrm{sech}[(\sqrt{2}/3)^{1/2}\xi]$, $\varphi(\xi) = -\sqrt{2}\ln\cosh[(\sqrt{2}/3)^{1/2}\xi]$, for the value of $\lambda_0 - \epsilon_g^2 = -\sqrt{2}/3 + i(4/3) \simeq -0.47 + i1.33$, which corresponds to the ground state of the corresponding complex nonlinear oscillator. Using Eqs. (4.210)–(4.212), the mode frequency and growth rate are then defined by the dispersion relation (computed at $x = x_0$)

$$D_n^{L\ell}(\omega)|_{x=x_0} - \frac{\lambda_0}{2\lambda_g^2}\mathbb{I}\mathrm{m}\delta\bar{W}_{nk}^L(\omega_0)|_{x=x_0} = 0, \tag{4.213}$$

where

$$D_n^{L\ell}(\omega) = i[\Lambda_T(\omega_0) - \mathbb{I}\mathrm{m}\delta\bar{W}_{nk}^L(\omega_0)] - [\delta\bar{W}_{nf}^L + \mathbb{R}\mathrm{e}\delta\bar{W}_{nk}^L(\omega_0)] - \left(\omega_0\frac{\partial\mathbb{R}\mathrm{e}\delta\bar{W}_{nk}^L(\omega_0)}{\partial\omega_0}\right)i\frac{\gamma}{\omega_0} \tag{4.214}$$

is the local linear EPM dispersion relation obtained from Eq. (4.210) neglecting the linear dispersiveness term $\propto \partial_x^2$. Equation (4.213) through the $\propto \lambda_g^{-2}$ term is the nonlinear extension of the linear EPM dispersion relation (Zonca and Chen, 2000). It describes a one-parameter family λ_g of EPM wave packets that are convectively amplified as they radially propagate with group velocity $\sim\hat{v}_{E\times B}$. The value of λ_g^2 for the dominant mode is determined by maximizing the wave-particle power transfer in the phase locking regime, i.e.,

$$\frac{d\gamma}{d\lambda_g^2} = \frac{\partial\gamma}{\partial\lambda_g^2} + \frac{\partial\gamma}{\partial\omega_0}\frac{d\omega_0}{d\lambda_g^2} = 0. \tag{4.215}$$

This equation has a solution $\lambda_g^2 \lesssim 1$ due to the optimal ordering in the nonlinear dispersion relation and to the fact that $d\gamma/d\lambda_g^2 > 0$ for $\lambda_g^2 \to 0$, while $d\gamma/d\lambda_g^2 < 0$ for $\lambda_g^2 \to \infty$. For typical tokamak parameters, one obtains $\lambda_g \simeq 0.5 - 0.6$ with a spread $\Delta\lambda_g \simeq \Delta\lambda_g^2 \simeq \gamma^{1/2}[-d^2\gamma/(d\lambda_g^2)^2]^{-1/2} \sim 0.1$. This is readily verified to yield phase locking of the EPM wave packet with the dominant resonant particle fraction contributing to wave-particle power exchange (Zonca *et al.*, 2015b).

In the initial EPM avalanche phase, characterized by phase locking and wave-packet convective amplification, Eq. (4.213) yields a frequency shift $\Delta\omega$ relative to the "linear" (initial) mode frequency ω_{0L} (Zonca *et al.*, 2005),

$$\frac{\Delta\omega}{\omega_{0L}} \simeq (s-1)\frac{x_0}{|sk_\vartheta r_0|} = \frac{s-1}{r_0}\int_0^t v_g(t')dt', \tag{4.216}$$

i.e., a frequency chirping rate that is proportional to the mode amplitude, as discussed at the beginning of Sec. IV.D.5. Meanwhile, Eq. (4.213) also shows that the EPM wave packet can be convectively amplified, yielding the avalanching process of Fig. 3, as long as the strengthening of the mode drive, due to pressure gradient steepening, compensates the reduced drive, due to equilibrium nonuniformities. Equilibrium geometry and plasma nonuniformities influence the wave-packet propagation speed and characteristic width as well. Because of its form, the intensity of the convectively amplified wave packet grows as the square of the distance in analogy with the superradiance (Dicke, 1954) operation regime of a free-electron laser (FEL), where the peak power also increases as the square of the distance along the undulator (Bonifacio *et al.*, 1990, 1994; Giannessi, Musumeci, and Spampinati, 2005; Watanabe *et al.*, 2007). The mechanism by which EPs eventually lose resonance by residual resonance detuning and are substituted by new resonant EPs reinforces this analogy (Zonca *et al.*, 2015b). The EPM wave-packet propagation could generally be in either radial directions. However, outward propagation is favored as the moving wave packet can more easily maintain the phase locking condition with the larger fraction of EPs that are transported outward while driving the mode, due to the conservation of the Hamiltonian in the extended phase space. Another important factor that may break the symmetry in the radial propagation direction is equilibrium nonuniformity, associated with both EP profiles and continuum damping. Thus, unless radial nonuniformity inhibits outward propagation, frequency chirping is predicted to be generally downward for EPM avalanche events, since characteristic EP resonant frequencies are radially decreasing for typical equilibrium radial profiles.

As a final point, we analyze the conditions under which radial corrugations in the EP profiles, discussed in connection with Eq. (4.202), are excited spontaneously (Zonca *et al.*,

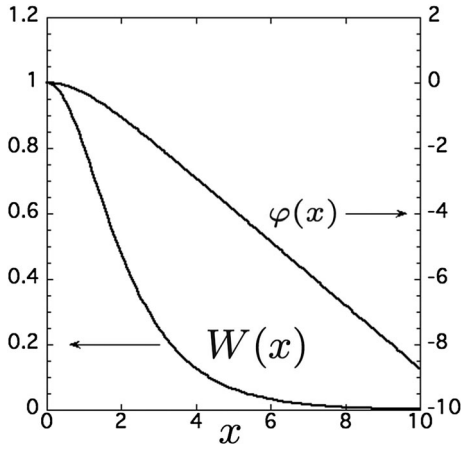

FIG. 5. The functions $W(x)$ and $\varphi(x)$ describing the self-similar shape $U(x) = W(x)e^{i\varphi(x)}$ of the EPM wave-packet propagation in the early phase of its nonlinear evolution (Zonca *et al.*, 2005, 2015b).

2000). Following the same procedure introduced in Sec. IV.C.2, the nonlinear dispersion relation for the EPM modulational instability can be written as

$$\left|\frac{\partial D_0}{\partial \omega_0}\right|^2 [\Delta_T^2 - (\omega_z + i\gamma_d)^2] + \frac{4i\gamma_M^2}{(\omega_z + 2i\gamma)^2}\left((\omega_z + i\gamma_d)\frac{\partial \mathbb{R}\mathrm{e}D_0}{\partial \omega_0} - i\Delta_T \frac{\partial \mathbb{I}\mathrm{m}D_0}{\partial \omega_0}\right) + \frac{3\gamma_M^4}{(\omega_z + 2i\gamma)^4} = 0. \tag{4.217}$$

Here D_0 stands for D_n of the EPM pump, γ_d is the sideband damping, and Δ_T the frequency mismatch, while

$$\gamma_M^2 = \frac{3\pi^2 (r/R_0)^{1/2}\alpha_E}{8\sqrt{2}|s|}\frac{\omega_0}{\bar{\omega}_{dF}} k_\vartheta^2 \rho_{LE}^2 k_z^2 v_E^2 |\bar{A}_0|^2. \tag{4.218}$$

Equation (4.217) shows common features with the dispersion relation of ZS induced by finite-amplitude TAE, discussed in Sec. IV.C.2. The novel element here is that resonant wave-particle interactions typically produce modulational instability of the EP pressure profile (Vlad *et al.*, 2004; Zonca *et al.*, 2006) characterized by both finite growth rate and real frequency shift (Zonca *et al.*, 2000). As pointed out in Sec. IV.C.2, all physical processes yielding fluctuation amplitude modulation may result in nonlinear splitting of the corresponding spectral lines. From ordering considerations, it is evident that the onset condition for the EPM induced modulational instability gives $|\omega_z| \sim \epsilon_0\omega_0 \sim \gamma_d \sim \gamma \sim \gamma_M/|\Delta_T/\omega_0|^{1/2}$, with $\Delta_T \sim \epsilon_0\omega_0$ (Zonca *et al.*, 2000; Zonca and Chen, 2014c). Thus, using Eq. (4.203) the threshold condition for $|\delta B_r/B_0|$ in this case is, respectively, $\sim \epsilon_0^{1/4}\alpha_E^{-1/2}$ and $\sim \epsilon_0^{1/2} q^{-1}\alpha_E^{-1/2}$ higher than when TAE induced ZS are dominated by the zonal current or zonal flows (cf. Sec. IV.C.2). These results suggest that for sufficiently strong EP drive, i.e., sufficiently high α_E, ZS are expected to not significantly modify the nonlinear EPM dynamics (Zonca *et al.*, 2000). In particular, when analyzing the modulational instability of EPM driven by EP transit resonance, the criterion for neglecting the effect of zonal flows becomes $\alpha_E \gg \epsilon_0^{3/2}/q^2$, as the EPM drive is not reduced by the trapped particle fraction. This is consistent with the empirical scaling $\alpha_E > \beta_e q^2$, β_e being the thermal electron plasma β, obtained from numerical gyrokinetic simulation results (Bass and Waltz, 2010).

Finally, it is worthwhile to make some further general remarks and comments on this analysis. Note that Eq. (4.212) is similar to that of a nonlinear oscillator in the so-called "Sagdeev potential" $V = (-U^2 + U^4)/2$, which generates the equation of motion

$$\partial_\xi^2 U = U - 2U^3, \tag{4.219}$$

and gives $U = \mathrm{sech}(\xi)$. This form appears in solitonlike solutions of NLSE, e.g., the Gross-Pitaevsky equation (Gross, 1961; Pitaevskii, 1961) describing the ground state of a quantum system of identical bosons using the pseudopotential interaction model, as well as the envelope of modulated water wave groups, as demonstrated by Zakharov (1968). The same form was also more recently shown to appear in the propagation of the short optical pulse of a FEL in the superradiant regime (Bonifacio *et al.*, 1990, 1994; Giannessi, Musumeci, and Spampinati, 2005) discussed earlier, as well as in the radial spreading of drift wave–zonal flow turbulence via soliton formation (Guo, Chen, and Zonca, 2009). The complex nature of Eq. (4.212), however, is novel and connected with the unique role of wave-particle resonances, which dominate the nonlinear dynamics of EPMs via resonant wave-particle power exchange. Maximization of such power exchange yields two effects: (i) the mode radial localization, similar to the analogous mechanism discussed for the linear EPM mode structure (Zonca and Chen, 2000, 2014c); and (ii) the strengthening of the mode drive ($\mathbb{I}\mathrm{m}\lambda_0 > 0$), connected with the steepening of the pressure gradient, convectively propagating with the EPM wave packet. These two effects are consistent with and clearly illustrated by the numerical simulation results of Fig. 3 (Zonca *et al.*, 2005).

More generally, Eqs. (4.201), (4.204), and (4.205) are of integrodifferential nature and thus they describe processes characterized by nonlocality in space and time connected with wave-particle resonant interactions. This case can be appreciated from the structure of Eq. (4.201) and the operator $\partial_t^{-2}\partial_r^2$. Assuming that Eq. (4.204) admits a self-similar solution in the form $\bar{A}_{n0}(\xi)$, as in Eq. (4.208), and that the radial profile of $\hat{F}_0(\omega)$ can be described by a stretched Gaussian distribution $\propto \exp[-|\xi - \xi_0|^\mu]$, with some fractional $\mu \in (1, 2)$, $\delta\bar{W}_{nk}^{NL}\bar{A}_{n0}$ can be rewritten in terms of fractional-derivative operators (Zonca *et al.*, 2006), $\propto \partial_\xi^{2-\mu}|\bar{A}_{n0}|^2$, with

$$\partial_\xi^{2-\mu}\Psi \equiv \frac{1}{\Gamma(\mu-1)}\frac{\partial}{\partial\xi}\int_{-\infty}^{\xi}\frac{\Psi(\xi')}{(\xi-\xi')^{2-\mu}}d\xi', \tag{4.220}$$

corresponding to the Weyl definition of fractional derivative [see, e.g., Metzler and Klafter (2000)]. Its appearance in the nonlinear evolution equation (4.204) reminds one of fractional generalizations of the Ginzburg-Landau and NLSE [(Weitzner and Zaslavsky, 2003; Milovanov and Rasmussen, 2005), reviewed by Zelenyi and Milovanov (2004)], characterized by a competition between a weak nonlinearity and space-time nonlocal properties. Indeed, equations built on fractional-derivative operators incorporate in a natural, unified way the key features of non-Gaussianity and long-range dependence that often break down the restrictive assumptions of locality and lack of correlations underlying the conventional statistical mechanical paradigm [see Metzler and Klafter (2004) for a review of this subject]. It is worthwhile noting that, following Eq. (4.220) and Zonca *et al.* (2006), when the free-energy source function in Eq. (4.201) is taken to be Gaussian, i.e., $\hat{F}_0(\omega) \propto \exp[-(\xi - \xi_0)^2]$, Eq. (4.204) can be reduced to the canonical form of the Ginzburg-Landau equation (Lifshitz and Pitaevsky, 1980), which finds many applications other than fusion plasma physics. Fractional time derivatives can also be introduced for the description of Eq. (4.205) nonlocality in time (and correspondingly in space), which is intrinsically connected with ballistic resonant particle transport but more

generally may describe a wider class of behaviors as well. Doing so naturally yields fractional Fokker-Planck equations and thus applications of general interest [see, e.g., the recent work by Górska *et al.* (2012)] with their further extension to nonlinear problems [cf. Eq. (4.205)]. This shows the special role of EPs in fusion plasmas, which introduce a completely novel class of nonlinear behaviors due to the existence of the SAW continuous spectrum, and the property of EPMs to lock onto the proper resonance for maximizing wave-particle power exchange and particle transport (Zonca *et al.*, 2006; Chen and Zonca, 2007a; Chen, 2008) due to phase locking.

7. The fishbone burst cycle

The observation of fishbone oscillations (McGuire *et al.*, 1983), interpreted as bursts of internal kink modes resonantly excited by EPs via precessional resonance (Chen, White, and Rosenbluth, 1984; Coppi and Porcelli, 1986), is the first key experimental evidence of the rich nonlinear dynamics involving the interaction of EPs with MHD and Alfvénic fluctuations. Nonlinear fishbone dynamics is determined by both nonlinear wave-wave (MHD) and wave-particle interactions. However, the key role played by EPs was clear from the early experimental evidence that fluctuations are locked onto the characteristic EP (precessional) frequency, while they are transported out preserving the resonance condition (White *et al.*, 1983). Thus, it is intuitive that for sufficiently strong power input fishbone dynamics should be dominated by wave-particle nonlinear interactions.

Early analyses of the fishbone burst cycle relied on simplified predator-prey models (Chen, White, and Rosenbluth, 1984; Coppi and Porcelli, 1986; Coppi, Migliuolo, and Porcelli, 1988) on which more detailed discussion is given below. Fishbone induced EP transport studies and comparisons with experimental observations were meanwhile based on test-particle numerical simulations (White *et al.*, 1983) (cf. Secs. V and V.A). The first nonlinear numerical studies of fishbone excitation by nonperturbative wave-EP interactions were reported by Candy *et al.* (1999), assuming a linear MHD description and mode structure given by a rigid $(m,n)=(1,1)$ radial displacement. The nonlinear EP kinetic response is computed numerically as a contribution to the potential energy in a kinetic energy principle, i.e., Eq. (3.17) with a simplified form of the inertia enhancement (Glasser, Green, and Johnson, 1975). Their results reproduce the dynamics of a fishbone burst, with downward frequency chirping and mode saturation at a level ~10 smaller than the dimensional estimate $|\delta\boldsymbol{\xi}_r/r_s|\sim 1$ with $\delta\boldsymbol{\xi}_r$ and r_s being, respectively, the radial displacement and the $q=1$ radial position. They also estimate that in their case the condition for neglecting MHD nonlinearity is marginally satisfied. The relative role of MHD and EP nonlinearities can, however, be more precisely estimated on the basis of Eq. (3.17), by comparing Λ_n^{NL} with $\delta\hat{W}_{nk}^{NL}$ due to EPs. Ödblom *et al.* (2002) demonstrated that Λ_n^{NL} is predominantly determined by ZS (flows and currents), generated self-consistently by the dominant $(m,n)=(1,1)$ component of the fishbone fluctuation. The MHD model employed by Ödblom *et al.* (2002) ignores kinetic thermal ion and geometry effects and yields

$$\Lambda^{NL}\sim\frac{|\delta\boldsymbol{\xi}_{r0}|^2}{\Delta^2}\Lambda\sim\frac{|\delta\boldsymbol{\xi}_{r0}|^2}{r_s^2(\gamma_L/\omega_0)^2}\frac{s^2}{\Lambda}, \tag{4.221}$$

where we dropped the $n=1$ subscript, $\delta\boldsymbol{\xi}_{r0}$ is the constant value of $\delta\boldsymbol{\xi}_r$, $\Delta\sim r_s(\Lambda/s)(\gamma_L/\omega_0)$ is the inertial layer width, s is the magnetic shear at the $q=1$ surface, and Λ can be estimated at its typical linear value. Including inertia enhancement, Eq. (4.221) still applies but a realistic estimate yields $|\Lambda|\sim|s|$ (Zonca *et al.*, 2007b). Meanwhile, the estimate for $\delta\hat{W}_{nk}^{NL}$ can be obtained as [cf. Eq. (4.231) and Sec. IV.D.5]

$$\delta\hat{W}_k^{NL}\sim\mathbb{I}\mathrm{m}\delta\hat{W}_k^{L}\frac{|\delta\boldsymbol{\xi}_{r0}|^2}{r_s^2(\gamma_L/\omega_0)^2}, \tag{4.222}$$

where $\mathbb{I}\mathrm{m}\delta\hat{W}_k^{L}\sim(R_0/r_s)\beta_{Er}$, with β_{Er} being the β_E value of resonant EPs. Thus, noting Eqs. (3.17), (4.221), and (4.222), one can conclude that EP nonlinearities dominate the precessional fishbone for $\beta_{Er}\gg|s|^3(r_s/R_0)|\Lambda|^{-1}$. However, for $|\Lambda|\sim|s|$ and near marginal stability, both nonlinear effects must be kept on the same footing. Here we focus on strongly

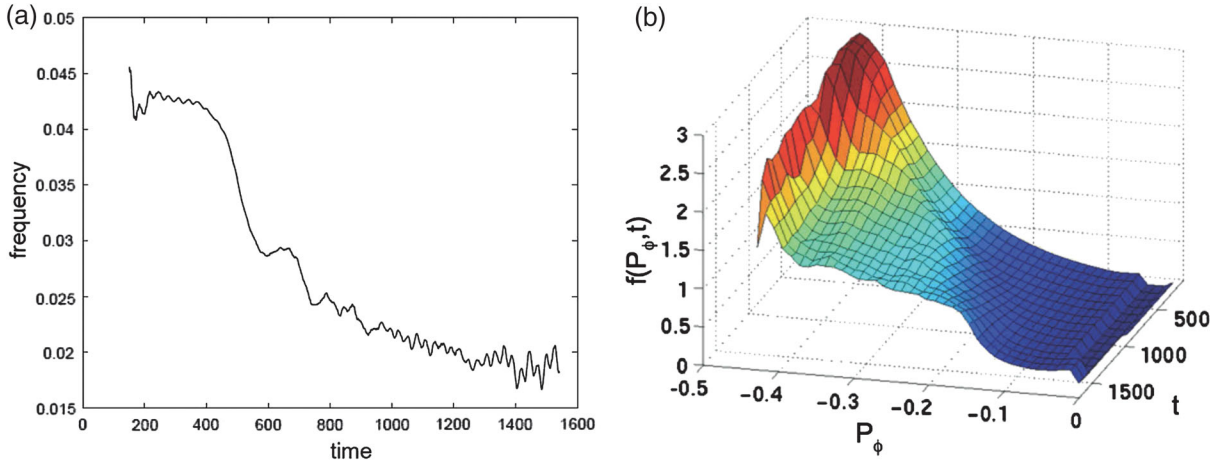

FIG. 6. (a) Evolution of the fishbone frequency vs time. The frequency is expressed in units of $\omega_{A0}=v_{A0}/R_0$ and the time in units of ω_{A0}^{-1}. (b) Evolution of the resonant EP distribution function for $v/v_{A0}=0.8$ and $\mu B_0/\mathcal{E}=1$. From Fu *et al.*, 2006.

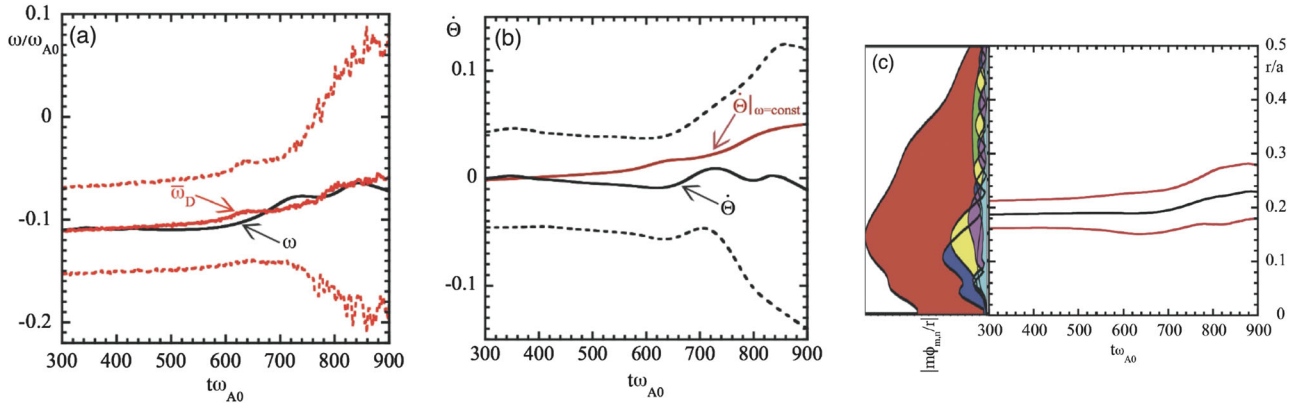

FIG. 7. (a) Time evolution of $\bar{\omega}_D$ (red line) and $\bar{\omega}_D \pm \delta\omega_D$ (dashed red lines), compared with the time evolving mode frequency from simulation results (black line). (b) Time evolution of $\bar{\dot{\Theta}}$ (black line) and $\bar{\dot{\Theta}} \pm \delta\dot{\Theta}$ (dashed black lines); $\bar{\dot{\Theta}}|_{\omega=\text{const}}$, obtained neglecting frequency chirping is also shown (red line). From Vlad *et al.*, 2013. (c) Time evolution of $\bar{r}$ (middle, black line) and of $\bar{r} \pm \delta r$ (top and bottom, red lines). The linear mode structure is also shown by $|(m/r)\delta\phi_{m,n}| \propto |\delta\boldsymbol{\xi}_{rm,n}|$ in abscissa vs the normalized radial position on the vertical axis. The harmonic in red refers to the dominant $(m,n) = (1,1)$ component. From Vlad *et al.*, 2013.

driven fishbones, where wave-wave (MHD) nonlinearities can be neglected.

Comprehensive numerical fishbone simulations based on the hybrid MHD-gyrokinetic model (cf. Sec. II) are more recent (Fu *et al.*, 2006; Vlad *et al.*, 2012, 2013). Fishbone linear stability analyses based on the same approach were reported by Park *et al.* (1999). Meanwhile, the first nonlinear simulation of a fishbone burst cycle was given by Fu *et al.* (2006), where it was shown that mode saturation and frequency chirping are connected with the secular outward motion of resonant EPs, as depicted in Fig. 6. More specifically, Fig. 6 shows both frequency variation in time and the change in the resonant EP distribution function for $v/v_{A0} = 0.8$ and $\mu B_0/\mathcal{E} = 1$ (cf. Sec. II.D), with v_{A0} the Alfvén speed on magnetic axis. The normalization of P_ϕ is such that $P_\phi = -0.42$ corresponds to the plasma center and $P_\phi = 0$ to the plasma boundary. In these numerical simulations, MHD nonlinearities are found to reduce the mode saturation level, but not drastically, showing that EPs dominate nonlinear dynamics, consistent with Eqs. (4.221) and (4.222).

Further demonstration of the nonlinear physics underlying the fishbone burst cycle was recently provided for "electron fishbones" (e-fishbones) (Vlad *et al.*, 2012, 2013), due to precessional resonance with suprathermal electrons (Wong *et al.*, 2000; Ding *et al.*, 2002; Zonca *et al.*, 2007a). Their simulation results are consistent with those of Fu *et al.* (2006) and demonstrate that nonlinear mode saturation is accompanied by downward frequency chirping. In addition, they illuminate and further clarify the nonlinear fishbone dynamics by means of the phase-space numerical diagnostics introduced by Briguglio (2012) and Briguglio and Wang (2013); see Vlad *et al.* (2012, 2013) for further details. The convective resonant particle motion yielding mode saturation by radial decoupling is demonstrated by a time sequence of kinetic Poincaré plots (White, 2012), which show EPs moving outward at essentially constant wave-particle phase and the formation of a steeper gradient region that is also outward moving. At the same time, a flatter region in the EP particle distribution is formed at smaller radii, which extends further inward as more EPs are convectively pumped outward. Meanwhile, as resonant EPs are convected outward and their $\bar{\omega}_d$ decreases, the mode chirps downward as shown in Fig. 7(a), which illustrates the time evolution of $\bar{\omega}_D$ and $\delta\omega_D$. Here $\bar{\omega}_D$ is the average of $\bar{\omega}_d$ of simulation particles weighted by the wave-particle power exchange in the linear phase, and $\delta\omega_D$ is the corresponding spread from $\bar{\omega}_D$. One can similarly define $\bar{\dot{\Theta}}$ and $\delta\dot{\Theta}$ as well as $\bar{r}$ and δr, shown, respectively, in Figs. 7(b) and 7(c). In particular, Fig. 7(b) shows that frequency chirping is due to phase locking (black line) and maximization of wave-particle power exchange, and that, with no frequency chirping accounted for, $\bar{\dot{\Theta}}|_{\omega=\text{const}}$ (red line) would yield rapid resonance detuning. Saturation of the fishbone burst instead is due to radial decoupling, as illustrated in Fig. 7(c), showing the time evolution of $\bar{r}$ (middle, black line) and $\bar{r} \pm \delta r$ (top and bottom, red lines), referred to the linear mode structure (in arbitrary units) $|(m/r)\delta\phi_{m,n}| \propto |\delta\boldsymbol{\xi}_{rm,n}|$.

The above nonlinear fishbone simulation results may be understood within the theoretical framework introduced in Sec. IV.D.5. Assuming deeply trapped EPs as in Sec. IV.D.6 and considering a rigid plasma displacement,[28] we have

$$\delta\hat{W}_k = 2\frac{\pi^2}{B_0^2} m\Omega^2 \frac{R_0}{r_s^2}\int_0^{r_s}\frac{r^3}{q}dr\int \mathcal{E}d\mathcal{E}d\lambda \times \sum_{v_\parallel/|v_\parallel|=\pm 1}\frac{\tau_b\bar{\omega}_d^2}{\omega(\tau)}\int_{-\infty}^{\infty}\frac{\omega+\omega(\tau)}{\bar{\omega}_d-\omega(\tau)-\omega} \times e^{-i\omega t}Q_{k,\omega(\tau)}\hat{F}_0(\omega)d\omega, \tag{4.223}$$

where as in Eq. (4.200) $\omega(\tau) = \omega_0(\tau) + i\gamma(\tau)$ is the time evolving complex frequency. The evolution equation for $F_0(t)$ is also obtained from Eq. (4.194):

[28] A fully self-consistent treatment must generally allow the mode structure to evolve due to nonperturbative redistributions of EPs.

$$\frac{\partial}{\partial t}F_0(t) \simeq \mathrm{St}F_0(t) + S(t) + 2\left(\frac{\bar{\omega}_d}{\omega_0(\tau)}\right) \times \frac{\partial}{\partial r}\left[\left(\int_{-\infty}^{+\infty}\frac{(\gamma - i\omega) - (\bar{\omega}_d - \omega_0)\gamma/\omega_0}{(\bar{\omega}_d - \omega_0)^2 + (\gamma - i\omega)^2} \times e^{-i\omega t}\frac{\partial \hat{F}_0(\omega)}{\partial r}|\omega_0(\tau)|^2|\delta\boldsymbol{\xi}_{r0}|^2 d\omega\right)\right]. \quad (4.224)$$

Equation (4.224) is the analog of Eq. (4.205) having maintained an explicitly external source and collision terms as well as the next order correction terms in the asymptotic expansion in γ/ω_0. With $\delta\hat{W}_k$ given by Eqs. (4.223) and (4.224), the GFLDR Eq. (3.17) provides a description of the fishbone burst cycle dominated by EP nonlinearity (Zonca *et al.*, 2007b), reducing to the case investigated numerically by Candy *et al.* (1999) if the core plasma response is described by ideal MHD (Glasser, Green, and Johnson, 1975). Because of the global nature of the fishbone mode structures, these equations generally require a numerical solution, which is not given in the literature except that in the MHD limit considered by Candy *et al.* (1999). However, further analytic progress is possible if one introduces subsidiary approximations, which help to elucidate the nature of the saturation process and EP transport due to fishbone bursts (Zonca *et al.*, 2007b).

Let us consistent with Fig. 7 assume that $\delta\hat{W}_k$ is predominantly provided by a localized radial region inside r_s. Using the formal decomposition $\delta\hat{W}_k \equiv \delta\hat{W}_k^L + \delta\hat{W}_k^{NL}$ as in Sec. IV.D.6, it can be readily verified that $\mathbb{R}\mathrm{e}\delta\hat{W}_k \simeq \mathbb{R}\mathrm{e}\delta\hat{W}_k^L$ at the leading order of the asymptotic expansion in γ/ω_0. For radially localized EP response,

$$[\bar{\omega}_d - \omega(\tau) - \omega]^{-1} \simeq \tilde{\omega}_d^{-1}[\mathcal{E} - \mathcal{E}_0 - i(\gamma - i\omega)/\tilde{\omega}_d]^{-1}, \quad (4.225)$$

with $\bar{\omega}_d(\bar{r}) \equiv \tilde{\omega}_d\mathcal{E}$ and $\omega_0 \equiv \tilde{\omega}_d\mathcal{E}_0$. Meanwhile, noting that $\tau_b = 2\pi q R_0 \mathcal{E}^{-1/2}(R_0/r)^{1/2}$ for deeply trapped particles, as well as $k_\vartheta \propto -nq/r$, $\bar{\omega}_d^2 \propto \tilde{\omega}_d^2 \propto (nq/r)^2$, and $|\omega_{*E}| \gg |\omega(\tau)|$, we can write

$$\mathbb{R}\mathrm{e}\delta\hat{W}_k \simeq \mathbb{R}\mathrm{e}\delta\hat{W}_k^L = -\frac{R_0}{r_s}\int_0^{r_s} q^2\frac{r}{r_s}\left(\frac{R_0}{r}\right)^{1/2} \times \frac{\partial}{\partial r}\left[\left(\frac{r}{R_0}\right)^{1/2}\hat{\beta}_E(r;\omega_0(\tau))\right]dr, \quad (4.226)$$

where

$$\hat{\beta}_E(r;\omega_0(\tau)) = 2\frac{\pi^2}{B_0^2}m|\Omega|\frac{r}{q^2}\int \mathcal{E}d\mathcal{E}d\lambda \times \sum_{v_\parallel/|v_\parallel|=\pm 1}\tau_b\bar{\omega}_d^2\int_{-\infty}^{\infty}\frac{(\bar{\omega}_d - \omega_0)}{(\bar{\omega}_d - \omega_0)^2 + (\gamma - i\omega)^2} \times e^{-i\omega t}\hat{F}_0(\omega)d\omega. \quad (4.227)$$

This definition assumes that modes have positive frequency when rotating in the EP diamagnetic direction; i.e., $n = 1$ for energetic ions and $n = -1$ for energetic electrons. The expression for $\hat{\beta}_E$ depends only on the ratio $\omega_0/\bar{\omega}_{dF}$, with $\bar{\omega}_{dF}$ being the characteristic EP precessional frequency. In the case considered in Sec. IV.D.6, it is the precessional frequency at the injection energy of the EP beam. Thus, Eq. (3.17) yields

$$\delta\hat{W}_f + \mathbb{R}\mathrm{e}\delta\hat{W}_k^L \simeq 0, \quad (4.228)$$

and Eq. (4.226) shows that the fishbone frequency is set by the condition $\omega_0/\bar{\omega}_{dF} \simeq$ const, to be computed at the position of the radial shell where the most significant EP contribution is localized. Meanwhile, we can write[29]

$$\mathbb{I}\mathrm{m}\delta\hat{W}_k = -\frac{R_0}{r_s}\int_0^{r_s} q^2\frac{r}{r_s}\left(\frac{R_0}{r}\right)^{1/2}\frac{\partial}{\partial r}\left[\left(\frac{r}{R_0}\right)^{1/2}\beta_{Er}(r;\omega_0(\tau))\right]dr = \frac{R_0}{r_s}\int_0^{r_s}\left[-rq^2\frac{\partial\beta_{Er}}{\partial r} - q^2\frac{\beta_{Er}}{2}\right]\frac{dr}{r_s}, \quad (4.229)$$

where the resonant EP β_E is defined as

$$\beta_{Er}(r;\omega_0(\tau)) = 2\frac{\pi^2}{B_0^2}m|\Omega|\frac{r}{q^2}\int \mathcal{E}d\mathcal{E}d\lambda \times \sum_{v_\parallel/|v_\parallel|=\pm 1}\tau_b\bar{\omega}_d^2\int_{-\infty}^{\infty}\frac{\gamma - i\omega}{(\bar{\omega}_d - \omega_0)^2 + (\gamma - i\omega)^2} \times e^{-i\omega t}\hat{F}_0(\omega)d\omega. \quad (4.230)$$

Substituting the formal solution of Eq. (4.224) into Eq. (4.229), it is possible to obtain

$$\beta_{Er} = \partial_t^{-1}(\dot{\beta}_{ErS} - \nu_{\mathrm{ext}}\beta_{Er}) + \partial_t^{-2}\left(\frac{R_0}{r}\right)^{1/2} \times \left\{\frac{q}{r}\frac{\partial}{\partial r}\left[\frac{r}{q}|\omega_0|^2|\delta\boldsymbol{\xi}_{r0}|^2\frac{\partial}{\partial r}\left(\left(\frac{r}{R_0}\right)^{1/2}\beta_{Er}\right)\right]\right\}. \quad (4.231)$$

Together with Eq. (4.229) this equation justifies the estimate for $\delta\hat{W}_k^{NL}$ given in Eq. (4.222), which yields the optimal ordering for the saturation amplitude as $|\delta\boldsymbol{\xi}_{r0}| \sim r_s|\gamma_L/\omega_0|$, consistent with simulation results (Vlad *et al.*, 2013). Here we have also introduced the effects of sources and collisions on the resonant EP population using the definitions

$$\dot{\beta}_{ErS} \equiv 2\frac{\pi^2}{B_0^2}m|\Omega|\frac{r}{q^2}\int \mathcal{E}d\mathcal{E}d\lambda \times \sum_{v_\parallel/|v_\parallel|=\pm 1}\tau_b\bar{\omega}_d^2\frac{\gamma}{(\bar{\omega}_d - \omega_0)^2 + \gamma^2}S(t), \quad (4.232)$$

$$\nu_{\mathrm{ext}}\beta_{Er} \equiv -2\frac{\pi^2}{B_0^2}m|\Omega|\frac{r}{q^2}\int \mathcal{E}d\mathcal{E}d\lambda \times \sum_{v_\parallel/|v_\parallel|=\pm 1}\tau_b\bar{\omega}_d^2\frac{\gamma}{(\bar{\omega}_d - \omega_0)^2 + \gamma^2}\mathrm{St}F_0(t), \quad (4.233)$$

[29]Note that here we use a slightly different definition than Zonca *et al.* (2007b) in order to take into account the assumption of deeply trapped EPs.

which explicitly separate these contributions as suggested by White (2010) in order to emphasize their different roles in the dynamics of the fishbone burst cycle on time scales longer than $\tau_{NL} \sim \gamma_L^{-1}$ (see the following discussion). Finally, the system of Eqs. (4.226)–(4.233) is closed by the evolution equation for $|\delta\boldsymbol{\xi}_{r0}|$; i.e.,

$$\frac{\partial}{\partial t}\ln|\delta\boldsymbol{\xi}_{r0}|^2 = \frac{2(R_0/r_s)}{-\partial\mathbb{R}\mathrm{e}\delta\hat{W}_k^L/\partial\omega_0}\left\{-\int_0^{r_s} q^2\frac{r}{r_s}\left(\frac{R_0}{r}\right)^{1/2} \times\frac{\partial}{\partial r}\left[\left(\frac{r}{R_0}\right)^{1/2}\beta_{Er}(r;\omega_0(\tau))\right]dr - \left(\frac{r_s}{R_0}|s|\Lambda(\omega_0)\right)\right\}. \tag{4.234}$$

Without sources and collisions, and assuming $q \sim$ const as well as $\omega_0/\bar{\omega}_{dF} \sim$ const, Eq. (4.231) describes the propagation of $(r/R_0)^{1/2}\beta_{Er}$ as a function of $r^2 - 2r|\omega_0\|\delta\boldsymbol{\xi}_{r0}|$, and resonant EP compression propagates with speed $\dot{r} \simeq |\omega_0\|\delta\boldsymbol{\xi}_{r0}|$, which is a function of r. This is the mechanism of mode-particle pumping (White *et al.*, 1983) that yields mode saturation by ejection of resonant particles from the $r = r_s$ surface when the ejection rate $\sim|\omega_0\|\delta\boldsymbol{\xi}_{r0}|/r_s$ balances the growth rate $\sim\gamma_L$. Thus, as resonant EPs are convected outward and the mode growth rate decreases, the downward frequency shift by phase locking can be computed by Eq. (4.216), with $v_g = |\omega_0\|\delta\boldsymbol{\xi}_{r0}|$. This picture is consistent with simulation results of Fig. 7(c) and is in essence similar to that of nonlinear EPM dynamics (cf. Sec. IV.D.6) with, however, different underlying mode structures. When EPs that most efficiently provide mode drive are transported sufficiently outward that radial decoupling becomes important, they are gradually replaced by lower energy particles, which resonate at smaller r value and continue driving the mode (White, 2000). In this way, particles can be extracted from increasingly lower energies and inner regions of the plasma core and be pumped outward, far beyond the r_s surface and up to the plasma boundary (White *et al.*, 1983). Proceeding further in the γ/ω_0 asymptotic expansion, the frequency sweeping rate can be determined with a better precision than based on the simple expression $\omega_0/\bar{\omega}_{dF} \sim$ const.

Equations (4.231) with sources and collisions and (4.234) can be used to derive reduced nonlinear models for the fishbone burst cycle. Without the nonlinear term, Eq. (4.231) gives the asymptotic solution $\beta_{Er} = \beta_{Er0} = \dot{\beta}_{ErS}/\nu_{\mathrm{ext}}$. For strongly driven fishbones, we may consider β_{Er0} significantly larger than the threshold condition $\beta_{Er} = \beta_c$, around which β_{Er} is linearly increasing in time due to $\dot{\beta}_{ErS}$. Formally acting with ∂_t on Eq. (4.231), estimating $\partial_r^2 \sim -1/r_s^2$, and considering the remaining $\partial_t^{-1} \sim \tau_{NL} \sim r_s/|\omega_0\|\delta\boldsymbol{\xi}_{r0}|$, Eqs. (4.231) and (4.234) can be modeled as

$$d\beta/d\tau = S - A\beta_c,$$
$$dA/d\tau = \gamma_0(\beta/\beta_c - 1)A, \tag{4.235}$$

where we dropped the subscript in β_{Er} and used notations by White (1989), τ is a normalized time, $A = |\delta\boldsymbol{\xi}_{r0}|/r_s$ is the normalized fishbone amplitude, and γ_0 is a measure of the linear growth rate. Equations (4.235) [cf. problem # 3 on p. 280 of White (1989)] are the same as those originally proposed by Chen, White, and Rosenbluth (1984).[30] As noted by Chen, White, and Rosenbluth (1984) and White (1989), the solution of Eqs. (4.235) is cyclic; i.e., it can be generally written as $F(A,\beta) =$ const, where $F(A,\beta)$ has a maximum at the fixed point position $\beta = \beta_c$, and $A = S/\beta_c$. A crucial feature of Eqs. (4.235) is the linear dependence on A of the loss term in the β evolution equation. From Eq. (4.231), this is readily recognized to be a consequence of the ∂_t^{-2} operator acting on the nonlinear response, which is the manifestation of secular resonant EP losses by mode-particle pumping (White *et al.*, 1983). This term constitutes the fundamental difference of the Chen, White, and Rosenbluth (1984) approach with respect to the predator-prey model discussed by Coppi and Porcelli (1986) and Coppi, Migliuolo, and Porcelli (1988), which adopts a loss term $\propto A^2$.

In the form of Eqs. (4.235), the temporal nonlocality built in Eq. (4.231) and more generally in Eq. (4.224) is lost. However, it was recently proposed in the context of predator-prey modeling of TAE bursting behavior (Heidbrink, Duong *et al.*, 1993) that nonlocal time behavior may be accounted for by introducing a time delay in the wave-particle power exchange and in the phase-space island-induced particle diffusion (Parker and White, 2010). Another worthwhile remark concerns the role of the collision term $\propto -\nu_{\mathrm{ext}}\beta_{Er}$ in Eq. (4.231). By definition, ν_{ext} reduces to the well-known (linear) effective collision frequency only in the weakly nonlinear case. For sufficiently strong nonlinear distortions, ν_{ext} may even change sign and, therefore, modify the nonlinear behavior of the dynamic system of Eqs. (4.235) with a formal substitution $S \to S + \nu\beta \to \nu\beta$, as hinted at by Zonca *et al.* (2007b), while the loss term may become $\sim -A\beta$ for large fluctuations. Both the time delay and the nonlinear ν_{ext} models, however, have not yet been fully explored.

Much richer physics is expected to become increasingly more relevant as plasma conditions approach marginal stability; e.g., MHD nonlinearities cannot be neglected (Ödblom *et al.*, 2002). Correspondingly, more theory and simulation studies are needed to fully understand and explain the diverse experimental evidence recently reported and summarized by Guimarães-Filho *et al.* (2012) for the specific case of electron fishbones. In general, the present understanding of wave-particle and wave-wave nonlinear effects calls for a comprehensive treatment addressing these physics on the same footing, while accounting for kinetic core plasma response in realistic toroidal geometry.

[30]Note that Chen, White, and Rosenbluth (1984) assumed that the nonlinear term in the β evolution equation is multiplied by the Heaviside function $H(\beta - \beta_{\min})$; i.e., it is considered effective only if β is above a minimum $\beta_{\min}$ value, considered to be that reached as a consequence of the secular expulsion of EPs from within the $r = r_s$ magnetic surface.

E. Further remarks on general theoretical issues and broader implications

By construction, Eq. (4.3) is inapplicable to investigations of broadband plasma turbulence. However, it has been used successfully to investigate nonlinear processes in DWT, where time-scale separation may be systematically applied. Examples are the excitation of ZS by coherent wave-wave interactions (Chen, Lin, and White, 2000; Chen *et al.*, 2001; Guzdar, Kleva, and Chen, 2001), turbulence spreading (Lin *et al.*, 2002; Hahm *et al.*, 2004; Lin and Hahm, 2004) enhanced by DW-zonal flow interaction (Chen, White, and Zonca, 2004; Zonca, White, and Chen, 2004; White, Chen, and Zonca, 2005; Guo, Chen, and Zonca, 2009), and saturation of electron temperature gradient driven turbulence due to inverse cascade via scatterings off driven low mode-number quasimodes (Chen, Zonca, and Lin, 2005; Lin, Chen, and Zonca, 2005). Equation (4.3) can also be used for addressing spatiotemporal cross-scale couplings between DAWs and EP dynamics and DWT and turbulent transport (cf. Sec. VI.B). Thus, the formal separation of nonlinear interaction with ZS on the right-hand side of Eq. (4.3) captures two different processes, i.e., the coherent nonlinear interaction with the ZS generated by the fluctuation itself (self-interaction) and the incoherent interaction with ZS generated by other fluctuating fields, including DWT (Zonca *et al.*, 2015a). Assuming, for illustration, nondispersive waves along with local nonlinear interactions in n space, the form of Eq. (4.3) becomes that of a discrete Anderson NLSE with randomness (Shepelyansky, 1993; Pikovsky and Shepelyansky, 2008; Iomin, 2010; Krivolapov, Fishman, and Soffer, 2010):

$$i\hbar\frac{\partial}{\partial t}\psi_n = \hat{H}_L\psi_n + \zeta|\psi_n|^2\psi_n, \tag{4.236}$$

where $\hat{H}_L$ is the Hamiltonian of the linear problem, accounting for the random transitions between nearest-neighbor states (Anderson, 1958). An important feature which arises in the analysis of Eq. (4.236) as well as Eq. (4.3) is competition between nonlinearity and randomness. It has been argued that when the nonlinearity parameter ζ is sufficiently small the random properties play the dominant role through the dynamics [see, e.g., Wang and Zhang (2009) and Krivolapov, Fishman, and Soffer (2010)], thus sustaining the phenomena of Anderson localization as in the linear case (Anderson, 1958). That means that the diffusion is suppressed and an initially localized wave packet will not spread to infinity. Despite this evidence, direct numerical simulations show that the phenomena of Anderson localization are destroyed above a certain critical strength of repulsive ($\zeta > 0$) nonlinearity (Pikovsky and Shepelyansky, 2008; Flach, Krimer, and Skokos, 2009), and an unlimited subdiffusive spreading of the wave field across the lattice occurs. This can be explained noting that the loss of Anderson localization in the presence of nonlinearity is a critical phenomenon (Milovanov and Iomin, 2012), and that the delocalization occurs spontaneously above a threshold value of ζ, similarly to the percolation transition in random lattices. Meanwhile, soliton solutions of Eq. (4.236) are typically found for attractive nonlinearity ($\zeta < 0$) (Zelenyi and Milovanov, 2004). Similarities with DWT spreading due to coherent DW-ZS interaction again become evident, considering that the zonal flow self-interaction term is attractive (Chen, White, and Zonca, 2004) and, therefore, that turbulence spreading may occur via soliton structure formation (Guo, Chen, and Zonca, 2009).

The theoretical analysis of Sec. IV.D.2 suggests a clear connection between AE nonlinear dynamics near marginal stability and autoresonance in driven 1D Vlasov-Poisson systems. Autoresonance (Meerson and Friedland, 1990) is the phenomenon of a nonlinear pendulum that can be driven to large amplitude, which evolves in time to instantaneously match the nonlinear frequency to that of an external drive with sufficiently slow downward frequency sweeping. This phenomenon is common in many fields of physics and "was first observed in particle accelerators, and has since been noted in atomic physics, fluid dynamics, plasmas, nonlinear waves, and planetary dynamics" (Fajans and Friedland, 2001). In fusion plasmas, the idea of autoresonance and resonant particle transport in buckets was proposed by Mynick and Pomphrey (1994) for removing helium ash from the plasma core and other possible applications, such as burn control, profile control, and diagnostic tool. The same notion has clear analogies to the idea of affecting the direct coupling of fusion alpha particle power, known as "alpha channeling" (Fisch and Rax, 1992) (cf. Sec. VI). Autoresonance is a process with a critical threshold in the amplitude of the external drive, which scales as $\sim\dot{\omega}^{3/4}$ and was observed in experiments with trapped electron clouds (Fajans, Gilson, and Friedland, 1999). Electron phase-space holes were formed and controlled in a plasma by adiabatic nonlinear phase locking (autoresonance) with a chirped frequency driving wave via Cherenkov-type resonance (Friedland, Khain, and Shagalov, 2006), for which a kinetic theory interpretation was given by Khain and Friedland (2007). As noted by Friedland, Khain, and Shagalov (2006), one important difference emerges when BGK structures (Bernstein, Greene, and Kruskal, 1957) are formed by instabilities, as they are poorly controllable. As long as the effect of EP transport on the plasma dielectric response can be considered small (cf. Secs. IV.D.1 and IV.D.2), the connection between autoresonance and the hole-clump nonlinear dynamics in the 1D beam-plasma problem with sources and sinks (Berk, Breizman, and Petiashvili, 1997; Berk *et al.*, 1999) is preserved. In the former case, the frequency sweeping is imposed by the external drive; in the latter one, chirping is set by balancing the rate of energy extraction of hole-clump dynamics in phase space with dissipation. However, when EP response is nonperturbative, resonant particle radial motion is secular as long as phase locking is maintained and frequency chirping is nonadiabatic, as discussed in Sec. IV.D.5 and, respectively, in Sec. IV.D.6 for EPMs and Sec. IV.D.7 for fishbones. The secular EP loss, predicted theoretically (White *et al.*, 1983) and observed experimentally (Duong *et al.*, 1993), may also be considered an autoresonant effect, spontaneously driven by EP transport for sufficiently strong drive. In between these two limiting behaviors there is a transition where the role of equilibrium geometry and plasma nonuniformity becomes increasingly more important for increasing mode drive (Wang *et al.*, 2012; Zhang, Lin, and Holod, 2012; Briguglio *et al.*,

2014). These physics, embedded in Eq. (4.3) by the integrodifferential nature of nonlinear terms and, more specifically, by the renormalized solution for the EP distribution function, Eqs. (4.192) and (4.194) (Dyson equation), suggest a number of possible model NLSEs, possibly with fractional partial derivatives, to be used for the description of multi spatiotemporal scale dynamics (cf. Secs. IV.D.6 and IV.D.7).

V. ENERGETIC-PARTICLE TRANSPORT IN FUSION PLASMAS

One fundamental issue in studies of collective mode excitation by EPs in burning plasmas is to assess whether significant degradation in the plasma performance could occur due to SAW fluctuations and what level of wall loading and damaging of plasma facing materials can be caused by energy and momentum fluxes due to collective fast particle losses. Losses up to 70% of the entire EP population have been both predicted theoretically and found experimentally (Duong *et al.*, 1993; Strait *et al.*, 1993; Heidbrink and Sadler, 1994).

The simplest prediction of fusion alpha density profiles in ITER is based on marginal stability arguments. This was proposed by Angioni *et al.* (2009), based on the assumption that fusion alpha transport from short-wavelength DWT is "stiff"; i.e., the profiles are maintained close to marginal stability to be computed by realistic linear gyrokinetic simulations. This work was recently extended by Waltz and Bass (2014) to include marginal stability transport due to long-wavelength AEs. In light of results discussed in this review, these predictions can capture only the averaged alpha density profiles on sufficiently long spatiotemporal scales, while more detailed investigations are needed to predict fluctuations about averaged profiles of EP density, temperature, etc., and to describe nonlinear dynamics of corresponding transport events (Chen and Zonca, 2007a, 2013; Zonca *et al.*, 2015a) [see also the recent reviews by Gorelenkov, Pinches, and Toi (2014) and Pinches *et al.* (2015)].

The standard approach to modeling EP losses due to a given spectrum of SAW fluctuations (AEs and EPMs) is based on test-particle transport studies. These are expected to well represent the actual transport phenomena provided that transport processes themselves do not significantly modify the fluctuation spectrum. It thus cannot describe the transition to secular transport phenomena, where the interplay of nonlinear mode dynamics and transport processes themselves is intrinsically nonperturbative as in the case of EPM avalanches discussed in Sec. IV.D.6 (cf. also Sec. VI.A). One important "exception" is the case of fishbones, where nonlinear transport processes do not significantly modify the MHD mode structure,[31] but predominantly causes the mode frequency to rapidly chirp downward (cf. Secs. IV.D.7 and V.B). In this case test-particle transport studies give good agreement between simulation results and experimental measurements of EP redistributions even assuming that the mode frequency is fixed. This is because the particle excursion in the radial coordinate is comparable to the machine size, due to the weak radial dependence of the precessional frequency (White *et al.*, 1983). Thus, accounting for the observed frequency sweeping is not crucial for EPs to be pumped out of the system. In many cases of practical interest, however, test-particle transport improves accuracy in comparisons of simulation results against experimental observations when the measured frequency sweeping is accounted for [see, e.g., Fredrickson *et al.* (2009) as well as Perez von Thun *et al.* (2011, 2012)]. This important point was noted in the early test-particle simulations of EPs by fast frequency chirping modes (White, 2000).

A. Suprathermal test-particle transport

The test-particle loss mechanism is essentially of two types (Hsu and Sigmar, 1992; Sigmar *et al.*, 1992): (1) transient losses, which scale linearly ($\approx \delta B_r/B$) with the mode amplitude, due to resonant drift motion across the orbit-loss boundaries in the EP phase space; and (2) diffusive losses, which scale as $\approx(\delta B_r/B)^2$, due to EP stochastic diffusion and eventually transport across the orbit-loss boundaries. Both mechanisms were observed experimentally [see, e.g., García-Muñoz *et al.* (2011)], as the result of accurate diagnostics for measurement of internal EP redistributions, the fast-ion D-alpha (FIDA) spectroscopy (Heidbrink *et al.*, 2004), and global losses by scintillator based fast-ion loss detectors (FILDs) (García-Muñoz, Fahrbach, and Zohm, 2009). Because of the large system size, mainly stochastic losses are expected to play a significant role in ITER, while the dominant loss mechanism below stochastic threshold is expected to be that of scattering of barely counterpassing particles into unconfined "fat" banana orbits (Hsu and Sigmar, 1992; Sigmar *et al.*, 1992).[32] After the first work on fishbone induced EP losses (White *et al.*, 1983), numerical simulations of test-particle transport were successfully adopted for investigating alpha-particle redistributions by MHD activity in TFTR (Zweben *et al.*, 1999), beam ion transport during tearing modes in the DIII-D tokamak (Carolipio *et al.*, 2002), EP confinement in the presence of stochastic magnetic fields in the Madison symmetric torus reversed field pinch (Fiksel *et al.*, 2005), and more recently to model neoclassical tearing mode induced EP losses in ASDEX Upgrade (García-Muñoz *et al.*, 2007).

Suprathermal particle transport by AEs has been addressed in many works (Sigmar *et al.*, 1992; Appel *et al.*, 1995; Todo and Sato, 1998; Candy *et al.*, 1999; Carolipio *et al.*, 2001; Todo, Berk, and Breizman, 2003; Pinches *et al.*, 2006), all yielding the similar conclusion that appreciable losses (above the stochastic threshold) require mode amplitudes on the order of $\delta B_r/B \sim 10^{-3}$, when single-$n$ (toroidal mode number) modes are considered. An actual quantitative estimate of the stochastic threshold in the multiple-n modes case depends on the specific features of the system being considered (see the following discussion), although it has been shown that the

[31]The linear fishbone mode structure may instead be importantly modified in the case of high-frequency fishbones (Nabais *et al.*, 2005; Zonca *et al.*, 2007a, 2009) as discussed by Kolesnichenko, Lutsenko, and White (2010).

[32]This same mechanism has been experimentally shown to be the dominant EP loss mechanism due to RSAE (Pace *et al.*, 2011) and energetic particle driven geodesic acoustic modes (Kramer *et al.*, 2011) in some recent DIII-D experiments.

multiple-mode stochastic threshold may be greatly reduced ($\delta B_r/B \lesssim 10^{-4}$) with respect to the single-n mode case (Hsu and Sigmar, 1992; Sigmar *et al.*, 1992). The critical aspects connected with the stochastic threshold for EP transport were discussed in a pair of recent works (White *et al.*, 2010a, 2010b), which analyzed the modification of deuterium beam distribution in DIII-D plasmas due to the interaction with AEs (TAE and RSAE). The main finding of test-particle transport analyses is that observed fluctuation levels are slightly above the stochastic threshold of the system, making simulation very sensitive not only to mode amplitudes but also to other small effects: e.g., omitting the scalar potential fluctuations component of the magnetic perturbations while retaining all other relevant features in the modeling "leads to beam transport more than an order of magnitude too small to explain the observed profile flattening." Near the onset of local stochasticity in the particle phase space (Chirikov, 1979; Lichtenberg and Lieberman, 1983, 2010), transport events due to resonance overlap of different-n AEs (Breizman, Berk, and Ye, 1993; Berk, Breizman, Fitzpatrick, and Wong, 1995; Berk *et al.*, 1996) (avalanches) may exhibit characteristic aspects of sandpile physics and were observed in numerical simulations of ITER plasmas (Candy *et al.*, 1997), showing negligible α-particle transport due to weakly damped core-localized modes, and of TAE mode bursting in a TFTR-like plasma during NBI (Candy *et al.*, 1999). These issues are closely connected with the crucial roles played by equilibrium geometry and plasma nonuniformity in the nonlinear EP phase-space dynamics and the onset of stochasticity.

Multimode hybrid MHD-gyrokinetic simulations were also used to analyze central flattening of the EP profile in reversed-shear DIII-D discharges, assuming an initial EP profile computed from classical NBI deposition (Vlad *et al.*, 2009). Simulation results show good agreement of the relaxed EP profile due to fast growing $n = 1$ and 2 EPMs with experiments measured with the FIDA diagnostics. Furthermore, in the EPM saturated phase, EPMs are transformed to weak RSAE modes, also in good agreement with experimental measurements in both frequency and radial localization. After the initial nonlinear evolution, simulation results for EP redistributions are remarkably consistent with those obtained by test-particle transport (White *et al.*, 2010a, 2010b). This suggests that with an adequate modeling of the EP source nonlinear gyrokinetic or equivalent numerical simulations (cf. Sec. II) have the capability of analyzing EP transport in the presence of multiple AEs, and the results may be comparable to test-particle transport calculations, if particle redistributions and nonlinear mode dynamics are not strongly interlinked.

B. Self-consistent nonperturbative energetic-particle transport

When the interplay of nonlinear mode dynamics and EP transport processes is intrinsically nonperturbative (cf. Secs. IV.D and VI.A), test-particle transport simulations may not reflect the underlying physics of EP redistributions. The first evidence of secular EP transport by EPM was given by Briguglio, Zonca, and Vlad (1998), showing that mode saturation occurs when the finite radial mode structure characteristic scale is comparable to the fluctuation-induced EP displacement (cf. Sec. IV.D.5).

Hybrid MHD-gyrokinetic simulations have confirmed the fact that rapid EP transport is expected when the system is significantly above marginal stability and that fast radial particle redistributions lead to fishbone mode saturation and downward frequency chirping (Fu *et al.*, 2006; Vlad *et al.*, 2012). Simulation results also indicate that fluid nonlinearities do not qualitatively alter the dynamics of the fishbone burst cycle and EP transport (Fu *et al.*, 2006).

Dramatic transport events, such as those observed in fishbones and EPMs, occur on time scales of a few inverse linear growth rates (generally, 100–200 Alfvén times) and have a ballistic character (White *et al.*, 1983) that differentiates them from the diffusive multiple-n AE induced transport. Experimental observations in the JT-60U tokamak have also confirmed macroscopic and rapid EP radial redistributions in connection with the so-called ALEs (Shinohara *et al.*, 2001). Numerical simulations of an $n = 1$ EPM burst (Briguglio *et al.*, 2007) show that radial profiles of EPs, computed before and after the EPM induced particle redistributions, agree qualitatively and quantitatively with experimental measurements (Shinohara *et al.*, 2004). Good agreement is also obtained on the burst duration. The EP transport meanwhile also explains the saturation of the ALE burst. These simulation results have been recently confirmed by further numerical studies of ALE nonlinear dynamics, with detailed investigations of the importance of equilibrium geometry (Bierwage *et al.*, 2011) and plasma compressibility effects (Bierwage *et al.*, 2012). Hybrid MHD-gyrokinetic simulations of single-n modes were also used to compare linear and nonlinear dynamics of Alfvénic oscillations in ITER burning plasma scenarios (Gorelenkov *et al.*, 2003; Vlad *et al.*, 2006).

In experimental conditions of practical interest, AE and EPM may coexist and be interlinked by nonlinear transport processes. This is the case of slow upward sweeping ACs observed in JET together with repeated rapid down-sweeping modes (Pinches *et al.*, 2004). This observation as suggested by hybrid MHD-gyrokinetic simulations of JET experimental conditions (Zonca *et al.*, 2002) may be explained in terms of early resonant excitation of a EPM within the q-minimum surface and followed later, due to nonlinear dynamic evolution of the fluctuations, by the formation of a cascade mode at the q-minimum surface. Similar coexistence of TAE and EPM are the plausible interpretation of TAE avalanches in NSTX (Fredrickson *et al.*, 2009, 2013; Podestà *et al.*, 2009, 2011), where the activity of quasiperiodic TAE fluctuations with limited frequency chirping is followed by the so-called TAE avalanche. Such phenomenon causes EP losses of up to ~30% over 1 ms and manifests itself as a larger burst amplitude with nonadiabatic frequency sweeping. Test-particle transport simulations show reasonable agreement of predicted particle losses with experimental observations, whose features are consistent with the onset of stochastic diffusion discussed by Berk, Breizman, Fitzpatrick, and Wong (1995) and Berk *et al.* (1996). On the other hand, the evidence of nonadiabatic frequency chirping suggests that resonance overlap may enhance the free-energy source in the first phase of quasiperiodic TAE fluctuations with limited frequency chirping. Once the EPM excitation threshold is

exceeded,[33] EPMs, characterized by nonadiabatic frequency sweeping and rapid secular particle redistributions, as discussed in Sec. IV.D.5, may then be triggered. Further indications of interesting nonlinear interplay between mode structures and EP transport in the case of TAE avalanches (Fredrickson *et al.*, 2009) come from the experimental growth rates $\sim 10^{-1}(\omega_0/2\pi)$ (Podestà *et al.*, 2011) that are typically larger than those computed from linear stability analyses $\sim 10^{-2}(\omega_0/2\pi)$ and from the mode structures that are not always the same as those reconstructed from reflectometry measurements (Podestà *et al.*, 2009). More recent analyses of these phenomena are given by Fredrickson *et al.* (2013).

The synergy between AE and MHD activity, notably sawteeth, is also connected with nonperturbative redistributions of EPs. In the case of DIII-D, the use of high harmonic ICRH generates an EP population that transiently stabilizes the sawtooth instability but destabilizes TAEs (Heidbrink *et al.*, 1999). In the further evolution of the plasma discharge, saturation of the central heating correlates with the onset of the TAEs, while sawtooth crash is eventually caused by the continued expansion of the $q = 1$ surface radius. Similar observations are made in TFTR plasmas (Bernabei *et al.*, 2000, 2001), where the eventual crash of long-period sawteeth is explained in terms of the loss of the stabilizing effect of EPs that are transported outward by EPM from within the $q = 1$ surface. An effect similar to that of EPM on sawteeth can also be induced by TAEs when, with high values of the safety factor at the plasma boundary, their mode structures are shifted deeper into the plasma core, where they can cause sufficient EP redistributions to affect sawtooth stabilization. Meanwhile, in some TFTR discharges, it has been demonstrated that the loss of ICRH efficiency may be due to the combined effect of EPM and TAE, which eventually redistribute EPs in a broader region of the plasma volume and may even cause global particle losses (Bernabei *et al.*, 1999). More recent analyses of the impact of strongly driven fishbones and AEs on EP losses in JET are given by Nabais *et al.* (2010), while comparisons of numerical simulations and fast-ion loss detector measurements for fishbones are discussed by Perez von Thun *et al.* (2011, 2012).

C. Transport of energetic particles by microscopic turbulence

The problem of EP transport by microscopic turbulence was addressed in the early work by Belikov, Kolesnichenko, and Yavorskij (1976), discussing the energy spectrum of α particles escaping from a plasma as a result of turbulent diffusion. A later and more systematic theoretical description of the fusion α-particle confinement in tokamaks was provided by White and Mynick (1989), demonstrating that suprathermal particle confinement is much less deteriorated by microturbulence than that of thermal plasma, due to orbit averaging and wave-particle decorrelation effects. This picture was also confirmed by numerical simulations of test-particle transport in strong electrostatic drift wave turbulence (Manfredi and Dendy, 1996) and more recently by numerical simulation of turbulent transport of a slowing down distribution of suprathermal particles with high birth energy compared to the thermal plasma energy (Angioni and Peeters, 2008; Zhang, Lin, and Chen, 2008; Angioni *et al.*, 2009). Experimental observations confirmed these general expectations and quantitatively estimated the turbulent diffusivity of EPs to be 1 order of magnitude less than that of thermal ions for particle energies $E/T_c \gtrsim 10$ (Heidbrink and Sadler, 1994; Zweben *et al.*, 2000), with T_c standing for the core plasma thermal energy. Significant interest in this topic was revived more recently by experimental observations in plasmas with NBI, showing evidence of anomalies in EP transport in AUG (Günter *et al.*, 2007), JT-60U (Suzuki *et al.*, 2008), and DIII-D (Heidbrink, Murakami *et al.*, 2009; Heidbrink, Park *et al.*, 2009), which might have raised concerns about the negative NBI efficiency in ITER. These observations were connected with theoretical (Vlad and Spineanu, 2005) and numerical simulation analyses (Estrada-Mila, Candy, and Waltz, 2005, 2006; Albergante *et al.*, 2009; Angioni *et al.*, 2009), supporting the fact that a significant level of EP transport could be driven by microturbulence. This discrepancy between experimental measurements and neoclassical predictions of cross-field diffusion of EPs was clarified by Heidbrink, Murakami *et al.* (2009) and Heidbrink, Park *et al.* (2009) looking at DIII-D plasmas, where EP diffusivity was dominated by ion temperature gradient (ITG) driven turbulence, and showing that anomalies were more pronounced at low E/T_c, where the effect of microturbulence is strongest. Numerical simulation results (Zhang *et al.*, 2010) demonstrated that EP diffusivities are consistent with quasilinear predictions (Chen, 1999), confirming the conclusions of original theoretical and numerical works. Thus, EP transport by microturbulence in reactor relevant conditions and above the critical energy (at which plasma ions and electrons are heated at equal rates by EPs) is negligible and EP turbulent diffusivities have intrinsic interest mostly in present day experiments with low characteristic values of E/T_c. The potential problem of EP transport due to magnetic fluctuations in ITER (Hauff *et al.*, 2009), as also reported by Breizman and Sharapov (2011), is resolved by these findings (Heidbrink, Murakami *et al.*, 2009; Heidbrink, Park *et al.*, 2009; Zhang *et al.*, 2010), and is further confirmed in dedicated numerical simulations (Albergante *et al.*, 2010, 2011, 2012) as well as experimental studies in DIII-D, supported by numerical and analytic modeling (Pace *et al.*, 2013). The main possible concern remains as the increased suprathermal particle diffusivities that may be expected in DEMO, due to the significantly larger operation temperature and consequently lower value of E/T_c (Albergante *et al.*, 2012).

VI. CONCLUDING REMARKS AND OUTLOOKS

This work addressed a wide range of linear and nonlinear physics issues related to SAWs and EPs in burning plasmas without, however, the intention of being comprehensive.

[33] Note that for sufficiently strong mode drive, of the order of the real frequency shift from the continuous spectrum accumulation point, there is no clear distinction between AE and EPM, as discussed in Sec. III.C, and EPMs could easily exist inside the SAW frequency gap. In addition, in typical NSTX experimental conditions, equilibrium mean flow shear is strong enough to significantly alter the SAW continuous spectrum and generally cause strong coupling of TAEs with the SAW continuous spectrum and thereby with EPMs (Podestà, 2012).

Among the physics issues addressed in this work, the theoretical formulation of the GFLDR provides a unified framework for linear as well as nonlinear physics studies and may serve as a useful interpretative tool for numerical simulation results and experimental observations. Linear stability problems essentially require the use of already available comprehensive gyrokinetic (or equivalent) codes along with careful modeling of realistic plasma equilibria and physical boundary conditions. The many benchmarking activities in progress worldwide give confidence that such predictions on linear physics will be available in the near future. As to nonlinear physics, we have shown that the governing equation for the fluctuation radial envelope has the theoretical structure of a NLSE with integrodifferential nonlinear terms. In simplified examples, this equation is shown to yield convective amplification of radially outward-moving EPM wave packets, accompanied by secular displacement of resonant EPs, as well as a fishbone burst cycle. Comparisons among reduced nonlinear theoretical models, numerical simulations, and experimental observations in present toroidal devices have already started providing new insight into the fundamental issues underlying these processes. Current theoretical understanding of nonlinear physics have, in particular, indicated the crucial importance of equilibrium geometry, plasma nonuniformities, radial mode structures, and kinetic processes. Simplified descriptions based on the analogy of the resonant excitation of SAWs by EPs with the 1D bump-on-tail problem are capable of capturing some of the important nonlinear dynamics near marginal stability, but, however, do not address the important roles of radial mode structures and plasma nonuniformities. Nonlinear physics therefore require substantially more significant effort to reach the level of maturity for reliable predictions of Alfvénic fluctuation and related transport in reactor relevant conditions. The rapid development of impressive diagnostics systems and numerical simulation capabilities renders it feasible that one can expect rapid advance in this important area.

The intended scope of this review has left out several important topics. For example, high-frequency fluctuations ($|\omega| \gtrsim \Omega_i$) have been neglected, although there is evidence of fusion alpha-particle driven ion cyclotron emission [see, e.g., Cauffman *et al.* (1995)], interpreted as resonantly excited compressional Alfvén eigenmodes (CAEs) (Belikov, Kolesnichenko, and Silivra, 1995; Gorelenkov and Cheng, 1995a, 1995b; Fülöp *et al.*, 1997). The CAE phenomenology has been widely studied in NSTX (Fredrickson *et al.*, 2002; Fredrickson, Gorelenkov, and Menard, 2004). Another important aspect involving the interaction of EPs with waves in the high radio-frequency (rf) range is the so-called alpha channeling (Fisch and Rax, 1992; Fisch, 2006, 2010, 2012), i.e., "the diversion of energy from energetic alpha particles to waves" (Fisch, 2000), as an "attempt at detailed control over plasma behavior" to facilitate the development of an economical fusion reactor. The use of bucket transport in fusion plasmas for removing helium ash from the plasma core as well as burn control, profile control, and diagnostic tool was proposed by Mynick and Pomphrey (1994) (cf. Sec. IV.E). Kolesnichenko, Yakovenko, and Lutsenko (2010) and Kolesnichenko, Yakovenko, Lutsenko, White, and Weller (2010) pointed out that DAW may channel the energy and momentum of EPs to different spatial regions, where waves are absorbed. In this way, EP-driven instabilities may not affect only the EP radial profiles, but alter thermal plasma transport as well, notably, the electron heat transport across the equilibrium magnetic field and the plasma rotation profile, consistent with observations in NSTX (Stutman *et al.*, 2009) and W7-AS (Kolesnichenko *et al.*, 2005). Furthermore, it is worthwhile mentioning that Wong *et al.* (2005) showed the possibility of producing an internal transport barrier, induced by radial redistribution of EPs due to Alfvénic instabilities. Finally, this review has not addressed important issues related to the intrinsic 3D nature of all real systems, including "axisymmetric" toroidal devices. For issues such as toroidal field ripple induced transport (Goldston and Towner, 1981; Goldston, White, and Boozer, 1981), which arise from the breaking of axisymmetry in 2D toroidal system, see the comprehensive ITER summaries (ITER Physics Expert Group on Energetic Particles, Heating and Current Drive, 1999; Fasoli *et al.*, 2007) and recent reviews by Gorelenkov, Pinches, and Toi (2014) and Pinches *et al.* (2015). Here we emphasized that AEs may cause global EP losses through induced ripple trapping, as discussed by White *et al.* (1995). For the similarities and differences between tokamaks and stellarators, recent and comprehensive reviews are given by Kolesnichenko *et al.* (2011) and Toi *et al.* (2011).

Looking beyond, we note that there are two issues which have received increasing attention within the fusion community. One deals with EP transport in the presence of many modes as expected in ITER. The other deals with the investigation of burning fusion plasmas as complex systems, with many interacting degrees of freedom, where the long time-scale behavior will ultimately determine the reactor performance. These two interlinked issues are further articulated in Secs. VI.A and VI.B, which then conclude this review.

A. Energetic-particle transport in the presence of many modes

Collective oscillations excited by EPs in burning plasmas are characterized by a dense spectrum of modes with characteristic frequencies and spatial locations (Chen and Zonca, 2007a; Chen, 2008). One crucial issue, as noted at the beginning Sec. V, remains the realistic prediction of global transport of EPs and fusion products and their impact on the system material walls. While quasilinear theory is suited for explaining EP transport by plasma turbulence (cf. Sec. V), it was argued that the onset of phase-space stochasticity may be described by a "line-broadened" quasilinear model (Berk, Breizman, Fitzpatrick, and Wong, 1995), accounting for a discrete spectrum of overlapping modes in the case of multiple AEs (Berk *et al.*, 1996) and which was recently extended and applied to the analysis of beams interacting with AEs in DIII-D (Ghantous *et al.*, 2012). A detailed discussion of model assumptions and validity limits was given by Ghantous, Berk, and Gorelenkov (2014). The actual transition to stochastic behavior in realistic systems, however, depends on the details of plasma nonuniformities and equilibrium geometries via resonance conditions and finite mode structures (cf. Sec. V), as recently shown by White *et al.* (2010a, 2010b). For this reason, the only presently viable modeling of EP losses by multiple AEs is test-particle transport or more sophisticated

nonlinear simulations with gyrokinetic or equivalent codes (cf. Sec. II). Simulations along these lines, using linear fluctuation spectra and mode structures, were carried out for ASDEX Upgrade (Schneller *et al.*, 2013) and are being pursued for ITER (Lauber, 2015; Schneller, Lauber, and Briguglio, 2016) (cf. Sec. IV.D.4). Other reduced nonlinear dynamic descriptions are possible as discussed in Secs. IV.A and IV.D.5, which may offer a useful tool for gaining deeper insights into the underlying physics.

The DAW spectrum in present day experiments is, in general, significantly different from that expected of burning plasmas (much lower mode numbers, corresponding to much larger relative EP orbits compared with machine size). The same holds for the associated kinetic processes and cross-scale couplings yielding to complex behavior, which will be further discussed in Sec. VI.B. Nonetheless, some aspects of complex behavior may still be addressed in existing machines, providing precious feedbacks for theory and modeling. One example is the analysis of EP transport during TAE avalanches in NSTX, where multiple modes are excited and the resultant EP redistributions are so far not completely understood (cf. Sec. V). Nonlinear simulation tools may be needed to yield more reliable interpretations of these observations (Fredrickson *et al.*, 2009, 2013).

B. Complex behavior in burning plasmas

A burning plasma is a complex self-organized system, where among the crucial processes to understand there are (turbulent) transport and fast-ion–fusion product induced collective effects (Zonca *et al.*, 2006). Complexity and self-organization are intrinsic to the very nature of burning plasmas, where the self-sustainment of fusion reactions for efficient power production requires that stationary conditions are achieved when in D-T plasmas almost the whole power density balance to compensate losses is provided by heating from fusion alphas. Meanwhile, fast ions in the same MeV energy range, produced mainly by ICRH and negative NBI (NNBI), will be used to heat and fuel the thermal plasma, provide rotation, and drive current. Together with fusion produced alpha particles, these fast ions are a potential free-energy source for driving collective plasma oscillations, which may induce or enhance transport processes. Complexity and self-organization are consequences of the interaction of EPs with plasma instabilities and turbulence; of the strong nonlinear coupling mediated by the EP population that will take place between fusion reactivity profiles, pressure driven currents, MHD stability, transport, and plasma boundary interactions; and, finally, of the long time-scale nonlinear (complex) behavior that may affect the overall fusion performance and eventually pose issues for the stability and control of the fusion burn. The role of EPs is also unique as mediators of cross-scale couplings, for they can drive instabilities on the mesoscales, intermediate between the microscopic thermal ion Larmor radius and the macroscopic plasma equilibrium scale length. EP-driven Alfvénic instabilities could also provide a nonlinear feedback onto the macroscale system via the interplay of plasma equilibrium and fusion reactivity profiles, as well as excite microscopic radial mode structures at SAW continuum resonances, which by mode conversion yield fluctuations that may propagate and be absorbed elsewhere (Kolesnichenko, Yakovenko, and Lutsenko, 2010). Furthermore, noting that instabilities may also be excited from microscales to mesoscales to macroscales (cf. Sec. III) has made the theoretical approach based on an extended inertial range dubious for burning fusion plasmas.

These physics are unique to burning plasmas and require a conceptual shift with respect to the way phenomena are currently investigated in present day experiments. For example, EP power density profiles and characteristic wavelengths of the collective modes in reactor relevant plasmas will be different. MeV energy ion tails, meanwhile, will provide the dominant electron heating and, thereby, introduce different weighting of the electron driven microturbulence. Furthermore, plasma operation scenarios will reflect different plasma edge conditions and plasma wall interactions at high density and low collisionality. For these reasons, important roles will be played by predictive capabilities based on numerical simulations (Batchelor *et al.*, 2007; Lauber, 2013) as well as by fundamental theories for developing simplified yet relevant models, to provide the necessary insight into the basic physics processes. Experiments in this respect have a key role in providing experimental evidence for modeling verification and validation. In the perspective of ITER (Tamabechi *et al.*, 1991; Aymar *et al.*, 1997), it is crucial to investigate these physics issues, exploiting positive feedbacks between experiment, numerical simulation, and theory, and integrating the largest number of aspects that are important for complexity in reactor relevant plasmas.

In addition to spontaneous generation by DWT, zonal flows including the finite-frequency geodesic acoustic mode (GAM) (Winsor, Johnson, and Dawson, 1968) or more generally ZS can also be generated by nonlinear AE and EPM dynamics, depending on proximity to marginal stability (cf. Sec. IV.C). Meanwhile, strongly driven EPMs cause radial modulations in EP profiles, affecting thus the EP distribution function (cf. Secs. IV.D.5 and IV.D.6), which may produce similar structures in the electron temperature profile and eventually alter the free-energy source driving DW turbulence and transport. In general, the ZS evolution must be self-consistently determined with that of all other relevant nonlinearly coupled degrees of freedom and could determine the long time-scale nonlinear dynamics of burning plasmas and, thereby, the reactor fusion performance.

In this respect, one important issue is the determination of hierarchy of relevant nonlinear time scales for the various cross-scale couplings including realistic conditions, such as proper equilibrium geometry, spatial nonuniformity, and kinetic effects (Zonca, 2008; Zonca and Chen, 2008; Zonca *et al.*, 2013, 2015a). Numerical simulations as well as experimental studies are beginning to address these issues.

ACKNOWLEDGMENTS

We are grateful to many colleagues for their contributions to this review: S. Bernabei, A. J. Brizard, A. Cardinali, N. Carlevaro, W. Chen, C. Z. Cheng, D. S. Darrow, G. Dattoli, J. Decker, R. O. Dendy, W. Deng, X. T. Ding, C. di Troia, J. Q. Dong, M. J. Engebretson, D. F. Escande, A. Fasoli, G. Fogaccia, G. Y. Fu, X. Garbet, L. Giannessi,

N. N. Gorelenkov, J. P. Graves, Z. O. Guimarães-Filho, Z. Guo, T. S. Hahm, P. Helander, C. Hidalgo, Ya. I. Kolesnichenko, A. Könies, M. Lesur, Y. Lin, Z. Lin, A. V. Melnikov, A. Merle, G. Montani, R. Nazikian, C. Nguyen, S. D. Pinches, B. D. Scott, K. Shinohara, P. K. Shukla, G. Sonnino, D. A. Spong, L. Stenflo, D. Testa, B. J. Tobias, Y. Todo, K. Toi, M. A. Van Zeeland, R. E. Waltz, A. Weller, H. S. Zhang, and L. J. Zheng. In particular, we are indebted to in depth discussions with A. Biancalani, A. Bierwage, S. Briguglio, I. Chavdarovski, E. D. Fredrickson, W. W. Heidbrink, Ph. Lauber, Z. X. Lu, A. V. Milovanov, M. Podestà, Z. Y. Qiu, G. Vlad, X. Wang, and R. B. White. We are also grateful to S. Briguglio, G. Y. Fu, G. Vlad, and X. Wang for granting their permission for reproducing in this review figures from their original works. This work was supported by the US DOE, NSF, the National Magnetically Confined Fusion Energy Research Program of China (NMCFERP-CN), and NSFC grants, and by Euratom Communities under the contract of Association between EURATOM/ENEA. This work was also partly supported by European Unions Horizon 2020 Research and Innovation Program under Grant No. 633053 as Enabling Research Projects ER14-ENEA_Frascati-01 and ER15-ENEA-03.

REFERENCES

Albergante, M., A. Fasoli, J. P. Graves, S. Brunner, and W. A. Cooper, 2012, Nucl. Fusion **52**, 094016.
Albergante, M., J. P. Graves, A. Fasoli, F. Jenko, and T. Dannert, 2009, Phys. Plasmas **16**, 112301.
Albergante, M., J. P. Graves, A. Fasoli, M. Jucker, X. Lapillonne, and W. A. Cooper, 2011, Plasma Phys. Controlled Fusion **53**, 054002.
Albergante, M., J. P. Graves, A. Fasoli, and X. Lapillonne, 2010, Nucl. Fusion **50**, 084013.
Alfvén, H., 1942, Nature (London) **150**, 405.
Alfvén, H., 1950, *Cosmical Electrodynamics* (Clarendon, Oxford, UK).
Al'tshul', L. M., and V. I. Karpman, 1965, Zh. Eksp. Teor. Fiz. **49**, 515 [Sov. Phys. JETP **22**, 361 (1966)].
Anderson, P. W., 1958, Phys. Rev. **109**, 1492.
Angioni, C., and A. Peeters, 2008, Phys. Plasmas **15**, 052307.
Angioni, C., A. G. Peeters, G. V. Pereverzev, A. Bottino, J. Candy, R. Dux, E. Fable, T. Hein, and R. E. Waltz, 2009, Nucl. Fusion **49**, 055013.
Annibaldi, S. V., F. Zonca, and P. Buratti, 2007, Plasma Phys. Controlled Fusion **49**, 475.
Antoni, M., Y. Elskens, and D. F. Escande, 1998, Phys. Plasmas **5**, 841.
Antoniazzi, A., R. S. Johal, D. Fanelli, and S. Ruffo, 2008, Commun. Nonlinear Sci. Numer. Simul. **13**, 2.
Antonsen, T. M., and B. Lane, 1980, Phys. Fluids **23**, 1205.
Antonsen, T. M., B. Lane, and J. J. Ramos, 1981, Phys. Fluids **24**, 1465.
Antonsen, T. M., and Y. C. Lee, 1982, Phys. Fluids **25**, 132.
Appel, L. C., H. L. Berk, D. Borba, B. N. Breizman, T. C. Hender, G. T. A. Huysmans, W. Kerner, M. S. Pekker, S. D. Pinches, and S. E. Sharapov, 1995, Nucl. Fusion **35**, 1697.
Appert, K., R. Gruber, F. Troyon, and J. Vaclavik, 1982, Plasma Phys. **24**, 1147.
Aymar, R., V. Chuyanov, M. Huguet, R. Parker, Y. Shimamura, and the ITER Joint Central Team and Home Teams, 1997, in *Proceedings of the 16th International Conference on Fusion Energy 1996*, Vol. 1 (International Atomic Energy Agency, Vienna), p. 3.
Bak, P., C. Tang, and K. Wiesenfeld, 1987, Phys. Rev. Lett. **59**, 381.
Barston, E. M., 1964, Ann. Phys. (N.Y.) **29**, 282.
Barth, I., L. Friedland, and A. G. Shagalov, 2008, Phys. Plasmas **15**, 082110.
Bass, E., and R. E. Waltz, 2010, Phys. Plasmas **17**, 112319.
Batchelor, D. A., *et al.*, 2007, Plasma Sci. Technol. **9**, 312.
Belikov, V. S., Ya. I. Kolesnichenko, and V. N. Oraevskij, 1968, Zh. Eksp. Teor. Fiz. **5**, 2210 [Sov. Phys. JETP **28**, 1172 (1969)].
Belikov, V. S., Ya. I. Kolesnichenko, and V. N. Oraevskij, 1974, Sov. Phys. JETP **39**, 828.
Belikov, V. S., Ya. I. Kolesnichenko, and O. A. Silivra, 1995, Nucl. Fusion **35**, 1603.
Belikov, V. S., Ya. I. Kolesnichenko, and V. A. Yavorskij, 1976, Nucl. Fusion **16**, 783.
Belova, E. V., N. N. Gorelenkov, and C. Z. Cheng, 2003, Phys. Plasmas **10**, 3240.
Bergkvist, T., and T. Hellsten, 2004, in *Theory of Fusion Plasmas*, edited by J. W. Connor, O. Sauter, and E. Sindoni (Editrice Compositori, Società Italiana di Fisica, Bologna, Italy), p. 123.
Bergkvist, T., T. Hellsten, and K. Holmström, 2007, Nucl. Fusion **47**, 1131.
Bergkvist, T., T. Hellsten, T. Johnson, and M. Laxåback, 2005, Nucl. Fusion **45**, 485.
Berk, H. L., D. N. Borba, B. N. Breizman, S. D. Pinches, and S. E. Sharapov, 2001, Phys. Rev. Lett. **87**, 185002.
Berk, H. L., C. J. Boswell, D. Borba, A. C. A. Figueiredo, T. Johnson, M. F. F. Nave, S. D. Pinches, S. E. Sharapov, and JET EFDA contributors, 2006, Nucl. Fusion **46**, S888.
Berk, H. L., and B. N. Breizman, 1990a, Phys. Fluids B **2**, 2226.
Berk, H. L., and B. N. Breizman, 1990b, Phys. Fluids B **2**, 2235.
Berk, H. L., and B. N. Breizman, 1990c, Phys. Fluids B **2**, 2246.
Berk, H. L., and B. N. Breizman, 1996, Comments Plasma Phys. Control. Fusion **17**, 129.
Berk, H. L., B. N. Breizman, J. Candy, M. Pekker, and N. V. Petiashvili, 1999, Phys. Plasmas **6**, 3102.
Berk, H. L., B. N. Breizman, J. Fitzpatrick, M. S. Pekker, H. V. Wong, and K. L. Wong, 1996, Phys. Plasmas **3**, 1827.
Berk, H. L., B. N. Breizman, J. Fitzpatrick, and H. V. Wong, 1995, Nucl. Fusion **35**, 1661.
Berk, H. L., B. N. Breizman, and M. Pekker, 1995, Phys. Plasmas **2**, 3007.
Berk, H. L., B. N. Breizman, and M. Pekker, 1996, Phys. Rev. Lett. **76**, 1256.
Berk, H. L., B. N. Breizman, and M. S. Pekker, 1997, Plasma Phys. Rep. **23**, 778.
Berk, H. L., B. N. Breizman, and N. V. Petiashvili, 1997, Phys. Lett. A **234**, 213.
Berk, H. L., B. N. Breizman, and H. Ye, 1992a, Phys. Rev. Lett. **68**, 3563.
Berk, H. L., B. N. Breizman, and H. Ye, 1992b, Phys. Lett. A **162**, 475.
Berk, H. L., R. R. Mett, and D. M. Lindberg, 1993, Phys. Fluids B **5**, 3969.
Berk, H. L., C. W. Nielson, and K. W. Roberts, 1970, Phys. Fluids **13**, 980.
Berk, H. L., M. N. Rosenbluth, R. H. Cohen, and W. M. Nevins, 1985, Phys. Fluids **28**, 2824.
Berk, H. L., J. W. Van Dam, D. Borba, J. Candy, G. T. A. Huysmans, and S. Sharapov, 1995, Phys. Plasmas **2**, 3401.
Berman, R. H., D. J. Tetreault, and T. H. Dupree, 1983, Phys. Fluids **26**, 2437.
Bernabei, S., *et al.*, 1999, Phys. Plasmas **6**, 1880.
Bernabei, S., *et al.*, 2000, Phys. Rev. Lett. **84**, 1212.
Bernabei, S., *et al.*, 2001, Nucl. Fusion **41**, 513.

Bernstein, I. B., E. A. Frieman, M. D. Kruskal, and R. M. Kulsrud, 1958, Proc. R. Soc. A **244**, 17.
Bernstein, I. B., J. M. Greene, and M. D. Kruskal, 1957, Phys. Rev. **108**, 546.
Betti, R., 1995, Phys. Rev. Lett. **74**, 2949.
Betti, R., and J. P. Freidberg, 1991, Phys. Fluids B **3**, 1865.
Betti, R., and J. P. Freidberg, 1992, Phys. Fluids B **4**, 1465.
Biancalani, A., L. Chen, F. Pegoraro, and F. Zonca, 2010a, Phys. Rev. Lett. **105**, 095002.
Biancalani, A., L. Chen, F. Pegoraro, and F. Zonca, 2010b, Phys. Plasmas **17**, 122106.
Biancalani, A., L. Chen, F. Pegoraro, and F. Zonca, 2011, Plasma Phys. Controlled Fusion **53**, 025009.
Bierwage, A., N. Aiba, Y. Todo, W. Deng, M. Ishikawa, G. Matsunaga, K. Shinohara, and M. Yagi, 2012, Plasma Fusion Res. **7**, 2403081.
Bierwage, A., Y. Todo, N. Aiba, K. Shinohara, M. Ishikawa, and M. Yagi, 2011, Plasma Fusion Res. **6**, 2403109.
Biglari, H., and L. Chen, 1986, Phys. Fluids **29**, 1760.
Biglari, H., and L. Chen, 1991, Phys. Rev. Lett. **67**, 3681.
Biglari, H., F. Zonca, and L. Chen, 1992, Phys. Fluids B **4**, 2385.
Biskamp, D., 1993, *Nonlinear Magnetohydrodynamics* (Cambridge University Press, Cambridge, UK).
Bondeson, A., and M. S. Chu, 1996, Phys. Plasmas **3**, 3013.
Bondeson, A., and D. J. Ward, 1994, Phys. Rev. Lett. **72**, 2709.
Bonifacio, R., L. De Salvo, P. Pierini, and N. Piovella, 1990, Nucl. Instrum. Methods Phys. Res., Sect. A **296**, 358.
Bonifacio, R., L. De Salvo, P. Pierini, N. Piovella, and C. Pellegrini, 1994, Phys. Rev. Lett. **73**, 70.
Boozer, A. H., 1981, Phys. Fluids **24**, 1999.
Boozer, A. H., 1982, Phys. Fluids **25**, 520.
Breizman, B. N., 2006, AIP Conf. Proc. **871**, 15.
Breizman, B. N., 2010, Nucl. Fusion **50**, 084014.
Breizman, B. N., 2011, Fusion Sci. Technol. **59**, 549.
Breizman, B. N., H. L. Berk, M. Pekker, F. Porcelli, G. V. Stupakov, and K. L. Wong, 1997, Phys. Plasmas **4**, 1559.
Breizman, B. N., H. L. Berk, and H. Ye, 1993, Phys. Fluids B **5**, 3217.
Breizman, B. N., and S. E. Sharapov, 2011, Plasma Phys. Controlled Fusion **53**, 054001.
Briguglio, S., 2012 (private communication).
Briguglio, S., G. Fogaccia, G. Vlad, F. Zonca, K. Shinohara, M. Ishikawa, and M. Takechi, 2007, Phys. Plasmas **14**, 055904.
Briguglio, S., G. Vlad, X. Wang, and F. Zonca, 2012, in Report on benchmark for nonlinear code, 8th Meeting of the ITPA Energetic Particle Physics Topical Group, held in conjunction with the 19th meeting of the ITPA MHD Stability Topical Group, Toki, Japan, March 5–9.
Briguglio, S., G. Vlad, F. Zonca, and G. Fogaccia, 2002, Phys. Lett. A **302**, 308.
Briguglio, S., G. Vlad, F. Zonca, and C. Kar, 1995, Phys. Plasmas **2**, 3711.
Briguglio, S., and X. Wang, 2013 (private communication).
Briguglio, S., X. Wang, F. Zonca, G. Vlad, G. Fogaccia, C. Di Troia, and V. Fusco, 2014, Phys. Plasmas **21**, 112301.
Briguglio, S., F. Zonca, and G. Vlad, 1998, Phys. Plasmas **5**, 3287.
Brizard, A., 1994, Phys. Plasmas **1**, 2460.
Brizard, A. J., 1989, J. Plasma Phys. **41**, 541.
Brizard, A. J., 1990, Ph.D. thesis (Princeton University, Princeton, NJ).
Brizard, A. J., 1992, Phys. Fluids B **4**, 1213.
Brizard, A. J., and T. S. Hahm, 2007, Rev. Mod. Phys. **79**, 421.
Brizard, A. J., and N. Tronko, 2012, arXiv:1205.5772v1.
Buratti, P., P. Smeulders, F. Zonca, S. Annibaldi, M. De Benedetti, H. Kroegler, G. Regnoli, O. Tudisco, and the FTU-team, 2005, Nucl. Fusion **45**, 1446.
Campbell, D. J., *et al.*, 1988, Phys. Rev. Lett. **60**, 2148.
Candy, J., H. L. Berk, B. N. Breizman, and F. Porcelli, 1999, Phys. Plasmas **6**, 1822.
Candy, J., D. Borba, H. L. Berk, G. T. A. Huysmans, and W. Kerner, 1997, Phys. Plasmas **4**, 2597.
Candy, J., and M. N. Rosenbluth, 1993, Plasma Phys. Controlled Fusion **35**, 957.
Candy, J., and M. N. Rosenbluth, 1994, Phys. Plasmas **1**, 356.
Carlevaro, N., D. Fanelli, X. Garbet, P. Ghendrih, G. Montani, and M. Pettini, 2014, Plasma Phys. Controlled Fusion **56**, 035013.
Carolipio, E. M., W. W. Heidbrink, C. Z. Cheng, M. S. Chu, G. Y. Fu, D. A. Spong, A. D. Turnbull, and R. B. White, 2001, Phys. Plasmas **8**, 3391.
Carolipio, E. M., W. W. Heidbrink, C. B. Forest, and R. B. White, 2002, Nucl. Fusion **42**, 853.
Cary, J. R., and A. J. Brizard, 2009, Rev. Mod. Phys. **81**, 693.
Catto, P. J., W. M. Tang, and D. E. Baldwin, 1981, Plasma Phys. **23**, 639.
Cauffman, S., R. Majeski, K. G. McClements, and R. O. Dendy, 1995, Nucl. Fusion **35**, 1597.
Chapman, I. T., R. Kemp, and D. J. Ward, 2011, Fusion Eng. Des. **86**, 141.
Chapman, I. T., *et al.*, 2007, Plasma Phys. Controlled Fusion **49**, B385.
Chavdarovski, I., and F. Zonca, 2009, Plasma Phys. Controlled Fusion **51**, 115001.
Chavdarovski, I., and F. Zonca, 2014, Phys. Plasmas **21**, 052506.
Chen, L., 1988, in *Theory of Fusion Plasmas*, edited by J. Vaclavik, F. Troyon, and E. Sindoni (Association EURATOM, Bologna), p. 327.
Chen, L., 1994, Phys. Plasmas **1**, 1519.
Chen, L., 1999, J. Geophys. Res. **104**, 2421.
Chen, L., 2008, Plasma Phys. Controlled Fusion **50**, 124001.
Chen, L., and A. Hasegawa, 1974a, Phys. Fluids **17**, 1399.
Chen, L., and A. Hasegawa, 1974b, J. Geophys. Res. **79**, 1024.
Chen, L., and A. Hasegawa, 1991, J. Geophys. Res. **96**, 1503.
Chen, L., J. Y. Hsu, P. K. Kaw, and P. H. Rutherford, 1978, Nucl. Fusion **18**, 1371.
Chen, L., Z. Lin, and R. B. White, 2000, Phys. Plasmas **7**, 3129.
Chen, L., Z. Lin, R. B. White, and F. Zonca, 2001, Nucl. Fusion **41**, 747.
Chen, L., and S. T. Tsai, 1983, Plasma Phys. **25**, 349.
Chen, L., J. Vaclavik, and G. W. Hammett, 1988, Nucl. Fusion **28**, 389.
Chen, L., R. B. White, G. Rewoldt, P. L. Colestock, P. H. Rutherford, M. N. Bussac, Y. P. Chen, F. J. Ke, and S. T. Tsai, 1989, in *Proceedings of the 12th International Conference on Plasma Physics and Controlled Nuclear Fusion Research, Nice (France)*, Vol. 2 (International Atomic Energy Agency, Vienna), p. 77.
Chen, L., R. B. White, and M. N. Rosenbluth, 1984, Phys. Rev. Lett. **52**, 1122.
Chen, L., R. B. White, and F. Zonca, 2004, Phys. Rev. Lett. **92**, 075004.
Chen, L., and F. Zonca, 1995, Phys. Scr. **T60**, 81.
Chen, L., and F. Zonca, 2007a, Nucl. Fusion **47**, S727.
Chen, L., and F. Zonca, 2007b, Nucl. Fusion **47**, 886.
Chen, L., and F. Zonca, 2011, Europhys. Lett. **96**, 35001.
Chen, L., and F. Zonca, 2012, Phys. Rev. Lett. **109**, 145002.
Chen, L., and F. Zonca, 2013, Phys. Plasmas **20**, 055402.

Chen, L., F. Zonca, and Z. Lin, 2005, Plasma Phys. Controlled Fusion **47**, B71.
Chen, L., F. Zonca, R. A. Santoro, and G. Hu, 1998, Plasma Phys. Controlled Fusion **40**, 1823.
Chen, W., *et al.*, 2011, Nucl. Fusion **51**, 063010.
Chen, Y., and S. E. Parker, 2011, Phys. Plasmas **18**, 055703.
Chen, Y., S. E. Parker, J. Lang, and G.-Y. Fu, 2010, Phys. Plasmas **17**, 102504.
Chen, Y., and R. B. White, 1997, Phys. Plasmas **4**, 3591.
Chen, Y., R. B. White, G.-Y. Fu, and R. Nazikian, 1999, Phys. Plasmas **6**, 226.
Cheng, C. Z., L. Chen, and M. S. Chance, 1985, Ann. Phys. (N.Y.) **161**, 21.
Cheng, C. Z., G. Y. Fu, and J. W. Van Dam, 1988, in *Theory of Fusion Plasmas*, edited by J. Vaclavik, F. Troyon, and E. Sindoni (Association EURATOM, Bologna), p. 259.
Chirikov, B. V., 1979, Phys. Rep. **52**, 263.
Chu, C., M.-S. Chu, and T. Ohkawa, 1978, Phys. Rev. Lett. **41**, 653.
Chu, M. S., J. M. Greene, L. L. Lao, A. D. Turnbull, and M. S. Chance, 1992, Phys. Fluids B **4**, 3713.
Chu, M. S., *et al.*, 1993, in *Plasma Physics and Controlled Nuclear Fusion Research 1992*, Vol. I CN-56/D-2-3 (International Atomic Energy Agency, Vienna), p. 855.
Cohen, R. H., and R. L. Dewar, 1974, J. Geophys. Res. **79**, 4174.
Connor, J. W., R. J. Hastie, and J. B. Taylor, 1978, Phys. Rev. Lett. **40**, 396.
Connor, J. W., R. J. Hastie, and J. B. Taylor, 1979, Proc. R. Soc. A **365**, 1.
Connor, J. W., W. M. Tang, and J. B. Taylor, 1983, Phys. Fluids **26**, 158.
Conte, R., and M. Musette, 1993, Physica (Amsterdam) **69D**, 1.
Coppi, B., 1977, Phys. Rev. Lett. **39**, 939.
Coppi, B., R. J. Hastie, S. Migliuolo, F. Pegoraro, and F. Porcelli, 1988, Phys. Lett. A **132**, 267.
Coppi, B., S. Migliuolo, and F. Porcelli, 1988, Phys. Fluids **31**, 1630.
Coppi, B., and F. Porcelli, 1986, Phys. Rev. Lett. **57**, 2272.
Cox, M., and MAST Team, 1999, Fusion Eng. Des. **46**, 397.
Curran, D., Ph. Lauber, P. J. Mc Carthy, S. da Graça, V. Igochine, and the ASDEX Upgrade Team, 2012, Plasma Phys. Controlled Fusion **54**, 055001.
Dewar, R. L., J. Manickam, R. C. Grimm, and M. S. Chance, 1981, Nucl. Fusion **21**, 493.
Dewar, R. L., J. Manickam, R. C. Grimm, and M. S. Chance, 1982, Nucl. Fusion **22**, 307.
Diamond, P. H., S.-I. Itoh, K. Itoh, and T. S. Hahm, 2005, Plasma Phys. Controlled Fusion **47**, R35.
Dicke, R. H., 1954, Phys. Rev. **93**, 99.
Ding, X. T., *et al.*, 2002, Nucl. Fusion **42**, 491.
D'Ippolito, D. A., and J. P. Goedbloed, 1980, Plasma Phys. **22**, 1091.
Drummond, W. E., and D. Pines, 1962, Nucl. Fusion Suppl. Pt. **3**, 1049.
Dubin, D., J. A. Krommes, C. Oberman, and W. W. Lee, 1983, Phys. Fluids **26**, 3524.
DuBois, D. F., and M. V. Goldman, 1965, Phys. Rev. Lett. **14**, 544.
DuBois, D. F., and M. V. Goldman, 1967, Phys. Rev. Lett. **19**, 1105.
Duong, H. H., W. W. Heidbrink, E. J. Strait, T. W. Petrie, R. Lee, R. A. Moyer, and J. G. Watkins, 1993, Nucl. Fusion **33**, 749.
Dupree, T. H., 1970, Phys. Rev. Lett. **25**, 789.
Dupree, T. H., 1972, Phys. Fluids **15**, 334.
Dupree, T. H., 1982, Phys. Fluids **25**, 277.
Edery, D., X. Garbet, J. Roubin, and A. Samain, 1992, Plasma Phys. Controlled Fusion **34**, 1089.
Elsasser, W. M., 1956, Rev. Mod. Phys. **28**, 135.
Engebretson, M. J., L. J. Zanetti, T. A. Potemra, W. Baumjohann, H. Lühr, and M. H. Acuna, 1987, J. Geophys. Res. **92**, 10053.
Estrada-Mila, C., J. Candy, and R. E. Waltz, 2005, Phys. Plasmas **12**, 022305.
Estrada-Mila, C., J. Candy, and R. E. Waltz, 2006, Phys. Plasmas **13**, 112303.
Fajans, J., and L. Friedland, 2001, Am. J. Phys. **69**, 1096.
Fajans, J., E. Gilson, and L. Friedland, 1999, Phys. Rev. Lett. **82**, 4444.
Fasoli, A., B. N. Breizman, D. Borba, R. F. Heeter, M. S. Pekker, and S. E. Sharapov, 1998, Phys. Rev. Lett. **81**, 5564.
Fasoli, A., D. Testa, S. Sharapov, H. L. Berk, B. Breizman, A. Gondhalekar, R. F. Heeter, M. Mantsinen, and contributors to the EFDA-JET Workprogramme, 2002, Plasma Phys. Controlled Fusion **44**, B159.
Fasoli, A., *et al.*, 2007, Nucl. Fusion **47**, S264.
Feng, Z., Z. Qiu, and Z. Sheng, 2013, Phys. Plasmas **20**, 122309.
Fiksel, G., B. Hudson, D. J. Den Hartog, R. M. Magee, R. OConnell, S. C. Prager, A. D. Beklemishev, V. I. Davydenko, A. A. Ivanov, and Yu. A. Tsidulko, 2005, Phys. Rev. Lett. **95**, 125001.
Finn, J., 1995, Phys. Plasmas **2**, 198.
Fisch, N., 2000, Nucl. Fusion **40**, 1095.
Fisch, N. J., 2006, Phys. Rev. Lett. **97**, 225001.
Fisch, N. J., 2010, J. Plasma Phys. **76**, 627.
Fisch, N. J., 2012, Internal Report PPPL-4766 (PPL, Princeton, NJ).
Fisch, N. J., and J. M. Rax, 1992, Phys. Rev. Lett. **69**, 612.
Fitzpatrick, R., and A. Y. Aydemir, 1996, Nucl. Fusion **36**, 11.
Flach, S., D. O. Krimer, and Ch. Skokos, 2009, Phys. Rev. Lett. **102**, 024101.
Fredrickson, E. D., N. N. Gorelenkov, and J. Menard, 2004, Phys. Plasmas **11**, 3653.
Fredrickson, E. D., *et al.*, 2002, Phys. Plasmas **9**, 2069.
Fredrickson, E. D., *et al.*, 2009, Phys. Plasmas **16**, 122505.
Fredrickson, E. D., *et al.*, 2013, Nucl. Fusion **53**, 013006.
Freidberg, J. P., 1987, *Ideal Magnetohydrodynamics* (Plenum Press, New York/London).
Friedland, L., P. Khain, and A. G. Shagalov, 2006, Phys. Rev. Lett. **96**, 225001.
Frieman, E. A., and L. Chen, 1982, Phys. Fluids **25**, 502.
Fu, G. Y., 1995, Phys. Plasmas **2**, 1029.
Fu, G. Y., 2008, Phys. Rev. Lett. **101**, 185002.
Fu, G. Y., and C. Z. Cheng, 1992, Phys. Fluids B **4**, 3722.
Fu, G. Y., J. Lang, Y. Chen, H. L. Berk, E. Fredrickson, N. Gorelenkov, and M. Podestà, 2010, in *Proceedings of the 23rd International Conference on Fusion Energy 2010* (International Atomic Energy Agency, Vienna), CD-ROM file THW/2-2Rb.
Fu, G. Y., and W. Park, 1995, Phys. Rev. Lett. **74**, 1594.
Fu, G. Y., W. Park, H. R. Strauss, J. Breslau, J. Chen, S. Jardin, and L. E. Sugiyama, 2006, Phys. Plasmas **13**, 052517.
Fu, G. Y., and J. W. Van Dam, 1989a, Phys. Fluids B **1**, 1949.
Fu, G. Y., and J. W. Van Dam, 1989b, Phys. Fluids B **1**, 2404.
Fu, G. Y., *et al.*, 1989, in *Plasma Physics and Controlled Nuclear Fusion Research 1988, Nice*, Vol. 1 (International Atomic Energy Agency, Vienna), p. 291.
Fujisawa, A., *et al.*, 2007, Phys. Rev. Lett. **98**, 165001.
Fülöp, T., Ya. I. Kolesnichenko, M. Lisak, and D. Anderson, 1997, Nucl. Fusion **37**, 1281.
Furth, H. P., J. Killeen, M. N. Rosenbluth, and B. Coppi, 1965, in *Plasma Physics and Controlled Nuclear Fusion Research 1964*, Vol. I (IAEA, Vienna), p. 103.
Galeev, A. A., V. I. Karpman, and R. Z. Sagdeev, 1965, Sov. Phys. Dokl. **9**, 681.

García-Muñoz, M., H.-U. Fahrbach, H. Zohm, and the ASDEX Upgrade Team, 2009, Rev. Sci. Instrum. **80**, 053503.
García-Muñoz, M., P. Martin, H.-U. Fahrbach, M. Gobbin, S. Günter, M. Maraschek, L. Marrelli, H. Zohm, and the ASDEX Upgrade Team, 2007, Nucl. Fusion **47**, L10.
García-Muñoz, M., *et al.*, 2011, Nucl. Fusion **51**, 103013.
Gerjuoy, E., A. Rau, and L. Spruch, 1983, Rev. Mod. Phys. **55**, 725.
Ghantous, K., H. L. Berk, and N. N. Gorelenkov, 2014, Phys. Plasmas **21**, 032119.
Ghantous, K., N. N. Gorelenkov, H. L. Berk, W. W. Heidbrink, and M. A. V. Zeeland, 2012, Phys. Plasmas **19**, 092511.
Giannessi, L., P. Musumeci, and S. Spampinati, 2005, J. Appl. Phys. **98**, 043110.
Gibson, A., and the JET Team, 1998, Phys. Plasmas **5**, 1839.
Gimblett, C. G., and R. J. Hastie, 2000, Phys. Plasmas **7**, 258.
Glasser, A. H., 1977, in *Finite Beta Theory Workshop, Varenna, 1977*, Vol. CONF-7709167 (U.S. Department of Energy, Washington, DC), p. 55.
Glasser, A. H., J. M. Green, and J. L. Johnson, 1975, Phys. Fluids **18**, 875.
Goedbloed, J. P., 1984, Physica (Amsterdam) **12D**, 107.
Goldston, R. J., and H. H. J. Towner, 1981, J. Plasma Phys. **26**, 283.
Goldston, R. J., R. B. White, and A. H. Boozer, 1981, Phys. Rev. Lett. **47**, 647.
Gorelenkov, N. N., H. L. Berk, R. Budny, C. Z. Cheng, G. Fu, W. W. Heidbrink, G. J. Kramer, D. Meade, and R. Nazikian, 2003, Nucl. Fusion **43**, 594.
Gorelenkov, N. N., H. L. Berk, E. Fredrickson, S. E. Sharapov, and JET EFDA Contributors, 2007, Phys. Lett. A **370**, 70.
Gorelenkov, N. N., Y. Chen, R. B. White, and H. L. Berk, 1999, Phys. Plasmas **6**, 629.
Gorelenkov, N. N., and C. Z. Cheng, 1995a, Phys. Plasmas **2**, 1961.
Gorelenkov, N. N., and C. Z. Cheng, 1995b, Nucl. Fusion **35**, 1743.
Gorelenkov, N. N., and W. W. Heidbrink, 2002, Nucl. Fusion **42**, 150.
Gorelenkov, N. N., S. D. Pinches, and K. Toi, 2014, Nucl. Fusion **54**, 125001.
Gorelenkov, N. N., M. A. Van Zeeland, H. L. Berk, N. A. Crocker, D. Darrow, E. Fredrickson, G. Fu, W. W. Heidbrink, J. Menard, and R. Nazikian, 2009, Phys. Plasmas **16**, 056107.
Gorelenkov, N. N., *et al.*, 2000, Nucl. Fusion **40**, 1311.
Gorelenkov, N. N., *et al.*, 2007, Plasma Phys. Controlled Fusion **49**, B371.
Górska, K., K. A. Penson, D. Babusci, G. Dattoli, and G. H. E. Duchamp, 2012, Phys. Rev. E **85**, 031138.
Grad, H., 1969, Phys. Today **22**, No. 12, 34.
Graves, J. P., I. T. Chapman, S. Coda, M. Lennholm, M. Albergante, and M. Jucker, 2012, Nat. Commun. **3**, 624.
Graves, J. P., *et al.*, 2010, Nucl. Fusion **50**, 052002.
Greene, J. M., and J. L. Johnson, 1968, Plasma Phys. **10**, 729.
Gregoratto, D., A. Bondeson, M. S. Chu, and A. M. Garofalo, 2001, Plasma Phys. Controlled Fusion **43**, 1425.
Gross, E. P., 1961, Nuovo Cimento **20**, 454.
Grossman, W., and J. Tataronis, 1973, Z. Phys. **261**, 217.
Grove, D. J., and D. M. Meade, 1985, Nucl. Fusion **25**, 1167.
Gruzinov, I., A. Das, P. H. Diamond, and A. Smolyakov, 2002, Phys. Lett. A **302**, 119.
Gryaznevich, M. P., and S. E. Sharapov, 2004, Plasma Phys. Controlled Fusion **46**, S15.
Gryaznevich, M. P., and S. E. Sharapov, 2006, Nucl. Fusion **46**, S942.
Gryaznevich, M. P., *et al.*, 2008, Nucl. Fusion **48**, 084003.
Guimarães-Filho, Z. O., *et al.*, 2012, Nucl. Fusion **52**, 094009.
Günter, S., *et al.*, 2007, Nucl. Fusion **47**, 920.
Guo, Z., L. Chen, and F. Zonca, 2009, Phys. Rev. Lett. **103**, 055002.
Guzdar, P. N., R. G. Kleva, and L. Chen, 2001, Phys. Plasmas **8**, 459.
Guzdar, P. N., R. G. Kleva, A. Das, and P. K. Kaw, 2001, Phys. Rev. Lett. **87**, 015001.
Hahm, T. S., 1988, Phys. Fluids **31**, 2670.
Hahm, T. S., and L. Chen, 1995, Phys. Rev. Lett. **74**, 266.
Hahm, T. S., P. H. Diamond, Z. Lin, K. Itoh, and S.-I. Itoh, 2004, Plasma Phys. Controlled Fusion **46**, A323.
Hahm, T. S., W. W. Lee, and A. J. Brizard, 1988, Phys. Fluids **31**, 1940.
Hasegawa, A., 1976, J. Geophys. Res. **81**, 5083.
Hasegawa, A., C. G. Maclennan, and Y. Kodama, 1979, Phys. Fluids **22**, 2122.
Hasegawa, A., and K. Mima, 1978, J. Geophys. Res. **83**, 1117.
Hasegawa, A., and T. Sato, 1989, *Space Plasma Physics—Stationary Processes*, Vol. 1 (Springer, New York).
Hasegawa, H., and L. Chen, 1974, Phys. Rev. Lett. **32**, 454.
Hasegawa, H., and L. Chen, 1975, Phys. Rev. Lett. **35**, 370.
Hasegawa, H., and L. Chen, 1976, Phys. Fluids **19**, 1924.
Hastie, R. J., T. C. Hender, B. A. Carreras, L. A. Charlton, and J. A. Holmes, 1987, Phys. Fluids **30**, 1756.
Hauff, T., M. J. Pueschel, T. Dannert, and F. Jenko, 2009, Phys. Rev. Lett. **102**, 075004.
Hazeltine, R. D., D. A. Hitchcock, and S. M. Mahajan, 1981, Phys. Fluids **24**, 180.
Heeter, R. F., A. F. Fasoli, and S. E. Sharapov, 2000, Phys. Rev. Lett. **85**, 3177.
Heidbrink, W. W., 1995, Plasma Phys. Controlled Fusion **37**, 937.
Heidbrink, W. W., 2002, Phys. Plasmas **9**, 2113.
Heidbrink, W. W., 2008, Phys. Plasmas **15**, 055501.
Heidbrink, W. W., K. H. Burrell, Y. Luo, N. A. Pablant, and E. Ruskov, 2004, Plasma Phys. Controlled Fusion **46**, 1855.
Heidbrink, W. W., H. H. Duong, J. Manson, E. Wilfrid, C. Oberman, and E. J. Strait, 1993, Phys. Fluids B **5**, 2176.
Heidbrink, W. W., E. D. Fredrickson, T. K. Mau, C. C. Petty, R. I. Pinsker, M. Porkolab, and B. W. Rice, 1999, Nucl. Fusion **39**, 1369.
Heidbrink, W. W., M. Murakami, J. M. Park, C. C. Petty, M. A. Van Zeeland, J. H. Yu, and G. R. McKee, 2009, Plasma Phys. Controlled Fusion **51**, 125001.
Heidbrink, W. W., J. M. Park, M. Murakami, C. C. Petty, C. Holcomb, and M. A. Van Zeeland, 2009, Phys. Rev. Lett. **103**, 175001.
Heidbrink, W. W., and G. J. Sadler, 1994, Nucl. Fusion **34**, 535.
Heidbrink, W. W., E. J. Strait, M. S. Chu, and A. D. Turnbull, 1993, Phys. Rev. Lett. **71**, 855.
Heidbrink, W. W., E. J. Strait, E. Doyle, and R. Snider, 1991, Nucl. Fusion **31**, 1635.
Heidbrink, W. W., *et al.*, 2008, Nucl. Fusion **48**, 084001.
Heidbrink, W. W., *et al.*, 2011, Plasma Phys. Controlled Fusion **53**, 085028.
Hinton, F. L., and R. D. Hazeltine, 1976, Rev. Mod. Phys. **48**, 239.
Hsu, C., and D. Sigmar, 1992, Phys. Fluids B **4**, 1492.
Hu, B., and R. Betti, 2004, Phys. Rev. Lett. **93**, 105002.
Iomin, A., 2010, Phys. Rev. E **81**, 017601.
Ionson, J. A., 1982, Astrophys. J. **254**, 318.
ITER Physics Expert Group on Energetic Particles, Heating and Current Drive and ITER Physics Basis Editors, 1999, Nucl. Fusion **39**, 2471.
Jaun, A., A. Fasoli, and W. W. Heidbrink, 1998, Phys. Plasmas **5**, 2952.
Jaun, A., A. Fasoli, J. Vaclavik, and L. Villard, 2000, Nucl. Fusion **40**, 1343.

Kaku, M., 1993, *Quantum Field Theory: A Modern Introduction* (Oxford University Press, Inc., New York).
Kaw, P. K., and J. M. Dawson, 1969, Phys. Fluids **12**, 2586.
Khain, P., and L. Friedland, 2007, Phys. Plasmas **14**, 082110.
Kieras, C. E., and J. A. Tataronis, 1982, J. Plasma Phys. **28**, 395.
Kimura, H., *et al.*, 1998, Nucl. Fusion **38**, 1303.
Kittel, C., 1971, *Introduction to Solid State Physics*, 4th ed. (Wiley, New York).
Kolesnichenko, Ya. I., 1980, Nucl. Fusion **20**, 727.
Kolesnichenko, Ya. I., V. V. Lutsenko, A. Weller, A. Werner, H. Wobig, Yu. V. Yakovenko, J. Geiger, and S. Zegenhagen, 2011, Plasma Phys. Controlled Fusion **53**, 024007.
Kolesnichenko, Ya. I., V. V. Lutsenko, and R. B. White, 2010, Nucl. Fusion **50**, 084017.
Kolesnichenko, Ya. I., and V. N. Oraevskij, 1967, At. Energ. **23**, 289.
Kolesnichenko, Ya. I., Yu. V. Yakovenko, and V. V. Lutsenko, 2010, Phys. Rev. Lett. **104**, 075001.
Kolesnichenko, Ya. I., Yu. V. Yakovenko, V. V. Lutsenko, R. B. White, and A. Weller, 2010, Nucl. Fusion **50**, 084017.
Kolesnichenko, Ya. I., Yu. V. Yakovenko, A. Weller, A. Werner, J. Geiger, V. V. Lutsenko, and S. Zegenhagen, 2005, Phys. Rev. Lett. **94**, 165004.
Kotschenreuther, M., 1986, Phys. Fluids **29**, 2898.
Kramer, G. J., C. Z. Cheng, G. Y. Fu, Y. Kusama, R. Nazikian, T. Ozeki, and K. Tobita, 1999, Phys. Rev. Lett. **83**, 2961.
Kramer, G. J., and G. Y. Fu, 2006, Plasma Phys. Controlled Fusion **48**, 1285.
Kramer, G. J., G. Y. Fu, R. Nazikian, R. V. Budny, C. Z. Cheng, N. N. Gorelenkov, S. D. Pinches, S. E. Sharapov, K. Zastrow, and JET-EFDA Contributors, 2008, Plasma Phys. Controlled Fusion **50**, 082001.
Kramer, G. J., S. E. Sharapov, R. Nazikian, N. N. Gorelenkov, and R. V. Budny, 2004, Phys. Rev. Lett. **92**, 015001.
Kramer, J. G., G. Y. Fu, R. Nazikian, M. A. Van Zeeland, R. K. Fisher, W. W. Heidbrink, L. Chen, and D. C. Pace, 2011, Bull. Am. Phys. Soc. **56**, 98 [http://meetings.aps.org/Meeting/DPP11/Session/GO4.12].
Krivolapov, Y., S. Fishman, and A. Soffer, 2010, New J. Phys. **12**, 063035.
Kruskal, M., 1962, J. Math. Phys. (N.Y.) **3**, 806.
Kruskal, M. D., and C. R. Oberman, 1958, Phys. Fluids **1**, 275.
Kulsrud, R. M., 1978, in *Important Advances in Twentieth Century Astronomy*, anniversary volume for Bengt Stromgren (Copenhagen University Observatory, Copenhagen), pp. 317–325.
Kulsrud, R. M., 1983, in *Basic Plasma Physics*, Vol. I, edited by A. A. Galeev and R. N. Sudan (North-Holland, Amsterdam), pp. 115–146.
Lang, J., and G. Y. Fu, 2011, Phys. Plasmas **18**, 055902.
Lang, J. Y., G. Y. Fu, and Y. Chen, 2010, Phys. Plasmas **17**, 042309.
Lashmore-Davies, C. N., and R. O. Dendy, 1989, Phys. Fluids B **1**, 1565.
Lauber, Ph., 2013, Phys. Rep. **533**, 33.
Lauber, Ph., 2015, Plasma Phys. Controlled Fusion **57**, 054011.
Lauber, Ph., M. Brüdgam, D. Curran, V. Igochine, K. Sassenberg, S. Günter, M. Maraschek, M. García-Muñoz, N. Hicks, and the ASDEX Upgrade Team, 2009, Plasma Phys. Controlled Fusion **51**, 124009.
Lauber, Ph., I. G. J. Classen, D. Curran, V. Igochine, B. Geiger, S. da Graça, M. García-Muñoz, M. Maraschek, P. J. McCarthy, and the ASDEX Upgrade Team, 2012, Nucl. Fusion **52**, 094007.
Lee, Y. C., and J. W. Van Dam, 1977, in *Finite Beta Theory Workshop, Varenna, 1977*, Vol. CONF-7709167 (U.S. Department of Energy, Washington, DC), p. 93.
Lesur, M., and P. H. Diamond, 2013, Phys. Rev. E **87**, 031101.
Lesur, M., and Y. Idomura, 2012, Nucl. Fusion **52**, 094004.
Lesur, M., Y. Idomura, and X. Garbet, 2009, Phys. Plasmas **16**, 092305.
Lesur, M., Y. Idomura, K. Shinohara, X. Garbet, and the JT-60 Team, 2010, Phys. Plasmas **17**, 122311.
Levin, M. B., M. G. Lyubarskii, I. N. Onishchenko, V. D. Shapiro, and V. I. Shevchenko, 1972, Zh. Eksp. Teor. Fiz. **62**, 1725 [Sov. Phys. JETP **35**, 898 (1972)] [http://jetp.ac.ru/cgi-bin/dn/e_035_05_0898.pdf].
Li, Y. M., S. M. Mahajan, and D. W. Ross, 1987, Phys. Fluids **30**, 1466.
Lichtenberg, A. J., and M. A. Lieberman, 1983, *Regular and Stochastic Motion* (Springer, Verlag).
Lichtenberg, A. J., and M. A. Lieberman, 2010, *Regular and Chaotic Dynamics*, 2nd ed. (Springer, Verlag).
Lifshitz, E. M., and L. P. Pitaevsky, 1980, *Statistical Physics. Pt. 2. Theory of Condensed Matter* (Pergamon Press, Oxford, UK).
Liljeström, M., and J. Weiland, 1992, Phys. Fluids B **4**, 630.
Lilley, M. K., and B. N. Breizman, 2012, Nucl. Fusion **52**, 094002.
Lilley, M. K., B. N. Breizman, and S. E. Sharapov, 2009, Phys. Rev. Lett. **102**, 195003.
Lilley, M. K., B. N. Breizman, and S. E. Sharapov, 2010, Phys. Plasmas **17**, 092305.
Lilley, M. K., and R. M. Nyqvist, 2014, Phys. Rev. Lett. **112**, 155002.
Lin, A. T., J. M. Dawson, and H. Okuda, 1978, Phys. Rev. Lett. **41**, 753.
Lin, Z., L. Chen, and F. Zonca, 2005, Phys. Plasmas **12**, 056125.
Lin, Z., S. Ethier, T. S. Hahm, and W. Tang, 2002, Phys. Rev. Lett. **88**, 195004.
Lin, Z., and T. S. Hahm, 2004, Phys. Plasmas **11**, 1099.
Lin, Z., I. Holod, L. Chen, P. H. Diamond, T. S. Hahm, and S. Ethier, 2007, Phys. Rev. Lett. **99**, 265003.
Littlejohn, R. G., 1982, J. Math. Phys. (N.Y.) **23**, 742.
Liu, Y. Q., A. Bondeson, Y. Gribov, and A. Polevoi, 2004, Nucl. Fusion **44**, 232.
Lu, Z. X., F. Zonca, and A. Cardinali, 2012, Phys. Plasmas **19**, 042104.
Lynden-Bell, D., 1967, Mon. Not. R. Astron. Soc. **136**, 101.
Mahajan, S. M., 1995, Phys. Scr. **T60**, 160.
Mahajan, S. M., W. Ross, and G. L. Chen, 1983, Phys. Fluids **26**, 2195.
Manfredi, G., and R. O. Dendy, 1996, Phys. Rev. Lett. **76**, 4360.
Marchenko, V. S., and S. N. Reznik, 2009, Nucl. Fusion **49**, 022002.
Mazitov, R. K., 1965, Zh. Prikl. Mekh. Tekh. Fiz. **1**, 27 [J. Appl. Mech. Tech. Phys. **1**, 22 (1965)].
McClements, K. G., M. P. Gryaznevich, S. E. Sharapov, R. J. Akers, L. C. Appel, G. F. Counsell, C. M. Roach, and R. Majeski, 1999, Plasma Phys. Controlled Fusion **41**, 661.
McGuire, K., *et al.*, 1983, Phys. Rev. Lett. **50**, 891.
Meerson, B., and L. Friedland, 1990, Phys. Rev. A **41**, 5233.
Mett, R. R., and S. M. Mahajan, 1992a, Phys. Fluids B **4**, 2885.
Mett, R. R., and S. M. Mahajan, 1992b, in *Theory of Fusion Plasmas*, edited by J. Vaclavik, F. Troyon, and E. Sindoni (Editrice Compositori, Società Italiana di Fisica, Bologna), p. 243.
Metzler, R., and J. Klafter, 2000, Phys. Rep. **339**, 1.
Metzler, R., and J. Klafter, 2004, J. Phys. A **37**, R161.
Mikhailovskii, A. B., 1975, Zh. Eksp. Teor. Fiz. **68**, 1772 [Sov. Phys. JETP **41**, 890 (1975)] [http://www.jetp.ac.ru/cgi-bin/e/index/e/41/5/p890?a=list].
Mikhailovskii, A. B., E. A. Kovalishen, M. S. Shirokov, A. I. Smolyakov, V. S. Tsypin, and R. M. Galvao, 2007, Plasma Phys. Rep. **33**, 117.

Mikhailovskii, A. B., and L. I. Rudakov, 1963, Sov. Phys. JETP **17**, 621 [http://www.jetp.ac.ru/cgi-bin/e/index/e/17/3/p621?a=list].
Mikhailovskii, A. B., and S. E. Sharapov, 1999a, Plasma Phys. Rep. **25**, 803 [http://adsabs.harvard.edu/abs/1999PlPhR..25..803M].
Mikhailovskii, A. B., and S. E. Sharapov, 1999b, Plasma Phys. Rep. **25**, 838 [http://adsabs.harvard.edu/abs/1999PlPhR..25..838M].
Mikhailovskii, A. B., M. S. Shirokov, S. V. Konovalov, and V. S. Tsypin, 2004, Dokl. Phys. **49**, 505.
Mikhailowskii, A. B., 1973, Nucl. Fusion **13**, 259.
Milovanov, A. V., and A. Iomin, 2012, Europhys. Lett. **100**, 10006.
Milovanov, A. V., and J. J. Rasmussen, 2005, Phys. Lett. A **337**, 75.
Montgomery, D., 1963, Phys. Fluids **6**, 1109.
Mynick, H. E., and A. N. Kaufman, 1978, Phys. Fluids **21**, 653.
Mynick, H. E., and N. Pomphrey, 1994, Nucl. Fusion **34**, 1277.
Nabais, F., D. Borba, M. García-Muñoz, T. Johnson, V. G. Kiptily, M. Reich, M. F. F. Nave, S. D. Pinches, S. E. Sharapov, and JET-EFDA contributors, 2010, Nucl. Fusion **50**, 115006.
Nabais, F., D. Borba, M. Mantsinen, M. F. F. Nave, S. E. Sharapov, and Joint European Torus-European Fusion Development Agreement JET-EFDA Contributors, 2005, Phys. Plasmas **12**, 102509.
Nazikian, R., *et al.*, 2006, Phys. Rev. Lett. **96**, 105006.
Nguyen, C., X. Garbet, V. Grandgirard, J. Decker, Z. Guimarães-Filho, M. Lesur, H. Lütjens, A. Merle, and R. Sabot, 2010, Plasma Phys. Controlled Fusion **52**, 124034.
Nguyen, C., H. Lütjens, X. Garbet, V. Grandgirard, and M. Lesur, 2010, Phys. Rev. Lett. **105**, 205002.
Nishikawa, K., 1968, J. Phys. Soc. Jpn. **24**, 916.
Northrop, T. G., 1963, *Adiabatic Motion of Charged Particles* (Wiley, New York).
Ödblom, A., B. N. Breizman, S. E. Sharapov, T. C. Hender, and V. P. Pastukhov, 2002, Phys. Plasmas **9**, 155.
Okabayashi, M., *et al.*, 2011, Phys. Plasmas **18**, 056112.
Okuda, H., and J. M. Dawson, 1973, Phys. Fluids **16**, 408.
O'Neil, T. M., 1965, Phys. Fluids **8**, 2255.
O'Neil, T. M., and J. H. Malmberg, 1968, Phys. Fluids **11**, 1754.
O'Neil, T. M., and J. H. Winfrey, 1972, Phys. Fluids **15**, 1514.
O'Neil, T. M., J. H. Winfrey, and J. H. Malmberg, 1971, Phys. Fluids **14**, 1204.
Onishchenko, I. N., A. R. Linetskii, N. G. Matsiborko, V. D. Shapiro, and V. I. Shevchenko, 1970a, Zh. Eksp. Teor. Fiz. Pis'ma Red. **12**, 407.
Onishchenko, I. N., A. R. Linetskii, N. G. Matsiborko, V. D. Shapiro, and V. I. Shevchenko, 1970b, JETP Lett. **12**, 281.
Onishchenko, O. G., O. A. Pokhotelov, R. Z. Sagdeev, L. Stenflo, R. A. Treumann, and M. A. Balikhin, 2004, J. Geophys. Res. **109**, A03306.
Ono, M., *et al.*, 2000, Nucl. Fusion **40**, 557.
Oyama, N., and the JT-60 Team, 2009, Nucl. Fusion **49**, 104007.
Pace, D. C., R. K. Fisher, M. García-Muñoz, W. W. Heidbrink, and M. A. Van Zeeland, 2011, Plasma Phys. Controlled Fusion **53**, 062001.
Pace, D. C., *et al.*, 2013, Phys. Plasmas **20**, 056108.
Park, W., E. V. Belova, G. Y. Fu, X. Z. Tang, H. R. Strauss, and L. E. Sugiyama, 1999, Phys. Plasmas **6**, 1796.
Park, W., *et al.*, 1992, Phys. Fluids B **4**, 2033.
Parker, J. B., and R. B. White, 2010, Bull. Am. Phys. Soc. **55**, BP9.117 [http://meetings.aps.org/Meeting/DPP10/Session/BP9.117].
Pegoraro, F., and T. J. Schep, 1978, in *Plasma Physics and Controlled Nuclear Fusion Research*, Vol. 1 (IAEA, Vienna), p. 507.
Perez von Thun, C., *et al.*, 2011, Nucl. Fusion **51**, 053003.
Perez von Thun, C., *et al.*, 2012, Nucl. Fusion **52**, 094010.
Pfirsch, D., and H. Tasso, 1971, Nucl. Fusion **11**, 259.
Pikovsky, A. S., and D. L. Shepelyansky, 2008, Phys. Rev. Lett. **100**, 094101.
Pinches, S. D., H. L. Berk, M. P. Gryaznevich, S. E. Sharapov, and JET-EFDA Contributors, 2004, Plasma Phys. Controlled Fusion **46**, S47.
Pinches, S. D., I. T. Chapman, Ph. W. Lauber, H. J. C. Oliver, S. E. Sharapov, K. Shinohara, and K. Tani, 2015, Phys. Plasmas **22**, 021807.
Pinches, S. D., V. G. Kiptily, S. E. Sharapov, D. S. Darrow, L. G. Eriksson, H. U. Fahrbach, M. García-Muñoz, M. Reich, E. Strumberger, A. Werner, ASDEX Upgrade Team, and JET-EFDA Contributors, 2006, Nucl. Fusion **46**, S904.
Pinches, S. D., *et al.*, 2004, Plasma Phys. Controlled Fusion **46**, B187.
Pitaevskii, L. P., 1961, Sov. Phys. JETP **13**, 451 [http://www.jetp.ac.ru/cgi-bin/e/index/e/13/2/p451?a=list].
Podestà, M., 2012 (private communication).
Podestà, M., R. E. Bell, N. A. Crocker, E. D. Fredrickson, N. N. Gorelenkov, W. W. Heidbrink, S. Kubota, B. P. LeBlanc, and H. Yuh, 2011, Nucl. Fusion **51**, 063035.
Podestà, M., *et al.*, 2009, Phys. Plasmas **16**, 056104.
Podestà, M., *et al.*, 2012, Nucl. Fusion **52**, 094001.
Pogutse, O. P., and E. I. Yurchenko, 1978, Nucl. Fusion **18**, 1629.
Pokhotelov, O. A., O. G. Onishchenko, R. Z. Sagdeev, M. A. Balikhin, and L. Stenflo, 2004, J. Geophys. Res. **109**, A03305.
Porcelli, F., and M. N. Rosenbluth, 1998, Plasma Phys. Controlled Fusion **40**, 481.
Qin, H., and W. M. Tang, 2004, Phys. Plasmas **11**, 1052.
Qin, H., W. M. Tang, and W. W. Lee, 2000, Phys. Plasmas **7**, 4433.
Qin, H., W. M. Tang, W. W. Lee, and G. Rewoldt, 1999, Phys. Plasmas **6**, 1575.
Qin, H., W. M. Tang, and G. Rewoldt, 1998, Phys. Plasmas **5**, 1035.
Qin, H., W. M. Tang, and G. Rewoldt, 1999, Phys. Plasmas **6**, 2544.
Qiu, Z., F. Zonca, and L. Chen, 2012, Phys. Plasmas **19**, 082507.
Rebut, P. H., R. J. Bickerton, and B. E. Kenn, 1985, Nucl. Fusion **25**, 1011.
Rewoldt, G., and W. M. Tang, 1984, Nucl. Fusion **24**, 1573.
Rosenbluth, M. N., 1982, Phys. Scr. **T2A**, 104.
Rosenbluth, M. N., and F. L. Hinton, 1998, Phys. Rev. Lett. **80**, 724.
Rosenbluth, M. N., and N. Rostoker, 1959, Phys. Fluids **2**, 23.
Rosenbluth, M. N., and P. H. Rutherford, 1975, Phys. Rev. Lett. **34**, 1428.
Ross, W., G. L. Chen, and S. M. Mahajan, 1982, Phys. Fluids **25**, 652.
Rutherford, P. H., and E. A. Frieman, 1968, Phys. Fluids **11**, 569.
Sagdeev, R. Z., and A. A. Galeev, 1969, *Nonlinear Plasma Theory* (W. A. Benjamin Inc., New York).
Sagdeev, R. Z., V. D. Shapiro, and V. I. Shevchenko, 1978a, Zh. Eksp. Teor. Fiz. Pis'ma Red. **27**, 361 [Sov. Phys. JETP **27**, 340 (1978)].
Schneller, M., Ph. Lauber, and S. Briguglio, 2016, Plasma Phys. Controlled Fusion **58**, 014019.
Schneller, M., Ph. Lauber, R. Bilato, M. García-Muñoz, M. Brüdgam, S. Günter, and the ASDEX Upgrade Team, 2013, Nucl. Fusion **53**, 123003.
Scott, B. D., 1997, Plasma Phys. Controlled Fusion **39**, 1635.
Sedláček, Z., 1971, J. Plasma Phys. **5**, 239.
Shapiro, V. D., 1963, Zh. Eksp. Teor. Fiz. **44**, 613 [Sov. Phys. JETP **17**, 416 (1963)] [http://www.jetp.ac.ru/cgi-bin/r/index/e/17/2/p416?a=list].
Shapiro, V. D., and V. I. Shevchenko, 1971, Zh. Eksp. Teor. Fiz. **60**, 1023 [Sov. Phys. JETP **33**, 555 (1971)] [http://www.jetp.ac.ru/cgi-bin/r/index/e/33/3/p555?a=list].

Sharapov, S. E., D. Borba, A. Fasoli, W. Kerner, L.-G. Eriksson, R. F. Heeter, G. T. A. Huysmans, and M. J. Mantsinen, 1999, Nucl. Fusion **39**, 373.
Sharapov, S. E., A. B. Mikhailovskii, and G. T. A. Huysmans, 2004, Phys. Plasmas **11**, 2286.
Sharapov, S. E., D. Testa, B. Alper, D. N. Borba, A. Fasoli, N. C. Hawkes, R. F. Heeter, M. Mantsinen, M. G. Von Hellermann, and contributors to the EFDA-JET work-programme, 2001, Phys. Lett. A **289**, 127.
Sharapov, S. E., *et al.*, 2013, Nucl. Fusion **53**, 104022.
Shepelyansky, D. L., 1993, Phys. Rev. Lett. **70**, 1787.
Shinohara, K., *et al.*, 2001, Nucl. Fusion **41**, 603.
Shinohara, K., *et al.*, 2004, Plasma Phys. Controlled Fusion **46**, S31.
Shukla, P. K., M. Y. Yu, H. U. Rahman, and K. H. Spatschek, 1984, Phys. Rep. **105**, 227.
Sigmar, D. J., C. T. Hsu, R. B. White, and C. Z. Cheng, 1992, Phys. Fluids B **4**, 1506.
Smolyakov, A. I., X. Garbet, and M. Ottaviani, 2007, Phys. Rev. Lett. **99**, 055002.
Spong, D. A., B. A. Carreras, and C. L. Hedrick, 1994, Phys. Plasmas **1**, 1503.
Spong, D. A., D. J. Sigmar, W. A. Cooper, D. E. Hastings, and K. T. Tsang, 1985, Phys. Fluids **28**, 2494.
Stix, T. H., 1972, Plasma Phys. **14**, 367.
Stix, T. H., 1992, *Waves in Plasmas* (AIP, New York).
Strait, E. J., W. W. Heidbrink, A. D. Turnbull, M. S. Chu, and H. H. Duong, 1993, Nucl. Fusion **33**, 1849.
Stutman, D., L. Delgado-Aparicio, N. Gorelenkov, M. Finkenthal, E. Fredrickson, S. Kaye, E. Mazzucato, and K. Tritz, 2009, Phys. Rev. Lett. **102**, 115002.
Suzuki, T., *et al.*, 2008, Nucl. Fusion **48**, 045002.
Takechi, M., *et al.*, 1999, Phys. Rev. Lett. **83**, 312.
Takechi, M., *et al.*, 2002, in *Proceedings of the 19th International Conference on Fusion Energy 2002* (International Atomic Energy Agency, Vienna), CD-ROM file EX/W-6, http://www.iaea.org/programmes/ripc/physics/fec2002/html/fec2002.htm.
Tamabechi, K., J. R. Gilleland, Y. A. Sokolov, R. Toschi, and ITER Team, 1991, Nucl. Fusion **31**, 1135.
Tang, J. T., and N. C. Luhmann, Jr., 1976, Phys. Fluids **19**, 1935.
Tang, W. M., J. W. Connor, and R. J. Hastie, 1980, Nucl. Fusion **20**, 1439.
Tataronis, J., 1975, J. Plasma Phys. **13**, 87.
Taylor, J. B., 1967, Phys. Fluids **10**, 1357.
Taylor, J. B., and R. J. Hastie, 1965, Phys. Fluids **8**, 323.
Taylor, J. B., and R. J. Hastie, 1968, Plasma Phys. **10**, 479.
Taylor, J. B., and B. McNamara, 1971, Phys. Fluids **14**, 1492.
Tennyson, J. L., J. D. Meiss, and P. J. Morrison, 1994, Physica (Amsterdam) **71D**, 1.
Tetreault, D. J., 1983, Phys. Fluids **26**, 3247.
Todo, Y., H. L. Berk, and B. N. Breizman, 2003, Phys. Plasmas **10**, 2888.
Todo, Y., H. L. Berk, and B. N. Breizman, 2010, Nucl. Fusion **50**, 084016.
Todo, Y., H. L. Berk, and B. N. Breizman, 2012a, Nucl. Fusion **52**, 033003.
Todo, Y., H. L. Berk, and B. N. Breizman, 2012b, Nucl. Fusion **52**, 094018.
Todo, Y., and T. Sato, 1998, Phys. Plasmas **5**, 1321.
Todo, Y., T. Sato, K. Watanabe, T. H. Watanabe, and R. Horiuchi, 1995, Phys. Plasmas **2**, 2711.
Todo, Y., T.-H. Watanabe, H.-B. Park, and T. Sato, 2001, Nucl. Fusion **41**, 1153.
Toi, K., K. Ogawa, M. Isobe, M. Osakabe, D. A. Spong, and Y. Todo, 2011, Plasma Phys. Controlled Fusion **53**, 024008.
Tsai, S., and L. Chen, 1993, Phys. Fluids B **5**, 3284.
Tsai, S. T., J. W. Van Dam, and L. Chen, 1984, Plasma Phys. Controlled Fusion **26**, 907.
Tsang, K. T., D. J. Sigmar, and J. C. Whitson, 1981, Phys. Fluids **24**, 1508.
Tuccillo, A. A., *et al.*, 2011, Nucl. Fusion **51**, 094015.
Turnbull, A. D., E. J. Strait, W. W. Heidbrink, M. S. Chu, J. M. Greene, L. L. Lao, T. S. Taylor, and S. J. Thompson, 1993, Phys. Fluids B **5**, 2546.
Van Dam, J. W., and M. N. Rosenbluth, 1998, Bull. Am. Phys. Soc. **43**, 1753 [http://flux.aps.org/meetings/YR98/BAPSDPP98/abs/S3100034.html].
Van Dam, J. W., M. N. Rosenbluth, and Y. C. Lee, 1982, Phys. Fluids **25**, 1349.
Vann, R. G. L., H. L. Berk, and A. R. Soto-Chavez, 2007, Phys. Rev. Lett. **99**, 025003.
Vann, R. G. L., R. O. Dendy, and M. P. Gryaznevich, 2005, Phys. Plasmas **12**, 032501.
Vann, R. G. L., R. O. Dendy, G. Rowlands, T. D. Arber, and N. d'Ambrumenil, 2003, Phys. Plasmas **10**, 623.
van Saarloos, W., and P. C. Hohenberg, 1992, Physica (Amsterdam) **56D**, 303.
Van Zeeland, M. A., G. J. Kramer, M. E. Austin, R. L. Boivin, W. W. Heidbrink, M. A. Makowski, G. R. McKee, R. Nazikian, W. M. Solomon, and G. Wang, 2006, Phys. Rev. Lett. **97**, 135001.
Vedenov, A. A., E. P. Velikhov, and R. Z. Sagdeev, 1961, Nucl. Fusion **1**, 82.
Vlad, G., S. Briguglio, G. Fogaccia, and F. Zonca, 2004, Plasma Phys. Controlled Fusion **46**, 1051.
Vlad, G., S. Briguglio, G. Fogaccia, F. Zonca, C. Di Troia, V. Fusco, and X. Wang, 2012, in *Proceedings of the 24th International Conference on Fusion Energy* (International Atomic Energy Agency, Vienna), http://www-naweb.iaea.org/napc/physics/FEC/FEC2012/papers/77_THP603.pdf.
Vlad, G., S. Briguglio, G. Fogaccia, F. Zonca, C. Di Troia, W. W. Heidbrink, M. A. Van Zeeland, A. Bierwage, and X. Wang, 2009, Nucl. Fusion **49**, 075024.
Vlad, G., S. Briguglio, G. Fogaccia, F. Zonca, V. Fusco, and X. Wang, 2013, Nucl. Fusion **53**, 083008.
Vlad, G., S. Briguglio, G. Fogaccia, F. Zonca, and M. Schneider, 2006, Nucl. Fusion **46**, 1.
Vlad, G., S. Briguglio, C. Kar, F. Zonca, and F. Romanelli, 1992, in *Theory of Fusion Plasmas*, edited by E. Sindoni and J. Vaclavik (Editrice Compositori Società Italiana di Fisica, Bologna), p. 361.
Vlad, G., C. Kar, F. Zonca, and F. Romanelli, 1995, Phys. Plasmas **2**, 418.
Vlad, G., F. Zonca, and S. Briguglio, 1999, Riv. Nuovo Cimento **22**, 1.
Vlad, M., and F. Spineanu, 2005, Plasma Phys. Controlled Fusion **47**, 281.
Walén, C., 1944, Ark. Mat. Astron. Fys. **30A**, 1.
Waltz, R. E., and E. M. Bass, 2014, Nucl. Fusion **54**, 104006.
Wang, Ge, 2013, Ph.D. thesis (University of Texas, Austin, TX).
Wang, Ge, and H. L. Berk, 2012, Nucl. Fusion **52**, 094003.
Wang, W.-M., and Z. Zhang, 2009, J. Stat. Phys. **134**, 953.
Wang, X., S. Briguglio, L. Chen, C. Di Troia, G. Fogaccia, G. Vlad, and F. Zonca, 2011, Phys. Plasmas **18**, 052504.
Wang, X., S. Briguglio, L. Chen, C. Di Troia, G. Fogaccia, G. Vlad, and F. Zonca, 2012, Phys. Rev. E **86**, 045401(R).
Wang, X., F. Zonca, and L. Chen, 2010, Plasma Phys. Controlled Fusion **52**, 115005.
Watanabe, T., X. J. Wang, J. B. Murphy, J. Rose, Y. Shen, T. Tsang, L. Giannessi, P. Musumeci, and S. Reiche, 2007, Phys. Rev. Lett. **98**, 034802.

Weiland, J., and L. Chen, 1985, Phys. Fluids **28**, 1359.
Weiland, J., M. Lisak, and H. Wilhelmsson, 1987, Phys. Scr. **T16**, 53.
Weitzner, H., and G. M. Zaslavsky, 2003, Commun. Nonlinear Sci. Numer. Simul. **8**, 273.
White, R., L. Chen, and F. Zonca, 2005, Phys. Plasmas **12**, 057304.
White, R., and H. Mynick, 1989, Phys. Fluids B **1**, 980.
White, R. B., 1989, *Theory of Tokamak Plasmas* (North-Holland, Amsterdam).
White, R. B., 2000 (private communication).
White, R. B., 2010 (private communication).
White, R. B., 2012, Commun. Nonlinear Sci. Numer. Simul. **17**, 2200.
White, R. B., L. Chen, F. Romanelli, and R. Hay, 1985, Phys. Fluids **28**, 278.
White, R. B., R. J. Goldston, K. McGuire, A. H. Boozer, D. A. Monticello, and W. Park, 1983, Phys. Fluids **26**, 2958.
White, R. B., N. Gorelenkov, W. W. Heidbrink, and M. A. Van Zeeland, 2010a, Phys. Plasmas **17**, 056107.
White, R. B., N. Gorelenkov, W. W. Heidbrink, and M. A. Van Zeeland, 2010b, Plasma Phys. Controlled Fusion **52**, 045012.
White, R. B., F. Romanelli, and M. N. Bussac, 1990, Phys. Fluids B **2**, 745.
White, R. B., P. H. Rutherford, P. Colestock, and M. N. Bussac, 1988, Phys. Rev. Lett. **60**, 2038.
White, R. B., *et al.*, 1995, Nucl. Fusion **35**, 1707.
Winsor, N., J. L. Johnson, and J. M. Dawson, 1968, Phys. Fluids **11**, 2448.
Wong, H. V., and H. L. Berk, 1998, Phys. Plasmas **5**, 2781.
Wong, K. L., W. W. Heidbrink, E. Ruskov, C. C. Petty, C. M. Greenfield, R. Nazikian, and R. Budny, 2005, Nucl. Fusion **45**, 30.
Wong, K. L., *et al.*, 1991, Phys. Rev. Lett. **66**, 1874.
Wong, K.-L., 1999, Plasma Phys. Controlled Fusion **41**, R1.
Wong, K.-L., *et al.*, 2000, Phys. Rev. Lett. **85**, 996.
Wu, D., 2012, *Kinetic Alfvén Wave: Theory, Experiment and Application* (Scientific Press, Beijing).
Wu, Y., C. Z. Cheng, and R. B. White, 1994, Phys. Plasmas **1**, 3369.
Wu, Y., R. B. White, Y. Chen, and M. N. Rosenbluth, 1995, Phys. Plasmas **2**, 4555.
Xiao, Y., and Z. Lin, 2011, Phys. Plasmas **18**, 110703.
Yi, L., *et al.*, 2012, Nucl. Fusion **52**, 074008.
Zakharov, V. E., 1968, J. Appl. Mech. Tech. Phys. **9**, 190.
Zakharov, V. E., and V. I. Karpman, 1962, Zh. Eksp. Teor. Fiz. **43**, 490 [Sov. Phys. JETP **16**, 351 (1963)].
Zelenyi, L. M., and A. V. Milovanov, 2004, Phys. Usp. **47**, 749.
Zhang, H. S., Z. Lin, and I. Holod, 2012, Phys. Rev. Lett. **109**, 025001.
Zhang, W., V. Decyk, I. Holod, Y. Xiao, Z. Lin, and L. Chen, 2010, Phys. Plasmas **17**, 055902.
Zhang, W., Z. Lin, and L. Chen, 2008, Phys. Rev. Lett. **101**, 095001.
Zhao, J. S., D. J. Wu, J. Y. Lu, L. Yang, and M. Y. Yu, 2011, New J. Phys. **13**, 063043.
Zheng, L.-J., and L. Chen, 1998a, Phys. Plasmas **5**, 444.
Zheng, L.-J., and L. Chen, 1998b, Phys. Plasmas **5**, 1056.
Zheng, L.-J., M. Kotschenreuther, and M. S. Chu, 2005, Phys. Rev. Lett. **95**, 255003.
Zimmermann, O., H. R. Koslowski, A. Krämer-Flecken, Y. Liang, R. Wolf, and TEC-team, 2005, in *Proceedings of the 32nd EPS Conference on Plasma Physics, Tarragona, Spain, 27 June–1 July, (2005), ECA*, Vol. 29C (EPS), CD-ROM file P4.059.
Zonca, F., 1993a, Plasma Phys. Controlled Fusion **35**, B307.
Zonca, F., 1993b, Ph.D. thesis (Princeton University, Princeton, NJ).
Zonca, F., 2008, Int. J. Mod. Phys. A **23**, 1165.
Zonca, F., A. Biancalani, I. Chavdarovski, L. Chen, C. Di Troia, and X. Wang, 2010, J. Phys. Conf. Ser. **260**, 012022.
Zonca, F., S. Briguglio, L. Chen, S. Dettrick, G. Fogaccia, D. Testa, and G. Vlad, 2002, Phys. Plasmas **9**, 4939.
Zonca, F., S. Briguglio, L. Chen, G. Fogaccia, T. S. Hahm, A. V. Milovanov, and G. Vlad, 2006, Plasma Phys. Controlled Fusion **48**, B15.
Zonca, F., S. Briguglio, L. Chen, G. Fogaccia, and G. Vlad, 2000, in *Theory of Fusion Plasmas*, edited by J. W. Connor, O. Sauter, and E. Sindoni (SIF, Bologna), p. 17.
Zonca, F., S. Briguglio, L. Chen, G. Fogaccia, and G. Vlad, 2005, Nucl. Fusion **45**, 477.
Zonca, F., S. Briguglio, L. Chen, G. Fogaccia, G. Vlad, and X. Wang, 2013, in *Proceedings of the 6th IAEA Technical Meeting on "Theory of Plasmas Instabilities"* (IAEA, Vienna, Austria).
Zonca, F., and L. Chen, 1992, Phys. Rev. Lett. **68**, 592.
Zonca, F., and L. Chen, 1993, Phys. Fluids B **5**, 3668.
Zonca, F., and L. Chen, 1996, Phys. Plasmas **3**, 323.
Zonca, F., and L. Chen, 2000, Phys. Plasmas **7**, 4600.
Zonca, F., and L. Chen, 2006, Plasma Phys. Controlled Fusion **48**, 537.
Zonca, F., and L. Chen, 2007, in *Proceedings of the 34th EPS Conference on Plasma Physics, Warsaw, Poland, 2–6 July, (2007), ECA*, Vol. 31F, CD–ROM file P4.071.
Zonca, F., and L. Chen, 2008, in *Frontiers in Modern Plasma Physics*, Vol. CP1061, edited by P. K. Shukla, B. Eliasson, and L. Stenflo (AIP, New York), p. 34.
Zonca, F., and L. Chen, 2014a, AIP Conf. Proc. **1580**, 5.
Zonca, F., and L. Chen, 2014b, Phys. Plasmas **21**, 072120.
Zonca, F., and L. Chen, 2014c, Phys. Plasmas **21**, 072121.
Zonca, F., L. Chen, A. Botrugno, P. Buratti, A. Cardinali, R. Cesario, V. P. Ridolfini, and JET-EFDA contributors, 2009, Nucl. Fusion **49**, 085009.
Zonca, F., L. Chen, S. Briguglio, G. Fogaccia, A. V. Milovanov, Z. Qiu, G. Vlad, and X. Wang, 2015a, Plasma Phys. Controlled Fusion **57**, 014024.
Zonca, F., L. Chen, S. Briguglio, G. Fogaccia, G. Vlad, and X. Wang, 2015b, New J. Phys. **17**, 013052.
Zonca, F., L. Chen, J. Q. Dong, and R. A. Santoro, 1999, Phys. Plasmas **6**, 1917.
Zonca, F., L. Chen, and R. A. Santoro, 1996, Plasma Phys. Controlled Fusion **38**, 2011.
Zonca, F., L. Chen, R. A. Santoro, and J. Q. Dong, 1998, Plasma Phys. Controlled Fusion **40**, 2009.
Zonca, F., L. Chen, and R. B. White, 2004, in *Theory of Fusion Plasmas*, edited by J. W. Connor, O. Sauter, and E. Sindoni (Editrice Compositori, Società Italiana di Fisica, Bologna, Italy), p. 3.
Zonca, F., F. Romanelli, G. Vlad, and C. Kar, 1995, Phys. Rev. Lett. **74**, 698.
Zonca, F., R. B. White, and L. Chen, 2004, Phys. Plasmas **11**, 2488.
Zonca, F., *et al.*, 2007a, Nucl. Fusion **47**, 1588.
Zonca, F., *et al.*, 2007b, arXiv:0707.2852v1.
Zweben, S. J., R. V. Budny, D. S. Darrow, S. S. Medley, R. Nazikian, B. C. Stratton, E. J. Synakowski, and G. Taylor for the TFTR Group, 2000, Nucl. Fusion **40**, 91.
Zweben, S. J., D. S. Darrow, E. D. Fredrickson, G. Taylor, S. von Goeler, and R. B. White, 1999, Nucl. Fusion **39**, 1097.